AD 290 493

ASD-TDR-62-509
Volume I

BERYLLIUM RESEARCH AND DEVELOPMENT PROGRAM

TECHNICAL DOCUMENTARY REPORT NO. ASD-TDR-62-509, Vol. I

October 1962

Directorate of Materials and Processes
Aeronautical Systems Division
Air Force Systems Command
Wright-Patterson Air Force Base, Ohio

Project No. 7351, Task No. 735104

(Prepared under Contract AF 33(616)-7065
by Nuclear Metals, Inc., Concord, Massachusetts,
S. H. Gelles, coordinator.)

Aeronautical Systems Division, Dir/Materials & Processes, Metals & Ceramics Lab, Wright-Patterson AFB, Ohio.
Rpt Nr ASD-TDR-62-509 Vol I. BERYLLIUM RESEARCH AND DEVELOPMENT PROGRAM. Final report, Oct. 1962, 214 pp. incl illus, tables, & 78 refs.

Unclassified Report

Summary of work conducted for the period April 1, 1960 through September 30, 1961 aimed at making Be more useful as an Air Force structural material. Report describes work in the field of purification, joining and flow and fracture. Volume I describes the preparation of high purity Be by the

(over)

decomposition of BeI_2, the joining of Be by ultrasonic welding and the resistance spot welding of Be. Also, a study of the distribution of BeO and voids in Be by replication electron microscopy, an investigation of the brittle behavior of Be by transmission electron microscopy, and a study of surface damage in Be are described.

1. Beryllium
2. Metallurgy
3. Welding
4. Surface Properties
I. AFSC Proj 7351-04
II. Contr Nr AF 33(616)-7065
III. Nuclear Metals, Inc. Concord, Mass.
IV. S. H. Gelles, Coordinator
V. Aval fr OTS
VI. In ASTIA collection

Aeronautical Systems Division, Dir/Materials & Processes, Metals & Ceramics Lab, Wright-Patterson AFB, Ohio.
Rpt Nr ASD-TDR-62-509 Vol I. BERYLLIUM RESEARCH AND DEVELOPMENT PROGRAM. Final report, Oct. 1962, 214 pp. incl illus, tables, & 78 refs.

Unclassified Report

Summary of work conducted for the period April 1, 1960 through September 30, 1961 aimed at making Be more useful as an Air Force structural material. Report describes work in the field of purification, joining and flow and fracture. Volume I describes the preparation of high purity Be by the

(over)

decomposition of BeI_2, the joining of Be by ultrasonic welding and the resistance spot welding of Be. Also, a study of the distribution of BeO and voids in Be by replication electron microscopy, an investigation of the brittle behavior of Be by transmission electron microscopy, and a study of surface damage in Be are described.

1. Beryllium
2. Metallurgy
3. Welding
4. Surface Properties
I. AFSC Proj 7351-04
II. Contr Nr AF 33(616)-7065
III. Nuclear Metals, Inc. Concord, Mass.
IV. S. H. Gelles, Coordinator
V. Aval fr OTS
VI. In ASTIA collection

Aeronautical Systems Division, Dir/Materials & Processes, Metals & Ceramics Lab, Wright-Patterson AFB, Ohio.
Rpt Nr ASD-TDR-62-509 Vol I. BERYLLIUM RESEARCH AND DEVELOPMENT PROGRAM. Final report, Oct. 1962, 214 pp. incl illus, tables, & 78 refs.

Unclassified Report

Summary of work conducted for the period April 1, 1960 through September 30, 1961 aimed at making Be more useful as an Air Force structural material. Report describes work in the field of purification, joining and flow and fracture. Volume I describes the preparation of high purity Be by the decomposition of BeI_2, the joining of Be by ultrasonic welding and the resistance spot welding of Be. Also, a study of the distribution of BeO and voids in Be by replication electron microscopy, an investigation of the brittle behavior of Be by transmission electron microscopy, and a study of surface damage in Be are described.

(over)

1. Beryllium
2. Metallurgy
3. Welding
4. Surface Properties
I. AFSC Proj 7351-04
II. Contr Nr AF 33(616)-7065
III. Nuclear Metals, Inc. Concord, Mass.
IV. S. H. Gelles, Coordinator
V. Aval fr OTS
VI. In ASTIA collection

Aeronautical Systems Division, Dir/Materials & Processes, Metals & Ceramics Lab, Wright-Patterson AFB, Ohio.
Rpt Nr ASD-TDR-62-509 Vol I. BERYLLIUM RESEARCH AND DEVELOPMENT PROGRAM. Final report, Oct. 1962, 214 pp. incl illus, tables, & 78 refs.

Unclassified Report

Summary of work conducted for the period April 1, 1960 through September 30, 1961 aimed at making Be more useful as an Air Force structural material. Report describes work in the field of purification, joining and flow and fracture. Volume I describes the preparation of high purity Be by the decomposition of BeI_2, the joining of Be by ultrasonic welding and the resistance spot welding of Be. Also, a study of the distribution of BeO and voids in Be by replication electron microscopy, an investigation of the brittle behavior of Be by transmission electron microscopy, and a study of surface damage in Be are described.

1. Beryllium
2. Metallurgy
3. Welding
4. Surface Properties
I. AFSC Proj 7351-04
II. Contr Nr AF 33(616)-7065
III. Nuclear Metals, Inc. Concord, Mass.
IV. S. H. Gelles, Coordinator
V. Aval fr OTS
VI. In ASTIA collection

FOREWORD

This report was prepar . by Nuclear Metals, Inc. under USAF Contract No. AF 33(616)-7065. This contract was initiated under Project No. 7351, "Metallic Materials," Task No. 735104, "Beryllium and Beryllium Alloys." The work was administered under the direction of the Directorate of Materials and Processes, Deputy for Technology, Aeronautical Systems Division, with Lt. S. S. Christopher, succeeded by Capt. L. F. Bubba, acting as project engineer.

This report covers work performed from 1 April 1960 to 30 September 1961.

ABSTRACT (VOLS. I AND II)

The report summarizes the work conducted on the Beryllium Research and Development Program for the period April 1, 1960 through September 30, 1961. The aim of this program is to make beryllium more useful as an Air Force structural material.

The program was divided into eleven major efforts, eight of which were subcontracted and three carried out at the site of the prime contractor, Nuclear Metals, Inc. Detailed abstracts of each program are presented in their respective sections. In addition, work contemplated for a future program is described in a separate section.

Two programs deal with the purification and evaluation of purified beryllium: (1) "The Preparation of Pure Beryllium Metal by the Iodide Decomposition Method" (Nuclear Materials and Equipment Corporation), (2) "Purification of Beryllium by Distillation" (Nuclear Metals, Inc.). In this effort it was found that high purity beryllium could be produced by a vacuum distillation process. Preparation of pure metal by decomposition of the iodide did not appear to be feasible.

Four programs deal with the joining of beryllium: (1) "Brazing of Beryllium" (The Brush Beryllium Company), (2) "The Forge Welding of Beryllium" (The Brush Beryllium Company), (3) "Investigation of the Ultrasonic Weldability of Beryllium Metal Sheet", (Aeroprojects Inc.), (4) "Resistance Welding of Beryllium Sheet" (Rensselaer Polytechnic Institute). The feasibility of joining beryllium by ultrasonic welding was shown. The resistance spot welding program led to definition of the welding parameters, and to methods of altering the weld nugget structure and of eliminating cracking and porosity. The application of warm working in the form of roll-planishing improved to some extent the mechanical behavior of welds made by the Tungsten-arc Inert Gas (TIG) process. In the brazing effort, the optimum time and temperature for brazing beryllium with silver was defined and the effects of post-braze heat treatment on the room temperature and elevated temperature mechanical properties were determined.

The remaining programs, dealing with the flow and fracture characteristics of beryllium and the effect of impurities and alloying additions are: (1) "The Role of Oxides and Voids in Beryllium" (Manufacturing Laboratories, Inc.), (2) "A Study of the Brittle Behavior of Beryllium by Means of Transmission Electron Microscopy" (The Franklin Institute), (3) "Surface Damage in Beryllium" (Lockheed Missiles and Space Company), (4) "Aging and Strain Aging in Beryllium" (Nuclear Metals, Inc.), (5) "Raising the Yield Strength of Beryllium" (Nuclear Metals, Inc.).

In this group of programs, heat-treatment of commercially pure Brush QMV beryllium was found to alter the mechanical properties. These changes were shown to be due to the precipitation of a fcc compound having a lattice parameter $a_o = 6.07$ Å. This appears to be associated with a precipitation reaction involving Fe and possibly Si and Al. The occurrence of a yield point in beryllium was shown to be consistent with the locking of dislocations by impurities.

Techniques for determining the distribution of beryllium oxides and voids in beryllium by replication electron metallography have been improved and the morphology of oxide layers artificially introduced between pressure bonded beryllium discs under different conditions were studied.

Many very fine precipitate particles were found, by transmission electron microscopy, to be present in commercially pure beryllium. These particles appeared to affect the movement of dislocations. Dislocation structures associated with "bend plane" formation were also found.

Twinning was found to be one of the major factors contributing to surface damage in beryllium. Cracks were found to be a relatively minor factor. Inclusions were found to play a role in the initiation of cracks.

A low reduction rolling process was developed that produced sheet having three-dimensional ductility superior to high reduction rolled sheet and equivalent tensile properties. A Be-1 w/o Cu alloy showed uniaxial properties superior to unalloyed Be but somewhat lower three dimensional properties.

PUBLICATION REVIEW

This technical documentary report has been reviewed and is approved.

I. Perlmutter
Chief, Physical Metallurgy Branch
Metals and Ceramics Division
Directorate of Materials and Processes

TABLE OF CONTENTS

TABLE OF CONTENTS (Continued)

TABLE OF CONTENTS (Continued)

LIST OF ILLUSTRATIONS

LIST OF ILLUSTRATIONS (Continued)

LIST OF ILLUSTRATIONS (Continued)

LIST OF ILLUSTRATIONS (Continued)

LIST OF ILLUSTRATIONS (Continued)

LIST OF ILLUSTRATIONS (Continued)

LIST OF TABLES

LIST OF TABLES (Continued)

SECTION 1

INTRODUCTION

This report* summarizes in detail the work carried out on the Beryllium Research and Development Program for the period April 1, 1960 through September 30, 1961.

The Beryllium Research and Development Program was the first attempt to coordinate within a "management" type contract all the research and development work on beryllium sponsored by Materials Central. Nuclear Metals, Inc., as prime contractor, has responsibility for the planning and performance of a series of projects aimed at making beryllium more useful as an Air Force structural material. It was intended that the approach to this goal be twofold. First, part of the program was to be aimed at changing the chemical and physical nature of the available beryllium by such processes as purification; second, part of the program was to be directed toward gaining a better understanding of beryllium in its current level of purity and developing the technology for its use.

Nuclear Metals, Inc. was to perform approximately 40% of the work at its site and was to let approximately 60% of the work to judiciously chosen subcontractors, subject to the approval of the Air Force.

It was the duty of the program manager to keep up with advances in research and technology as applied to beryllium. This involved continuing study of the literature, as well as visits to sites engaged in beryllium research and development work. The program manager was also required to impart to the subcontractors information that would help in the performance of their work, and to arrange for meetings at which the subcontractors and other people involved in beryllium research and development could review their programs and keep up with current advances in beryllium technology.

There were twelve projects in all: eight of these were subcontracted and four were conducted at Nuclear Metals, Inc. The following is a list of the projects, the sites at which they were carried out, and the principal investigators:

PROJECT	SITE	PRINCIPAL INVESTIGATORS
Preparation of Pure Beryllium Metal by the Iodide Decomposition Process	Nuclear Materials and Equipment Corporation	L. Pepkowitz B. Vondra
Ultrasonic Welding of Beryllium	Aeroprojects Inc.	J. B. Jones N. Maropis J. G. Thomas H. L. McKaig, Jr.
Oxide and Void Distribution in Beryllium	Manufacturing Laboratories, Inc.	S. Allen
Role of Dislocations in Beryllium	Franklin Institute	F. Wilhelm H. G. F Wilsdorf

- - - - - - - - - - - - - -

* Manuscript released May 1962 by the author for publication as an ASD Technical Documentary Report.

PROJECT	SITE	PRINCIPAL INVESTIGATORS
Surface Damage in Beryllium	Research Laboratories, Lockheed Missiles and Space Division	E. C. Burke M. I. Jacobson F. A. Almeter
Brazing of Beryllium	Brush Beryllium Company	B. M. MacPherson R. B. Magalski R. G. O'Rourke
Forge Welding of Beryllium	Brush Beryllium Company	B. M. MacPherson W. W. Beaver
Resistance Spot Welding	Rensselaer Polytechnic Institute	E. Nippes W. Savage F. Wassell
Distillation of Beryllium	Nuclear Metals, Inc.	J. P. Pemsler
Evaluation of Products	Nuclear Metals, Inc.	E. D. Levine
Aging and Strain Aging in Beryllium	Nuclear Metals, Inc.	L. R. Aronin A. K. Wolff
Raising the Yield Strength of Beryllium	Nuclear Metals, Inc.	E. D. Levine L. R. Aronin

The sections to follow summarize in detail the work that has been accomplished on the different projects. The final section of the report describes the future plans for the program.

SECTION 2

THE PREPARATION OF PURE BERYLLIUM METAL BY THE IODIDE DECOMPOSITION METHOD

B. L. Vondra, F. J. Shipko, and L. P. Pepkowitz

(Nuclear Materials and Equipment Corporation
Apollo, Pennsylvania)

ABSTRACT

The work under this contract was undertaken to determine the feasibility of producing high purity ductile beryllium metal by the iodide decomposition process. The activities included preparation of stoichiometric BeI_2; static and dynamic methods for the thermal decomposition of the halide and evaluation of materials of construction. It was concluded that filament temperatures compatable with a beryllium metal filament are not sufficiently high to decompose BeI_2 in an irreversible manner or that the rate of distillation of the deposited Be metal from the filament exceeds the rate of dissociation of BeI_2 on the filament. Suggestions are presented for future work.

2-1 INTRODUCTION

This program was undertaken to determine the feasibility of producing high purity ductile beryllium by the iodide decomposition (van Arkel-De Boer) process. Production of other highly purified metals by this technique has reached an advanced state of development, allowing tonnage quantities to be produced. Among these metals are zirconium, hafnium and vanadium. No success has been reported in producing beryllium by this method.

Two variations of the process are possible. In the first, the dynamic process, the metal iodide is simply distilled or sublimed at a low vapor pressure through an evacuated chamber containing a heated filament. As the vapor contacts the heated filament the iodide is thermally decomposed, depositing the metal on the filament and releasing iodine which is pumped from the system.

The mechanism of the second or static process is also basically simple but more readily adaptable to large scale production. The volatile iodide of the metal is vaporized at a low pressure in an evacuated vessel. A thin filament in this chamber is heated to a suitably high temperature. Dissociation of the iodide occurs at the temperature of the filament and the metal is deposited on it. The iodide is prepared continuously by the reaction of the iodine released in the dissociation with a crude metal supply in the deposition vessel. Undesirable impurities in the crude metal are left behind as the cyclic process transfers pure metal to the filament.

For either process to be applicable, the metal must have the following properties:

(1) The metal should react with iodine at a reasonable temperature.

(2) The iodide must have a suitable vapor pressure - temperature relationship so that adequate volatility will occur at moderate temperatures (i.e., room temperature to $\sim 600^{\circ}C$).

(3) The iodide should be highly compatible with reasonable materials of construction.

(4) Decomposition of the iodide at the filament should take place below the melting point of the metal to be deposited.

(5) The rate of vaporization of the metal deposit at the filament temperature must be lower than the rate of deposition.

Investigations into the physical and chemical properties of beryllium indicate that its iodide forms and has a suitable vapor pressure within a favorable temperature range. Experiments with various materials of construction have uncovered a major problem area that has not yet been adequately investigated.

Requirements (4) and (5) place an upper limit for the beryllium system of $1283^{\circ}C$, the melting point of beryllium. Temperatures below $1100^{\circ}C$ may be required to minimize vaporization of the metal.

It is not possible to make any exact calculations for the reaction

$$BeI_{2(V)} \longrightarrow Be_{(S)} + I_{2(V)}$$

since reliable thermodynamic values are not available and the species involved in the reaction are unknown. However, it can be assumed that the reaction is controlled by kinetic considerations such as the rate of thermal decomposition at the filament, the rate of diffusion of free iodine away from the filament, and the rate of BeI_2 diffusion toward the filament.

2-2 LITERATURE SURVEY

A survey of the literature was made on the thermal decomposition and hydrogen reduction processes for beryllium halides. Very little work on beryllium has been reported except for a few papers in which the formation of pure beryllium was assumed, but not unequivocally demonstrated or reduced to a practical process.

The history and application of the van Arkel - De Boer technique of preparing pure metals by the pyrolytic decomposition of volatile iodides is presented[1] in detail by Shapiro. A beryllium iodide decomposition method was reported[2] by Sloman. His work was carried out in evacuated Pyrex equipment, decomposing the BeI_2 on a tungsten filament at 700 - 900°C. He reported the deposition of a 1 - 3 mm thickness of beryllium which contained considerable boron and silicon. The deposit was coarsely crystalline and very brittle. It was indicated that Ni-Cr alloys might be suitable as container materials instead of glass; however, the program was not continued.

Kopelman and Bender reported[3] on the dissociation of BeI_2 in platinum equipment. They observed an interaction of BeI_2 with the platinum at 575 - 1060°C, forming a Be-Pt alloy of undetermined composition with the evolution of elemental iodine. However, when a beryllium crucible insert was used, free iodine was not obtained at 1200°C. It was concluded that the decomposition of the iodide in the absence of platinum is controlled solely by kinetic considerations.

Kellog, in reference to the thermal decomposition process, calculated[4] that 3.6% of the BeI_2 present would be dissociated at 1500°K and 10^{-2} atmospheres. He suggested that decomposition of the halides in an arc would overcome the temperature limitation of the hot wire process.

Hackspill and Besson report[5] the reduction of $BeCl_2$ with hydrogen on the surface of a hot tungsten wire. They obtained a deposit of beryllium or a Be-W alloy, depending on the filament temperature.

2-3 EXPERIMENTAL

2-3.1 Preparation of Pure BeI_2. Since the successful preparation of pure beryllium metal will depend on the purity and stoichiometry of the starting material, the first step in the present program was to prepare pure BeI_2. It was mandatory that no elemental iodine be present in the product since it has been shown[1] that trace excesses of iodine can reverse the direct reaction. Various methods of

preparing BeI_2 were evaluated. These relied on direct reaction of elemental beryllium and iodine, or reaction of Be_2C with HI.

(1) Preparation at Atmospheric Pressure by Direct Reaction. Several batches of BeI_2 were prepared in both Pyrex and stainless steel systems. The procedure employed the vaporization of iodine in a stream of argon (0.1 liter per minute) at a temperature of 80 - 90°C. The iodine vapor contacted a bed of Pechiney beryllium flake maintained at 450 - 500°C. The resultant product deposited in the cooler portions of the reaction chamber in the form of a white crystalline powder. However, as the reaction was continued, the product became slightly brownish due to unreacted iodine becoming adsorbed on the BeI_2. The BeI_2 was then sublimed from the reaction chamber to collection bulbs. Even after several resublimations the iodine coloration in the product could not be completely eliminated. The results were the same in both steel and Pyrex reactors.

(2) Preparation Under Vacuum by Direct Reaction. Due to the inability to rid the iodide of iodine in the flow system, BeI_2 was prepared under vacuum in a Pyrex apparatus. To achieve this purpose, a versatile vacuum apparatus (Figure 1) was designed and constructed for iodide preparation as well as for thermal decomposition studies. Several batches of pure white crystalline product were prepared. Iodine was vaporized at 90°C from the iodine reservoir through a bed of beryllium metal flake maintained at 450°C. The iodine pressure in the system was kept low with the aid of a liquid nitrogen trap attached directly to the reaction chamber. The iodide collected in the chamber directly above the beryllium metal, with any excess iodine removed by continuous pumping. The BeI_2 was sublimed from this chamber into side arm sampling tubes in which it was collected and sealed off for analysis. Free iodine could not be detected in the product.

(3) Preparation from Be_2C and HI. Essentially pure Be_2C was obtained from Nuclear Metals, Inc. and used as the starting material. The HI was prepared by mixing purified H_2 with iodine at 100°C and passing the mixture through a bed of platinized asbestos at 700°C. Unreacted iodine was collected in a cold trap (-30°C) beyond the reaction zone.

Be_2C was reacted with the HI in an hydrogen atmosphere.

$$Be_2C + 4HI \longrightarrow 2BeI_2 + 2H_2 + C$$

The Be_2C was contained in a carbon liner inside a quartz tube and heated to 550°C. The product of the reaction (BeI_2) had a brownish tint similar to that prepared from direct reaction of the elements at atmospheric conditions. This coloration was not removed after sublimation.

The experiment was repeated under vacuum conditions. Liquid nitrogen was used to freeze HI in a bulb connected to the reaction tube. After degassing the system at 550°C, the HI was slowly evolved from the bulb by gradual warming. A white crystalline powder collected beyond the reaction zone. This material had a composition similar to that prepared directly from the elements and was free of iodine.

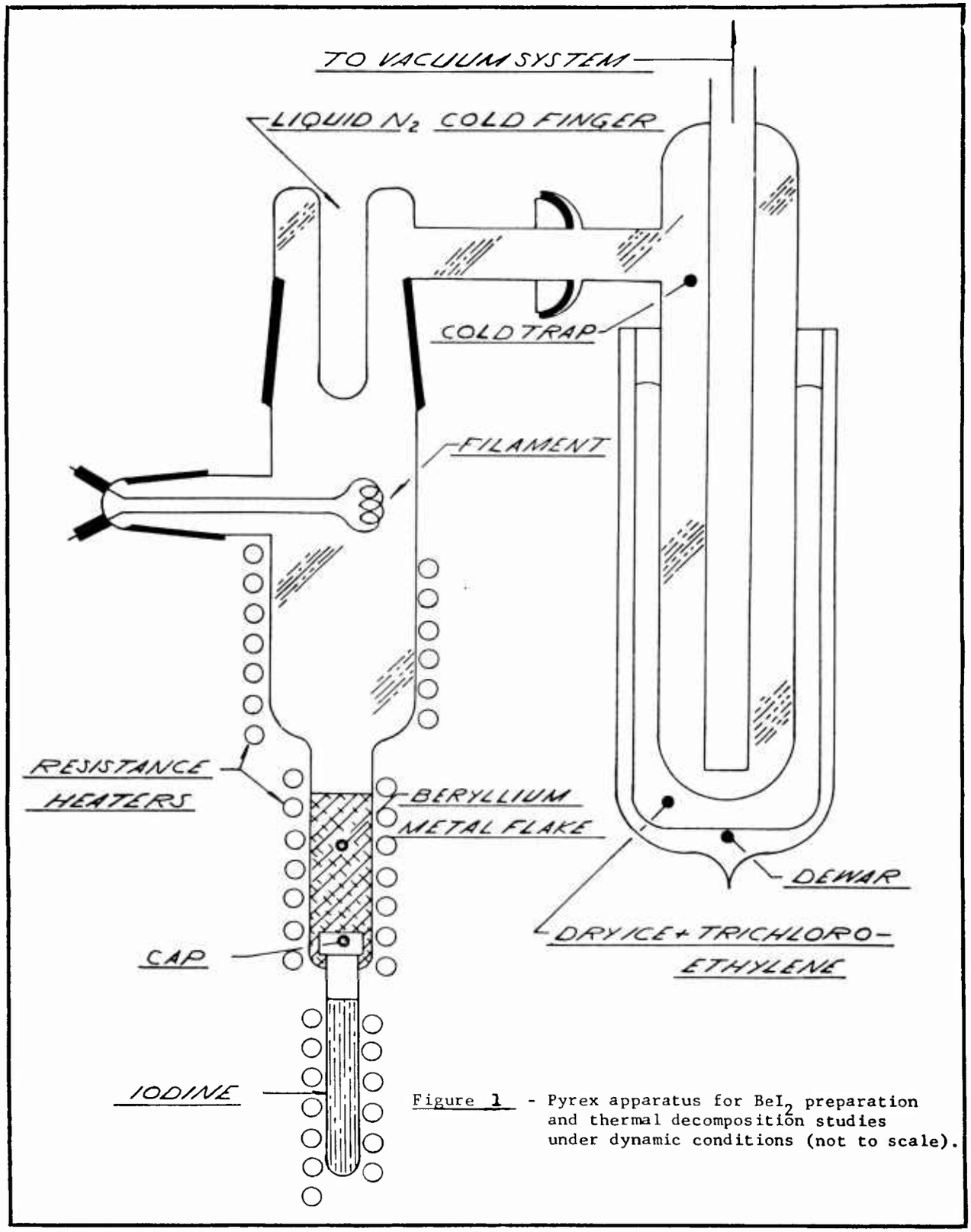

Figure 1 - Pyrex apparatus for BeI_2 preparation and thermal decomposition studies under dynamic conditions (not to scale).

(4) Selection of Best Preparation Method and Evaluation of Product. The preparation of BeI_2 from the elements under vacuum conditions proved to be the most acceptable method and was chosen for further preparations of the compound. The starting materials are readily available in high purity and do not require any preliminary preparation or manipulations which easily introduce undesirable impurities. The use of Pyrex for the apparatus was not found to be detrimental since only trace quantities of silicon could be found in the product and no attack on the glass was evident.

Spectrographic analysis of a typical BeI_2 preparation is presented in Table 1.

Several batches of BeI_2 were prepared and sublimed into small Pyrex tubes which were subsequently analyzed for Be, I, and free I_2 (Table 2). The individual sample tubes were broken under deionized water and the BeI_2 hydrolyzed to HI and $Be(OH)_2$. A glass stoppered flask was used to prevent escape of HI vapors. The solution was made to known volume and aliquots taken for analyses. Beryllium was determined by precipitation with ammonium hydroxide, drying and igniting to BeO. Titration of the sample with sodium thiosulfate solution gave the free iodine content. Total iodine in an aliquot was determined by oxidation of the HI to I_2 by sodium nitrite and titration with sodium thiosulfate.

2-3.2 Decomposition of BeI_2.

(1) Dynamic Experiments in an Hydrogen Atmosphere. Several experiments were made to study the behavior of BeI_2 in a flow system in an hydrogen atmosphere. If decomposition of the halide takes place, the hydrogen should act as a carrier to remove iodine from the vicinity of the filament and favor the formation of a beryllium deposit. The hydrogen might also effect the reduction of the iodide at a temperature lower than required for ordinary thermal decomposition. This reaction would decrease the concentration of iodine by the formation of HI.

$$BeI_2 + H_2 \xrightarrow{\text{Hot filament}} Be + 2HI$$

The conditions and results of these experiments are shown in Table 3. With the exception of run H-1 the iodide was prepared from the elements under vacuum conditions and sublimed into Pyrex bulbs that were subsequently transferred to the reaction tube under an argon atmosphere. The resulting iodide was a pure white powder, as compared to that used in run H-1 which was prepared in a flow system at atmospheric conditions in argon and had a brown tint due to iodine contamination.

In the first three experiments there was a definite reaction with the Pyrex, since the walls were seriously etched in the vicinity of the filament. The deposit on the filament was analyzed by X-ray methods and was found to be elemental silicon. Boron and beryllium were detected spectrographically. Figure 2 shows the filament from run H-2.

An interaction of beryllium iodide and the silica in the glass probably occurred

$$2BeI_2 + SiO_2 \longrightarrow 2BeO + SiI_4$$

$$SiI_4 \xrightarrow{\Delta} Si + 2I_2$$

Table 1. ANALYSIS OF BeI_2 AND STARTING MATERIAL

BeI_2 (%)	
Fe	.03
Al	.05
Mg	.005
Cu	.03
Si	<.1
Ti	.02
Ag	.01

Table 2. BeI_2 ANALYSIS

Sample No.	Be (millimoles)	I (millimoles)	Free I_2 (%)	I_2/Be Mole Ratio
1	2.32	3.89	.01	1.68
2	3.08	5.24	.05	1.70
3	2.23	4.27	.01	1.91
4	3.74	6.78	.03	1.81
5	4.09	7.09	.03	1.74
6	2.14	3.74	.05	1.75
7	3.15	5.97	.06	1.90
8	2.29	4.03	.06	1.75
9	2.03	3.62	.16	1.78
10	2.42	4.45	.02	1.83
11	3.09	5.79	.06	1.87
			Average	1.79

Table 3. DYNAMIC EXPERIMENTS IN AN HYDROGEN ATMOSPHERE

Run No.	Fila-ment	Filament Temp.(°C)	H_2 Pressure and/or Flow Rate	Vapori-zation Temp. of BeI_2 (°C)	Length of run (hrs.)	Comments	Results	Deposit on Filament
H-1	Mo	1000	.4 LPM at atmospheric pressure	440	1.5	Bulb containing BeI_2 placed 2" in front of filament in horizontal Pyrex tube. Corrosion of Pyrex tube.	Thick, dark gray deposit; brittle; looks metallic	High Si Some B Low Be*
H-2	Mo	1075	.4 LPM at atmospheric pressure	440	1.5	Similar to above run. Corrosion of Pyrex tube.	Thick deposit as globules and crystals	High Si Slight B Low Be*
H-3	Mo	1200	.4 LPM at atmospheric pressure	350	2	Similar to run 1. Evidence of erosion of filament. Corrosion of Pyrex tube.	Crystalline, brittle deposit. Deposit broke away from filament.	High Mo High Si Trace Be*
H-4	Mo	1100	100-200 micron leak with continuous pumping	220	2.5	BeI_2 prepared in reactor beforehand and sublimed in H_2 past filament. No attack on Pyrex.	I_2 collected in cold trap.	None
H-5	Mo	1250	.1 LPM at atmospheric pressure.	220	2	No corrosion of Pyrex.	No deposit on filament.	None

* spectrographic analysis - not distinguished as metallic Be

60X

Figure 2 - Filament from experiment H-2 showing character of deposit.

with subsequent thermal decomposition (or hydrogen reduction) of the silicon iodide to metallic silicon. In all these experiments there was evidence of elemental iodine beyond the reaction zone.

In runs H-4 and H-5 no interaction of BeI_2 with the Pyrex was observed. Spectrographic analysis of the BeI_2 that sublimed past the filament showed only a trace (< .1%) of silicon. The elimination of the reaction with the Pyrex is attributed to the lower temperature used to vaporize the halide. Such a temperature appears unfavorable for the formation of SiI_4. In none of these experiments was there any significant deposition of metallic beryllium, although traces of beryllium were detected spectrographically.

(2) Dynamic Experiments under Vacuum Conditions. Several analyses of BeI_2 that was prepared by reacting the elements under vacuum in a Pyrex system showed only a trace (< .05%) of silicon. These results and other advantages of Pyrex, including transparency and ease of construction, led to its selection as the reactor material for these experiments.

A schematic diagram of this reactor is shown in Figure 1. The diameter of the tube at the filament is 1.5 inches and the length from the iodine reservoir to and including the cold finger is 21 inches. Apiezon wax was used to make a vacuum seal on the filament leads and at the ground glass connections. Removable Nichrome-wound resistance heaters were designed so that they could be readily inserted or removed. This reactor was attached to a cold trap and a high vacuum pumping system. A dry ice-trichloroethylene mixture was used in the cold trap in all the experiments.

The apparatus was thoroughly cleaned for each experiment. It was dried by rinsing with acetone, air drying, and finally evacuating without cooling the trap. C.P. iodine was then added to the reservoir and a Pyrex cap placed over the end. Pechiney beryllium metal flake was introduced to a depth of approximately three inches. The iodine reservoir was cooled under liquid nitrogen during evacuation of the system.

In a typical experiment the beryllium flake was heated to 450°C and the iodine reservoir gradually raised to 90°C. Beryllium iodíde collected in the narrow tube above the metal bed. This reaction was continued until all of the iodine in the reservoir was consumed. Finally the iodide was sublimed into the reaction chamber to about 3 inches below the filament. The upper resistance heater was then positioned so that the heated zone would extend up to the filament.

This heater was set at the predetermined temperature of the run; the beryllium flake bed being maintained at 450°C to prevent back sublimation of halide. The filament was heated after the desired sublimation temperature was reached. In experiments involving cooling of the cold finger, liquid nitrogen was added before heating the filament and maintained at constant level throughout the experiment.

The temperature of the heaters was monitored with Chromel-Alumel thermocouples in contact with the Pyrex walls, and the filament temperature was controlled with the aid of an optical pyrometer. Suitable corrections for emissivity were made depending on the type of filament used.

Table 4 lists the dynamic experiments performed in the Pyrex apparatus with the above-mentioned general conditions. A constant vacuum was applied in all runs except for run D-7 in which the reactor and cold trap were isolated from the pumping system.

The BeI_2 prepared for each of the runs was a pure white crystalline powder. Its preparation in situ eliminated transfer problems with the attendant possible contamination and hydrolysis of the iodide. This compound is so unstable that when a leak develops in the apparatus an immediate brown coloration due to the release of elemental iodine is observed.

Filaments made from 0.020-inch diameter tungsten or molybdenum wire proved to be the most acceptable. Their high vaporization temperature coupled with non-reactivity toward BeI_2 made them quite suitable for these experiments. Beryllium wire (0.020-inch diameter) was very brittle and difficult to coil into a filament. Its high vapor pressure (1 micron at 1130°C) and reactivity toward iodine limits its use. Platinum filaments were found unsuitable because of their reactivity with the iodide. The following detailed discussion of the dynamic experiments will clarify the data in Table 4.

Runs D-1 and D-2 were performed by a method that has been used in the past to deposit such metals as zirconium and molybdenum. The iodide was not prepared beforehand but was synthesized in situ. Iodine was released from the reservoir at an estimated 10-micron vapor pressure by warming it to approximately -35°C. The beryllium metal bed was maintained at 450°C. The reaction chamber was heated to the same temperature to prevent condensation of any iodide on the walls. White BeI_2 collected beyond the filament, indicating a very low elemental iodine concentration in the atmosphere. No metallic deposit was observed on the filament at 800 or 1100°C.

Runs D-3 through D-8 were a series of tests using a molybdenum filament in which a range of filament temperatures and beryllium iodide vapor pressures were tried. The iodide was prepared before each experiment as described above. Approximately 20 to 30 grams of iodide were prepared in each case to assure an adequate supply of vapor throughout the run. The vapor pressures listed in the table are those that would be present under equilibrium conditions but are not necessarily those that were attained since the system was in a dynamic condition. These relative pressures were maintained throughout since an excess of iodide remained in the vaporization section at the end of each run.

Experiments D-3 and D-4 were made without using any coolant in the cold finger. Although no deposit on the filament was observed, elemental iodine collected in the dry-ice trap. No effect was observed by varying the BeI_2 vapor pressure between 50 and 200 microns.

Runs D-5, D-6 and D-8 were conducted to determine the effect of elemental iodine concentration on the deposition or resublimation of beryllium. All three runs were made with coolant in the cold finger: liquid nitrogen was used in runs D-5 and D-6 and a mixture of dry ice-trichloroethylene was used in D-8. The inside end of the finger was located about 1.5 inches from the filament. This cold surface,

Table 4. DYNAMIC EXPERIMENTS UNDER VACUUM CONDITIONS

Run No.	Filament	Filament Temp. (°C)	Vaporization Temp. of BeI_2 (°C)	Vapor Pressure of BeI_2 (microns)	Length of Run (hrs.)	Comments	Results	Deposit on Filament
D-1	Mo	1100	450	-	3	BeI_2 prepared throughout run by passing I_2 from -35°C reservoir through 450°C Be.	BeI_2 collected beyond filament.	None
D-2	Mo	800	450	-	3	BeI_2 prepared throughout run by passing I_2 from -35°C reservoir through 450°C Be.	BeI_2 collected beyond filament.	None
D-3	Mo	975	250	200	2	No liquid N_2 finger	I_2 collected in cold trap.	None
D-4	Mo	1300-1350 (ends,1100)	220	50	3	BeI_2 remained white during sublimation past filament. No liquid N_2 in finger.	I_2 collected in cold trap.	None
D-5	Mo	1300-1350 (ends,1100)	220	50	2.5	Liquid N_2 in finger during sublimation.	I_2 collected on finger.	None
D-6	Mo	1500 (ends, 1200)	200	15	3	Liquid N_2 in finger during sublimation.	I_2 collected on finger.	None
D-7	Mo	1200	200	15	2	Static run. Vacuum off during sublimation of BeI_2. No liquid N_2 in finger.	I_2 collected in cold trap.	None
D-8	Mo	1000	200	15	2	Dry ice - trichloroethylene (-80°C) in finger.	I_2 collected on finger.	None
D-9	W	1050	200	15	1.5	Liquid N_2 in finger.	I_2 collected on finger.	None
D-10	Pt	1150	250	200	0.5	Liquid N_2 in finger.	Filament alloyed with deposit and melted. Much I_2 collected on finger.	Pt_5Be_{13}

Table 4 (Continued)

Run No.	Filament	Filament Temp. (^{o}C)	Vaporization Temp. of BeI_2 (^{o}C)	Vapor Pressure of BeI_2 (microns)	Length of Run (hrs.)	Comments	Results	Deposit on Filament
D-11	Pt	800-850	250	200	2.5	Liquid N_2 in finger.	Trace I_2 collected on finger.	None
D-12	Pt	1000	200	15	1	Liquid N_2 in finger.	Metal deposit. No apparent alloying. I_2 collected on finger.	Pt_5Be_{13}
D-13	Pt	1000	200	15	4	Liquid N_2 in finger.	Metal deposit. Build-up on filament stopped after 1 hr. I_2 collected on finger.	Pt_5Be_{13}
D-14	Be	1050	200	15	1.5	Liquid N_2 in finger.	Filament slightly eroded at center. I_2 collected on finger.	None
D-15	Be	975	200	15	2	Liquid N_2 in finger.	No change in filament. I_2 collected on finger.	None

in close proximity to the heated filament, should accelerate the removal of elemental iodine and possibly prevent a recombination of the thermally dissociated iodide. The coolant was placed in the cold finger just before the filament was heated. In each case iodine collected on the finger even though no deposit was formed on the filament.

Experiment D-7 was run under static conditions; i.e., no pumping was used after the filament was heated. The transfer of iodide past the filament was not impeded, since the vapor always tends to condense on cooler sections of the reactor. Pressure checks made on a McLeod gauge beyond the cold trap indicated a vacuum of less than one micron throughout the run. Iodine was collected in the dry-ice trap but there were no positive indications of beryllium metal deposited on the heated filament.

Run D-9 was made under conditions similar to those used in D-8 except that a tungsten filament was used instead of molybdenum. The change in the type of filament had no affect on the results.

In order to check the work of Kopelman and Bender[3], wherein platinum was used as a container material, a series of experiments, D-10 through D-13, were performed using a platinum filament. Run D-10, performed at a filament temperature of 1150°C, yielded a Be-Pt alloy. Melting of the alloy was observed, and droplets collected on the lower portion of the filament. X-ray diffraction indicated a structure agreeing with that of Pt_5Be_{13}.[6] Figure 3 shows the droplets of the alloy formed. Liquid nitrogen was used in the cold finger and a quantity of iodine that was large as compared to previous results was collected. A BeI_2 vapor pressure of 200 microns was used. The run had to be discontinued after 0.5 hour because an electrical short circuit developed in the filament.

In an attempt to stop the alloying of beryllium with the filament, the filament temperature was lowered to 800 - 850°C for run D-11. A trace of iodine collected on the cold finger but the temperature was too low to induce a reaction with the platinum filament and no deposit was formed.

Figures 4 and 5 show the type of deposit formed in runs D-12 and D-13. The platinum filament was maintained at 1000°C and a light gray deposit was formed with no apparent alloying. In an attempt to build up the deposit into a thick coating, the duration of experiment D-13 was extended to four hours. However, after an initial deposition period (approximately 1 hour) little or no increase in coating thickness was observed. This indicates that thermal decomposition of the iodide was not taking place; instead, an interaction between the platinum and the BeI_2 was occurring. When no more elemental platinum was exposed to the BeI_2 atmosphere, the reaction stopped.

Repetition of the above experimental conditions employing a beryllium filament (0.020-inch diameter wire) showed iodine collecting on the cold finger as normally observed, but no apparent deposition on the filament (runs D-14 and D-15). There was a slight erosion of the filament at 1050°C, possibly due to vaporization of the beryllium or to a reaction with iodine formed at the filament.

4X

Figure 3 - Pt-Be alloy droplets formed on platinum filament at 1150°C.

4X

Figure 4 - Pt-Be coating formed on platinum filament at 1000°C.

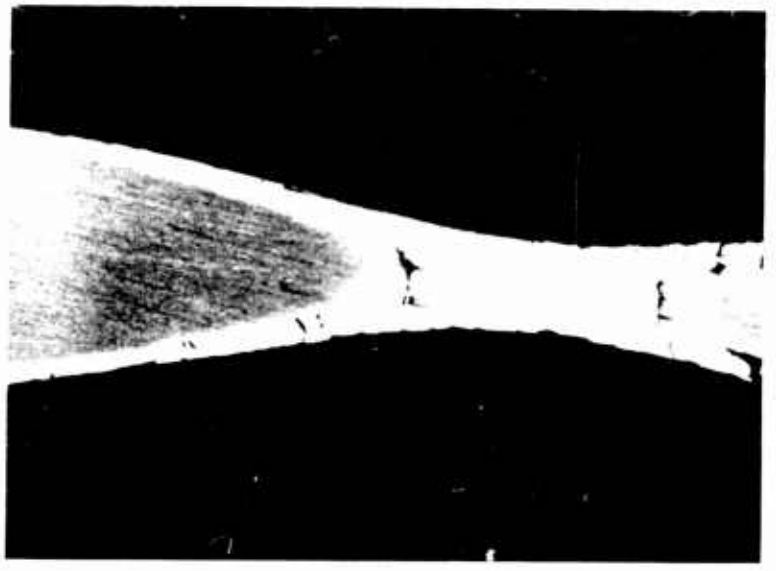

70X

Figure 5 - Cross section through platinum filament showing Pt-Be alloy coating formed at 1000°C.

It is quite possible that the limitation placed on the temperature of the filament because of the low vaporization temperature of metallic beryllium is a serious drawback to the feasibility of this method. Even though the halide might dissociate at some suitable higher temperature, recombination with iodine would occur because of vaporization from the hot surface. With this thought in mind, two experiments were made employing tungsten filaments at higher temperatures.

In one experiment a tungsten filament that ran the length of an 0.75-inch diameter by 12-inch-long quartz tube was heated to approximately 1400°C. The tube was maintained at 1000°C. Beryllium iodide, prepared in the usual manner, was sublimed through the tube under conditions of continuous pumping at a maximum pressure of 15 microns. Iodine was collected in the dry-ice trap but the major portion of the BeI_2 passed through the hot zone unaffected. There was no effect on the filament but the walls of the quartz tube were badly etched and had a brown coloration, indicating extensive interaction of BeI_2 with SiO_2.

After observing the interaction with the quartz tube, a second approach was taken using the standard Pyrex reactor. A cylindrical molybdenum shield 1.5 inches in length and 0.5 inch in diameter was mounted around a coiled tungsten filament in a vertical position. The shield (approximately 3/16 inch from the filament) was heated by radiation from the filament and was to serve as the deposition surface rather than the walls of the container. It was hoped that the elevated temperature of the shield would minimize recombination of the metal with the halogen and leave a beryllium deposit on the molybdenum.

The filament was heated to 1500°C. The shield reached a temperature of 950 - 975°C on the lower half and 775 - 800°C at the top. BeI_2 was vaporized through the chamber at 200°C (V.P. of 15 microns). Some free iodine collected in the cold trap, but the major portion of the BeI_2 collected on the relatively cool walls above the hot zone. There was no reaction with the filament or deposit on, or interaction with, the shield.

(3) Static Systems. Although the dynamic system did not provide conditions favorable for the deposition of beryllium metal, such work did yield data regarding the behavior of BeI_2 toward certain reactor materials and was very valuable in the design of further reactors. Based on the experience and data obtained in the dynamic systems, the static system appears more attractive for the following reasons:

(1) Allowance for the establishment of equilibrium conditions.

(2) Attainment of uniform temperatures.

(3) Greater ease of maintaining a temperature differential between BeI_2 and the filament, especially over a long period of time.

(4) Use of less iodine to transport beryllium from the bed of raw material to the filament; i.e., a situation closer to an ideal diffusion controlled process.

Consequently, a series of experiments were made to study the effects of static conditions as well as the compatability of various reactor materials with a BeI_2 atmosphere.

Table 5 shows the results of a series of static experiments made with various reactor materials. The experimental procedures are outlined in the following discussion of the individual experiments.

(a) Pyrex Systems. A 100 cc Pyrex bulb was fabricated with provisions for evacuation and halide preparation. It was equipped with a tungsten filament with electrical leads through the walls of the bulb. A tube connected directly to the bulb contained beryllium metal and a reservoir of iodine. The iodide was prepared in this tube in the usual manner and sublimed into the bulb, in which 3 grams of beryllium metal had previously been placed.

This tube was then removed from the bulb by fusing a constriction between the two sections. After thoroughly evacuating the bulb, the tube leading to the vacuum pump was removed in the same manner, thus isolating the unit.

In experiment S-1 the entire bulb was heated to 450°C to vaporize the BeI_2 (V.P. approximately 250 mm Hg) and the filament was heated to 900 - 950°C. These conditions were maintained for 66 hours. (The temperature probably dropped slightly after the first day but it was not possible to observe it optically.)

After 17 hours the walls were badly etched, but no iodine coloration was apparent. Toward the end of the experiment the walls became opaque with a slight yellow coloration.

No evidence of elemental iodine was found after opening the cell, and the beryllium metal appeared as if it had reacted considerably. The filament had a crystalline coating approximately 2 mils thick and was very brittle. X-ray diffraction analysis showed only metallic silicon on the wire. (The X-ray method cannot usually detect components of less than 5% concentration.) Spectrographic analysis indicated boron ($\sim$5%) and beryllium (.15%) as well.

A second experiment (S-2) was made in a similar Pyrex system except that the cell was maintained at 325°C instead of 450°C. The glass was only slightly etched at this temperature. The filament, however, had a deposit on it that was similar in composition to the first run except that is was not as thick.

(b) Quartz Systems. In order to affirm the interaction of BeI_2 and SiO_2 a quartz reaction cell was constructed. Three grams of beryllium metal were added to the cell and approximately 2-3 grams of BeI_2 were sublimed into the cell. The tungsten filament was heated to 900 - 950°C and the entire cell was maintained at 300 - 325°C. A good vacuum was maintained throughout the experiment (S-3), which lasted for 72 hours.

A slight attack on the quartz was noted but the cell remained transparent throughout the run. BeI_2 was still present as such at the end and no iodine coloration was evident.

Table 5. STATIC EXPERIMENTS

Run No.	Material of Construction for Reactor	Temp. of Tungsten Filament (°C)	Reactor Temp. (°C)	Vapor Pressure of BeI_2 (mm of Hg)	Length of Run (hrs.)	Results	Examination of Filament	
							Spectographic	X-Ray
S-1	Pyrex	800-900	450	250	66	Glass seriously etched. Thick crystalline deposit on filament.	Si 90-100% B 5% Be .15 %	Metallic Si
S-2	Pyrex	800-900	325	5	64	Glass slightly etched. Crystalline deposit on filament.	Si 90-100% S 5% Be .1%	Metallic Si
S-3	Quartz	950	325	5	72	Slight attack on quartz. Thick brittle coating on filament.	Si, Be*	Metallic Si
S-4	Inconel (Ni-20% Cr) **	950	325	5	48	Black deposit containing Si and Be and some Mg, Cu, Cr and Ni on walls of reactor. No coating on filament.	High in Fe, Cr; traces of Be, Si, Ni, and Co. (wall deposit)	Possibly $FeBe_2$ and metallic Cr. (wall deposit)
S-5	Inconel **	825	325	5	48	Black deposit on walls indicated interaction of BeI_2 with reactor. Thin deposit on filament.	Negative	Negative
S-6	Mo **	950	325	5	72	No interaction of BeI_2 with reactor. Few globules of deposit on filament.	Trace of Si	Negative

Table 5 (Continued)

Run No.	Material of Construction for Reactor	Temp. of Tungsten Filament (°C)	Reactor Temp. (°C)	Vapor Pressure of BeI_2 (mm of Hg)	Length of Run (hrs.)	Results	Examination of Filament	
							Spectrographic	X-Ray
S-7	Mo **	1000	325	5	65	No interaction of BeI_2 with reactor. No deposit on filament.	Negative	Negative
S-8	Mo **	975	283	1	28	No deposit on filament and no interaction of BeI_2 with reactor. BeI_2 recovered from reactor at end.	Negative	Negative
S-9	Ni **	975	225	.06	25	Same as S-8	Negative	Negative
S-10	Ni **	1050	225	.06	25	Same as S-8	Negative	Negative
S-11	Mo **	1100	225	.06	24	Same as S-8	Negative	Negative

* Not distinguished as metal.
** See Figure 2-7 for design of reactor.

A thick deposit was formed on the filament (see Figure 6). It was very brittle and easily broken off. Spectrographic analysis indicated a trace of beryllium and a high silicon content, but X-ray analysis revealed only metallic silicon.

It is concluded that BeI_2 reacts with SiO_2 as follows:

$$2\ BeI_2 + SiO_2 \longrightarrow 2BeO + SiI_4$$

$$SiI_4 \longrightarrow Si + 2I_2$$

$$I_2 + Be \longrightarrow BeI_2$$

(c) Inconel, Molybdenum and Nickel Systems. Reactors constructed entirely of each metal were 3 inches long and 1.25 inches in diameter. A schematic diagram of the design is shown in Figure 7. The chamber was designed to be vacuum tight under high temperature operating conditions. A heavy tungsten lead was brought through a ceramic tube that completely filled the side arm. The end of this tube was sealed with a Teflon plug that was compressed into a machined seat by means of a metal cap. This end of the reactor was maintained at a lower temperature than the rest of the reactor in order to prevent thermal decomposition of the Teflon. The needle valve made a vacuum seal at the reactor entrance. After evacuation of the reactor through the needle valve, the valve was closed and the cap containing the rubber O-rings was removed. In order to prevent the possibility of leakage during a run, the entire reactor was contained in a Pyrex tube under a constant vacuum of less than 1 micron. This tube was heated in a resistance furnace, the temperature being measured with a thermocouple in contact with the reactor wall.

The tungsten filament was precalibrated in an evacuated Pyrex tube with an optical pyrometer. It was then attached to a metal plug that was welded to a fitting in the reactor wall.

In a typical experiment the reactor was thoroughly cleaned and then dried under vacuum with heat. After a thorough flushing with argon, three grams of Pechiney flake beryllium and approximately three grams of BeI_2 were added through the side arm. The ceramic tube was then inserted over the filament and the seal was made at the Teflon gasket. The needle valve was closed after evacuating to a pressure of less than one micron.

The results with Inconel and molybdenum reactors at a reactor temperature of 325°C are shown in runs S-4 through S-7 of Table 5.

There was extensive interaction of BeI_2 with the Inconel that produced a black powdery deposit on the walls. This deposit contained Si, Be, Mg, Cu, Cr and Ni as determined by spectrographic analysis. Figure 8 illustrates the coating obtained on the filament at 950°C. It was high in Fe and Cr with traces of Si, Ni, Co and Be. X-ray analysis revealed metallic Cr and possibly $FeBe_2$. No deposit was produced on the filament at 825°C.

40X

Figure 6 - Heavy silicon deposit on filament, formed by interaction of BeI_2 and quartz.

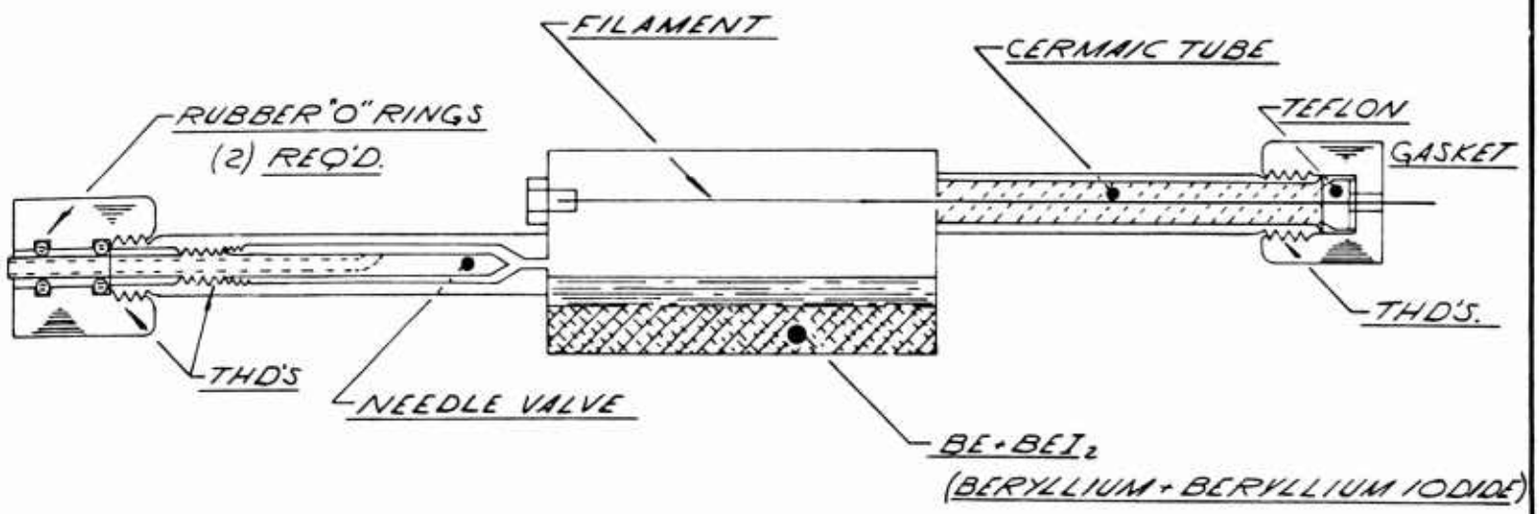

Figure 7 - Schematic drawing of static system for thermal decomposition of BeI_2.

60X

Figure 8 - Enlargement of deposit formed on filament by interaction of BeI_2 and Inconel.

Molybdenum proved to be an excellent reactor material, showing no interaction with BeI_2. The trace of Si on the filament in run S-6 may have resulted from an impurity in the halide. No trace of beryllium was detected on the filaments.

Runs S-8 through S-11 were made with lower BeI_2 temperatures to determine if the relatively high BeI_2 vapor pressures in the previous tests were having an inhibiting effect on thermal decomposition, as has been observed in other processes. Vapor pressures of 1 and 0.06 mm Hg were employed as compared to 5 mm in the previous tests.

Nickel, which had reacted with BeI_2 at 325°C, showed no adverse affect at 225°C. The lower temperature was undoubtedly unfavorable for an interaction with the reactor material.

In all of these cases BeI_2, free of iodine, was recovered from the reactor at the end of the experiments, and the filaments showed no indication of any deposit.

(d) Static Experiments with Beryllium and Elemental Iodine. In order to facilitate further thermal decomposition experiments, a new apparatus was fabricated (Figure 9). It was designed to permit studies involving beryllium metal and elemental iodine directly rather than the intermediate synthesis of BeI_2. A beryliium lining was used to minimize any interaction with the reactor.

A schematic diagram of this apparatus is shown in Figure 10. It consists of an outer salt-bath chamber and an inner reaction cell. The Inconel reactor can be readily assembled and dismantled, a vacuum seal being made on the lid by compressing a gold wire (non-reactive with iodine) between the flanges. The filament lead is introduced through a Mullite tube and connected to the tungsten filament, with the reactor acting as the second terminal. A vacuum seal is made at the filament entry port by compressing a Teflon plug into a machined seat with a threaded metal cap. This type of seal proved leak tight up to 150°C in earlier experiments. The needle valve for evacuating and isolating the cell is located in the salt bath to prevent condensation of BeI_2 or I_2. The reactor lid, designed with an 0.005-inch clearance to the flange, was tightened against an 0.035-inch-diameter gold wire by twelve bolts distributed around the circumference. Ten foot pounds of torque applied to each bolt compressed the gold to a 1/16-inch-wide seal. Only hand tightening was needed to make a vacuum tight seal at the needle valve.

Two types of beryllium liners were used. The first was a beryllium metal tube two inches in diameter and a .125-inch wall thickness. This liner was constructed with a beryllium bottom and lid that were held fast by molybdenum bolts. The filament entered the lid through Mullite insulators, the bore of which was sufficiently large to allow entry of iodine vapors and still minimize diffusion of vapors between the liner and the outer chamber.

The second type of lining consisted of a 1/4-inch layer of Pechiney metal flake along the wall and bottom of the reactor. It was held in place by a 40 mesh molybdenum screen. This type of liner provided a higher surface area of metal for reaction with iodine, but required longer periods for degassing.

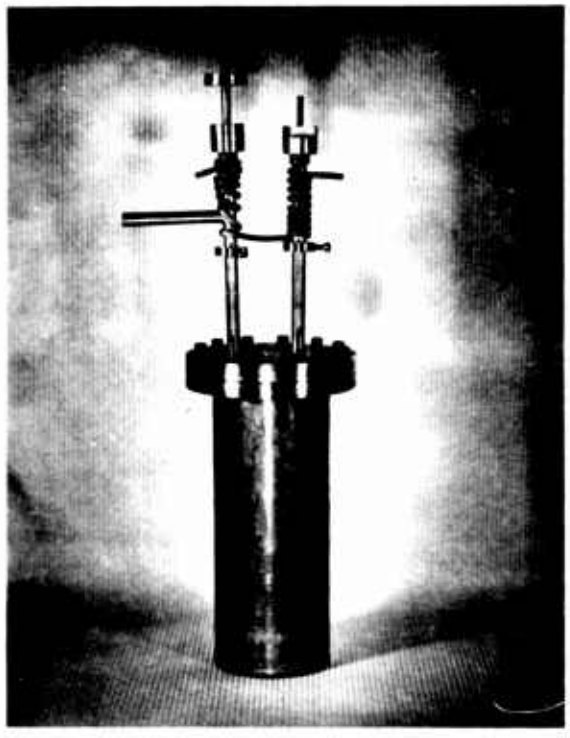

Figure 9 Assembled static reactor for use with beryllium metal and elemental iodine. One fifth actual size.

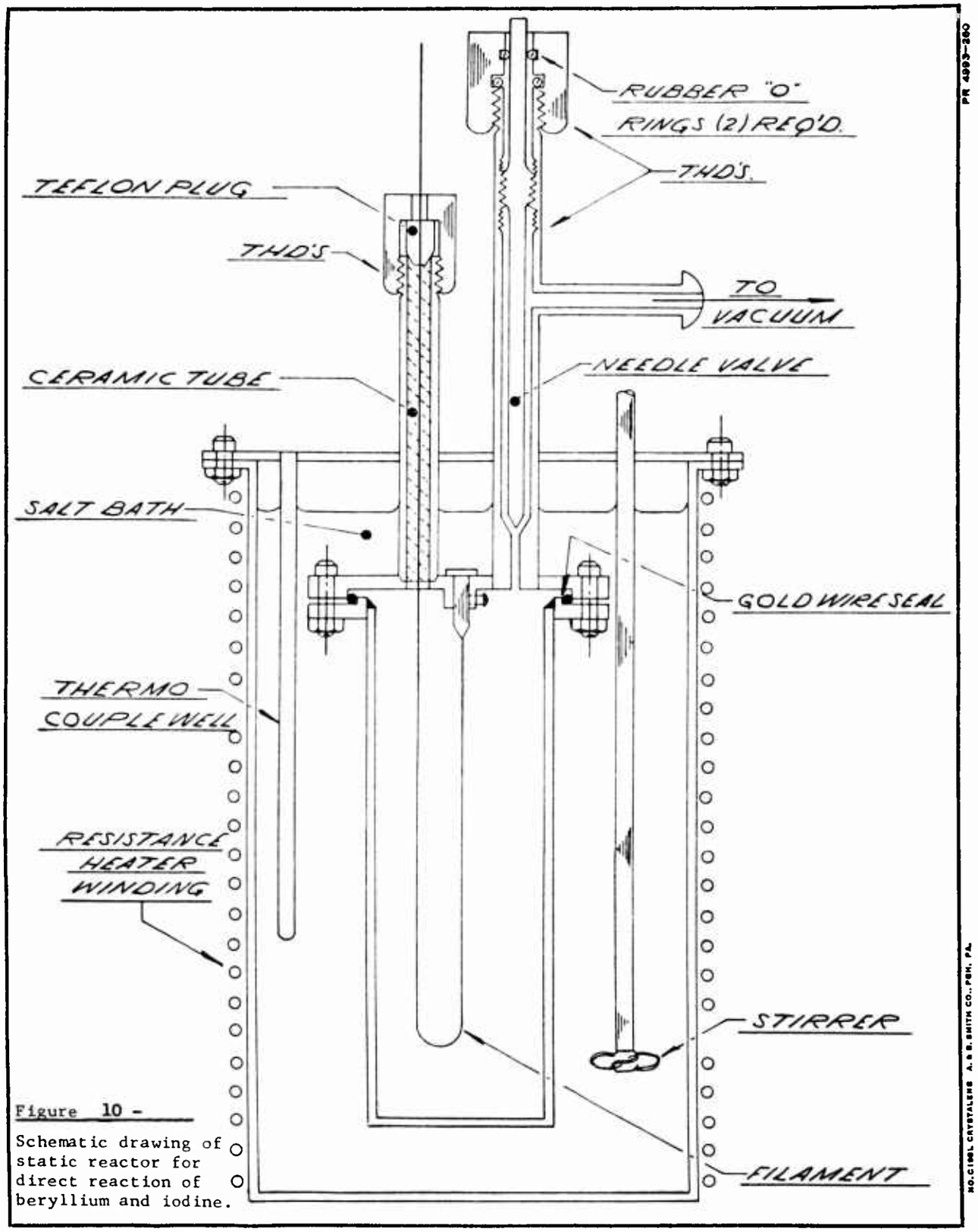

Figure 10 -

Schematic drawing of static reactor for direct reaction of beryllium and iodine.

Before each experiment the tungsten filament to be used was calibrated in an evacuated Pyrex tube to a predetermined temperature. The voltage and current necessary to maintain this temperature were recorded. The calibration was done with the Pyrex tube at the temperature to be maintained in the reactor in order to compensate for heat radiation effects that would alter the filament temperature.

Table 6 outlines the experiments performed under static conditions with elemental iodine and beryllium. The objective was to determine the effect of iodine rather than BeI_2 as the reactant. The temperature of the reactor was to be maintained in a range favorable toward the reaction of Be with I_2, the concentration of iodine and iodide being regulated by the quantity of iodine added.

The iodine was added to the reactor by vaporization from an external bulb. The amount of iodine added was determined by controlling the time of diffusion from the bulb.

In order to establish the effectiveness of this system, the well established method for the deposition of zirconium by iodide decomposition was tested. Zirconium turnings were packed along the wall of the reactor behind a molybdenum screen and, after a preliminary degassing at 400°C, the reactor was lowered to 300°C. Iodine was admitted from the reservoir at room temperature for 15 minutes. The filament was then heated to 1250°C after a ten minute induction period.

There was no apparent deposition for a period of fifteen minutes. After this time, however, there was a gradual increase of current flow through the filament. Control of the potential difference across the filament maintained it at a constant temperature. There was a continuous increase of current flow for 3.5 hours after which time the run was discontinued. A deposit of zirconium metal 0.010-inch thick was found on the tungsten filament, thus proving the effectiveness of the design.

The first three experiments listed in Table 6 (S-11 through S-13) were run using the beryllium-tube liner and 7 grams of Pechiney metal flake. In each case the reactor was degassed at 475°C overnight to a rate of approximately 10 microns/liter/hour. Upon lowering to 300°C, the degassing rate fell to about 2 microns/liter/hour. The filament was degassed at 1300 - 1400°C. The same temperature conditions were used in all three tests. The only important variations were in the iodine added and the induction period before heating the filament. There was no indication of any change of current flow through the filament or deposit on the filament in any of these attempts.

The remainder of the tests listed in Table 6 were carried out with a lining of Pechiney metal flake behind a molybdenum screen. A very high degassing rate was initially observed because of the large surface area, and 24 hours of constant pumping were required to get <10 microns/liter/hour at 400°C.

Run S-14 was similar to the previous series except that a higher temperature was used on the feed material (350°C) and a larger quantity of iodine was admitted. Negative results were obtained.

Table 6. STATIC EXPERIMENTS WITH BERYLLIUM-LINED REACTOR*

Run No.	Type of Liner	Filament Temp. (°C)	Reactor Temp. (°C)	Exposure Time of Reactor to I_2 Vapor (0.3 mm V.P.) (min.)	Induction Period Before Heating Filament (min.)	Length of Run (hrs.)	Results
S-11	Be tube (+ 7 g Be flake)	1050	300	2	10	12	No deposit on filament. No side effects observed. No interaction with reactor.
S-12	Be tube (+ 7 g Be flake)	1050	300	10	10	8	Same as for S-11.
S-13	Be tube (+ 7 g Be flake)	1050	300	5	60	8	Same as for S-11.
S-14	Be flake behind Mo screen	1050	350	15	60	18	Same as for S-11.
S-15	Same as for S-14	1250	300	10	10	11	Same as for S-11.
S-16	Same as for S-14	1130	300	15	60	9	Same as for S-11.
S-17	Same as for S-14	1100	225	30	60	9	Same as for S-11.
S-18	Same as for S-14	1500	300	10	0	8	No deposit on shield positioned near filament. No interaction with filament.

* See Figures 2-9 and 2-10 for illustration of reactor.

Repeated negative results obtained in the static experiments over a wide range of I_2 and BeI_2 pressures, indicate that the filament temperatures employed are unfavorable for thermal decomposition of the iodide. Consequently, higher filament temperatures were tried in runs S-15, -16 and -17. No positive indications of metal deposition were observed at filament temperatures of 1100, 1130 or 1250°C. (There is a temperature limitation imposed on the filament because of the volatility of beryllium metal. Figure 11 shows the vapor pressure of beryllium with respect to temperature.)

In run S-18 the filament was heated to 1500°C in an attempt to deposit beryllium on a molybdenum shield in close proximity to the filament. The shield was 3-inches long by 1-inch wide, and was positioned so it was 1/8 inch from the filament at the bottom with a gradual increase to 1 inch from the filament at the top. This run also produced completely negative results.

2-4 DISCUSSION

As stated in the introduction (Section 2-1), the purpose of this program was to attempt the production of ductile beryllium metal by achieving very high purity through the iodide decomposition method. This goal was based on the assumption that trace impurities are the reason for the brittleness of presently available beryllium metal. High purity zirconium and hafnium have been made by the iodide procedure with resulting ductility. Hafnium metal currently being produced at Nuclear Materials and Equipment Corporation by such an iodide decomposition method has a total impurity level of less than 500 parts per million. By analogy the same situation might apply to beryllium.

The requirement for high purity makes it mandatory that the process take place in a beryllium or BeO container and the metal be grown on a beryllium wire. It is emphasized in the experimental part of this report that the wire temperature that can be achieved with beryllium wire (m.p. $\sim$1280°C) is too low for the thermal decomposition of BeI_2. In addition the high vapor pressure of beryllium metal (See Figure 11) at temperatures near the melting point poses a major problem, since it is quite possible that the rate of volatilization of beryllium from the wire (and recombination with the free iodine in the atmosphere to form BeI_2) can exceed the deposition rate of beryllium metal. Some slight evidence that this occurs at the higher wire temperatures is found in the brightly polished surface of the filament after a trial run as compared to the duller initial finish. It is also possible that brightening of the wire could be brought about by a combination of Be and I_2 on the wire surface to form BeI_2; however, previous experience would lead one to expect a pitting effect to occur under such chemical attack.

The experiments with the platinum wire filament indicate that BeI_2 can be reduced to form beryllium metal and that the recombination of the beryllium metal with I_2 to form BeI_2 is prevented or inhibited by the formation of a Pt-Be alloy. These results confirm the work of Kopelman and Bender[3] but do not lead to a feasible method of producing the desired product. The experimental data obtained under this contract do not confirm the work of Hackspill and Besson[5] in that no evidence of beryllium metal production was obtained in the presence of hydrogen as the reductant.

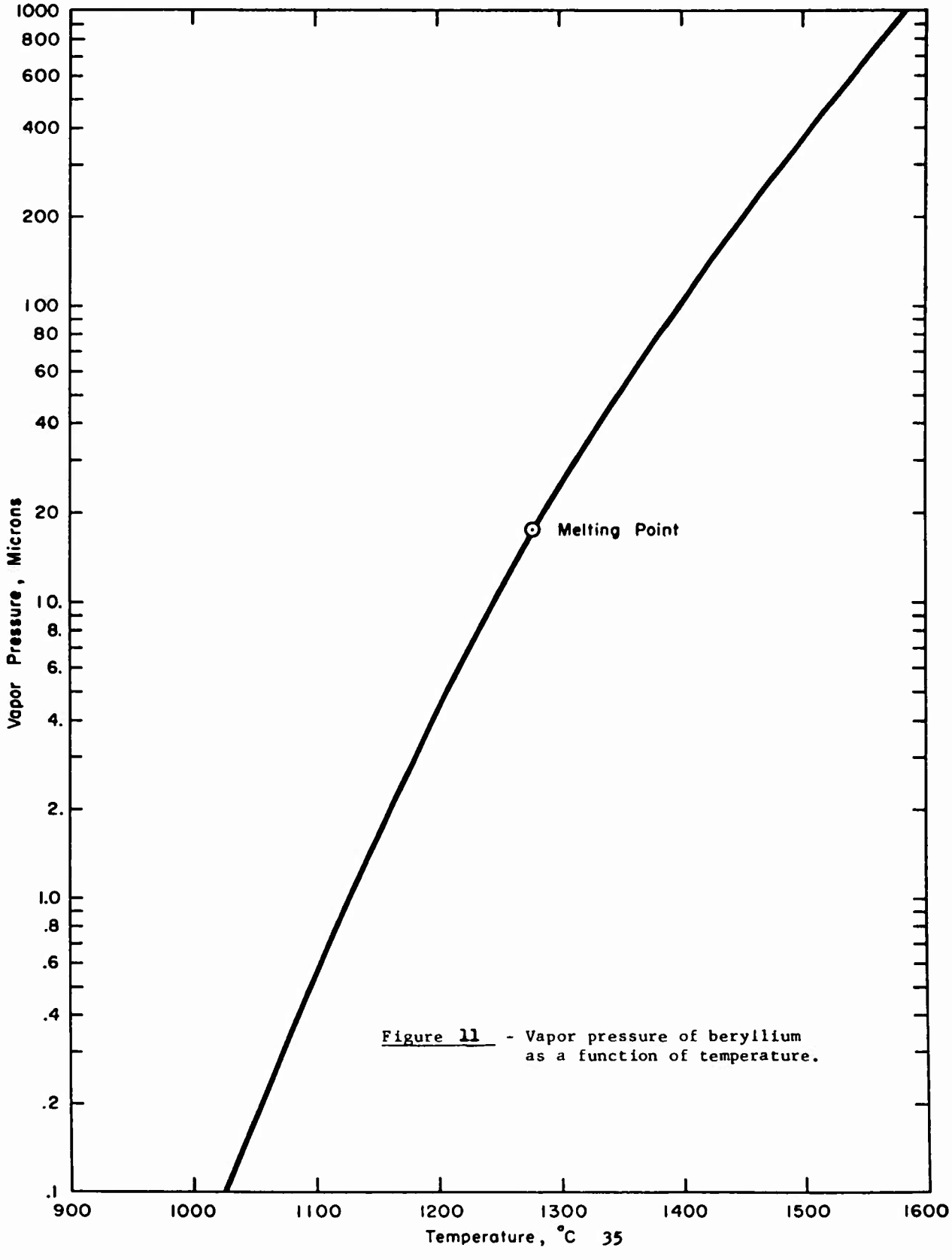

Figure 11 - Vapor pressure of beryllium as a function of temperature.

One of the major positive contributions of this effort was the establishment of suitable materials of construction for any future work involving BeI_2. Glass, quartz, stainless steel, nickel and Inconel were shown to react with BeI_2 and produce other iodides that decomposed on the heated filament. At relatively low temperatures ($\sim 200^{\circ}C$) and associated low BeI_2 vapor pressures (<1 mm) the interaction between BeI_2 and Inconel or nickel was essentially eliminated and made possible the use of the reactor shown in Figures 9 and 10. Molybdenum proved to be quite stable toward the iodide but it was difficult to fabricate into a leak tight reactor. Tungsten also proved to be inert and provided suitable filaments for higher temperature tests.

The first work performed under the contract was the preparation of stoichiometric BeI_2. The need for this stoichiometric compound was twofold. First, it was necessary to determine the compatability of BeI_2 with materials of construction. Although the corrosive properties of BeI_2 were known, it had to be shown that this was not caused by excess iodine attached to such a covalent compound (i.e., $BeI_2 \cdot I_2$). In addition, the availability of stoichiometric BeI_2 permits the mixing of excess beryllium metal with BeI_2 in a number of known ratios to enable measurement of the effect of vapor concentration on the deposition rate. The second need for stoichiometric BeI_2 was to use this material in simple flow systems to determine the thermal decomposition parameters if it proved to be possible to thermally decompose BeI_2 on a heated wire at temperatures below the melting point of beryllium.

The various experiments conducted under this contract were designed not only to ascertain whether beryllium could be deposited on a hot filament by the thermal decomposition of BeI_2 but also simultaneously to measure, if possible, some of the important controlling parameters known to be limiting in the van Arkel-De Boer process. Unfortunately, since no indication of beryllium metal production was obtained, an investigation of these parameters was not possible.

It may be of interest to indicate briefly what some of the specific experiments were designed to measure.

One of the main controlling parameters, as pointed out by Z. M. Shapiro[1], is the free iodine concentration at the filament. An excess of I_2 will inhibit the reaction by reversing the decomposition step and re-forming the volatile iodide. In the case of zirconium, the allowable concentration of free iodine is vanishingly small. Accordingly the dynamic-type experiments were designed with a liquid nitrogen cold finger close to the filament in order to freeze out the free iodine and promote the decomposition reaction. A drawback to this type of experimental design is that the BeI_2 vapor concentration is also kept at a low level. Varying the cold finger temperature over a wide range did not give the desired result.

The static experiments were designed in part to determine the controlling diffusion process and to determine whether the desired reaction would proceed in a "cyclic" process as is the case for zirconium, hafnium, etc. Tests with both BeI_2 as the starting material and with beryllium metal plus I_2 to determine whether BeI_2 or some other compound (e.g., subhalide), formed in situ, was the important reactive species (see Shapiro[1] for a detailed discussion regarding ZrI_4, ZrI_3, ZrI_2 and I_2). The experiments using BeI_2 as the initial compound gave negative results at vapor pressures of BeI_2 from 0.06 to 5 mm. The runs were made

over long periods of time in case a long induction period was operative or in case the deposition rate was very slow.

In none of these experiments was there any visual indication of free iodine at the end of the experiment. This indicated that no decomposition of BeI_2 had occurred. In addition there was no indication of deposition of beryllium metal on the filament.

The main purpose of the experiments in the beryllium-lined equipment (runs S 11 through S-18), besides the prevention of impurity pickup from the reactor, was to determine the effect of low iodine concentrations and varying reactor temperatures. At low added I_2 amounts ($\sim$ 0.1 g), the excess iodine vapor would react with the excess beryllium metal (present as chips or reactor liner) to form BeI_2 and insure that the free iodine concentration was negligible. The BeI_2 vapor pressure, under these conditions, would be controlled by the reactor temperature and might have been as high as 2 mm at 300°C or 13 mm at 350°C. But even under these theoretically optimum conditions no beryllium metal was deposited on the filament.

Based on the foregoing interpretations and experimental evidence, it must be concluded that either filament temperatures compatible with a beryllium metal filament are not high enough to decompose BeI_2 in an irreversible manner or the vapor pressure of the deposited beryllium metal is excessive; i.e., the rate of evaporation of beryllium metal from the filament exceeds its rate of deposition.

2-5 FUTURE WORK

By agreement with Nuclear Metals, Inc. the work at Nuclear Materials and Equipment Corporation was confined to the investigation of the iodide decomposition process. There are many other avenues to explore for the production of high purity beryllium by the van Arkel - de Boer process, which has proved so fruitful in producing other high purity, ductile metals.

(1) Utilization of a bromide system ($BeBr_2$) instead of the iodide system.

The equivalent bromide system should prove to be less corrosive than the iodide system thus simplifying the equipment problem. The vapor pressure of the bromide is higher than that of the iodide, indicating that thermal decomposition may take place at a lower filament temperature.

(2) Arc decomposition of the halide.

It has been suggested by Kellog[4] that the decomposition of the halide could take place in an arc without introducing unwanted contaminants. This is a very intriguing possibility and should be experimentally investigated. By this means the higher temperature required for the dissociation of BeI_2 can be easily attained and the beryllium metal vapor produced can be collected on a cooled surface.

(3) Preparation of beryllium metal by the thermal decomposition of metal-organic compounds.

The use of metalorganics to prepare pure metals is a very attractive possibility. At Nuclear Materials and Equipment Corporation, high purity chromium has been prepared from the dicumene compound and pure aluminum has been prepared by the decomposition of aluminum alkyls at temperatures below 100°C. It is suggested that pure beryllium can be deposited by similar techniques. In particular it is suggested that beryllium diphenyls may be quite advantageous, since there is no oxygen or nitrogen present in the organic grouping. Further, the polyphenyls are very stable at elevated temperatures and would not contaminate the beryllium product.

REFERENCES

1. Z. M. Shapiro, in Chp. 5 of The Metallurgy of Zirconium (B. Lustman and F. Kerze, Jr., Eds.), McGraw-Hill Book Co., New York (1955).

2. H. A. Sloman, Researches on Beryllium, J. Inst. Metals, p. 365, (1932).

3. B. Kopelman and H. Bender, The Dissociation of Beryllium Iodide in Platinum Containers, J. Electrochem. Soc., p. 89 (1951).

4. H. H. Kellog, in Chp. IV A of The Metal Beryllium (D. W. White, Jr. and J. E. Burke, Eds.), Amer. Soc. Metals (1955).

5. L. Hackspill and J. Besson, Bull. Soc. Chim. France, 113 (1949).

6. W. B. Pearson, Handbook of Lattice Spacings and Structure of Metals, Pergamon Press (1958).

SECTION 3

INVESTIGATION OF THE ULTRASONIC WELDABILITY OF BERYLLIUM METAL SHEET

J. Byron Jones, Nicholas Maropis, John G. Thomas
H. L. McKaig and J. Devine

(Aeroprojects Incorporated, West Chester, Pennsylvania)

ABSTRACT

Investigations to determine the ultrasonic weldability of beryllium sheet material indicated the maximum weldable gage with available equipment (4 kw) to be approximately 0.020 inch. A number of variables in the process were investigated to determine the conditions most favorable for the production of high-quality welds. Difficulties were encountered because much of the sheet material received for the investigation exhibited deep surface scratches and grooves which could not be completely removed even with electropolishing or chemical etching.

Welding machine settings were established for sheet materials in the range of 0.010 to 0.020 inch. At a weld interval of 0.5 second and a clamping force of 500 pounds, 2400 watts input power was required to weld 0.012 inch beryllium with a 3-inch radius sonotrode tip. Welds of better quality were obtained with tips of larger radii (6 or 9 inches), but the power requirements were greater. Sonotrode tips of Astroloy were superior to those of other materials investigated.

No correlation was established between the direction of the applied vibratory energy and the preferred orientation of the beryllium sheet. The possibility of increasing the ductility and thus the weldability, of beryllium sheet by power programming was investigated briefly, but the temperature readily obtained in the weld zone was less than the approximately 400^{o}C required for substantially increased ductility. Improving the weldability of beryllium by power-programming requires further study.

Of several foil inserts evaluated, only soft aluminum foil interleaf completely eliminated weld cracking. Foil inserts of harder materials, zirconium and molybdenum, require further study. Beryllium interleaf appeared promising, but was not completely evaluated.

The most satisfactory beryllium welds were obtained with sheet material that was generally smooth, flat, and free from surface defects. Annealed sheet appeared to be more readily weldable than the as-received material, but the extent of the improvement was not established.

Visual and X-ray inspection of beryllium panels assembled from 0.010-inch sheet with ultrasonic spot welds on 3/4 inch centers indicated the feasibility of producing high-quality beryllium bonds free from internal discontinuities.

3-1 INTRODUCTION

The requirement for a satisfactory method to join beryllium to itself and to other metals is emphasized by the increased interest in the use of beryllium sheet for aircraft and space structures and in nuclear applications. The present use of beryllium for such purposes is limited by the difficulty of producing bonds of high quality in this material with available joining techniques.

The major technical problems with beryllium are associated with its room-temperature ductility and anisotropic properties, particularly in sheet form[1-4]. It has been noted that the tensile ductility of beryllium increases above room temperature, and that there are two ductility peaks; one occurring at about 300-400°C and a slightly lower one occurring at 700 - 800°C[5]. Above this temperature, ductility again decreases. Current joining techniques, which include fusion welding, brazing, diffusion welding, and resistance welding[6-12], have not been entirely satisfactory, particularly for production use, because of requirements for meticulous surface preparation, cracking, weld porosity, etc. Only when very careful control is exercised over the variables in these processes can satisfactory welds be obtained.

To take advantage of the unusual properties of beryllium, such as its light weight and high modulus, a joining method that produces reliable, high-strength, ductile, crack-free bonds is necessary. Ultrasonic welding is a potentially satisfactory method for producing these high-quality bonds, since under ideal conditions it produces a fine grained beryllium joint. Brief studies conducted prior to the work reported herein demonstrated the feasibility of joining beryllium to itself and to other materials by ultrasonic techniques and suggested that further experimentation and development would lead to a satisfactory and practical method for joining this material.

3-1.1 Characteristics of Ultrasonic Welding. Ultrasonic welding is a non-fusion, solid-state process for joining metals without the aid of solder, fluxes, or filler metal[13]. It has proved a satisfactory means for joining a wide variety of metals and alloys in combinations and geometries that are often difficult or impossible to join by other techniques. This process is used routinely in production operations in such diverse fields as the fabrication of nuclear fuel elements and the manufacture of transistors.

Essentially, ultrasonic welding involves clamping the pieces to be joined at moderate static force between an active sonotrode and an anvil, that serves as a reaction element to the clamping force and the applied vibration. The active sonotrode tip is usually spherical, while the anvil face is usually flat.

Electrical energy of proper frequency is delivered from an ultrasonic generator to a transducer which converts the electrical energy to mechanical energy in the form of vibration at the resonant frequency of the transducer coupling system. The mechanical vibration is then transmitted by the coupling system and sonotrode tip into the weldment material, where a weld is produced by dissipation of the shear-type vibratory energy at the weld interface. A sound metallurgical bond is formed without the cast structure that is characteristic of resistance welds and without the excessive deformation that usually accompanies pressure welding. No fluxes are used, and only rarely are filler materials used. No electric current passes through the weld metal, and usually no external heat is applied.

The unique characteristics of ultrasonic welds make the process useful for a variety of applications, not necessarily as a substitute for the more conventional processes, but as a supplementary process in applications for which other methods are impractical, unreliable, or uneconomical. It is adaptable to a wide variety of joint designs. In many cases, variations can be made in sonotrode tips and anvil faces to accommodate specific geometries, or special tooling or positioning devices can be utilized. Since no current passes through the joint, there is no problem in fixturing with respect to providing either conducting or insulating members.

The finest wires and the thinnest foils can be welded to pieces of almost any size or shape; the bonds are clean and show minimum penetration of the wire or foil material into the other component. Welds can even be produced through certain types of surface coatings with no damage to the foil and without introducing impurities to shorten the life of the joint. Furthermore, various metals can be bonded to metallized glass surfaces by ultrasonic welding techniques. These applications are illustrative of the many advantages inherent in the use of ultrasonic techniques to join similar and dissimilar materials.

Investigation of the fundamentals of ultrasonic welding[14,15] suggests that the effect of the ultrasonic welding process on the properties of beryllium may facilitate the production of sound, crack-free junctions. Although localized temperature rise does occur during ultrasonic welding, the temperature does not approach the melting point of the metal. Furthermore, by appropriate adjustment of the welding machine settings, some control can be exercised over the maximum temperature obtained. More effective control may be obtained, however, by the application of auxiliary heat immediately prior to or during the ultrasonic welding process. If the temperature can be controlled within the ranges of the ductility peaks of beryllium, it should be possible to produce crack-free junctions.

With beryllium and other hard metals of low ductility, experience has shown that high power and short weld intervals are required to produce high quality welds. Moreover, a good impedance match between the vibratory energy source and the weldment is necessary to achieve efficient power delivery.

A number of materials exhibiting characteristics similar to those of beryllium have been experimentally joined viz.:

(1) High-modulus materials such as molybdenum with a modulus of 55×10^6 psi (the elastic modulus of beryllium is about 44×10^6 psi).

(2) Sintered powdered materials, such as pure molybdenum and M-257 aluminum.

(3) High-strength, high-temperature materials, such as Inconel X, Zircaloy-2, 17-7 PH, 15-7 PH (precipitation-hardened) stainless steels, and tungsten.

Prior to this program, brief experimentation had been carried out in the ultrasonic welding of beryllium to itself and to other metals. This early work was exploratory in nature; only metallographic studies were made. Figure 12 shows a photomicrograph of an ultrasonic weld in 0.020-inch-thick QMV cross-rolled beryllium sheet. With lighter gage material, apparently satisfactory welds have also

Figure 12 - Ultrasonic solid-state weld between two sheets of 0.020-inch-thick QMV cross-rolled beryllium (polarized light; 250X).

been produced between beryllium and certain other materials, such as aluminum, copper, iron, and titanium (Figure 13). Photomicrographs of several dissimilar-metal welds, shown in Figure 14, illustrate the potential soundness of these bonds.

3-1.2 Objectives of the Program. Review of background information indicated that effort expended in the specific areas listed below should lead to an early estimate of the potential quality and the properties of ultrasonic welds between two sheets of beryllium:

(1) By means of available ultrasonic welding machines endeavor to produce spot-type welds between sheets of thickness in the range of 0.020 to 0.060 inch and to ascertain the approximate welding machine settings for power, clamping force, and weld interval that are required.

(2) Investigate impedance matching problems between the hard, low-ductility beryllium and the sonotrodes, considering the criticality of clamping force in this connection.

(3) Consider welding machine tip radii and tip materials of several moduli with the view to eliminating weldment cracking, reducing tip sticking, and extending tip life.

(4) Correlate weld properties with the direction of vibratory excursion of the welding tip in relationship to the anisotropic mechanical properties of rolled beryllium sheet.

(5) Consider the feasibility of transiently improving the ductility of beryllium sheet during vibratory welding by the use of elevated temperatures in the range of 400°C.

(6) Evaluate inserts of similar and dissimilar metal foils as a means of shortening weld intervals and/or reducing power requirements.

(7) Utilize inert atmosphere during welding and endeavor to determine its effect on weld contamination.

3-2 EXPERIMENTAL EQUIPMENT, MATERIALS, AND TECHNIQUES

3-2.1 Equipment. Available ultrasonic spot-type welding equipment capa. of handling 4000 watts (see Figure 15) was used in this program. In this machi... magnetostrictive nickel stacks convert high frequency alternating electrical power into vibratory power and a wedge-reed coupling system delivers it to the weld locale. Static force is applied normal to the plane of the weld interface, by means of a hydraulic system, while the weld interval, automatically controlled by electronic timers, is actuated by a foot switch. The interrelationship of the components in the 4000-watt ultrasonic spot-type welding machine of Figure 15 is shown in Figure 16.

3-2.2 Materials.

(1) Beryllium. Beryllium sheet from three sources was used in this work:

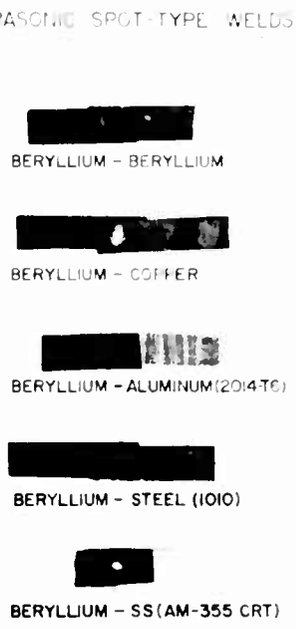

Figure 13 - Ultrasonic spot-type welds between beryllium and dissimilar metals.

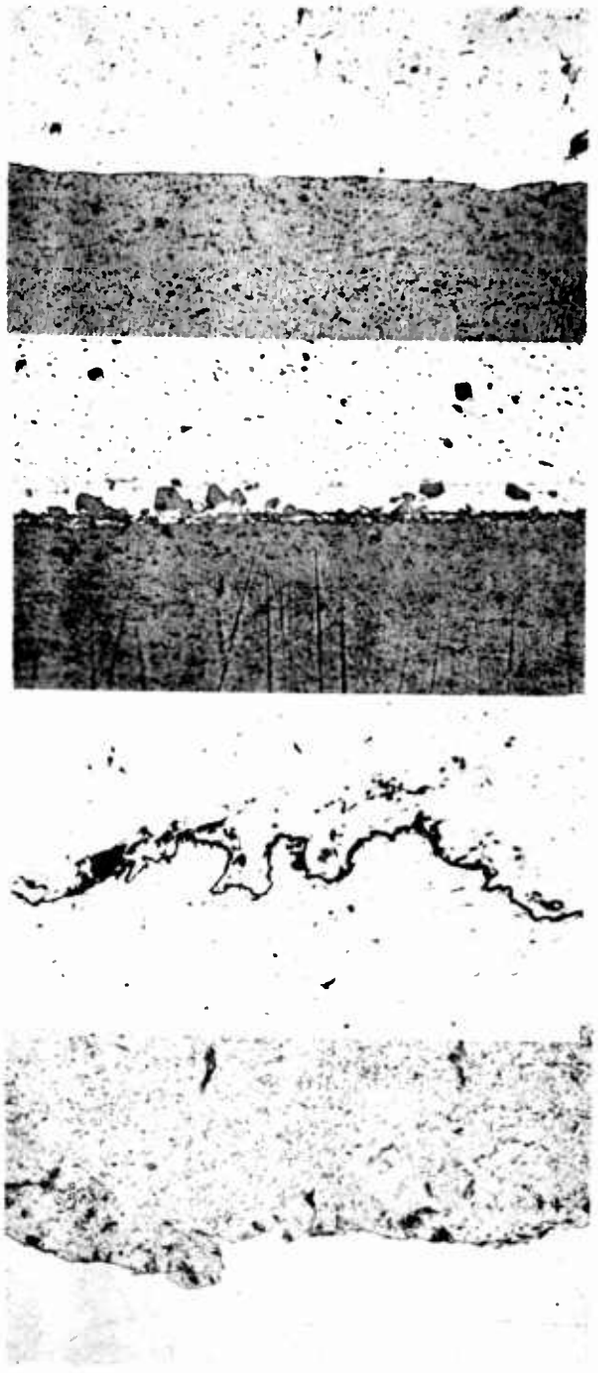

(a). 0.009-inch aluminum to 0.050-inch beryllium (400X; 0.5% HF).

(b). 0.009-inch aluminum to aluminum-tinned 0.050-inch beryllium (400X; 0.5% HF).

(c). 0.032-inch iron to 0.010-inch beryllium (250X; 1% Nital)

(d). 0.003-inch titanium foil to 0.050-inch beryllium (400X; 9 HNO_3 + 3 HF + 88 H_2O).

Figure 14 - Photomicrographs of ultrasonic welds between beryllium and dissimilar metals.

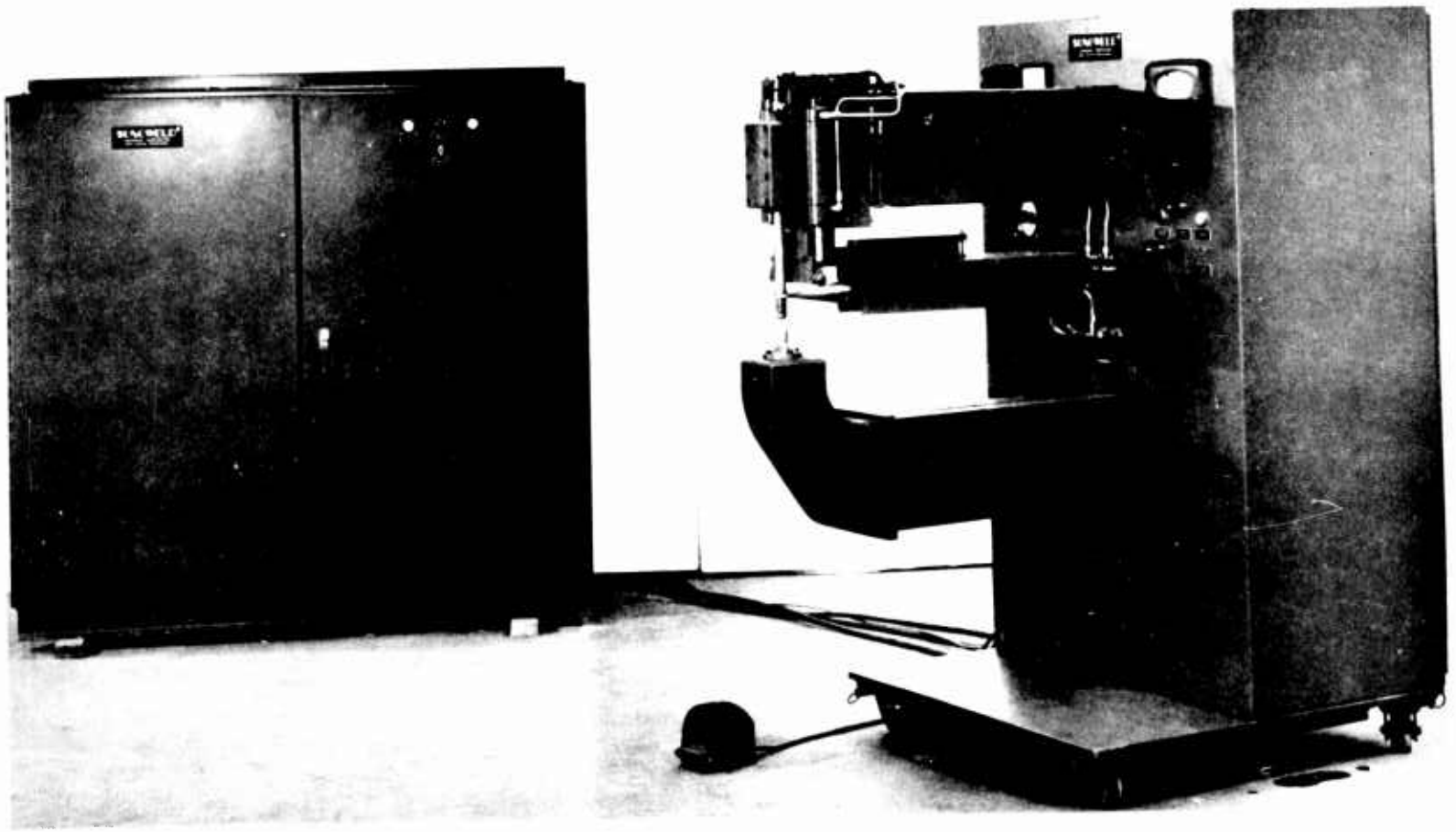

Figure 15 - Typical 4000-watt ultrasonic spot-type welding machine.

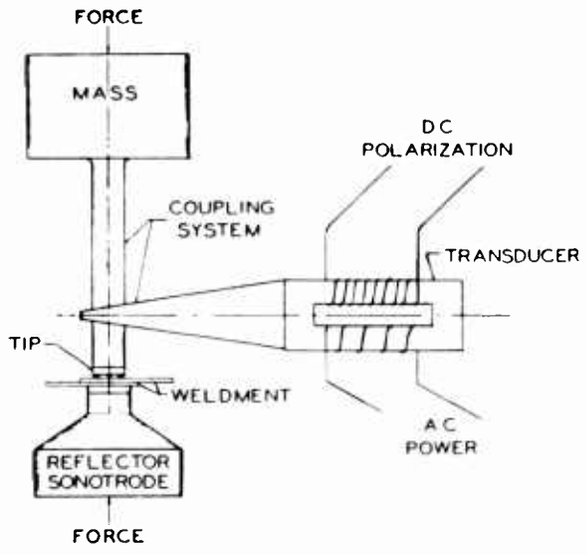

Figure 16 Schematic diagram of a wedge-reed transducer-coupling system.

(1) AOH: 0.010-inch material on hand at Aeroprojects,

(2) AMC*: 0.020- and 0.060-inch and, later in the program, coupons cut from 0.020-inch annealed beryllium from the same source,

(3) BBC: 0.003-, 0.005-, and 0.010-inch material supplied by Brush Beryllium Corporation.

The original AMC sheet had been lacquered, scribed, chemically etched along the scribed portion, and broken into individual 1- by 4-inch test coupons. In several cases, the edges were irregular and cracked, and the surface of the sheet contained deep scratches and grooves as well as an unidentified contaminant.

In an effort to obtain specimens of reproducible surface finish, some of the material was electropolished in a solution, consisting of 10 parts H_3PO_4, 3 parts glycerine, 3 parts H_2SO_4, and 3 parts methanol at a current density of approximately 3 amperes per square inch. Uniform surface finish was not obtained even after electropolishing for 12 minutes. Although the surface roughness was reduced from 100-120 microinches to 40-50 microinches**, the specimens still retained severe surface defects, and a waviness of the surface was apparent. The time and effort required for this process indicated the need for an alternate method. Subsequent specimens were given a 3-minute immersion in the electropolishing solution at 175°F. A bright etched surface was obtained, and the thickness of the sheet was simultaneously reduced. Both techniques were used for the AMC specimens welded in these investigations.

(2) Tips. The high level of dynamic stress associated with the delivery of ultrasonic energy into hard metals and alloys during welding imposes severe requirements on the sonotrode tips. Ordinary tool steels are satisfactory for welding aluminum or copper alloys, but for hard, brittle materials, the life of tool-steel tips may be short. Inconel X-750*** is preferred for welding mild steels, titanium, and zirconium, but for certain materials this material may not be suitable. Astroloy, a relatively new nickel alloy (General Electric Company) with good high-temperature properties, was also considered.

3-2.3 Welding Machine Settings. As a result of recent fundamental research[14,15] into the principles underlying the ultrasonic welding process, a better understanding of the factors governing welding machine settings was obtained. Values for clamping force, power, and time (weld interval) were delineated for beryllium on the basis of these earlier investigations.

(1) Clamping Force. Techniques had previously been established[15] for determining the clamping force required to produce an ultrasonic bond in a given material thickness under minimum energy conditions (MEC). With the clamping force

- - - - - - - - - - - - -

* Prepared by Brush Beryllium Company for the Air Force AMC Sheet-Rolling Program

** Measured with a Brush Surfindicator

*** Previously designated as Inconel X

established, the optimum impedance match between the sonotrode tip and the weldment is obtained; hence, the delivery of energy into the weld area is maximized. Several methods for establishing clamping-force levels are discussed below.

(a) Nugget Pull-Out Method. With sonotrode tips of specific radius, clamping force values for reasonably malleable materials are established by selecting a single clamping force and a fixed weld interval (based on previous experience). Welds are then produced at gradually decreasing power until the bond no longer fails by nugget pull-out in a peel test. This procedure is repeated at different clamping forces until sufficient data are obtained to establish a power-clamping force curve. The minimum of this concave-upward curve corresponds to the optimum clamping-force value and indicates the threshold power necessary for welding (Figure 17).

(b) Thermal-Response Method. For relatively brittle materials, such as beryllium, the nugget pull-out test is not feasible. However, it has also been shown[15] that, for any fixed and reasonable value of vibratory power (even though the power level may be too low to produce an actual weld), the temperature achieved in the intended weld locale is maximum at the clamping force associated with the minimum value of the power-clamping force threshold curve described above. Thus, for brittle materials, a convex-upwards curve of temperature as a function of clamping force is obtained. Power levels productive of satisfactory welding are then determined at this value of clamping force by making and evaluating welds at various power levels.

(c) Standing-Wave Ratio (SWR) Method. Since the power delivered by any ultrasonic system can be measured by the elastic standing-wave ratio in the coupler[15], this technique is used to establish clamping-force values at a fixed level of input power. Dynamic microphone-type strain gages are used to detect the standing-wave pattern along uniform sections of the acoustic transmitting system and to measure the associated standing-wave ratio (the ratio of maximum to minimum particle displacement along the acoustic coupler). These signals give an elliptical oscillogram pattern in which the power passing through the instrumented section during any instant and the energy delivered to the weld locale are proportional to the area of the ellipse. This technique was used near the end of this program to spot-check the clamping-force values obtained by the thermal-response method.

(2) Weld Energy. During recent fundamental research into the phenomena of ultrasonic welding[15], an equation was developed which permits the calculation of the approximate energy required to generate an ultrasonic weld between two sheets of the same metal in terms of the hardness and thickness of one of the sheets:

$$E = 300\, t^{3/2}\, H^{3/2} \qquad \text{(Equation 3-1)}$$

where

E = electrical energy input, watt-seconds.

t = material thickness, inches.

H = Vickers microindentation hardness number.

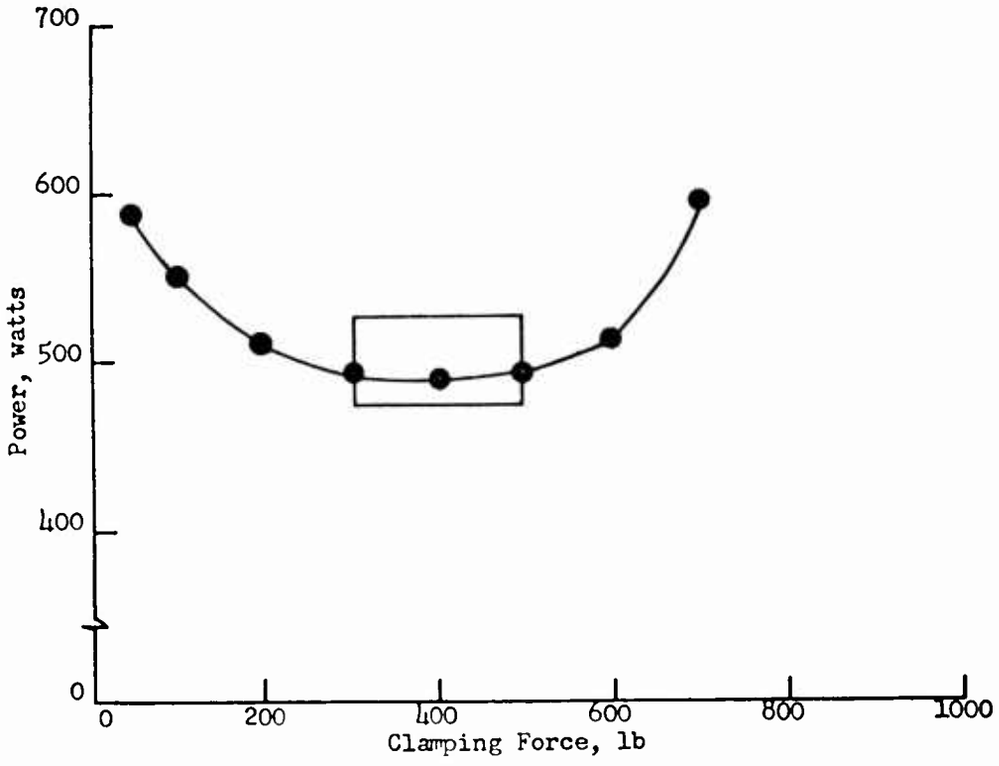

Figure 17 - Threshold curve for welding 0.020-inch 1100-H18 aluminum.

By substituting in the equation the measured hardness value of the material and the contemplated thicknesses, it was possible to approximate electrical energy requirements for welding various gages of beryllium.

3-2.4 Impedance Matching. Because of losses in electromechanical conversion, transmission and reflection at impedance discontinuities, only a portion of the electrical power delivered to the transducers reaches the weld zone as acoustic power. Consequently, in determining energy delivery into the weld zone, the impedance presented by the weldment to the terminal tip is the fundamental factor to be considered. The weld-zone impedance depends on the clamping force, tip radius, the hardness and thickness of the weldment material and, possibly, to some undetermined extent, upon the power level[14] at which the welding is done.

The impedance presented by the weldment to the sonotrode tip may be determined by the standing-wave ratio technique in which sensing elements are mounted on the acoustic transmitting coupler. This information is then used to modify the tip configuration or terminal coupler to get a higher or lower transverse vibratory force at the weldment and thus improve the impedance match between the tip and the weldment.

While the transmission of energy from the welding tip to the weldment is maximum when the impedance ratio between them is unity, in general, the ratio of weldment to tip impedance is found to vary between 0.2 and 0.5. Several instances have been noted, however, in which this ratio does approach unity. As shown in Figure **18,** the ratio reaches a value as high as 0.9 when 0.040-inch 2024-T3 aluminum is welded.

3-2.5 Effect of Tip Radius. The radius of the sonotrode tip greatly affects the area of its contact with the sheet, and, hence, the delivery of vibratory energy into the weldment. It also affects the weld impedance and, thus, the ability of the acoustic system to deliver the necessary energy efficiently. In addition, the stresses resulting from the normal clamping force are controlled by the tip radius.

As the sonotrode tip radius is increased, the contact area between the tip and the weldment and, thus, the weld areas are increased. It was anticipated that a 3-inch, spherical tip would excessively concentrate the vibratory power, as well as produce excessive stresses due to the clamping force, and, thus, contribute to early cracking of the beryllium specimens. To confirm this, tips with 1.5-, 3-, 6- and 9-inch radii were investigated.

For the best impedance match between weldment and tips, a higher clamping force is required for a larger tip radius. Moreover, a larger tip radius extends the weld area so that still greater power is required. As might be predicted from the Hertz theory[16], however, the clamping-force does not increase sufficiently to produce the same unit stress. Actually, with tips of larger radius the stress gradients adjacent to the weld zone are reduced, and the incidence of cracking is decreased.

3-2.6 Evaluation Techniques. Since the relatively low ductility of beryllium precludes the fabrication of the usual type of tensile-shear specimens, welded beryllium coupons were joined, as shown in Figure **19,** to aluminum support strips

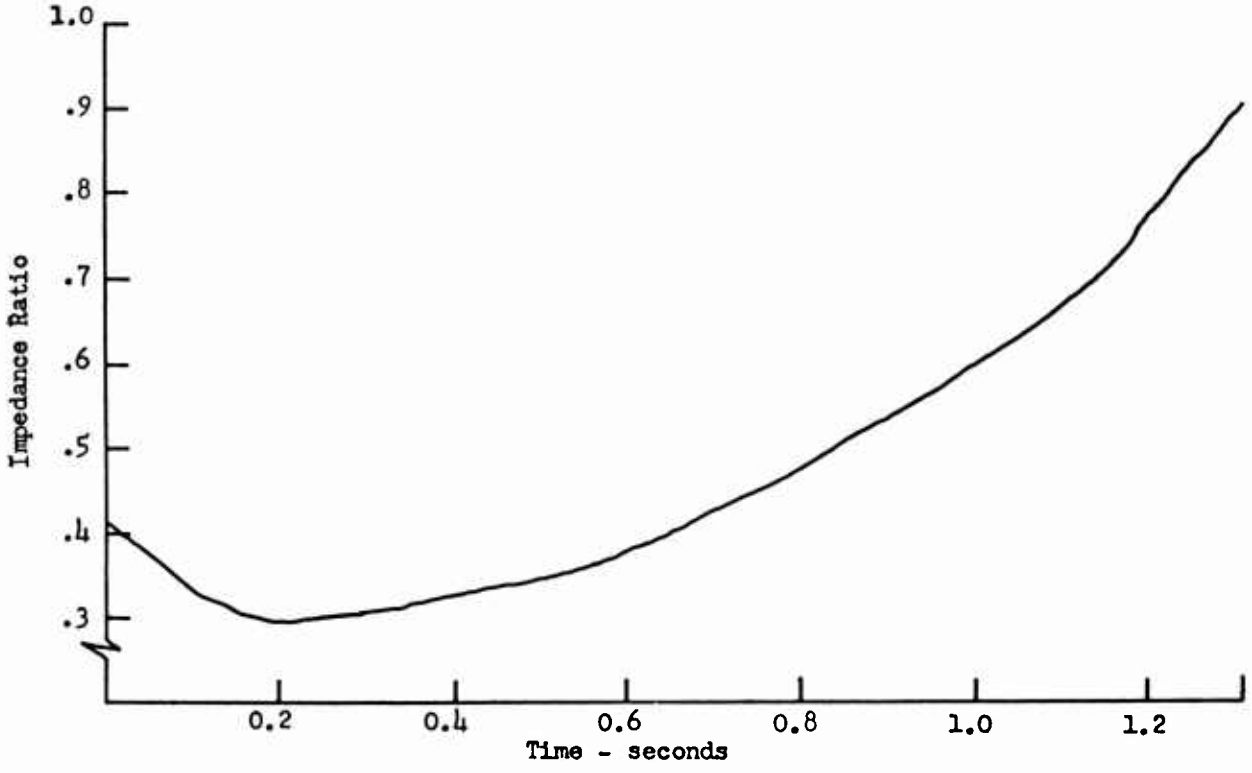

Figure 18 - Impedance ratio for 0.040-inch bare 2024-T3 aluminum alloy. (power, 2000 watts; clamping force, 900 lb; welding interval, 1.5 sec).

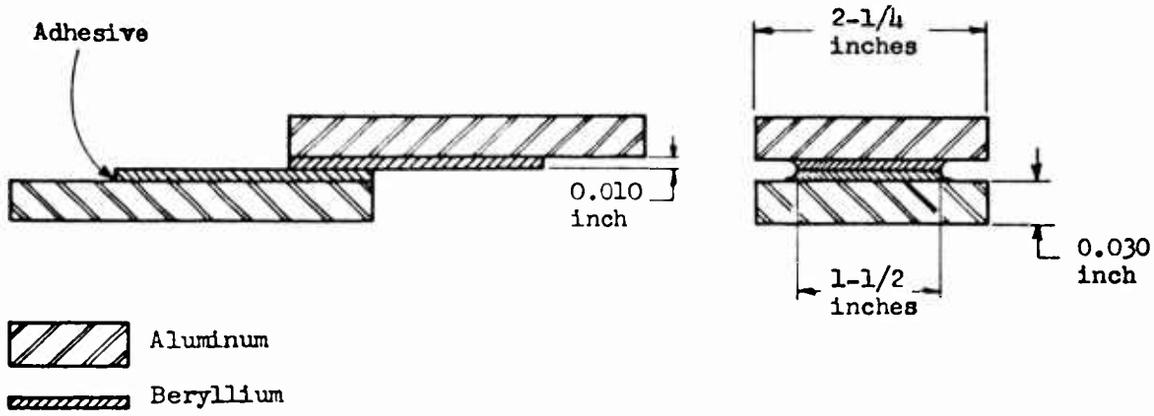

Figure 19 - Tensile-shear testing setup.

by means of quick-setting epoxy-type adhesive. The cross-sectional area of the aluminum strip was about four times that of the beryllium to compensate for the disparity in the modulus and the support plates were wider than the beryllium coupon to permit testing of the weld without interference from cracks due to flaws in the sheet edge. In these experiments, each beryllium weld was inspected with the aid of a stereoscopic microscope before the aluminum support plates were cemented in place for the tensile-shear test. Similar inspection was also carried out on fracture surfaces after tensile testing.

For metallographic evaluation, specimens were sectioned outside the weld zone with an abrasive cut-off wheel and mounted in Formvar, and then ground to expose the weld. This procedure was adopted to reduce the likelihood of cracking during sectioning. The specimens were polished with laps moistened in 5% oxalic acid[17], and examined under polarized light. Weld quality was then evaluated on the basis of:

(1) Microscopic inspection of the surfaces in and around the weld zone prior to the tensile test.

(2) Microscopic inspection of the surfaces sheared in testing to determine the continuity of the weld.

(3) Metallographic studies of weld integrity with particular attention to weld structure, bond area, bond-envelope area, and the incidence of cracks and inclusions.

3-3 SUMMARY OF EXPERIMENTAL WORK

Prior to the receipt of the AMC material, tentative requirements for welding beryllium were determined from tests with 0.010-inch beryllium (AOH). On the basis of this initial work and later information obtained from welding 0.020-inch AMC material, before and after chemical etching (which reduced the sheet thickness to 0.015-inch), welding machine settings and conditions for 0.020-, 0.040-, and 0.060-inch beryllium sheet were established. However, as noted below, welding 0.040- and 0.060-inch material was beyond the capcity of the existing equipment. Consequently, studies involving these heavier gages were abandoned.

3-3.1 Welding-Machine Settings. The optimum clamping force was established by the thermal response method in which the temperature in the weld zone was measured by means of a 0.003-inch Constantan wire-to-beryllium thermocouple junction in which the end of the fine Constantan wire was located between the beryllium sheets in the weld area. Typical strip-chart recordings produced by such a single wire thermocouple are shown in Figure 20. Data obtained with 0.012-inch beryllium (Figure 21) indicate that the maximum temperature (270°C was obtained with a clamping force of about 500 lb. Under these conditions, however, the power was too low to produce a bond. A clamping force of approximately 850 lb (see Figure 22) was required to weld 0.018-inch material when a 6-inch radius spherical sonotrode tip was used.

The weld energy requirements were estimated from the energy Equation 3-1 ($E = 300\ t^{3/2}\ H^{3/2}$). Vickers microindentation hardness (500-gram load) number for beryllium (approximately 248) was substituted in this equation and weld energy was calculated as a function of material gage. A curve showing this relationship is presented in Figure 23.

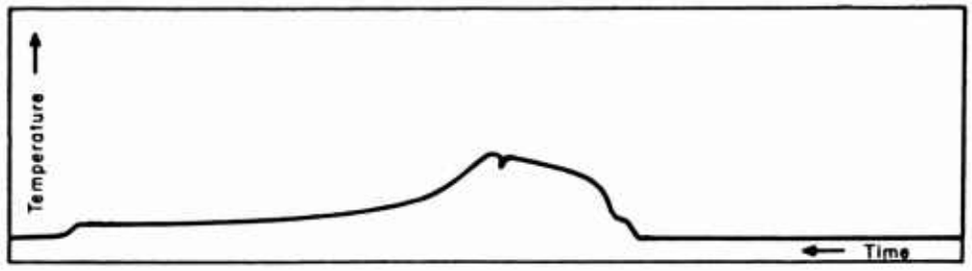

Test No. 7: 400-lb Clamping Force

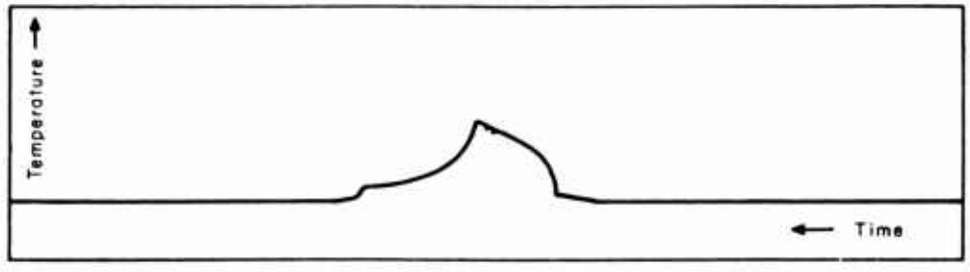

Test No. 12: 600-lb Clamping Force

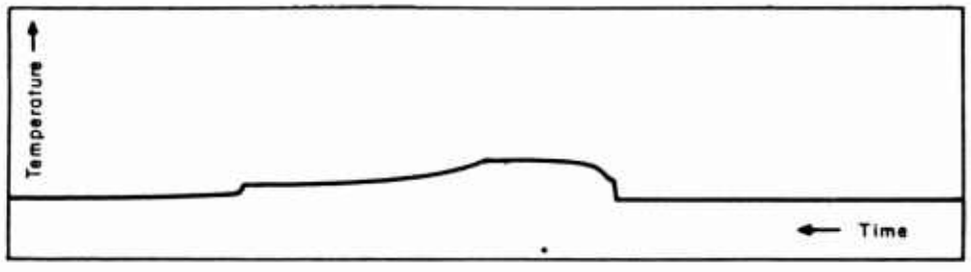

Test No. 9: 700-lb Clamping Force

Figure 20 - Typical temperature traces. (Input power, 1200 watts; weld interval, 0.4 sec; tip radius, 3 inches.) Drawing No. RA-1859

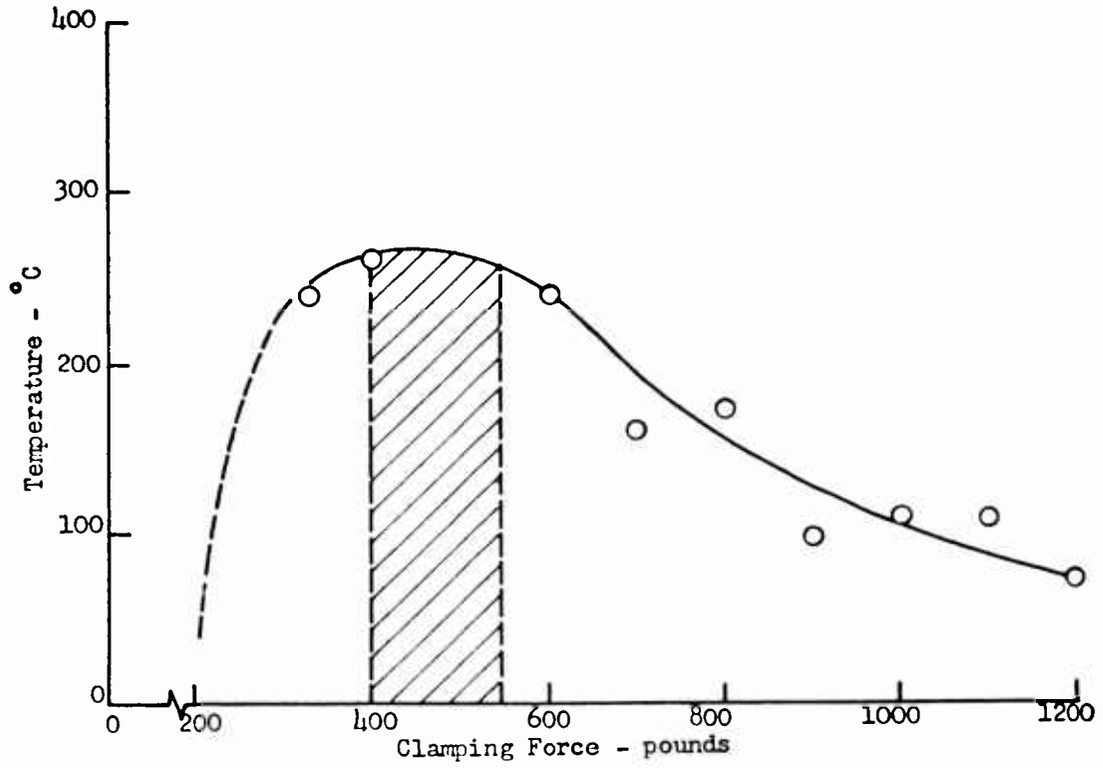

Figure 21 - Preliminary delineation of clamping force required for welding 0.010- to 0.012-inch beryllium (power, 1200 watts; welding interval, 0.4 sec; tip radius, 3 inches).

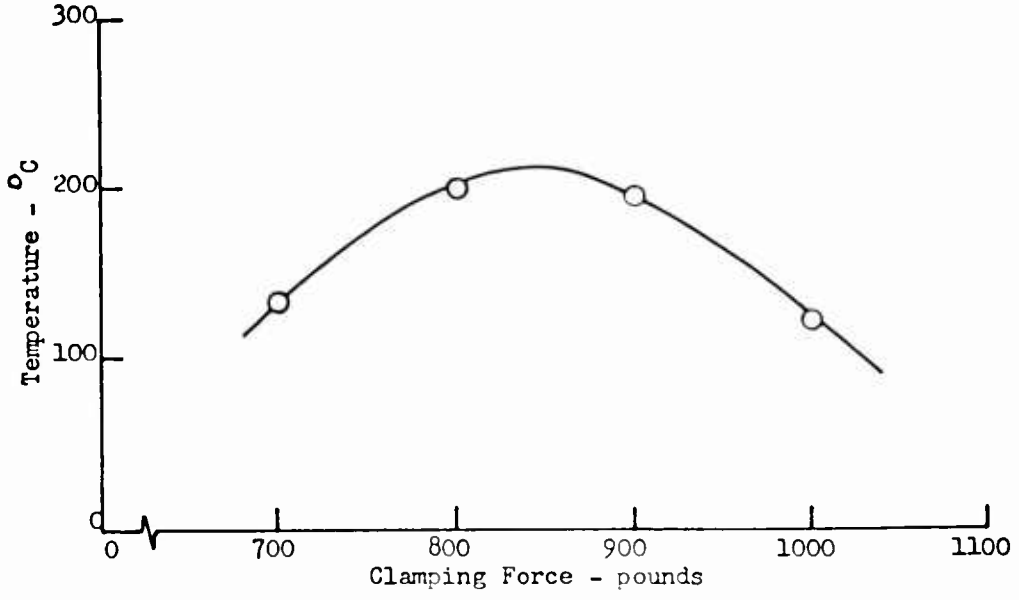

Figure 22 - Preliminary delineation of clamping force required for welding 0.018-inch beryllium (tip radius, 6 in.; power, 3400 watts; welding interval, 0.4 sec).

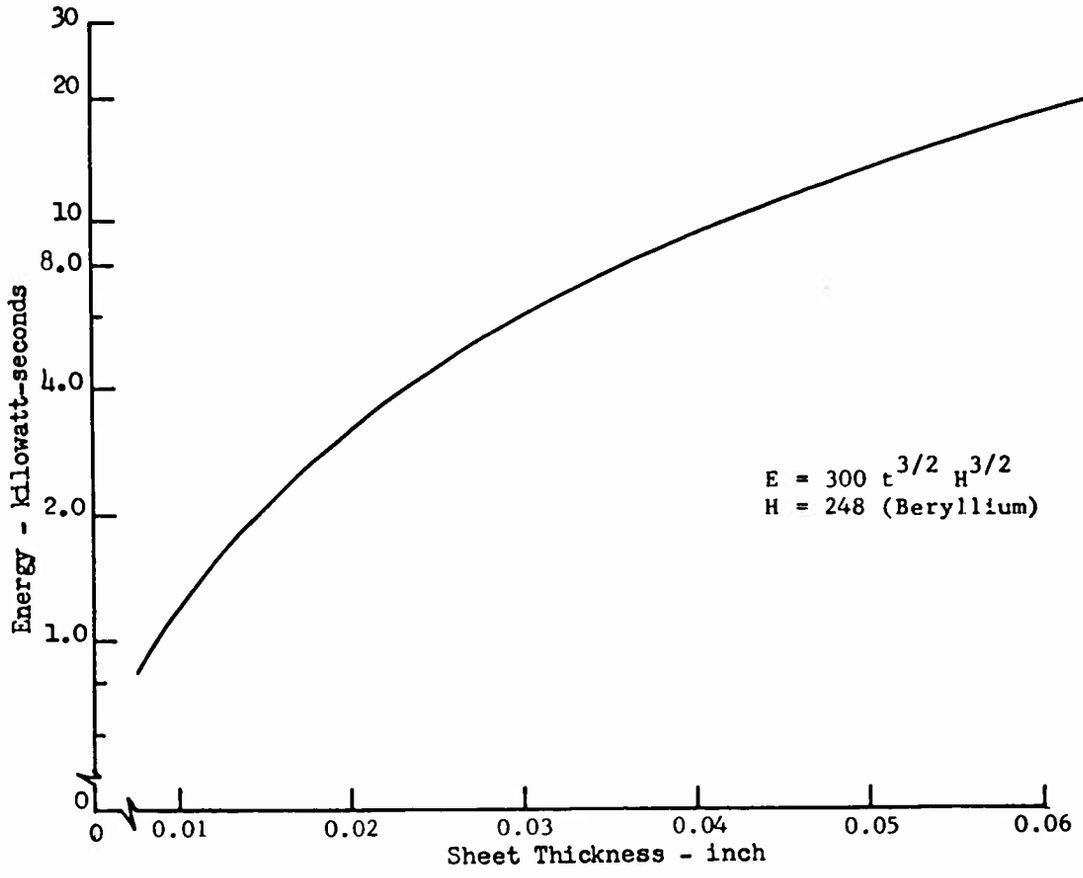

Figure 23 - Estimated energy as a function of beryllium sheet thickness.

The results of previous work[18], which were confirmed by this investigation, indicated that a weld interval of 0.5 seconds or less is mandatory to avoid cracking in the beryllium weld specimens. The smaller weld interval requires more power to deliver a given amount of energy. With a weld interval of 0.5 second, about 2400 watts of power delivered to the transducer and a clamping force of 500 pounds were required to weld 0.010- to 0.020-inch beryllium when a 3-inch sonotrode tip was used.

3-3.2 Impedance Matching. The limits of time and funds precluded study of the impedance between the transducer-coupling system and the beryllium weldment for the various gages of the beryllium sheet or for the four tip radii used in the program. However, two sets of measurements were made with 0.015-inch material showing the weld-zone impedance as a function of weld interval for tips of 3- and 6-inch radii. These results, shown in Figure 24, indicate a ratio of weld-zone impedance to coupler impedance in the range of 0.35 to 0.6.

This impedance information obtained for beryllium, added to data previously obtained for certain other materials, indicates the possibility that a universal type of ultrasonic welding machine can be designed to weld a broad range of materials of many different gages.

3-3.3 Effect of Sonotrode Tip on Weld Characteristics. Astroloy, a relatively new General Electric nickel alloy with good high-temperature properties, was used previously in several pilot-type experiments to determine its potential as a tip material. Those results indicated its superiority over Inconel X-750 for welding tungsten and several refractory metals. Accordingly, the tips used for this work were fabricated from Astroloy. The performance of these tips in welding beryllium sheet was satisfactory; no substantial evidence of damage was noted after more than 500 welds per tip.

Beryllium sheet, 0.010- to 0.012-inch was welded with spherically contoured tips, 1.5-, 3.0-, and 6.0-inch radii (Table 7). Each weld was subjected to:

(1) Microscopic inspection of the surface and of the exposed weld area after fracture or nugget peel-out test.

(2) Measurements of weld envelope area.

(3) Tensile shear test.

(4) Metallographic evaluation of interface quality after sectioning and polishing of weld interface.

The incidence of cracking appeared to be least when a 6-inch tip was used (Table 3-1). In an effort to reduce cracking further, a tip with a radius of 9 inches was utilized in joining material that had been reduced to a thickness of 0.015-inch by chemical etching. With this larger tip, a clamping force of 900 pounds was required. Welds were made at a fixed power level to the transducers of 3800 watts and at weld interval ranging from 0.1- to 1.5 seconds.

Microscopic study of the weld surfaces revealed small hairline cracks in the sonotrode contact zone; this condition was more marked at the longer intervals. In contrast with results obtained, using tips of larger radii, however, no gross

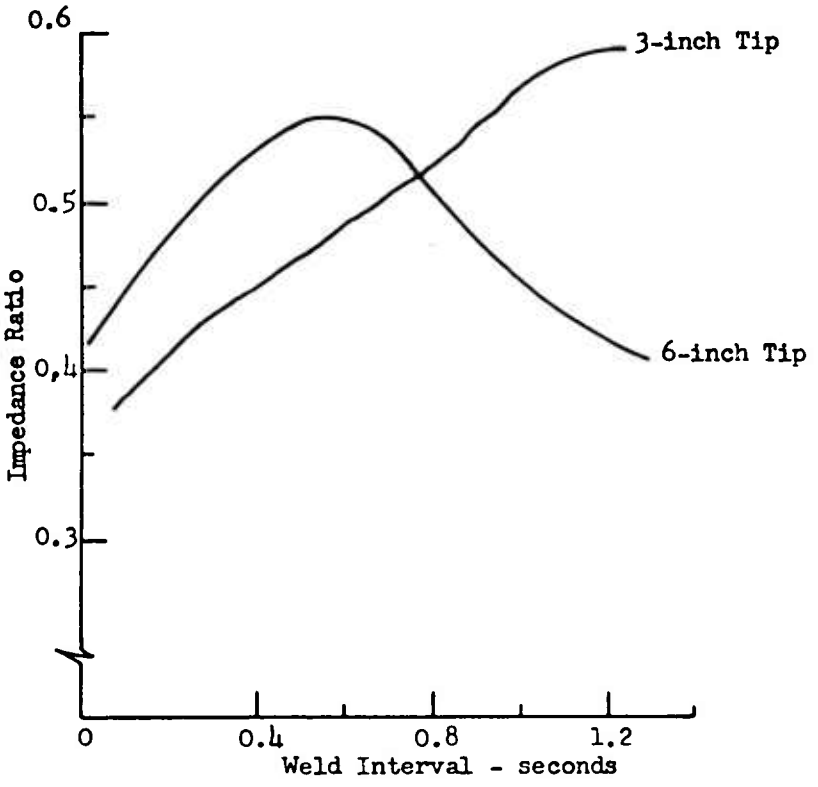

Figure 24 - Weld-zone impedance as a function of weld interval and tip radius.

Table 7. EFFECT OF TIP RADIUS AND WELD INTERVAL ON INCIDENCE OF CRACKING IN BERYLLIUM SHEET

Sheet Thickness, (inch)	0.010-0.012[c]			0.015[d]
Tip Radius, (inch)	1.5	3.0	6.0	9.0
Clamping Force, (pound)	350-400	500-550	800	900
Weld Interval, (second)[a]	Incidence of Cracking[b]			
0.03	None	None	None	--
0.05	None	None	None	--
0.10	None	None	None	None
0.15	None	None	None	--
0.20	None	None	None	None
0.30	Some	Occasional	None	None
0.35	Some	Some	None	--
0.40	Some	Some	Occasional	None
0.50	--	--	Occasional	None
0.60	--	Some	--	None
0.80	--	--	--	None
0.90	--	--	--	None
1.50	--	--	--	None

(a) The short welding intervals were investigated to determine whether cracking might have occurred piror to the formation of a weld.

(b) Gross cracking as opposed to microscopic hairline surface cracks. Occasional cracking occurred as a result of the application of clamping force and the superposed ultrasonic vibration.

(c) 2400 watts.

(d) 3800 watts.

cracking nor specimen fragmentation was noted, even at longer weld intervals. Photographs of representative specimens after tensile-shear tests are shown in Figure 25.

3-3.4 Improving Ductility by Use of a Preheat. A previously investigated power programming system was explored further as a means of circumventing the limitations imposed by the power capacity of the 4-kw equipment and, simultaneously, of studying the practicability of preheating the weld interface to increase the ductility of beryllium and thus facilitate the formation of a high quality bond. Three separate timers were preset to deliver, sequentially, three levels of power output from the ultrasonic generator. In this fashion, the applied power was increased in controlled steps to raise the temperature in the weld zone.

Previous work[15] showed that the energy dissipation during ultrasonic welding usually produces measurable temperatures in the range of 35 - 50% of the absolute melting point of the weldment material. A temperature increase of this magnitude might be expected to improve the ductility of beryllium. With a 6-inch tip and a power level of 3400 watts, a maximum temperature of about 240°C was recorded while welding 0.018-inch beryllium (about 0.3 second after initiation of the welding pulse). This is considerably less than 35% of the absolute melting point of beryllium, and it is doubtful that the ductility improved substantially.

3-3.5 Effect of Machine Variables on Weld Strength. Data concerning welding conditions and the strength of the ultrasonic welds between sheets of 0.010- and 0.012-inch beryllium, as well as between sheets of 0.018- and 0.020-inch, are summarized in Tables 8 and 9; the Vickers microindentation hardness for these specimens was 254. Since the unit tensile-shear-strength was calculated from weld-envelope area measurements and these are only approximate, the strength values are probably underestimated.

Inspection of the aluminum support plates, after tensile-shear testing of the 0.015-inch beryllium specimens showed that the beryllium specimens were somewhat loosely held to the supports in the area of the welds. Apparently, the epoxy bonding between the test coupon and the support plates was incomplete (a condition which was not evident in any other tests). These specimens had therefore been subjected to a partial peel load so the resulting strength data are somewhat low.

Furthermore, the fact that these specimens fractured when subjected to the partial peel load made it difficult to determine the true weld area. Hence, the unit-strength values (given in Table 10), calculated from the shear strength data which is too low and the weld area data which are possibly too high are probably conservative.

3-3.6 Orientation of Vibratory Energy with Rolling Direction of Sheet. Since beryllium sheet is anisotropic and the delivery of the vibratory energy during standard ultrasonic spot-welding is unidirectional, the excursion of the sonotrode with respect to the direction of maximum ductility existing in the beryllium sheet was investigated. One series of test welds was made in which the direction of vibratory excursion was oriented transverse to the long axis of the tab specimens (1-inch and 2-3/4 inches long) and a second series was made with vibratory excursion oriented parallel to the longitudinal axis.

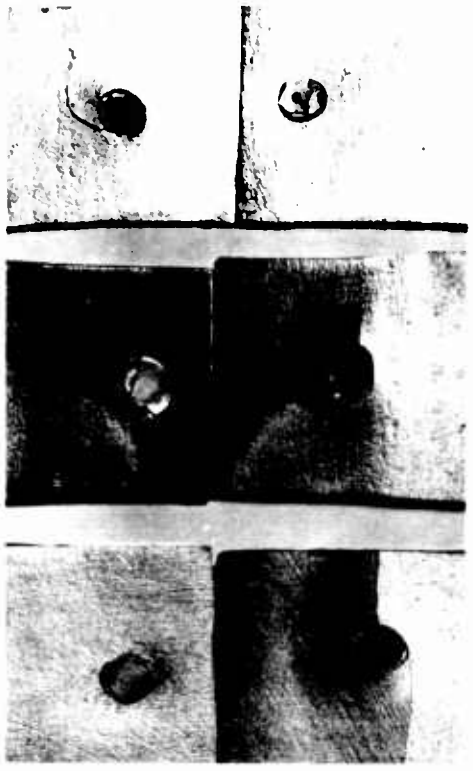

0.6-sec welding interval

0.8-sec welding interval

1.5-sec welding interval

Figure 25 - Weld area growth and nugget pullout in beryllium bonds after tensile-shear tests (power, 3800 watts; clamping force, 900 lb; tip radius, 9 in.)

Table 8. TENSILE-SHEAR STRENGTH OF ULTRASONIC BONDS IN BERYLLIUM SHEET[a]

Tip Radius, in.	Clamping Force, lb	Energy, watt-sec	Tensile Strength, lb/spot	Unit Strength, psi
1.5	350-400	720	22	1594
		840	46	2930
3.0	400-550	960	155	10900
			200	13150
			210	12650
			195	8500
6.0	800-850	720	116	5044
			195	7500
		800	198	6900
		960	166	6650
		1200	190	7100

(a) 0.010- to 0.012-inch sheet welded at 2400 watts.

Table 9. TENSILE-SHEAR STRENGTH OF ULTRASONIC BONDS IN BERYLLIUM SHEET[a]

Energy,[b] watt-sec	Tensile Strength, lb/spot	Unit Strength, psi
2120	95	3710
2200	200	9300
2290	280	12960
2300	278	9965
	150	5475
2400	260	12560
	210	7840
	170	7370
2500	155	5920
	445	18860
2600	235	11460
2660	330	18000
	152	5480
2680	78	3805
	50	3155
2800	202	8230
3040	305	--
3060	220	8300

(a) 0.018- to 0.020-inch sheet welded with a clamping force of 800 - 850 lb and a tip radius of 6.0 in.

(b) Power programmed; see Section 3-3.4 for details.

Table 10. TENSILE-SHEAR STRENGTH OF ULTRASONIC BONDS IN BERYLLIUM SHEET[a]

Energy, watt-sec[b]	Tensile Strength, lb/spot	Unit Strength, psi
400	No weld	--
750	57	3677
1150	102	6623
1500	217	12260
1900	207	11070
2300	152	6972
2650	205	5409
3050	208	7909
3400	206	5869
5700	222	4980

(a) 0.015- to 0.016-inch sheet welded with a clamping force of 900 lb and a tip radius of 9.0 in.

(b) Power programmed; see Section 3-3.4 for details.

These experiments were conducted with a 9-inch radius tip and 0.015-inch material at welding machine settings of 3800 watts to the transducer, 900-pounds clamping force, and a 0.5-second weld interval. All beryllium tab specimens (1 x 2-3/4 inches) were cut from a sheet so that the 2-3/4 inch dimension was parallel to the major rolling direction.

The interfacial weld zones obtained were annular, with the inner boundary of the weld area not well defined, so the area measurements (and, hence, the unit-strength data) are not very accurate. In addition, the weld area for several of these specimens could not be measured because of material transfer or parent-metal fracture during the tensile-shear tests.

Shear strength data, reported in Table 11, showed a wide scatter and gave no indication that the quality of the welds or the cracking tendencies were affected by the direction of the vibratory motion or the preferred orientation of the beryllium sheet.

An experiment, that includes investigation of such variables as thicknesses of material and radius of sonotrode tip would be necessary to establish whether an orientation effect exists.

3-3.7 Use of Foil Interleaf to Improve Weld Strength. To evaluate spot-type weldments incorporating a foil interleaf, beryllium specimens were prepared with each of six foil materials: molybdenum, zirconium, titanium, gold, aluminum, and beryllium. The results of an initial study indicated that zirconium, gold, and aluminum inserts improved weld strength and merited further consideration (Figure 26 and Table 12).

The solubility of aluminum in beryllium is probably less than 0.1 $^{w}/_{o}$[19] and no compounds are formed in this system. The beryllium-gold system contains an extensive series of compounds, and the reported solubility of gold in beryllium is approximately 2 $^{w}/_{o}$[19]. The solid solubility of beryllium in molybdenum, determined by hardness measurements, is given as 0.05 w/o at 1850°C, decreasing to 0.01 w/o at 1300°C[20]. Although the solubility of beryllium in α-titanium and in α-zirconium is uncertain, recent estimates are 0.15 - 1.0 $^{w}/_{o}$[21,22] and approximately 1.0 $^{w}/_{o}$[23], respectively. Compound formation is prevalent in both the titanium-beryllium and the zirconium-beryllium systems.

In previous studies[14,18] involving the use of a foil interleaf and beryllium, the weld energy could be reduced, but the optimum clamping force was not affected. Accordingly, the machine settings used in these tests were those established as minimal for welding beryllium alone.

High quality welds, free from cracks, were obtained with 0.001-inch aluminum interleaf; these welds also showed the highest single-spot strength obtained with any of the interleaf materials. Two of these specimens exhibited single-spot strengths of 340 and 430 pounds and considerable interfacial disturbance was noted as well as dispersion of the foil layer in the weld periphery. Gold and zirconium were less satisfactory than aluminum.

Table 11. EFFECT OF VIBRATORY ORIENTATION ON TENSILE-SHEAR STRENGTH OF BONDS IN 0.015-INCH BERYLLIUM[a]

Orientation of Vibratory Excursion	Tensile Strength, lb/spot	Unit Strength, psi
Transverse to long axis of tabs	133(b)	9,070
	362	--
	164	8,410
	234(c)	--
	75	6,050
Longitudinal to axis of tabs	266	15,670
	223(b)	12,350
	117	7,360
	90	3,760

(a) Welded at 3800 watts with a clamping force of 900 lb, a tip radius of 9.0 in., and a welding interval of 0.5 sec.

(b) Partial nugget pullout.

(c) Fracture in parent metal.

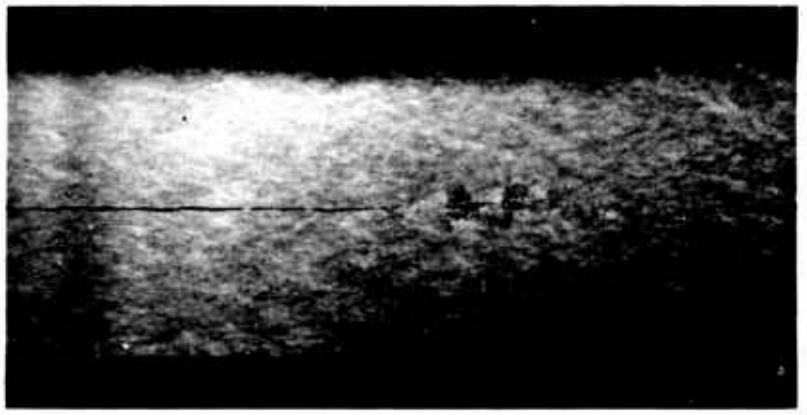

(a). aluminum interleaf

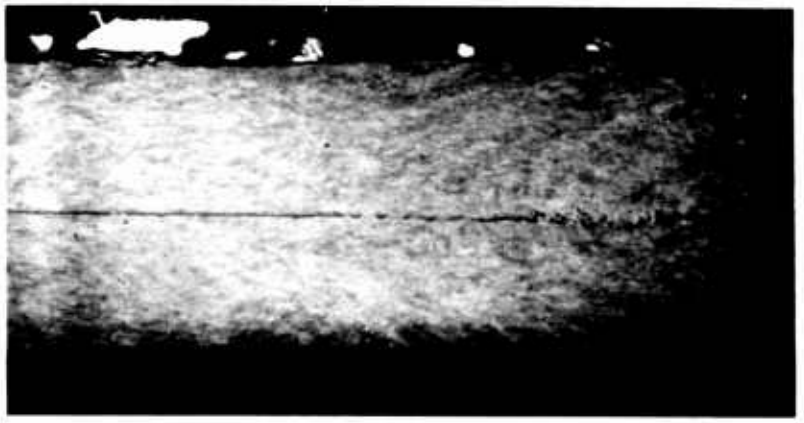

(b). zirconium interleaf

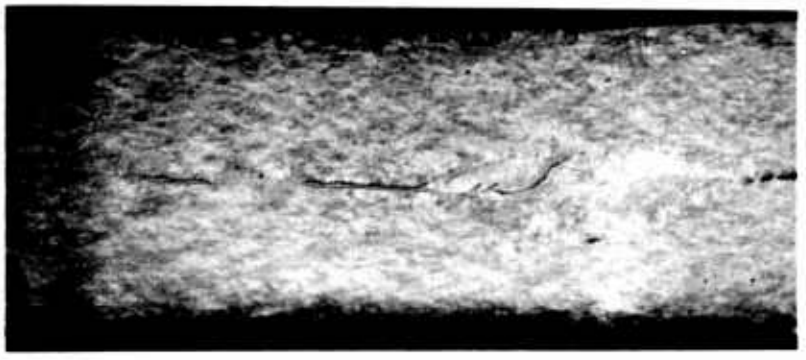

(c). gold interleaf

Figure 26 - Diametrical section of ultrasonic welds made in 0.018-inch beryllium sheet with various interleaves, showing annular bond locale (polarized light; 50X).

Table 12. EFFECT OF FOIL INTERLEAF ON ULTRASONIC BONDS IN BERYLLIUM[a]

Interleaf		Beryllium Thickness, in.	Energy, watt-sec	Tensile Strength, lb/spot	Unit Strength, psi	Microscopic Evaluation[b]	
Material	Gage, in.					Surface	Interface
Al	0.001	0.013/0.0135	600	450[c]	(c)	0	0
		0.019/0.019	2400	430	(c)	0	0
		0.019/0.019	2400	340	(c)	1(d)	0
Au	0.001	0.013/0.015	600	40	4320	3(d)	3
		0.019/0.019	2400	370	(c)	1	2
		0.0195/0.019	2400	250	(c)	1	2
Be	0.001	0.019/0.020	2000	200		2	
				250		2	
			2400	165		2	
				225		2	
				185		2	
				320		3	
				310		2	
			3200	170		3	
				49		3	
				92		3	
				200		3	
Mo	0.0005	0.0095/0.010	600	No weld	--	--	--
Ti	0.0005	0.0135/0.0137	600	60	2700	1	1
Zr	0.00046	0.0125/0.0130	600	250	9520	(d)	0
		0.0195/0.020	2400	50	3380	3	2
		0.019/0.019	2400	260	7023	1	2

(a) 0.0125- to 0.020-inch sheet welded with a clamping force of 500 lb for the thinner sheet and 850 lb for the thicker sheet, using a tip radius of 6.0 in.

(b) 0: No cracks evident.
1: Small hairline cracks radiating outward from weld center, apparently not extending to weld locale.
2: Small cracks which may or may not extend to weld locale.
3: Large cracks which extend to weld locale and may extend through both sheets.

(c) Fractured across the sheet and through the bonding cement which sheared away from aluminum backing plate so that no area measurement was possible.

(d) Small cracks may be extension of surface imperfections.

A small quantity (3 in^2) of 0.001-inch beryllium foil was also tested as an interleaf material, but the results were inconclusive. Because of the limited amount of beryllium foil available, only one series of experiments, involving three energy levels, was performed. The results of these tests are included in Table **12.** The need for a more comprehensive investigation is clearly indicated by these findings.

3-3.8 Welding in Inert Atmosphere. Previous experience with easily oxidized materials indicated that oxidation and the associated surface embrittlement are suppressed when these materials are welded in an inert atmosphere. To determine the effect of an inert atmosphere on the welding characteristics of beryllium, several beryllium joints were made with helium flooding the weld zone. The results of this scouting experiment are summarized in Table **13.** Evaluation of strength and metallographic structure in a small number of coupons failed to reveal any difference between these welds and those made in air.

3-3.9 Weldability of Annealed Beryllium Sheet. A brief study of the ultrasonic weldability of annealed AMC beryllium sheet was made to determine if beryllium sheet, heat-treated to enchance third dimensional ductility[24], would show improved welding characteristics. Coupons prepared from the original AMC beryllium sheet were annealed* at NMI and then resubmitted for welding.

From a preliminary inspection of these specimens (see Table **14),** it appeared doubtful that they could be welded. In particular, evidence of warping was noted, which would probably lead to cracking when the necessary clamping force was applied.

The superficial hardness of the annealed specimens as shown in Table **15** was essentially the same as that of the original as-received beryllium sheet. A decrease in hardness would have allowed a corresponding reduction in the welding energy, but since the decrease apparently did not occur, attempts were made to weld the annealed specimens at the machine settings and welding interval established for the as-received, 0.020-inch material.

While the superficial hardness test did not indicate a difference between the annealed and the as-received material, the annealed coupons, in spite of the cracking tendency associated with their lack of flatness, did respond more readily to ultrasonic welding. Metallographic studies indicated that these were the best beryllium bonds produced without foil inserts during the course of these studies. The bond interface was almost totally indistinguishable in many regions of the weld. The photomicrographs of Figure **27 (a) and 27 (b)** show the interface regions for two welds. Figure **27 (c)** is a photograph of an overall weld in the annealed material.

Surface damage and weld cracking, however, were somewhat more severe than that encountered in the as-received sheet thus indicating that a considerable excess of welding power was used.

- - - - - - - - - - - - -

* Annealed in 1 atmosphere of argon for 6 minutes at 1050°C.

Table 13. EFFECT OF INERT ATMOSPHERE (HELIUM) ON WELD INTEGRITY OF 0.016-INCH BERYLLIUM[a]

Tensile Strength, (lb/spot)	Microscopic Evaluation of Weld Surface
80	Small cracks that may or may not extend into weld locale.
115	Small hairline cracks radiating outward from center of weld but not extending to weld locale. Small nugget pulled from weld zone.
250	Small hairline cracks radiating outward from center of weld but not extending to weld locale.

(a) Welding energy of 2800 watt-sec, using a clamping force of 900 lb and a tip radius of 9.0 in.

Table 14. INSPECTION DATA FOR ANNEALED BERYLLIUM SAMPLES

Sample No.	Dimensions, in.			Comments
	Thickness	Width	Length	
T-2	0.019	1	2-3/4	One edge cracked. Surface contains wavy scratches.
B-12	.0185-.0195	1	2-3/4	Surface contains scratches. Coupon has complex curvature in both planes.
J-7	.020-.022	1	2-3/4	Surface contains scratches. Coupon has complex curvature in both planes.
T-12	.018-.0195	1	2-3/4	Best surface of group. Coupon has complex curvature in both planes, sample slightly warped.
B-2	.021-.022	1	2-3/4	Similar to Sample No. T-2.
5 Random Samples	.018-.022	3/4	1-1/4	Surfaces very irregular and warped. Unsatisfactory for ultrasonic welding.
4 Samples	0.019-.022	3/4	2-3/4	Surfaces very irregular and warped. Unsatisfactory for ultrasonic welding.

Table 15. HARDNESS VALUES FOR 0.020-INCH BERYLLIUM SHEET BEFORE AND AFTER ANNEALING

Material	Hardness Values[a]	
	15-T Scale	45-T Scale
As-Received	85	58
	82	61
	85	
Annealed	85	59
	87	63
	85	63
		60

(a) Rockwell Superficial Hardness Tester.

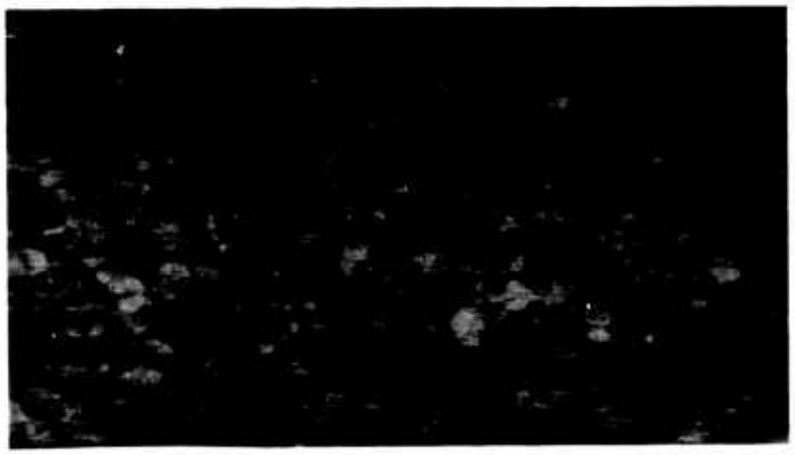

(a). sheet interface (150X)

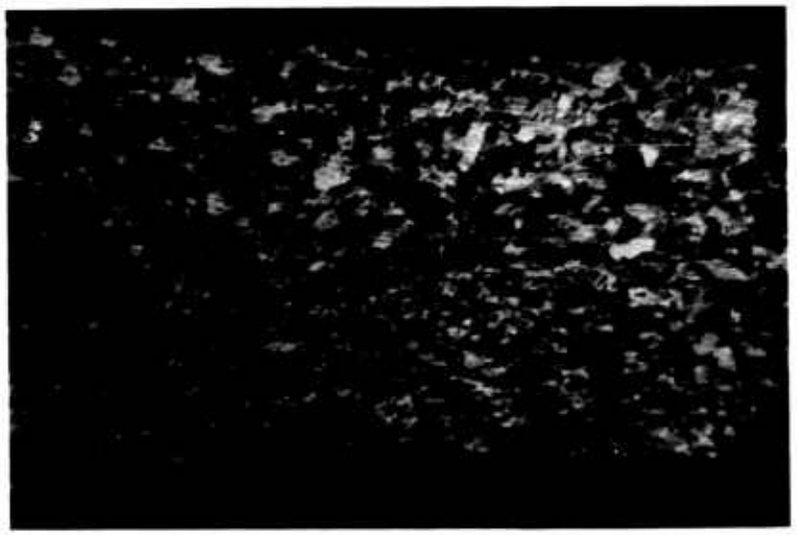

(b). sheet interface (90X)

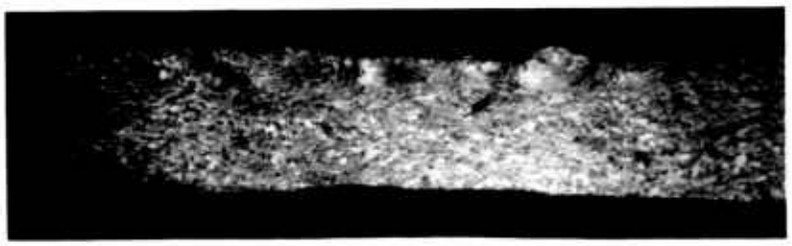

(c). over-all weld (28X)

Figure 27 - Ultrasonic welds made in annealed 0.018-inch (AMC) beryllium.

3-3.10 Metallographic Studies. Initial investigations with available 0.010-inch beryllium sheet resulted in ultrasonic welds of the type shown in Figure 28. This is probably characteristic of sound beryllium-to-beryllium bond. Several important features of the bond are apparent from the photomicrograph:

(1) The bonded area is annular and the central portion of the weld area is unbonded. This is characteristic of ultrasonic welds in several materials.

(2) The total thickness reduction (indentation) at the weld zone is small. The sonotrode tip caused some surface irregularities, but gross surface damage did not occur.

(3) The bonding is accompanied by extensive internal deformation of the sheet adjacent to the sonotrode. This degree of internal local plasticity is remarkable, especially in beryllium, and provides an insight into the mechanism by which ultrasonic energy produces crack-free welds in brittle material.

(4) Effective dispersion of surface oxide and/or surface contaminant occurred in the bonded portion of the specimen (Figure 29).

(5) The small fissure at the edge of the weld area (right side of Figure 28 was probably caused by attempts to fracture the weld with a knife. Small fissures along the mating surfaces are observed (arrow in Figure 29) in the peripheral regions of the weld area.

Because of the thickness and the surface condition of the AMC beryllium, good welds could not be obtained with this material in the as-received condition. As-received sheet was reduced to about 0.013 inch, by electropolishing and to approximately 0.015- to 0.018-inch by chemical etching. The results of investigations with electropolished and /or chemically etched material are summarized below:

(1) Electropolished 0.013-Inch Sheet. The bonded areas of welds (made either without interleaf or with interleaves of gold, zirconium, or aluminum) in 0.013-inch electropolished sheet were annular and the aluminum interleaf welds were generally crack-free. The cracks observed in specimens welded with other interleaf materials were usually normal to the sheet surface and extended either completely through both sheets of the weldment or through the sheet adjacent to the sonotrode tip. When cracks occurred at the outside edge of the annular bond zone, they usually extended only through the sheet that was in contact with the sonotrode tip; the cracks penetrating both sheets were ordinarily found in the central portion of the weld areas.

Examination of the surface of as-welded samples showed a definite crack pattern. Both radial cracks originating at the center of the weld spot and circumferential cracks were observed. After sectioning the samples for metallographic examination, the circumferential cracks noted on the surface were correlated with the annular edge cracks in the microsection; the radial cracks on the surface were observed as the center cracks in the microsection.

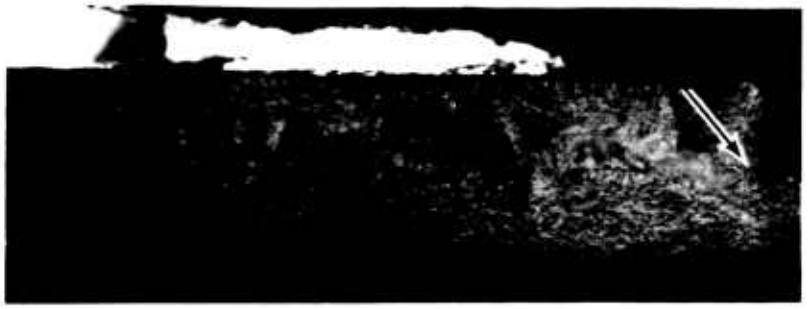

Figure 28 - Ultrasonic weld between two sheets of 0.010-inch beryllium. Note small fissure at arrow. (polarized light; 50X; tip radius, 6 in.)

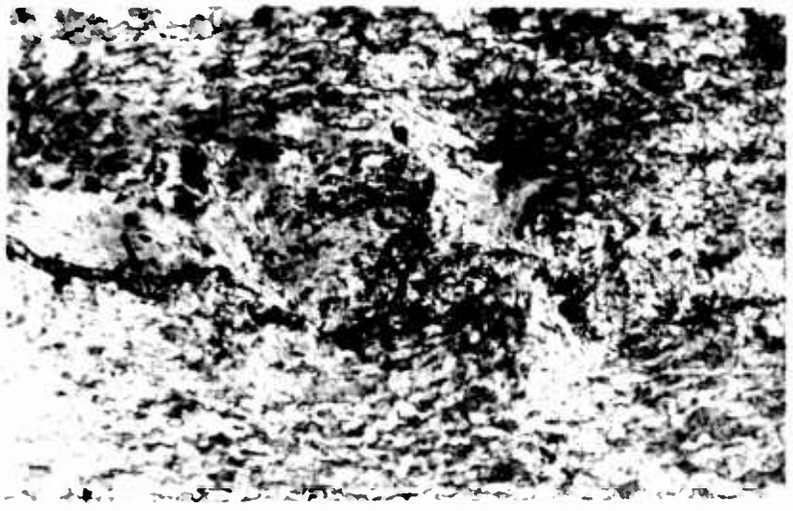

Figure 29 - Detail of weld interface of Figure 3-17. (Polarized light; 200X; etchant, 0.5% HF.)

(2) Chemically Etched 0.015-Inch Sheet. The 0.015 inch chemically etched specimens were welded at 3800 watts and 900 pounds clamping force with a 9-inch radius spherical tip. Only non-interleaf welds were investigated in this group. Bonding, as indicated by interfacial disturbance, occurred at the periphery of the contact area, and cracks were observed near the bond centers in those welds that were sectioned. However, no edge-cracks were observed in this group of specimens, and it appears that further effort in the area of tip-geometry will probably resolve the cracking problems. By using aluminum foil as an interleaf material, reproducible high quality welds (at both surface and interface) of good strength were produced in the 0.015-inch chemically etched sheet.

(3) Chemically Etched 0.018-Inch Sheet. The 0.018-inch chemically etched sheet was welded with a 6-inch tip at energy levels of 3400 watt-seconds (programmed power) and a clamping force of 850 pounds. Metallographic examination showed that the welds in this material were similar to those described for the 0.015-inch specimens. Bonding occurred only in the peripheral zone of the contact surface (annular bond pattern), and hairline surface cracks were observed in three specimens that were welded without an interleaf.

(4) As-Received 0.020-Inch Sheet. Samples of the 0.020-inch AMC beryllium sheet were welded with a 0.001-inch beryllium foil interleaf. Since microscopic surface inspection of these specimens showed through cracking (i.e., cracks extending from the weld to the surface of the specimen) the samples were not sectioned for metallographic examination.

(5) Annealed 0.020-Inch AMC Material. When two specimens of the 0.020-inch annealed AMC beryllium were examined for surface cracks by a stereoscopic microscope, small cracks at the tip surface were noted. One specimen was completely fractured by application of only static clamping force but was then welded through the cracks.

3-3.11 Results with BBC Material. Beryllium supplied in 0.003-, 0.005-, and 0.010-inch sheet by the Brush Beryllium Company was used in the final welding studies. The surfaces of these coupons were smooth, and there was evidence that some of the samples may have been electropolished.

BBC coupons having equal thickness were welded at the machine settings given in Table 16. This material responded to ultrasonic welding considerably better than the beryllium sheet previously investigated probably, because of the improved surface finish. Incipient welds were achieved with the 0.010-inch material at weld energies of only 200 watt-seconds. While these bonds were not of high-strength, welding at these conditions had not been possible with the materials investigated earlier. However, examination revealed surface cracks in all but two of the 0.010-inch specimens. Attempts to section those coupons for metallographic inspection were unsuccessful because the joints were not sufficiently strong to withstand the sectioning operation. Metallographic examination of some of the 0.003- and 0.005-inch specimens revealed surface cracks that although very small, extended through the sheet into the weld interface (Figure 30). The very small amount of this material available, did not permit establishing the proper machine settings for welding the BBC beryllium.

Table 16. WELD CHARACTERISTICS OF BERYLLIUM SHEET PRODUCED BY BRUSH BERYLLIUM COMPANY[a]

Material Thickness, in.	Clamping Force, lb	Weld Energy, watt-sec	Microscopic Evaluation of Weld Surfaces
0.003	300	80	No apparent cracks (3 specimens)
		200	Cracks
0.005	300	96	No apparent cracks
0.010	300	200	No apparent cracks (3 specimens)
		200	One small crack
0.010	350	300	Small nugget in weld; radial cracks
	400	270	Severe tip sticking; radial cracks
	425	1128	Welded through nugget to anvil
	450	210	Cracks
		220	Small spot; some cracks[b]
		270	Small spot; good weld
		300	Fair welds; radial cracks
		1050	Cracks
		1200	Welded through surface and cracks
		1200	Cracks

(a) Welded at 800 - 3500 watts, using a tip of 3.0-inch radius and welding intervals of 0.1 - 0.5 sec.

(b) Using 0.001-inch beryllium interleaf.

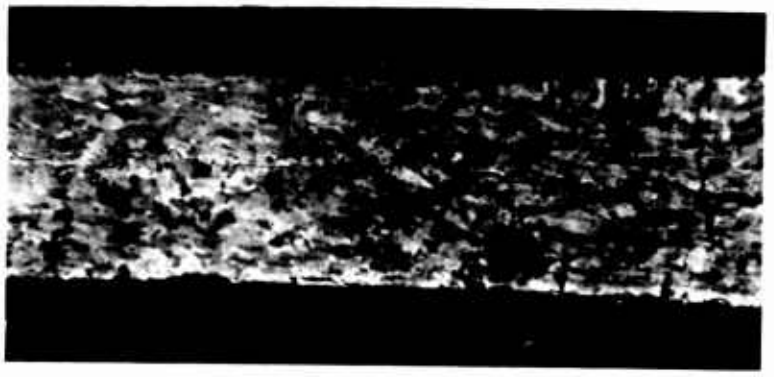

Figure 30 - Cracks in weld zone of 0.005-inch BBC Beryllium (polarized light; 100X).

3-3.12 Multiple Spot-Welded Panels. Recently, 13 beryllium panels, each of which consisted of two pieces of 0.010-inch sheet, were assembled by means of ultrasonic spot-welds on 3/4-inch centers. One of these panels is shown in Figure **31.** Visual and X-ray inspection indicated that the multiple-spot beryllium assemblies were crack-free.

3-4 CONCLUSIONS

Conclusions pertaining to the specific areas investigated in this program are summarized generally under the headings of the previously outlined objectives to the program.

3-4.1 Determination of Welding Machine Settings.

(1) Calculations of the energy requirements to weld beryllium sheet indicated that the power required to weld 0.040- and 0.060-inch sheet exceeded the power-handling capacity of available equipment, and the experimental work was limited to gages of 0.020 inch and less.

(2) These studies confirmed previous work which indicated that a weld interval of 0.5 second or less is necessary to avoid cracking of the beryllium sheet.

(3) Machine settings for welding 0.010 - 0.012 inch beryllium with a 3-inch radius sonotrode tip were selected at 2400 watts, 0.5 second, and 500 pounds clamping force.

3-4.2 Investigation of Impedance Matching.

(1) Limited determinations of weld zone impedance indicated a ratio of weld zone impedance to coupler impedance in the range of 0.35 to 0.6; the transmission of energy from the welding tip to the weldment is maximum when this impedance ratio is unity.

3-4.3 Effect of Sonotrode Tip Radius and Material.

(1) Sonotrode tips of Astroloy demonstrated satisfactory wear characteristics; a tip life of more than 500 welds per tip was achieved.

(2) Sonotrode tips of 6- and 9-inch radii appeared to be more effective and produced less crack incidence than tips of smaller radii; a more thorough statistical analysis of this variable is indicated.

3-4.4 Effect of Orientation of Vibratory Energy with Sheet Rolling Direction.

(1) Studies related to the weldability of beryllium with respect to the preferred orientation of the material and the direction of applied vibratory force failed to establish a relationship between these factors; a statistically designed experiment will be required to develop any relationship that exists.

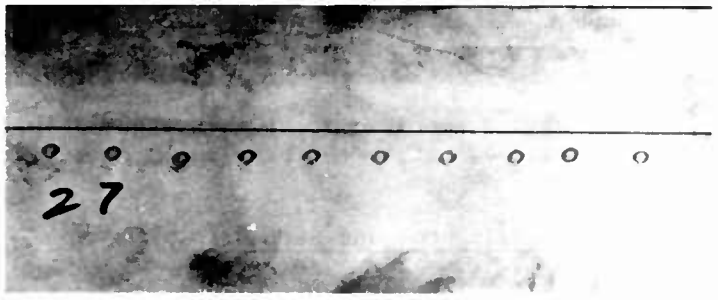

(a). Side of panel in contact with tip.

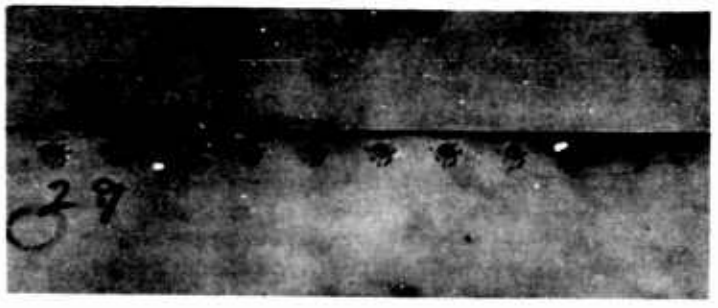

(b). Side of panel in contact with anvil.

Figure 31 - Ultrasonically welded panels of 0.010-inch beryllium; spot welds spaced 3/4 inch apart.

3-4.5 Effect of Preheat.

(1) The use of power programming apparently failed to induce an initial temperature of 400°C which is required to achieve a substantial increase in ductility; thorough investigation of this system of applying power, possibly with the addition of force programming, is expected to improve the weldability of beryllium.

3-4.6 Effect of Welding with Foil Interleaf.

(1) The use of an aluminum foil interleaf eliminated weld cracking in 0.013- and 0.019-inch beryllium.

(2) Harder insert materials, such as zirconium, molybdenum, and beryllium, were ineffective in alleviating cracking tendencies.

(3) The gold interleaf, of intermediate hardness, did not entirely eliminate cracking. Localized plastic flow, as well as diffusion in the bonded regions, was observed.

3-4.7 Effect of Annealing Treatment.

(1) The weldability of annealed beryllium, even though of the same measured hardness as the as-received sheet material, was superior to that of the as-received sheet; metallographic examination showed good bonding, with the interface almost totally eliminated in many regions of the weld area.

3-4.8 Metallographic Characteristics of Welds.

(1) In both interface and non-interleaf welds, bonding occurred at the periphery of the contact area, and the central portions of the weld areas were generally only partially bonded, or in some cases, entirely unbonded; this is characteristic of ultrasonic welds.

(2) Most of the satisfactory beryllium welds were obtained with sheet material that was generally smooth, flat, and free from surface defects.

3-5 RECOMMENDATIONS

From the results of the experimental work reported herein, the development of a satisfactory welding procedure (i.e. machine settings for power, clamping-force and weld interval; etc.) appears promising for joining structural members of 0.010-inch (or less) beryllium sheet. The criticality of the machine settings can be substantially reduced if interleaf materials, such as aluminum foil, can be tolerated at the weld interface. While the foil inserts are not deleterious to weld strength at room temperature, strength as well as other properties may be affected at elevated temperatures.

With further development effort, the use of ultrasonic welding appears feasible as a more versatile method for joining beryllium of 0.060-inch and thicker gages. It is recommended that further experimental work be initiated and specifically directed toward the following objectives:

(1) The Development of High Power Ultrasonic Welding Equipment.[a] The higher powered equipment will extend the weldable thickness of the ultrasonic joining process to heavier gages, permit the use of shorter weld intervals for joining thin gage material, and reduce or eliminate any tendency toward material cracking.

(2) The Development of Power- and Force-Programming Systems for Available Ultrasonic Equipment. With power-and force-programming, the criticality of the welding schedule now required for the production of crack-free structural welds in beryllium can be greatly reduced. Also, longer weld intervals can probably be used with less danger of material cracking; thus, a usable energy increase, or extension of the weldable thickness to heavier gages, can be realized with the existing ultrasonic equipment.

(3) Continuation of The Study of Interleaf Materials. Since the proper selection of interleaf material is effective in increasing the weldable gage at a fixed power level and in eliminating cracking, a study of interleaf materials should be carried out to develop a criterion for selecting insert materials that are compatable with beryllium from the standpoint of corrosion resistance and operating characteristics at elevated temperatures. The foil interleaf may also be effective in the production of leak-tight closures.

Successful completion of these recommended investigations will provide an ultrasonic welding process for production-line assembly of beryllium structures for missile and space craft.

- - - - - - - - - - - - - -

(a) Since the conclusion of the work reported herein, a program for the development of ultrasonic welding equipment of greater power handling capacity has been initiated by the Directorate of Processes and Materials, ASD. The inclusion of beryllium as a material of interest in the ASD program would adequately satisfy the requirements of the action recommended in No. 1 above.

REFERENCES

1. A. R. Kaufmann, The Relation of Purity to Brittleness in Beryllium, Chp. VII-A in The Metal Beryllium, (D. W. White, Jr. and J. E. Burke, Eds.), pp. 367-371, Amer. Soc. Metals, Cleveland, 1955.

2. G. L. Tuer and A. R. Kaufmann, Ductility of Beryllium as Related to Single Crystal Deformation and Fracture, Chp. VII-B in The Metal Beryllium (D. W. White, Jr. and J. E. Burke, Eds.), pp. 372-424, Amer. Soc. Metals, Cleveland, 1955.

3. J. L. Klein, V. Macres, D. Woodard, and J. Greenspan, Ductility of Beryllium as Related to Preferred Orientation and Grain Structure, Chp. VII-C in The Metal Beryllium (D. W. White, Jr. and J. E. Burke, Eds.), pp. 425-465, Amer. Soc. Metals, Cleveland, 1955.

4. G. L. Tuer, D. H. Woodard, D. B. Lister, and A. R. Kaufmann, Recovery and Recrystallization of Cold Worked Beryllium, Chp. VII-D in The Metal Beryllium (D. W. White, Jr. and J. E. Burke, Eds.), pp. 466-504, Amer. Soc. Metals, Cleveland, 1955.

5. D. W. Lillie, The Physical and Mechanical Properties of Beryllium Metal, Chp. VI-A in The Metal Beryllium (D. W. White, Jr. and J. E. Burke, Eds.), pp. 304-327, Amer. Soc. Metals, Cleveland, 1955.

6. R. E. Monroe, D. C. Martin, and C. B. Voldrich, Welding and Brazing of Beryllium to Itself and to Other Metals, USAEC Report BMI-836, Battelle Memorial Institute, May 1953.

7. D. C. Martin, Joining of Beryllium, Chp. V-G in The Metal Beryllium (D. W. White, Jr. and J. E. Burke, Eds.), pp. 283-294, Amer. Soc. Metals, Cleveland, 1955.

8. N. A. Brown, Joining of Beryllium - A Survey of the Unclassified Literature, USAEC Report CF-58-6-9, Oak Ridge National Laboratory, June 1958

9. N. E. Weare and R. E. Monroe, Joining of Beryllium, DMIC-Memo-13, Battelle Memorial Institute, March 1959.

10. E. M. Passmore, Beryllium Joining; WADC Sponsored Program, Report No. RAD-SR-8-59-7 (Quarterly Progress Report No. 2), Air Force Contract AF 33(616)-5913, Avco Manufacturing Corporation, Jan 1959.

11. E. M. Passmore, Beryllium Joining; WADC Sponsored Program, Report No. RAD-SR-59-40 (Quarterly Progress Report No. 4), Air Force Contract AF 33(616)-5913, Avco Manufacturing Corporation, Oct 1959.

12. Aeroprojects Incorporated, unpublished data.

13. A. L. Phillips (Ed.), Ultrasonic Welding, Chp. 52 in The Welding Handbook, Sec. 3, 4th ed., Amer. Welding Soc., New York, 1960.

14. J. B. Jones, N. Maropis, J. G. Thomas, and D. Bancroft, Fundamentals of Ultrasonic Welding, Phase I, Final Report on Navy BuAer Contract NOas 58-108-c, RR-59-105, Aeroprojects Incorporated, May 1959.

15. J. B. Jones, N. Maropis, J. G. Thomas, and D. Bancroft, Fundamentals of Ultrasonic Welding, Phase I, Final Report on Navy BuAer Contract NOas 59-6070-c, RR-60-91, Dec 1960.

16. A. E. H. Love, A Treatise on the Mathematical Theory of Elasticity, Dover Publications, 1934.

17. Procedures for the Metallographic Preparation of Beryllium, Titanium, and Refractory Metals, DMIC Memo. 37, p. 3, Battelle Memorial Institute, 1959.

18. Exploration and Development of Ultrasonic Welding, Reports on Army Contract DA-36-034-ORD-3254 RD, Aeroprojects Incorporated.

19. A. R. Kaufmann and P. Corzine, Chp. X in The Metal Beryllium (D. W. White, Jr. and J. E. Burke, Eds.), Amer. Soc. Metals, Cleveland, 1955.

20. Arc-Cast Molybdenum-Base Alloys, Second Annual Report, Climax Molybdenum Co., 1951.

21. L. W. Craighead, et al, Trans AIME, 188:485 (1950).

22. R. I. Goldhoff, et al, Trans ASM, 45:941 (1953).

23. E. T. Hayes, in The Metallurgy of Zirconium (Lustman and Kerze, Ed.), McGraw-Hill, New York, 1955.

24. F. M. Yans, A. K. Wolff and A. R. Kaufmann, Development of Randomly Oriented Wrought Beryllium Sheet, NMI-9611, Nuclear Metals, Inc. Oct. 17, 1960.

SECTION 4

THE ROLE OF OXIDE AND VOIDS IN BERYLLIUM

Steven Allen

(Manufacturing Laboratories, Inc., Cambridge, Massachusetts)

ABSTRACT

The effect of beryllium oxide as a grain growth inhibitor and some effects of other precipitates and inclusions in beryllium were studied using replication electron metallography as the principal tool. It proved to be difficult to distinguish and identify the various precipitates but carbides, aluminum-silicon complexes and iron-beryllides were found to be identifiable. The identification of oxide was assured by employing an artificially simplified system, obtained by pressure welding surface oxidized beryllium, in which the location of the oxide thus was pre-determined. It was demonstrated that an oxide layer could be in a nearly continuous form or in a spheroidized state depending on the temperature and deformation involved in welding. In both of these conditions it will act as a grain growth inhibitor.

4-1 INTRODUCTION

4-1.1 Background. Powder metallurgy beryllium of commercial purity contains oxygen as a major impurity (about 1%). Because of its limited solid solubility in beryllium, oxygen appears in the form of oxide. Much of the oxygen is present as a surface layer that forms on the powder during the attrition milling and subsequent handling[1]. In material fabricated from powder, this oxide acts as a grain growth inhibitor. At a sufficiently high temperature, this effect is overcome and accelerated grain growth occurs. With a fine grain size, powder metallurgy beryllium possesses relatively good room temperature ductility. However, the reason for this is not clear.

Although some correlation exists between oxide content and mechanical properties of beryllium[2], relatively little is known in detail about the role of the oxide. Work has been done on the oxidation rate of beryllium[3] and on the structure and growth of the oxide crystals[4], but little attention has been given to the condition of oxide layers or film-metal interface. A coherent protective film of molar volume greater than the base metal is probably formed around individual grains before compacting, and calculation shows that the average thickness should be about 300A[5] Boundary inclusions have been observed by electron microscopy[6], but only very limited work has so far been done on the morphology of oxides in beryllium[7,8].

4-1.2 Method of Investigation. The principal difficulty in determining the morphology of oxides or other inclusions in beryllium is that of unequivocal identification. Many of the inclusions are submicroscopic in size, therefore requiring electron microscopy for observation. In such a complex system as powder metallurgy beryllium, a systematic investigation is needed to ensure identification of different types of inclusions.

The problem was pursued in three directions

(1) improvement of techniques for preparation of specimens and replicas;

(2) examination of some of the complex systems of beryllium;

(3) preparation and examination of simplified systems of beryllium with beryllium oxide.

Since Manufacturing Laboratories does not have the facilities for safe handling of beryllium, most of the bulk specimen preparation and all of the metallographic preparation were undertaken by Nuclear Metals, Inc.

4-2 EXPERIMENTAL PROCEDURES AND RESULTS

4-2.1 Development of Techniques. The most readily available specimens at the beginning of this study were from a series of solution treated, quenched and aged samples of hot-extruded QMV rod. These were employed in checking and developing the techniques needed for electron microscopy.

These samples were given standard metallographic preparation and then cathodically etched in an argon atmosphere. This resulted in surfaces with numerous inclusions, precipitates, and boundaries that were visible, because of surface relief, even without the use of polarized light (Figure 32). While relief is necessary for electron microscopy, the brittle nature of the protruding particles resulted in some replication difficulties.

A convenient, general purpose, replication method is a double replica technique in which the primary replica is obtained by pressure molding with hot polyethylene. Unfortunately, with the specimens used, this resulted in gross surface distortions and the removal of most of the free inclusions. Films continuous over some sections of boundaries and 0.2 - 0.5μ wide were occasionally found (Figure 33), but the resolution of structural details was not good, probably because of distortion of the sample.

A number of techniques using dissolved plastics for the primary replica were explored. It was found that some of these after drying could be stripped from the sample by a softened thin cellulose acetate tape; Formvar replicas, thus removed, proved to be the most satisfactory. The amount of disturbance of the surface features was checked quantitatively, and less than 2% of the surface features 0.5μ or larger in size was found to be affected even after four replications using this technique.

Manipulations in and variations of the Formvar technique were developed to ensure that pits, voids and inclusions could be correctly differentiated, and that specific areas on the specimen could be examined on the electron micrographs. The veracity of the Formvar technique was checked by replicating some specimens with both Formvar and carbon and comparing the results. It was found that, except for a slight loss in contrast and definition, the much more easily obtained Formvar replicas were almost identical with carbon replicas. The Formvar method was therefore used throughout the rest of the investigation.

In the initial development of the Formvar replica technique, it was noted that the appearance of the specimens was very non-uniform and it was difficult to determine what might be "characteristic" about the structure. Since quite different structures were found after re-preparation of specimens, it was necessary to investigate the methods of metallographic preparation in more detail. It was learned that many of the observed features originated as polishing artifacts, and that others originated so early in the cathodic etching process that they might well be artifacts. It was also observed that the attack-polishing normally employed in metallographic preparation gives considerable relief and therefore is advantageous for electron microscopy. The most successful method of preparation found is the following variation of that of Boyd and Richards[9]:

(1) Grind specimen successively through 400 grit SiC paper.

(2) Attack-polish on a fast silk lap using 5% oxalic acid and Linde "A" abrasive.

(3) Attack-polish on a fast Gamal covered lap using dilute bright dip[10] and Linde "B" abrasive.

Figure 32 - Cathodically etched, solution treated, quenched and aged beryllium hot extruded from QMV -200 mesh powder.

EP1333A 23302-36T1 20,000X

Figure 33 - Electron micrograph of specimen shown in Figure 4-1.

(4) Chemically attack on the lap of stage (3), using a small amount of bright dip only for several seconds, and repeat if necessary.

This metallographic preparation can result in a generally smooth surface on the beryllium, but such a surface was not consistently obtained. Furthermore, inclusions were frequently removed by polishing, and the positive distinction of the resulting depressions from pits and voids that are normally encountered in powder metallurgy products of less than theoretical density could not always be made.

4-2.2 Examination of Precipitates. In order to identify the precipitates in powder metallurgy beryllium by their structural characteristics, a number of precipitates in a piece of vacuum melted Pechiney beryllium and in a piece of vacuum melted beryllium of uncertain history (probably QMV) were examined in some detail. Figure 34 shows an aluminum-silicon mixture in the latter beryllium, as identified from light microscopy, by color and morphology[11], and Figure 35 shows a somewhat similar appearing but smaller area in the Pechiney beryllium that may also be an aluminum-silicon mixture.

Within the aluminum-silicon mixture of the unidentified beryllium (Figure 34) are several polygonal particles which display a smoother surface than, and protrude from, the mixture. These are not carbide particles, a striking example of which is shown in Figure 36, but probably are silicon or iron-beryllide. It was also noted in the unidentified beryllium that there was a definite tendency for voids to be associated with groups of these particles. Furthermore, voids were sometimes present in groups or strings. All such voids were probably caused by solidification contraction.

4-2.3 Precipitates and Inclusions in Solution Treated and Aged Beryllium. It has been found that mechanical properties of commercial beryllium can be modified by solution treating and aging[12]. Gelles and Wolff[13] followed the aging by measuring changes in electrical resistivity and showed by X-ray diffraction that this was related to an increase in the quantity of precipitates, although these could not be identified. Electron microbeam probe work indicated increased segregation, possibly at grain boundaries, of iron, aluminum and silicon due to aging treatment.

Two specimens of Gelles and Wolff's series were examined in detail for distribution of inclusions and precipitates. The specimens had been hot extruded (30:1 reduction at 1950°F) from cold compacted Brush QMV -200 mesh beryllium powder, solution treated for 1 hour at 1100°C and quenched. One specimen was in the as-solution-treated condition; the other specimen had been aged 4 weeks at 600°C, which gives the maximum aging effect as determined by the change in electrical resistivity.

The specimens were prepared by the previously described polishing technique. Initial electron microscopic examination showed that there were no major differences in the appearance of the specimens, and that grain boundaries were not in sufficient relief to enable them to be located in the elctron micrographs (Figure 37). Many

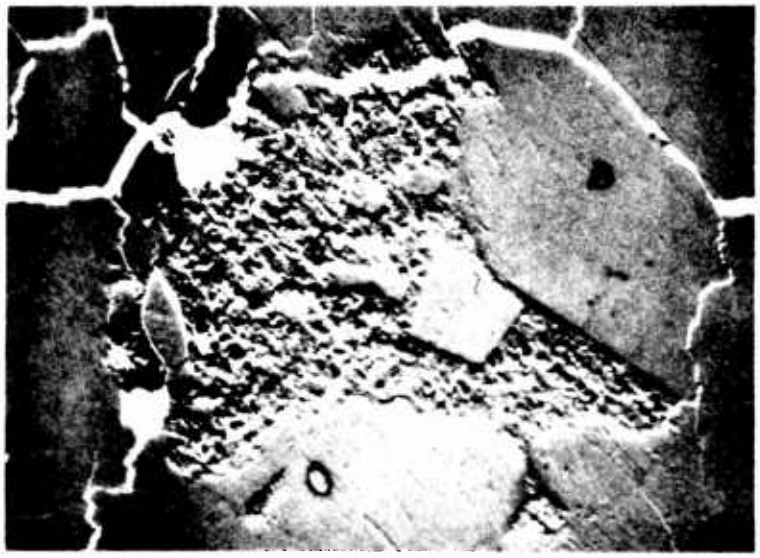

EP1800D PfBe-1B2-B-F2 7,500X

Figure 34 - Group of precipitates in vacuum melted beryllium (probably aluminum-silicon mixture interspersed with other precipitates of regular shape).

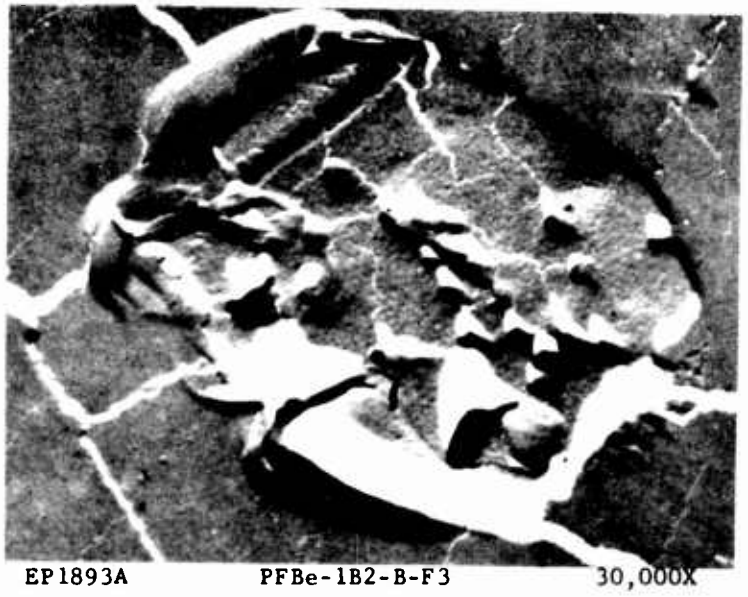

Figure 35 - Unidentified precipitate in vacuum melted Pechiney flake beryllium (precipitate is probably harder than the beryllium matrix, since it protrudes above the plane of polish).

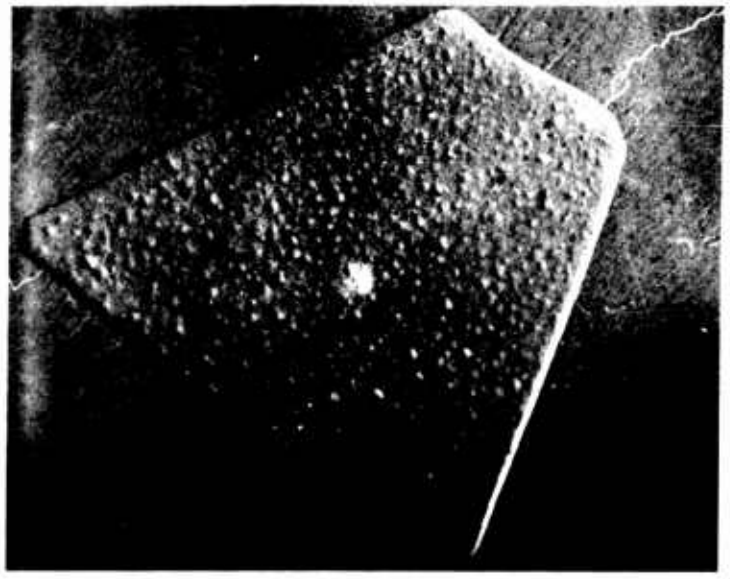

EP1800E PfBe-1B2-B-F3 7,500X

Figure 36 - Particle tentatively identified as beryllium carbide found in vacuum melted beryllium, showing the surface texture and polygonal shape.

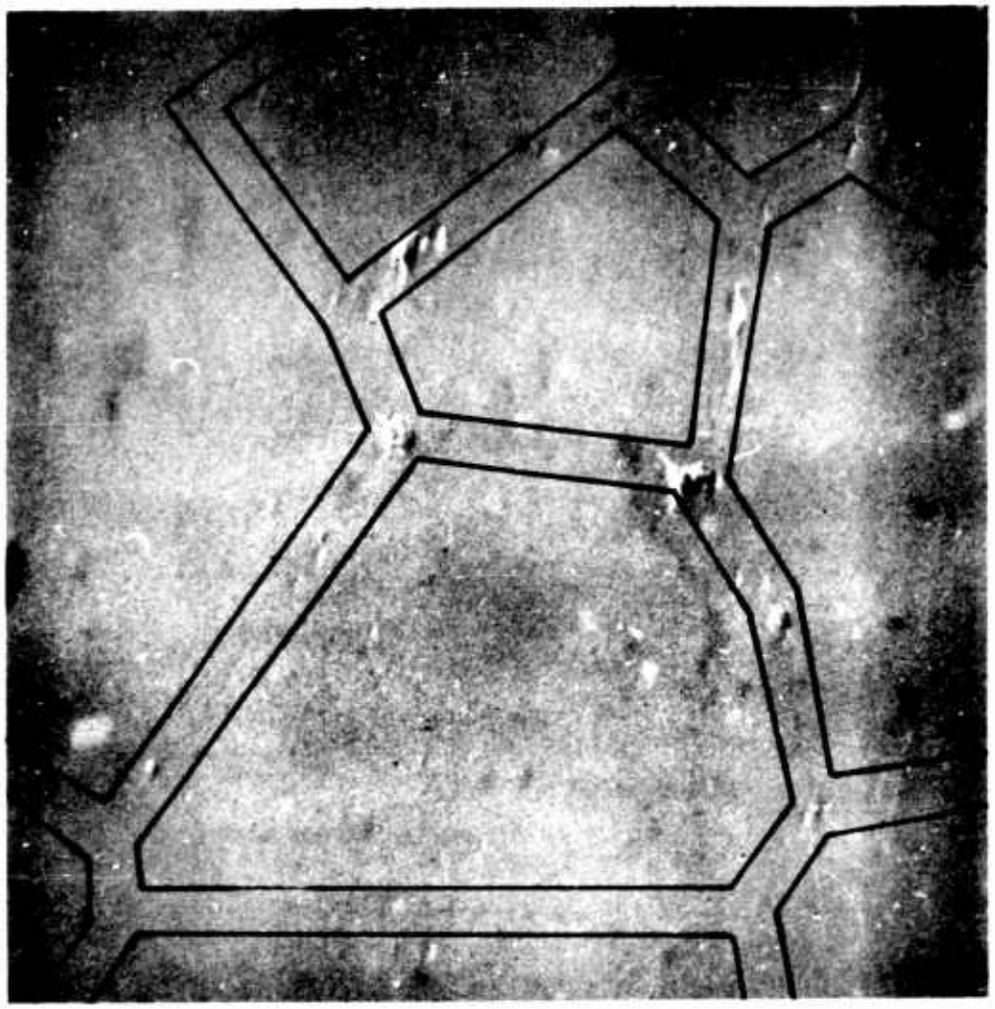

EP2177C 23302-6T2-F3 10,000X

Figure 37 - Solution treated and aged beryllium that had been hot extruded from Brush -200 mesh QMV powder. The paired lines border the approximate location of grain boundaries as determined from polarized light metallography.

of the precipitates and inclusions were not retained on the surface of the specimens, but were represented by pits and voids. A large fraction of the inclusions had regular shapes, which were often six-sided (Figure 38). Occasional voids also corresponded to these shapes. The size of these features ranged from 0.1 - 0.4μ. Pits were usually rounded or irregular shaped and ranged in size from 0.03 - 0.1μ with a rare occurrence of sizes up to 0.6μ. These features appeared to be disconnected, so that it was not in general possible to locate the grain boundaries from them in the electron micrographs. Since the relative amounts of inclusions and precipitates at grain boundaries and within the matrix were of interest, it was necessary to determine the position of the grain boundaries. It was possible to approximately locate such boundaries by matching electron micrographs with polarized light photographs.

It was found that the six-sided precipitates (which were mostly raised above the plane of polish) only appeared at grain boundaries, and with about the same frequency in both specimens. The appearance of these particles suggests the outline of the prism planes of a hexagonal crystal that is elongated along one "a" axis, which is aligned approximately 30° to the grain boundary in the plane of polish. It was further noted (taking the hexagonal shape as an approximation), that the "basal planes" appeared randomly oriented in the solution treated specimen and predominantly perpendicular to the extrusion direction in the aged specimen. Although these precipitates somewhat resemble the beryllium carbide identified previously in another specimen, both their frequency and presence at the grain boundaries suggest that they may be oxides.

Because of the high magnifications needed to observe inclusions and pits in the specimens, only relatively small areas of 100 - 150μ^2 revealing about 50μ of grain boundaries could be surveyed in detail. Based on the limited data this provided on the density of inclusions and pits in grains and grain boundaries, only one apparently significant difference between the two specimens was found. The density of large and medium size pits within the grains decreased drastically on aging, from 0.7/μ^2 to 0.1/μ^2. This may have been caused by a change in etching characteristics on aging, or by solution of particles with possible migration of the dissolved constituents to the grain boundary.

4-2.4 Examination of Surface Oxides. Simplified beryllium-beryllium oxide systems were prepared by surface oxidizing of small solid specimens at elevated temperatures. In order to reduce the complexity still further, commercial high-purity beryllium, produced as flake by Pechiney in France, was used as the starting material. It was anticipated that a substantial oxide layer could be produced, thereby presenting an opportunity for detailed examination of the metal-oxide interface in the as-oxidized condition.

Oxidation times and temperatures were selected on the basis of weight gains[3,14] in order to obtain a range of thicknesses. The specimens were prepared from vacuum melted Pechiney flake by 2-hour exposures to tank oxygen at 1 atmosphere at temperatures of 500, 600, 700 and 800°C. The surface of these specimens was quite irregular and contained numerous pits. This did not seem to be connected with prior surface preparation, since it was not ameliorated by

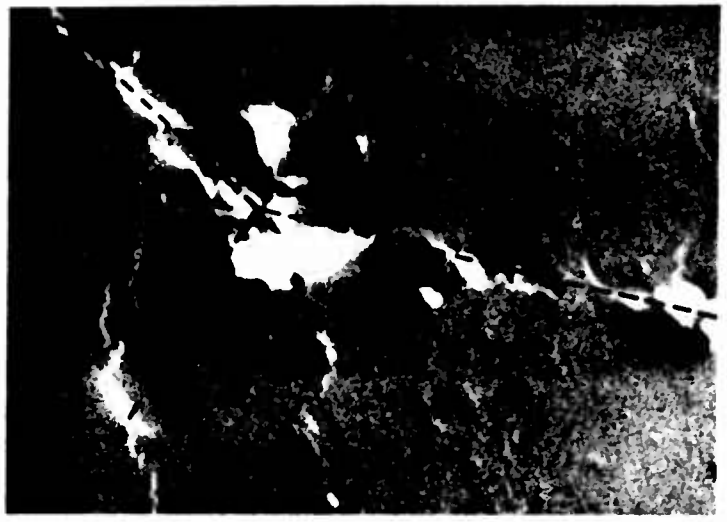

EP2054C 23302-30T2-F2 40,000X

Figure 38 - Large six-sided particles in grain boundaries of solution treated beryllium that had been hot extruded from Brush -200 mesh QMV powder. Grain boundaries are indicated by lines. A number of small pits can also be seen within the grains.

metallographic polishing before exposure. The pits were mostly of regular shape. They were usually considerably larger and more widely spaced when formed at the higher temperatures. The orientation of the pits varies from grain to grain. A few of the pits exhibited steps spaced about 0.1μ apart (Figure 39); however, most of the pits were more irregular and did not exhibit steps (Figure 40).

The lower temperature specimens did not differ substantially from these; in fact, the differences between two specimens oxidized at the same temperature often was greater than that between specimens oxidized at different temperatures.

The observations in a recent extensive investigation[14] of high temperature oxidation of beryllium are in consonance with the variations in oxidation and other variations observed during the present work. In the work cited, oxidation rates of individual specimens at the same temperature were found to differ greatly, although the kinetics for each specimen were self-consistent. Small discontinuities were found in the oxidation rates, and the authors concluded that the oxide may not be completely protective above 500°C. It was stated that no evaporation of the metal occurred, and, at least after long exposure at 700°C, blistering of the surface was observed. Subsequent work[15] by the same authors showed that, at least in wet oxygen, pitting occurred and corrosion products appeared below the surface.

The appearance of the specimens examined in the present investigation suggests two processes:

(1) Penetration of the oxygen along crystallographic planes of the base metal. This has been observed in the oxidation of tantalum[16] and has been attributed to either dislocation-enhanced diffusion or dislocation-aided nucleation.

(2) A subsequent detachment of some oxide and/or beryllium from the surface.

(1) Oxides Protected by Plating. In order to examine the interface between metal and oxide in section, it was necessary to protect the outer surface during metallographic preparation. Vacuum coating of the outer surface was used for this purpose. Initial attempts at vacuum plating were made with chromium, Nichrome, copper and nickel. Of these, only Nichrome and nickel adhered satisfactorily, and a sufficient thickness of nickel could not be achieved. The plating was protected during sectioning by butting a flat piece of beryllium against the sample, and this assembly was prepared metallographically. The Nichrome deposit was found to be below the plane of polish of the beryllium pieces after metallographic preparation. Considerable difficulty was encountered in subsequent replication because of this difference in level; it was not possible to completely replicate the Nichrome deposit and its interfaces with the beryllium pieces without the occurrence of some defects or artifacts in the replica. These difficulties were somewhat reduced but not completely eliminated by a number of improvements in the replication technique. After a number of trials it was possible to examine identical regions on two or more replicas, which increased confidence in the observations made. Location 1 of Figure 41 is ascribed to the Nichrome deposit.

EP1389B PFBe-1A 5,000X

Figure 39 – Pit in surface of vacuum melted beryllium that was oxidized 2 hrs. at 800°C.

EP1390C PFBe-1A 30,000X

Figure 40 - Corner of typical pit in surface of vacuum melted beryllium that was oxidized 2 hrs. at 800°C.

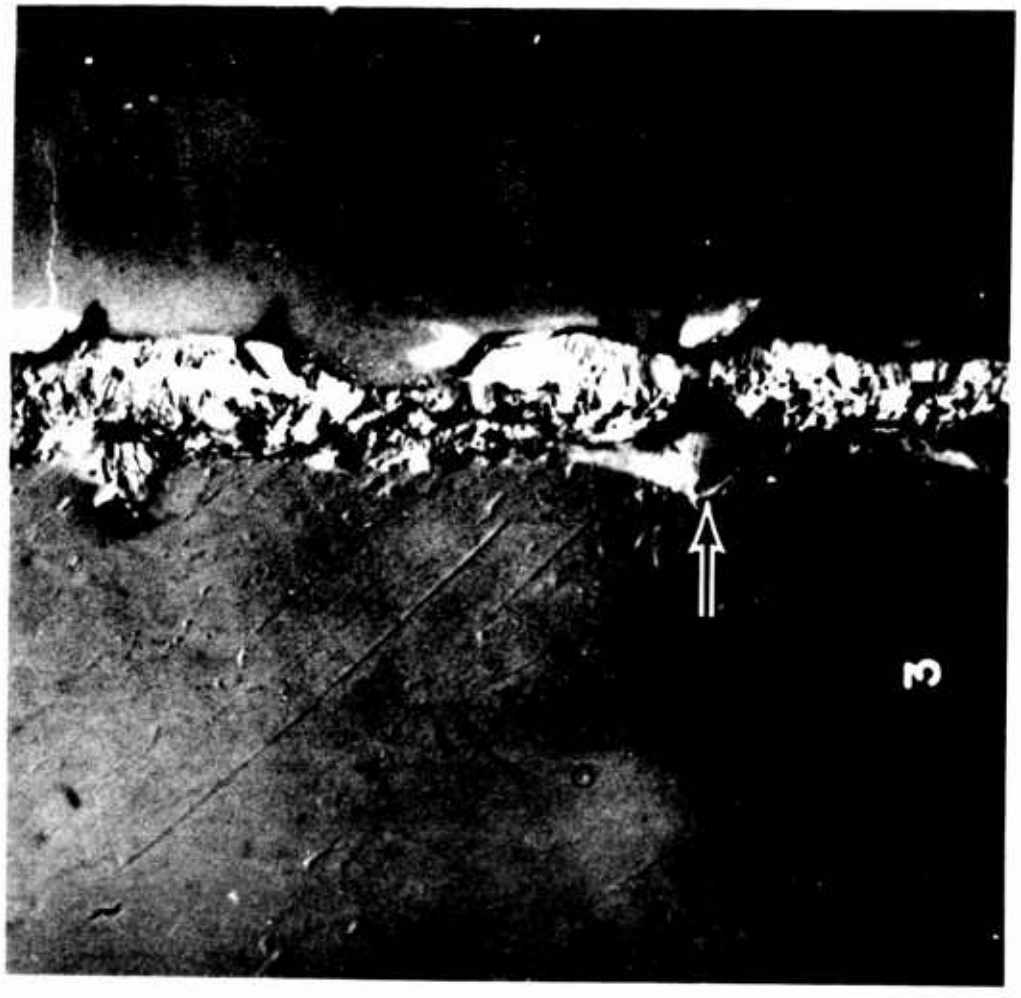

EP1191E PFBe-1B2-B-F5 25,000X

Figure 41 - Assembly consisting of surface-oxidized beryllium, nichrome deposit, and beryllium backing piece (see text for explanation).

Location 2, which resembles a boundary, probably represents a crack between the specimen and the Nichrome deposit. Location 3, within the vacuum melted and oxidized Pechiney beryllium, contains a number of pits and short, often curved markings in addition to long straight polishing scratches. The short markings were reproduced in detail in those replicas where the same area could be obtained, therefore it is certain that they are not replication artifacts. Among the pits and resembling them, occasional raised features (circled in Figure 41) were detected. One unusual area was observed where nearly half of the pit-like features were raised.

The beryllium backing piece was also examined in the region adjoining the Nichrome deposit. In general, this piece contained none of the pits and short markings that were found near the oxidized surface of the Pechiney beryllium. The only exception occurred in an area next to the unusual area in the Pechiney beryllium, and therefore was discounted.

The region of the pits and short markings was confined to a depth of about 6 - 10μ from the surface of the oxidized Pechiney specimen. This region might be either an artifact of specimen preparation, or a feature of the Pechiney beryllium associated with the surface oxidation treatment. The evidence is insufficient to discriminate between these possibilities.

Figure 41 also shows the polyhedral pits on the surface of the oxidized Pechiney specimen. These pits, indicated by an arrow, were not completely filled with Nichrome deposit and therefore appear as triangular forms near the interface.

If a crack is present at the surface of a specimen at the time of oxidation, it is reasonable to expect that the internal surfaces of this crack would be oxidized. Therefore, in addition to areas near the oxidized surface, a number of cracks starting from the surface were examined. No evidence of an oxide layer could be found. However, it is not certain whether any of the cracks examined were present in the specimen at the time of oxidation or whether they all occurred subsequently.

Because of the lack of interference colors on the surfaces of the oxidized specimen, it seems possible that the oxidation treatment resulted in a layer thinner than the 500 - 1500 A that was anticipated from the oxidation treatment. Furthermore, it appeared that polishing an assembly of three materials, beryllium, beryllium oxide and Nichrome, would not provide a sufficiently planar surface to permit detailed examination of the metal-oxide interface. Therefore, investigation of these specimens was terminated.

(2) Pressure Welds of Oxidized Surfaces. The bonding of two oxidized surfaces appeared to be the most logical method of observing an oxide at a definitely identifiable location without the disadvantages introduced by protective layers of a second metal.

A series of specimens of cylindrical shape were prepared from an extruded rod of doubly vacuum melted Pechiney Flake beryllium. Flat surfaces were metallographically prepared by grinding through 4/0 papers, diamond polishing with 1μ abrasive, bright dipping[14] for 30 seconds at 100°C, and rinsing in distilled

water and alcohol. The oxidation was carried out at 550°C for 5 hours in a previously evacuated tube that had been backfilled to 1/3 atmosphere with purified oxygen.

The oxidation conditions were chosen to give a layer of the order of 500 to 1000 A[3,14] under the expectation that this would be adherent. All specimens after oxidation exhibited colored films on the polished surfaces, with the colors ranging from iridescent blue to mottled brown. Especially in specimens of the latter coloration, adjacent grains were distinguishable by color; even within a single grain, however, there was a range of colors of the surface film. Such appearances roughly confirm the expected magnitude of oxide thickness[17] and also indicate that the films were not uniform.

Several unsuccessful attempts were made to achieve bonds between two oxidized surfaces by uniaxial loading at elevated temperature. It was therefore decided that hydrostatic pressure, in which the flow stress of beryllium could be exceeded, would be necessary for bonding. Subsequent runs were made in the high pressure apparatus, shown in Figure 42, at Manufacturing Laboratories, Inc. In this apparatus, the specimens must be protected from reaction with the cell components, for which a platinum foil wrapping was tried at first. A temperature of 1150°C and a pressure of 10 kilobars (for one hour) were chosen for the first hydrostatic pressure weld. Because of failure of the platinum/platinum-rhodium thermocouple, the first run exceeded the planned temperature. In excess of 1500°C was reached, as evidenced by phase transformation in the pyrophyllite of the surrounding cell. The specimen, when recovered, appeared to have melted.

Since the cause of the thermocouple failure was not evident, a repeat of the first run was made. Instead of increasing the power to the specimen cell to compensate for the lower apparent temperature, as was done for the first run, the power was held constant at the level that first gave a temperature reading of 1150°C. The outer surfaces of the successfully welded specimens showed evidence of reaction with the platinum of the protective foil and thermocouple, but the reaction products did not penetrate appreciably along the plane of the weld.

The problem created by the reaction of the beryllium specimens with platinum was subsequently eliminated by substituting tantalum as the protective foil. This resulted in only a slight reaction, and the thermocouple was unaffected.

Since the cylindrical specimens were not fully supported around their circumference during the initial high pressure loading, some plastic deformation occurred. Therefore, the specimens were measured before and after the welding runs.

Figure 43 shows a micrograph, taken with polarized light, of the sectioned specimen produced by the second run. The plane of the weld can be clearly distinguished by its trace, which is the horizontal line near the center. The welded beryllium pieces underwent considerable grain growth during the process, the grain size increasing from a range of 0.01 - 0.1 mm to 0.3 - 1.0 mm. The oxide layer served as a very effective grain growth inhibitor; no grains crossed the bond plane. Electron microscopic examination of the specimen bonded at 1150°C showed that the oxide was not in the form of a continuous film, but rather consisted of a series

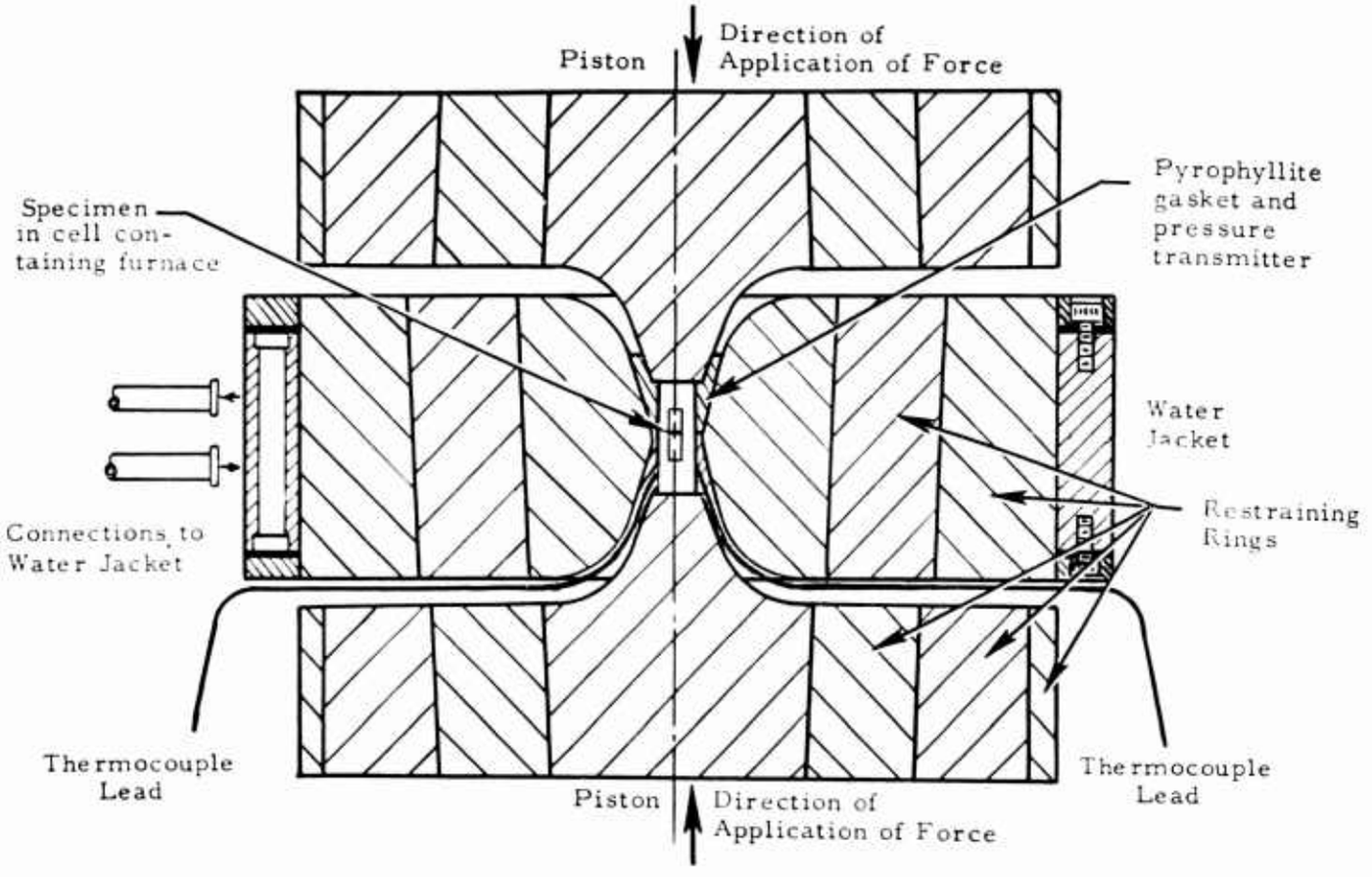

Figure 42 - High pressure apparatus used for pressure welding surface-oxidized beryllium specimens.

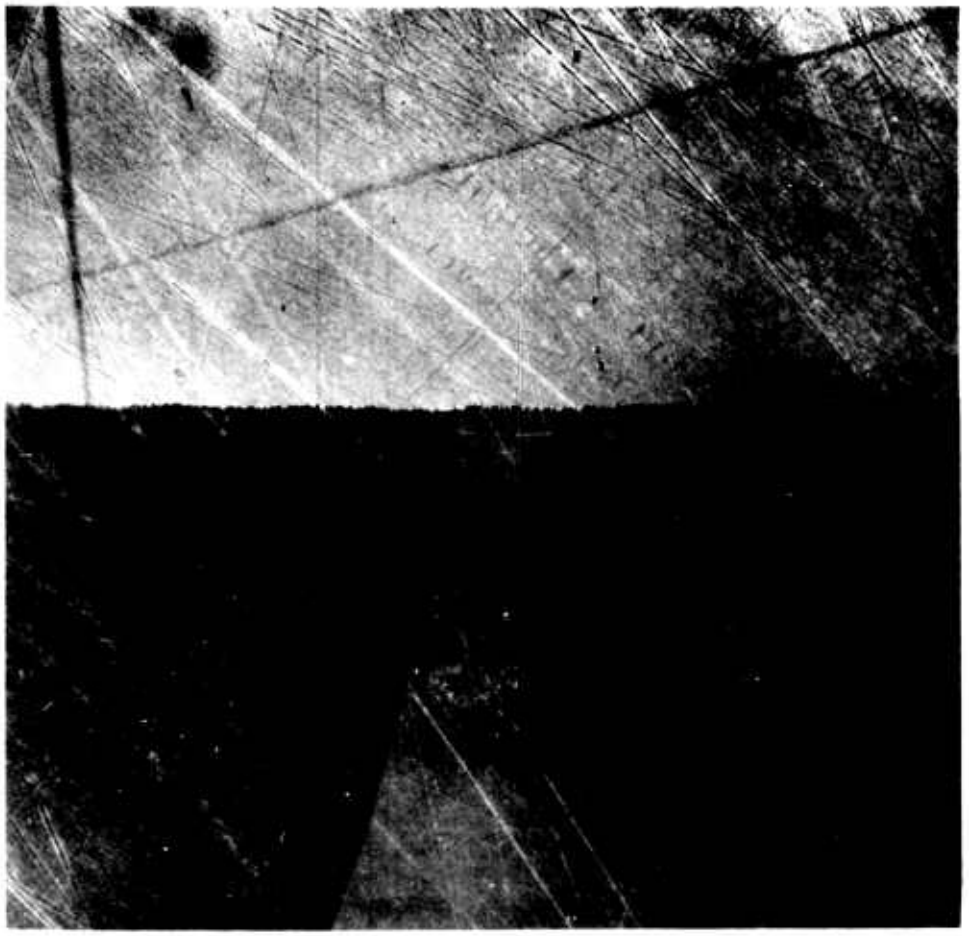

LD19-121 1151-3-DC-BC 1000X

Figure 43 - Section transverse to weld interface in surface-oxidized beryllium pressure welded at 1150°C and 10 kilobars for one hour (polarized light).

of disconnected particles, many of which were removed in polishing (Figure 44, 45 and 46). The replicas of Figures 44 and 45 were shadowed approximately along this layer, with a shadow angle of 27°. The voids, which apparently represent oxide particles, range in size from about 0.25μ to an occasional 3μ, and are spaced 0.5 - 5μ apart; the larger spacing is associated with the larger particles. The void appearance suggests coagulation or spheroidization of the oxide layer. Since the outlines of the voids are indistinct, an accurate measurement of the original thickness of the layer cannot be made. However, assuming the original oxide was a uniform film of equal thickness of both oxidized surfaces, a reasonable estimate of the original film thickness is 400 - 2000 A, which is in good agreement with the previously mentioned estimates. Figure 46 shows a replica in which the shadow direction was perpendicular to the trace of the weld plane. An unusually acute shadow angle (12°) was used to accentuate elevations. The replica was from the same region as the one of the previous two figures. The weld surface as a whole protrudes slightly above the plane of polish; probably because the presence of the oxide caused some retention of the surrounding beryllium. The particulate form of the oxide is again observed, with the majority of the particles represented by pits or voids.

Another pressure welding run was made using a temperature of 800°C and a pressure of 5 kilobars for 1 hr., so chosen to reduce spheroidization of the oxide and grain growth in the beryllium. This resulted in a very successful bond. Since there was little reaction with the tantalum protective foil, it was possible to determine that the linear extension parallel to the plane of the weld was less than 5%. It is believed that the deformation in the previous run was about the same.

Figures 47 and 48 show light and electron micrographs of the specimen bonded at 800°C. There appears to have been some grain growth at the bonding temperature, yielding grain sizes ranging from 0.01 - 0.2 mm. However, a number of the grains still exhibit the strained appearance of unrecrystallized material and some of them have large mechanical twins undoubtedly caused by deformation in the high pressure apparatus. No grains were found to cross the bond plane. The appearance of the weld plane was found to differ substantially from that of the specimen bonded at 1150°C, apparently since no spheroidization occurred. The weld was delineated by numerous short parallel depressions. These were found to be about 0.2μ long, 0.05μ wide and spaced about 0.1μ apart. Since the presence of the oxide layer in the form of a series of parallel rods is extremely unlikely, the appearance of the weld is interpreted as showing a fairly continuous layer, with the short grooves caused either by a peculiar fracturing characteristic of the as yet unrecrystallized beryllium oxide[2] or, more likely, by scratches in the oxide layers caused by polishing. The length of these marks again approximately confirms the anticipated thickness of the oxide layers.

4-3 CONCLUSIONS

(1) The most successful approach to the study of oxides in powder metallurgy beryllium has been pressure welding of surface-oxidized beryllium specimens.

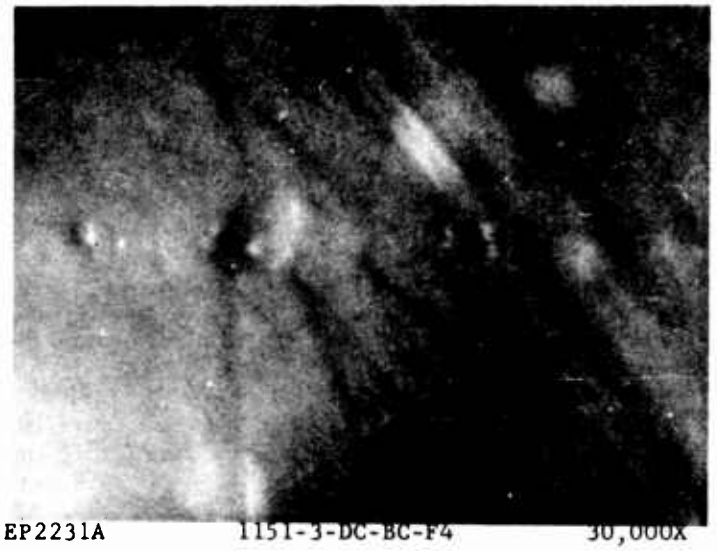

Figure 44 - Weld interface in surface-oxidized beryllium pressure welded at 1150°C and 10 kilobars for 1 hr. Shadow along trace of weld plane; shadow angle, 27°

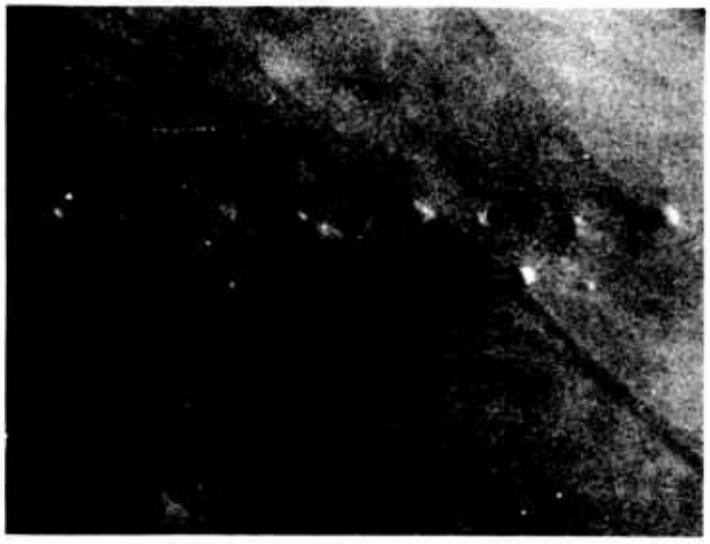

EP2233A 1151-3-DC-BC-F4 30,000X

Figure 45 - Weld interface in surface-oxidized beryllium pressure welded at 1150°C and 10 kilobars for 1 hr. Shadow along trace of weld plane; shadow angle, 27°

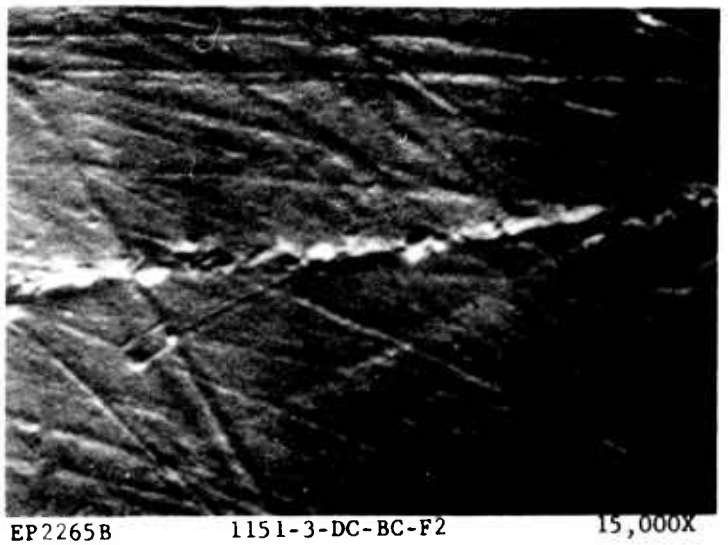

Figure 46 - Weld interface in surface-oxidized beryllium pressure welded at 1150°C and 10 kilobars for 1 hr. Shadow perpendicular to trace of weld plane; shadow angle, 12°.

LD19-122 1151-3-DC-GE 500X

Figure 47 - Section transverse to weld interface in surface-oxidized beryllium pressure welded at 800°C and 5 kilobars for 1 hr (polarized light).

EP2269E 1151-3-DC-GE-F2 30,000X

Figure 48 - Weld interface in surface-oxidized beryllium pressure welded at 800°C and 5 kilobars for 1 hr.

(2) Evidence was found that if the pressure welding is carried out below about 1000°C, a fairly continuous oxide layer is formed; whereas at higher temperature the oxide may take a spheroidized form.

(3) Oxide films present during pressure welding appear to act as grain growth inhibitors, which is a useful function in powder metallurgy beryllium.

(4) Metallographic preparation appears critical with respect to retaining oxides prior to replication for electron microscopy.

4-4 RECOMMENDED FUTURE WORK

The most successful approach of this work, using surface-oxidized, pressure-welded specimens to yield a predetermined location of oxide layer, should be followed further to elucidate the behavior of oxide in beryllium.

(1) The investigation of an oxide layer in the form of a film should be extended, with checks on the electrical resistivity of the junction.

(2) The investigation of the coagulation or spheroidization of the oxide layer should be extended to yield information on the kinetics of spheroidization and grain boundary diffusion.

(3) The effect of the oxide layer in inhibiting grain growth should be investigated. The important variables are believed to be the thickness and continuity of the layer and the size and spacing of the oxide particles.

(4) The effect of deformation on the morphology of the oxide, especially after heat treatment, should be studied.

4-5 ACKNOWLEDGEMENTS

Mrs. Imogene DiBello performed all the electron microscopy and associated tasks, James E. Boyd assisted with metallographic preparation and Bernard S. Lement assisted with the technical direction of the program.

REFERENCES

1. W. W. Beaver, Fabrication of Beryllium by Powder Metallurgy, The Metal Beryllium (D. W. White, Jr. and J. E. Burke, Eds.), Amer. Soc. Metals, Cleveland, 1955.

2. G. E. Darwin and H. H. Buddery, Beryllium, Academic Press, New York, 1960.

3. E. A. Gulbransen and K. F. Andrew, The Kinetics of the Reactions of Beryllium with Oxygen and Nitrogen and the Effect of Oxide and Nitride Films on its Vapor Pressure, J. Electrochem. Soc., 97:383 (1950).

4. I. S. Kerr and H. Wilman, The Structure and Growth of Oxide Layers Formed on Beryllium, J. Inst. Metals, 84:379 (1956).

5. J. L. Klein, V. G. Macres, D. H. Woodard, and J. Greenspan, Ductility of Beryllium as Related to Preferred Orientation and Grain Structure, The Metal Beryllium (D. W. White, Jr. and J. E. Burke, Eds.) Amer. Soc. Metals, Cleveland, 1955.

6. R. Syre, A. Saulnier, and M. Perez, Comparison des demiproduits en béryllium préparés à partir de métal coulé ou à partir de poudre frittée, Rev. Métall., 56:359 (1959).

7. A. Saulnier and P. Mirand, Determine par micrographie électronique de la répartition de l'oxyde dans le béryllium fritté, Comptes rendus, 250:3834 (1960).

8. A. Saulnier, Étude structurale du béryllium, J. of Nuclear Materials, 2:299 (1960).

9. J. E. Boyd and J. F. Richards, An Improved Technique for Metallographic Preparation of Beryllium and Beryllium Alloys, Metal Progress, in press.

10. C. O. Matthews, Lockheed Aircraft Corp., LMSD 5099, October 1958.

11. A. R. Kaufmann, P. Gordon and D. W. Lillie, The Metallurgy of Beryllium, Trans. ASM, 42:785 (1950).

12. D. R. Mash, Aging Effects in Commercially Pure Beryllium, J. of Metals, 7:1235 (1955).

13. S. H. Gelles and A. K. Wolff, Impurity Effects in Commercially Pure Beryllium, NMI-1238, Nuclear Metals, Inc., February 10, 1961.

14. D. W. Aylmore, S. J. Gregg, and W. B. Jepson, The High Temperature Oxidation of Beryllium, Part I, in Dry Oxygen, J. of Nuclear Materials, 2:169 (1960).

15. D. W. Aylmore, S. J. Gregg and W. B. Jepson, The High Temperature Oxidation of Beryllium, Part III, in Wet Oxygen, J. of Nuclear Materials, 3:190 (1961).

16. R. Bakish, Metallographic Manifestation of the Air Oxidation of Tantalum at 750°C, J. Electrochem. Soc., 105:71 (1958).

17. F. H. Constable, The Cause of the Colours shown during the Oxidation of Metallic Copper, Proc. Roy. Soc., 115A:570 (1929).

SECTION 5

A STUDY OF THE BRITTLE BEHAVIOR OF BERYLLIUM BY MEANS OF TRANSMISSION ELECTRON MICROSCOPY

F. Wilhelm and H. G. F. Wilsdorf

(The Franklin Institute, Philadelphia, Pennsylvania)

ABSTRACT

The electron microscope was used to study glide dislocations directly in deformed beryllium. After developing techniques which permitted the production of electron-transparent specimens from bulk beryllium, two materials with different impurity content were investigated.

Glide dislocations in vacuum melted Pechiney flake beryllium exhibited different features that depended greatly on the history of the samples; i.e., whether they were carefully furnace cooled from the annealing temperature or whether they were quenched. A strong resistance to glide was clearly discernible from all results.

In furnace-cooled single crystals of commercial purity, very small precipitates that affected dislocation motion very decisively were detected. "Bend-planes" that are considered to be the cause for early fracture of this material have been observed.

The frictional force of dislocations was deduced to be very high in both the vacuum melted Pechiney flake and commercial purity materials.

5-1 INTRODUCTION

This project was undertaken to investigate the factors that contribute to the brittle behavior of beryllium. It was proposed to examine dislocation patterns in deformed beryllium having different impurity contents by means of a new experimental technique that allows dislocations to be seen directly in electron micrographs of high resolution and magnification. The only previous study of dislocations in beryllium found in the literature was carried out by Baird, Hartree and Phillips, who examined undeformed polycrystalline beryllium flakes and single crystals of beryllium of unspecified purity.(1)

5-2 PREPARATION OF SPECIMENS FOR DIFFRACTION ELECTRON MICROSCOPY

Beryllium samples having dimensions 12 x 12 mm or larger and 0.5 - 1.2 mm thick were received from Nuclear Metals, Inc. Subsequent cutting and polishing of the samples was done electrolytically. All samples that were to be heat treated were cut into strips approximately 6 mm wide and electropolished to remove surface twins and other surface damage; the strips were heat treated after being placed in quartz tubes that were evacuated and filled with Purgon (pure argon). After heat treatment, the specimens were mechanically strained if this was required for the particular experiment.

One of the main problems in studying dislocations in the beryllium specimens by means of transmission electron microscopy was in finding a suitable method of thinning the specimens to a final thickness of 1000 - 5000 Å. In the process developed, a small depression was first electrolytically etched in the center of the specimen by means of a fine jet stream of dilute nitric acid. With a current of approximately 100 ma flowing, the center portion was thus thinned down to approximately 50 - 100 μ. The specimen was then cut to size (3 x 3 mm) so that it fitted into the specimen holder of the electron microscope. An electrolytic jet that ejected a thin, extended stream of dilute HNO_3 against the specimen permitted fairly accurate and fast cutting.

After cutting to size, the whole specimen was thinned down electrolytically in the apparatus shown in Figure 49. The beryllium specimen, which was held in the electrolyte by aluminum tweezers (protected by Microstop lacquer), formed the anode, while a thin plate of stainless steel covering the bottom of the cell served as the cathode. A strong light beam was focused on the specimen from below (through a small hole in the cathode). The specimen was observed constantly by means of an optical microscope of about 50X magnification until the first breakthrough of light was detected at the center. At this moment the specimen was removed from the bath, washed and dried. An area both large enough for study and thin enough for electron transmission was usually produced. The electropolishing solution consisted of 100 parts orthophosphoric acid, 30 parts concentrated sulphuric acid, 30 parts ethanol and 30 parts glycerol. This bath was agitated and kept at room temperature. The electropolishing process was slow; the reduction in thickness being approximately 4 μ per hour. A voltage of between 1 and 15 volts was employed, resulting in a current density of approximately 20 ma/cm^2. The current observed was remarkably independent of the cell voltage; the current density remained almost unchanged between 2 and 20 volts (Figure 50). Best polishing was obtained between 10 and

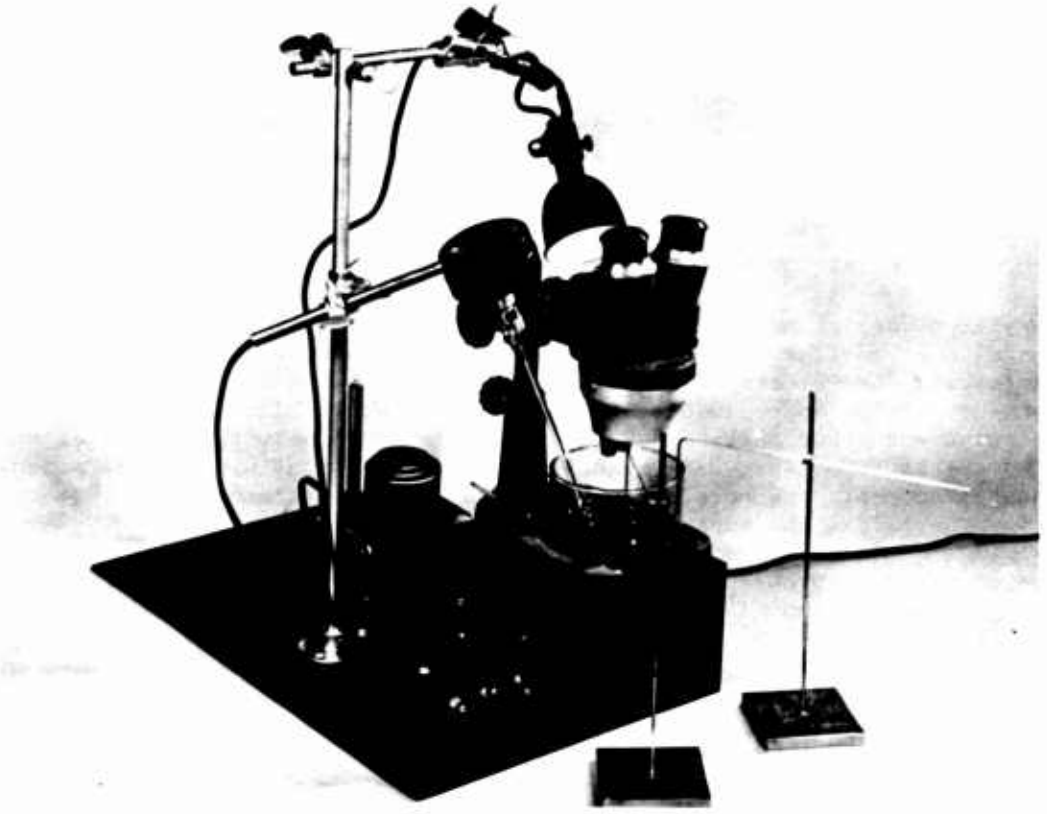

Figure 49 - Electropolishing apparatus used for the preparation of thin specimens for transmission electron microscopy.

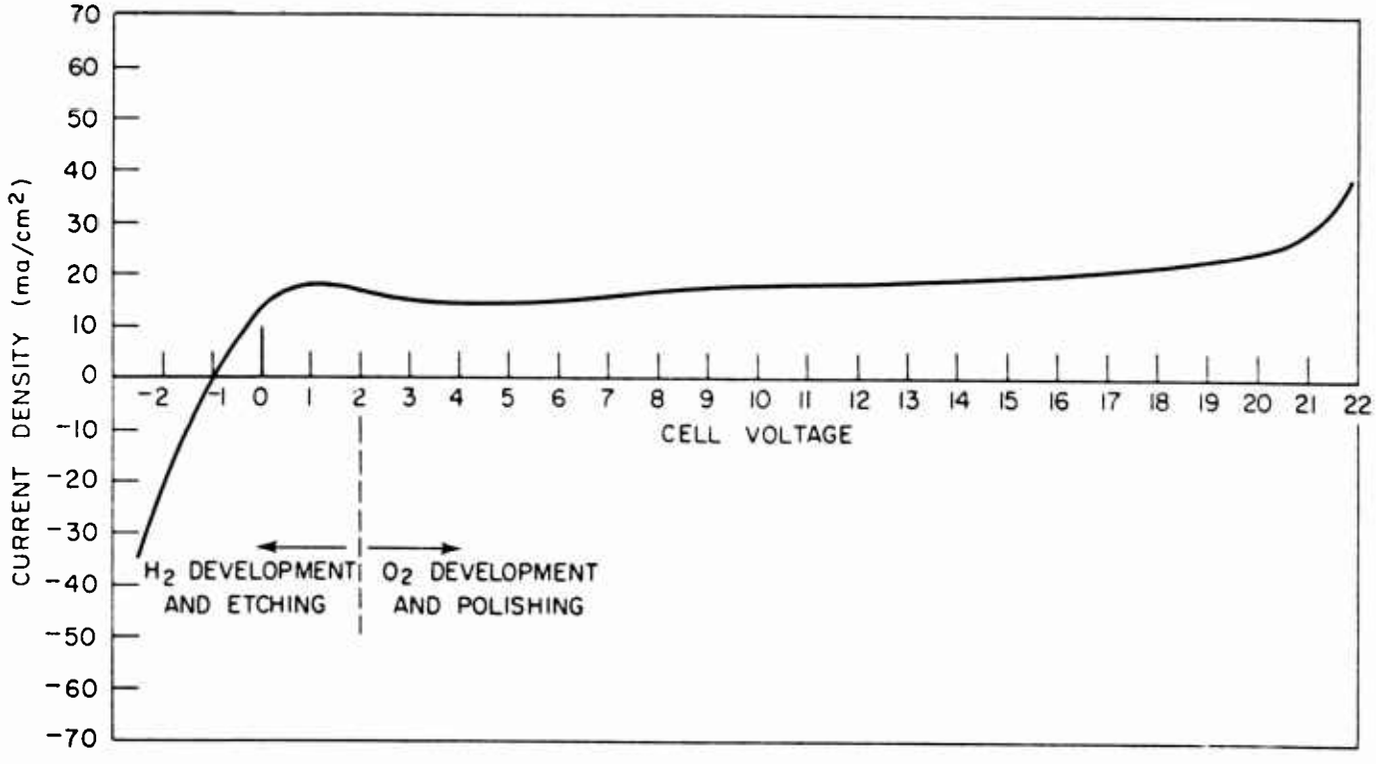

Figure 50 - Current-voltage diagram for beryllium electropolishing cell.

15 volts. Above 15 volts unstable conditions occurred occasionally, resulting in a strong current surge and etching under gas evolution. At voltages near 2 volts the gas development (oxygen) ceased, and below 1.5 volts hydrogen was generated. Polishing at these low voltages was poor, with etch pits becoming a serious problem. However, it has been observed that specimens prepared under hydrogen development show, when studied in the electron microscope, a cleaner background than is usually found in specimens prepared under oxygen development. It seems that the oxygen reacts with the beryllium surface, causing a dark, spotty surface film to form. A compromise has to be made between optimum polishing conditions (negligible pitting) and a clean, smooth surface. It has also been observed in polycrystalline beryllium that the optimum polishing voltage depends on the particular grain orientation. Slight variations in voltage cause one or the other grain to be polished while a neighboring grain may retain its dull appearance.

5-3 DISLOCATIONS IN BERYLLIUM FABRICATED FROM PECHINEY FLAKE

Samples prepared from vacuum-melted Pechiney flake beryllium were supplied by Nuclear Metals, Inc. in the as-melted condition after mechanical machining and grinding to the size of 12 x 12 x 0.5 mm. Further cutting and thinning of the specimens involved only electrolytic etching and polishing processes. The spectrographic analysis of the starting flake material in parts per million is as follows:

Al	80
Ca	< 50
Mg	< 50
Si	< 25
Fe	190
Ni	190
Cr	25
Mn	15
Cu	< 5

The specimens, as received, were polycrystalline and contained grains 1 - . in diameter.

Specimens with various treatments were investigated:

(1) as received

(2) annealed at 900°C in Purgon for 2 hours and furnace cooled; some specimens undeformed and others deformed by bending around a cylinder of 2-inch diameter.

(3) quenched in ice water from 1150°C; undeformed; some specimens annealed at 300°C for 2 hours after quenching.

5-3.1 As-Received Vacuum-Melted Specimens. A typical electron micrograph with diffraction contrast caused by dislocations in as-received samples is shown in Figure **51.** Narrow, elongated loops a few hundred angstroms in width are seen near glide dislocations; their length varies between 300 and 4,000 Å. Many dark dots are also noted; their diameter may be as small as 50 Å or less and was not observed to be larger than 200 Å. One is tempted to interpret the dots as impurity clusters. However, they disappear as soon as the diffraction conditions are not suitable for dislocation contrast; it is therefore concluded that the black dots are small prismatic dislocation loops. It should be noted that the dislocations are predominantly straight. If curved, they have either a large curvature (a radius of about 1 μ or greater) or a very small curvature (a radius of a few hundred angstroms). Dislocation cusps, which are anchored at dark spots, are frequent. The length of the cusps may reach nearly 1 μ, although most of them have a length of a few thousand angstroms. Sharply-kinked dislocations, often in the shape of a "V", occur in large numbers. The angle between the legs of the "V" is between 20 and 100° of arc.

The above observations can be construed as direct evidence for an extremely effective dislocation pinning. Many of the dark spots are seen to anchor the dislocations. In this context it is of particular significance that most of the long narrow loops, the V-shaped dislocations and the drawn-out cusps are pointing in the same direction.

In previous papers a particular type of interaction between dislocations and point defects and their aggregates, named "mushrooming", has been described.[2] This leads to dislocation tangles with interspersed prismatic loops. The as-received vacuum melted Pechiney flake beryllium exhibited dislocation tangles with interspersed prismatic loops so similar in many respects to those observed in fcc metals that they are also believed to be the result of "mushrooming". Figure **52** gives a further illustration of the dislocation structure found. Typical for such dislocation tangles are the long, narrow loops that have previously[3] been explained as the results of a combined glide and climb mechanism. It should be pointed out that the long, narrow dislocation loops in the tangles, which presumably occur only at right angles to their Burgers vector, occur only in one direction in Figure **52.** This observation seems to preclude the alternate interpretation that dislocation interactions between two systems are responsible for the tangles; thus "mushrooming" remains the most likely explanation.

5-3.2 Specimens Annealed at 900°C for 2 Hours. Vacuum-melted Pechiney flake material that was annealed at 900°C for 2 hours in Purgon and electropolished exhibited many fine cracks when examined with an optical microscope. Under tensile stress, fracture occurred along the basal plane at an elongation of less than 0.1%. Optical microscopic inspection revealed small bands of slip lines confined to the immediate fracture zone, whereas the remainder of the tensile specimen showed no visible slip lines. In order to induce more uniform strain throughout the material, subsequent samples were bent around a metal cylinder of 2-inch diameter. However, the strain produced in bending a sample was inhomogenous because some of the cracks present widened and new ones became visible.

The surface of beryllium specimens that were strained after annealing and then electropolished showed many fine lines when viewed with an optical microscope at 260X magnification. It appears that electropolishing preferentially attacks rows

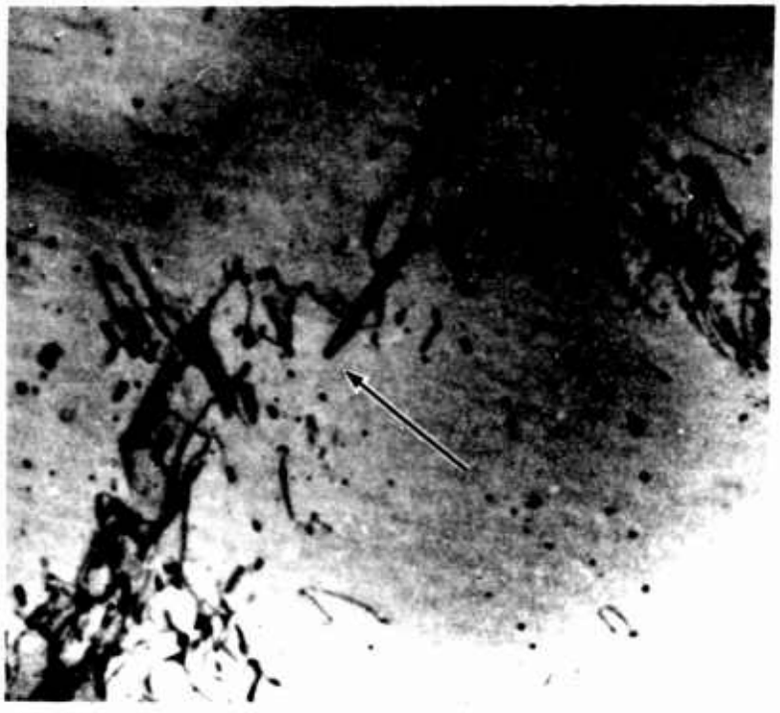

40,000X

Figure 51 - Dislocations in polycrystalline beryllium (vacuum-melted Pechiney flake, as-received). Arrow indicates pinning of glide dislocations.

40,000X

Figure 52 - Dislocation pattern in polycrystalline beryllium (vacuum-melted Pechiney flake, as-received). Small round spots represent dislocation loops, some of which act as obstacles pinning glide dislocations (see arrows).

of dislocations. Electron microscope specimens made from this strained material showed a widely varying dislocation density. Dense bands of dislocations running nearly parallel to each other bordered on regions almost free of dislocations (see Figure 53). In some cases regular networks of dislocations were seen. The dislocations in Figure 54 very likely represent basal glide with Burgers vectors inclined 120° to each other. However, it was not possible to confirm this since the crystal orientation could not be determined. On the other hand, the basal plane is the major slip plane in beryllium, and it is believed that grains that polished extremely well in the polycrystalline samples often had an (0001) orientation. On many intersections no dislocation reactions seem to have taken place but on a small fraction of intersections the original four-fold nodes had clearly split into two three-fold nodes (see arrow in Figure 54). This is of particular interest for three reasons:

(1) For metals with a low or moderate stacking fault energy, three-fold nodes should be clearly extended. No indication of extended nodes was, however, found, nor have any dislocations been seen which were split into partials. Thus, the stacking fault energy of beryllium must be high. Referring back to the observation reported in Section 5-3.1, it should be noted that the presence of tangles in the as-received vacuum melted Pechiney flake beryllium and its absence in the annealed and furnace-cooled specimens precludes the explanation that the dislocation tangling is somehow dependent on the magnitude of the stacking fault energy, since the two types of specimens cannot differ much in this respect.

(2) The observation that the dislocations indicated in Figure 54 have interacted with each other proves that at least two different slip systems are involved; nonetheless, no tangling has taken place. However, the dislocations in the tangle of Figure 52 presumably belong to only one system. This is a further argument that neither the formation of intersection jogs nor dislocation interactions can be the major cause for the dislocation tangles.

(3) Although a favorable dislocation reaction was clearly possible between the two systems of Figure 54 three-fold nodes have formed only infrequently at dislocation intersections. This indicates that a strong frictional stress prevents the dislocations from rotating at the four-fold nodes, presuming that the dislocations all lie in the same plane.

Two observations appear to cast doubt that the dislocation tangles are, as previously suggested, due to mushrooming: First, the dislocations observed in the tangles are more angular than in fcc metals, and second, the specimens prepared from vacuum-melted Pechiney flake material that were annealed at 900°C and furnace cooled yielded no tangles whatsoever. The first of these effects is almost certainly due to a higher Peierls-Nabarro stress, as is subsequently discussed in Section 5-5. The absence of tangling in furnace-cooled specimens, on the other hand, may be explained by a very low vacancy concentration after furnace cooling, coupled with the assumption that vacancies do not condense into voids in beryllium.

5-3.3 Quenched Specimens. In order to study the effect of impurity atoms on the mobility of glide dislocations, quenched specimens were examined. The specimens were heated to 1150°C in Purgon for 30 minutes and then rapidly quenched

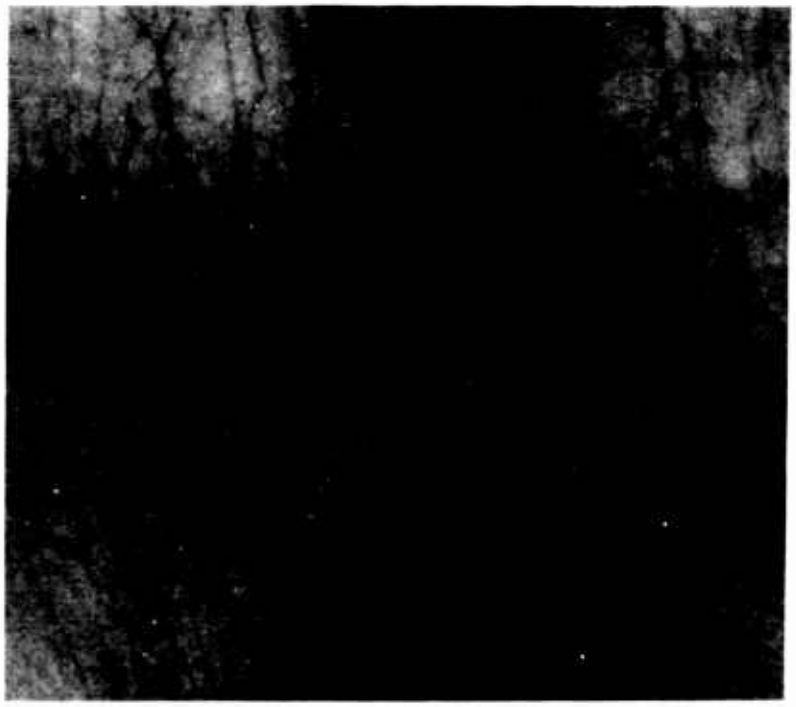

40,000X

Figure 53 - Banded dislocation pattern in deformed beryllium (vacuum-melted Pechiney flake annealed at 900°C for 2 hours).

40,000X

Figure 54 - Typical dislocation pattern in deformed beryllium (vacuum-melted Pechiney flake annealed at 900°C for 2 hours). Long, straight dislocations belong to two slip systems. Arrow points to a double three-fold dislocation node.

in ice water. The observations with the electron microscope indicate that the dislocation density was extremely low, and that the dislocations had formed rather irregular patterns. Anticipating a clustering of point defects at elevated temperatures, some of the quenched material was annealed at 300°C for two hours, thinned down and examined. Although some small loops were seen, the results are not conclusive since they occurred together with irregular arrays of dislocations, similar to those observed in as-received samples.

5-4 DISLOCATIONS IN BERYLLIUM OF COMMERCIAL PURITY

Beryllium of commercial purity was available in the form of single crystals with dimensions of 50 x 6 x 1 mm, and with the basal planes inclined 46° to the large surface of the samples. The [$10\bar{1}0$] direction was perpendicular to the long axis of the samples.

The analysis of this material in parts per million by weight is as follows:

Al	970
Ca	< 50
Mg	< 5
Si	35
Fe	1000
Ni	105
Cr	100
Mn	95
Cu	5
C	3000*
O	600
N	134

The studies were made on crystals that were annealed in a Purgon atmosphere at 1150°C for one hour and furnace cooled. The specimens were strained in compression with a load of 50,000 psi perpendicular to their largest face. Optical examination before and after electropolishing did not reveal any slip lines or strain markings; however, some twinning had occurred.

A strikingly high density of small, dark spots that are strongly suspected to be precipitates was observed. The average distance between the spots, projected in the plane of observations, is 700 Å; their diameter varies between 50 and 400 Å with an average of about $\bar{d}$ = 250 Å. From the known orientation of the crystal in the electron microscope and the measurable length of dislocations lying in the basal plane, the thickness of the beryllium film is calculated to be 2500 A.

- - - - - - - - - - - - - -

* This value appears to be too high and may be due to a local enrichment of C.

The ratio of particle volume (precipitates) to total specimen volume is calculated to be between 2×10^{-4} and 1×10^{-3} for areas of lowest and highest spot density respectively. The density of the fine precipitates is determined as $N = 3 \times 10^{14}/cm^3$. They clearly represent obstacles against dislocation motion, as may be seen in Figure 55. The dislocations, similar to those marked by arrows, are pinned where they are in contact with precipitates. However, the free dislocation lengths between precipitates are usually bowed only slightly, and no loops encircling precipitates have been observed. This indicates that the dislocations either penetrate through the precipitates or move around them by climb or cross-slip before the critical stress, τ_{cr}, has been reached, at which point the free lengths between precipitates would begin to act as sources as envisaged by Orowan[4]. Using Orowan's formula

$$\tau_{cr} = \frac{a\mu b}{\ell} = a\mu b\sqrt{Nd}$$

with μ the modulus of rigidity, b the Burgers vector, ℓ the distance between pinning points for a dislocation moving on a slip plane, and "a" a constant of the order of unity, the critical stress becomes about 10 Kg/mm^2. τ_{cr} is the stress which must be applied in addition to τ_o if loops are to be released from the free lengths between pinning points, while τ_o is the stress which would move the dislocations if the beryllium were free of precipitates. However, the value of 10 Kg/mm^2 is substantially higher than the critical resolved shear stress of about 3 Kg/mm^2,* in agreement with the experimental observations mentioned above concerning dislocation bowing and loops encircling particles.

The orientation of the single crystal specimen with respect to the direction of the applied stress is known for the sample the structure of which is shown in Figure 55. Under the conditions present, single slip on the basal plane with the Burgers vector 1/2 $[2\bar{1}\bar{1}0]$ is expected. The majority of the single dislocations visible in Figure 55 presumably belong to this slip system. Also a dislocation array of high density in $(1\bar{2}10)$ is observed. The appearance of this structure seems to indicate that it consists of two types of dislocations. It is suggested that some unpredicted slip, also on the basal plane but with $b_2 = 1/2\ [\bar{1}\bar{1}20]$, has taken place and that dislocations of these two systems meeting in $(1\bar{2}10)$ have reacted as 1/2 $[2\bar{1}\bar{1}0]$ + 1/2 $[\bar{1}\bar{1}20]$ = 1/2 $[1\bar{2}10]$ to form a wall of edge dislocations. There is little doubt that this dislocation wall is a so-called "bend-p' the occurrence of which has been assumed to be necessary for the formation o' on (0001). Moreover, because of the way the specimens were deformed, $(1\bar{2}10)$ likely fracture plane. Thus, it is tempting to speculate that the high dens dislocation array in Figure 55 represents an incipient crack in the same plan

- - - - - - - - - - - - - -

* This value was taken from H. T. Lee and R. M. Brick, "Deformation of Beryllium Single Crystals at 25 to 500°C", Trans. ASM, 48, p. 1003 (1956).

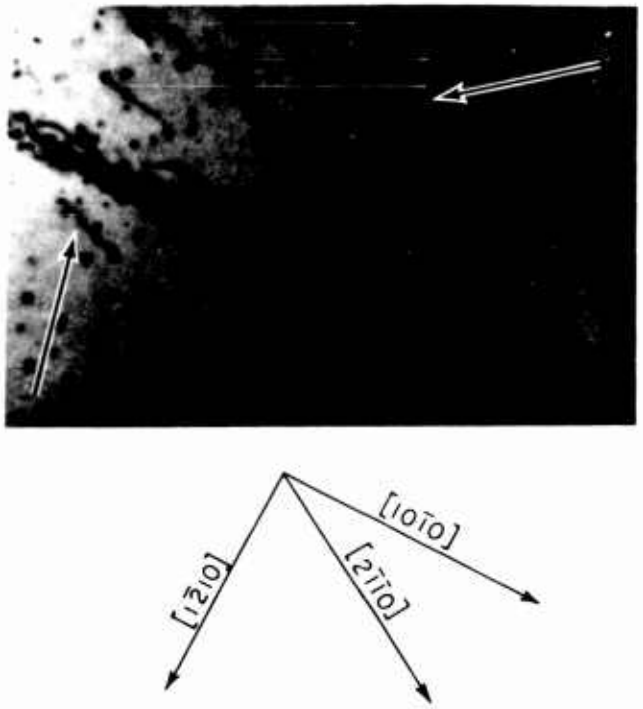

40,000X

Figure 55 Dislocations and fine precipitates in beryllium single crystal of commercial purity. Note the dislocation array apparently lying in (1$\bar{2}$10). Arrows point to dislocations pinned by precipitates.

Another example of precipitates in commercial purity material is shown in Figure 56. No dislocations are visible. Electron micrographs showing similar results have not yet been fully evaluated.

5-5 SOME ADDITIONAL OBSERVATIONS AND COMMENTS

In the purer Pechiney flake material relatively few precipitates were found. These lay predominantly along grain and sub-grain boundaries. Figure 57 shows a string of precipitate clusters in vacuum-melted Pechiney flake after annealing. Particles sometimes appeared to be lined up without the presence of a boundary (as for the chain of smaller, darker spots in Figure 58 which was observed in vacuum-melted Pechiney flake material, quenched and annealed). It is thought that these dots mark the site of former grain boundaries that moved during heat treatment. That the presence of these particles is observed in quenched specimens as well as in annealed ones indicates that there is a considerable amount of insoluble material present. Their average diameter is approximately 500 A.

The dislocations in any of the beryllium specimens studied were always immobile while under observation in the electron microscope, whereas, under similar conditions, dislocations in fcc metals are observed to move freely and even multiply. This observation, together with the strong tendency of the dislocations to align in crystallographic directions (Figure 54) coupled with the apparent suppression of the favorable dislocation reaction as discussed in Section 5-3.2, shows that the Peierls-Nabarro force in beryllium is high. Moreover, as further evidence for a high Peierls-Nabarro stress it was already deduced (Section 5-3.2) that the stacking fault energy on the basal plane is high, indicating that the stacking fault position does not represent a configuration of effective minimum energy for the atoms.

The high Peierls force is not surprising in the light of a recent theoretical investigation[5]. Due to its low c/a ratio, the basal plane in beryllium is not close-packed. Consequently, the critical resolved shear stress at which slip along the basal plane would take place in the absence of dislocations must be high, and thus the Peierls-Nabarro stress must also be high.

Another interesting observation involving precipitates has been made on single crystals of such orientation that the basal plane is normal to the large specimen surface. The specimens were annealed at 1150°C for one hour and furnace-cooled. After electropolishing, they were studied with an optical microscope. A substructure similar to that frequently observed in zinc was found (see Figure 59). A network of cells elongated in the direction of the basal plane trace is formed. These cell boundaries are undoubtedly due to a concentration of impurities produced during the solidification process. Similar observations[6] have been made on zinc, in which this phenomenon has been extensively studied.

The evidence collected and described indicates three logical reasons for the relative brittleness of beryllium: commercially pure beryllium contains a profusion of very small precipitates which hinder dislocation motion; the Peierls-Nabarro stress in beryllium is very high; and there is evidence for the presence of high density dislocation boundaries lying in $(\bar{1}2\bar{1}0)$. These effects together may well raise the yield stress close to or beyond the level at which the cleavage stress is exceeded on the most favorably oriented cleavage or fracture planes. In that case fracture would take place before an appreciable amount of plastic deformation.

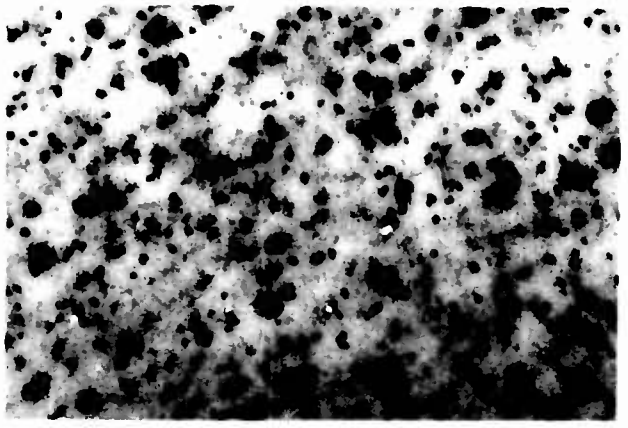

60,000X

Figure 56 Precipitates of two distinctly different particle sizes in beryllium of commercial purity. Note the definite directional alignment of the finer particles.

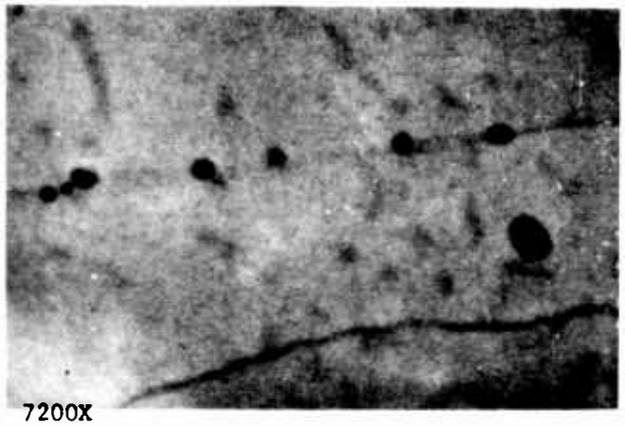

Figure 57 Impurity clusters in annealed beryllium (vacuum-melted Pechiney flake).

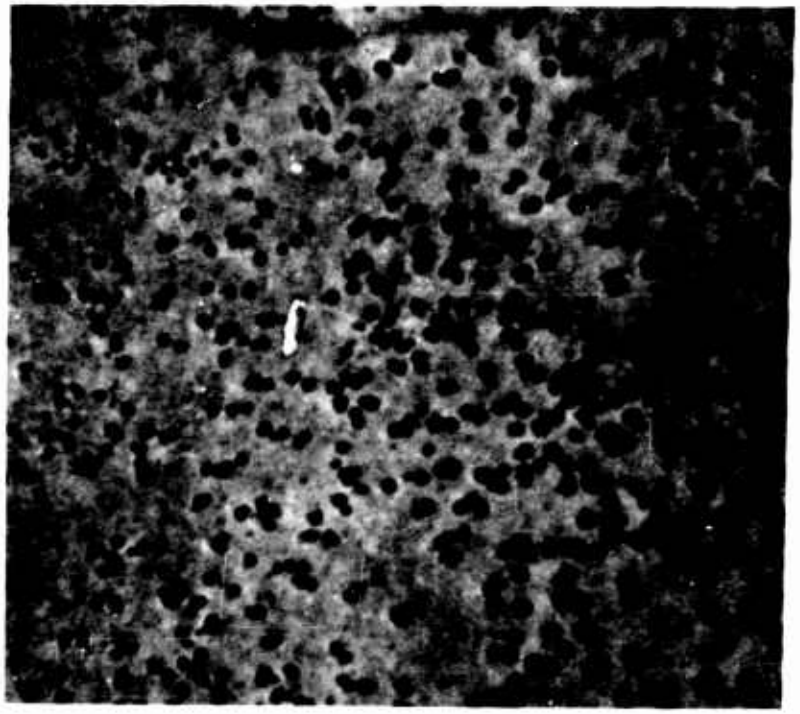

16,000X

Figure 58 Precipitates in quenched and annealed (300°C for 2 hours) beryllium (vacuum-melted Pechiney flake).

350X

Figure 59 - Substructure in annealed beryllium single crystal of commercial purity (line in upper left corner indicates trace of basal plane).

REFERENCES

1. J. D. Baird, O. P. Hartree and R. Phillips, Nature, 182, 1660 (1958).

2. H. G. F. Wilsdorf and D. Kuhlmann-Wilsdorf, Phys. Rev. Letters, 3, 170 (1959).

3. J. T. Fourie and H. G. F. Wilsdorf, J. Appl. Phys., 31, 2219 (1960).

4. E. Orowan, Discussion, Symposium on Internal Stresses, 451 Inst. Metals, London (1947).

5. D. Kuhlmann-Wilsdorf, Phys. Rev., 120, 773 (1960).

6. V. Damiano and M. Herman, Trans. AIME, 215, 136 (1959).

SECTION 6

SURFACE DAMAGE IN BERYLLIUM

M. I. Jacobson, F. M. Almeter, and E. C. Burke

(Lockheed Missiles and Space Company, Sunnyvale, California)

ABSTRACT

A study was made of the nature and effects of surface damage in hot-pressed, hot-rolled, and hot-upset beryllium sheet, all of the same composition. Metallographic examinations showed the presence of considerable surface damage in the form of twins and cracks in as-received hot-pressed and hot-rolled sheet. Limited twinning was seen in the surface grains of hot-upset sheet. Mechanical properties were improved when as-received samples were annealed to remove twins, or annealed and etched to remove all surface damage.

Specimens with controlled surface damage, induced by grinding 2, 5, or 10 mils off in one pass, were machined from sheet that had all previous surface damage removed by annealing and etching. The degree of surface damage (i.e., the extent of twins and cracks) increased as depth of grinding increased. Hot-upset sheet was more resistant to surface damage than the other materials. Annealing to remove twins and relieve residual stresses resulted in sharp increases in ductility for all types of sheet, as indicated by tensile, bend, and impact tests. In some cases etching after annealing produced further increases in properties, particularly for hot-upset sheet, but in other cases etching had little or no effect. Etching alone also effected considerable improvements in properties.

The detrimental nature of twins was indicated by studying deformation and fracture in polished cross sections. Fracture was observed to initiate in twinned regions and at the intersections of twins and grain boundaries, and to propagate along twin-matrix interfaces. These studies also showed that cleavage fractures initiated at impurity particles located in grain boundaries, and that intergranular cracks formed readily at room temperature.

Electron diffraction studies revealed the presence of a thin layer of basal planes oriented parallel to the surface of ground samples. Although this layer was not directly related to mechanical properties, it was thought to have a detrimental effect since it places $(11\bar{2}0)$ planes in a favorable orientation for fracture.

The poor ductility in machined beryllium is attributed to highly twinned areas acting as the favored loci for crack formation. The presence of cracks is less detrimental, since cracks apparently do not grow unless they are suitably oriented. When many twins are present, the possibility of nucleating favorably oriented cracks is greater.

The experiments performed here emphasize the fact that if beryllium is to be used in structural applications requiring maximum properties, considerable care must be taken to ensure that all surface damage is removed.

6-1 INTRODUCTION

Lockheed Missiles and Space Company completed in January 1960 an investigation[1] of crack propagation in beryllium for the Wright Air Development Division materials laboratory. The study showed that surface damage introduced by machining beryllium resulted in lowered mechanical properties. Removal of the surface damage by chemical etching restored these properties.

The current program was initiated to provide a better understanding of the exact nature of surface damage and of the means of removing it. Three types of beryllium sheet, all fabricated from the same lot of powder, were studied:

(1) Sheet sawed from hot-pressed QMV block

(2) Hot-rolled sheet

(3) Hot-upset sheet

The program was designed to determine whether twinning or cracking was more detrimental to mechanical properties. Samples were tested in the as-received, as-ground, annealed, annealed and etched, or etched only condition. The as-received and as-ground samples contained twins and cracks; annealing removed the majority of the twins, and etching removed both twins and cracks.

Tensile, bend, and impact tests were supplemented by electron diffraction and metallographic studies. The bend samples were designed with a small width: thickness ratio ($\sim$2.5:1) so that there would be sufficient bending to distinguish between the different surfaces. The previous investigation[1] had shown that bend samples with a high width:thickness ratio were all brittle.

Samples were prepared with metallographically polished cross sections, so that the relation of surface damage to deformation and fracture characteristics could be observed.

6-2 EXPERIMENTAL PROCEDURE

6-2.1 Material. Surface damage studies were made on three types of beryllium sheet: (1) hot-pressed, (i.e., sheet sawed from hot pressed QMV block), (2) hot-rolled, and (3) hot-upset. These sheets were fabricated from the same lot of QMV powder, with the following chemical composition, as reported by the Brush Beryllium Company:

Constituent	Percent by Weight
Be	98.9
BeO	1.00
Fe	0.118
Si	0.03
Al	0.06
Mg	0.06
Mn	0.09
Ni	0.018
Cr	0.013
C	0.12

Each sheet had a nominal thickness of 0.100 in. and a maximum deviation from flatness of 2 percent. Brush Beryllium Company supplied the hot-pressed sheet, which had been cut from QMV block, and also the hot-rolled sheet.

Nuclear Metals, Inc., fabricated the following pieces of hot-upset sheet:

(1) Disk, 7-1/2 in. diameter, 0.100 in. thick, with no defects

(2) Disk, 7-3/8 in. diameter, 0.100 in. thick, with a cracked circumference

(3) Disk, 7-1/2 in. diameter, 0.100 in. thick, which cracked during upsetting

(4) Disk, 7 in. diameter, 0.100 in. thick, with a cracked circumference

These disks were etched to the 0.100 in. thickness after upsetting.

Basal pole figures were made for the three types of sheet. The pole figures and the technique used to obtain them are described in Appendix 6A.

Metallographic examinations were made of the sheet surfaces, and of sections cut perpendicular to the surfaces. The results of these studies are presented in Section 6-3.1.

6-2.2 Preparation of Specimens. Tensile, bend and unnotched Charpy-type impact specimens, with the dimensions shown in Figure 60, were machined from the three types of beryllium sheet. Specimens were cut from both the longitudinal and transverse directions of the hot-rolled sheet. For the hot-pressed and hot-upset sheets, specimens were not cut in any specific direction, since these materials were assumed to have no preferred direction lying in the plane of the sheet. The cut edges of each specimen were given a 16-μ-in. rms finish and ground with 120 emery paper to remove machining marks and edge burrs. Specimens prepared in this manner are herein referred to as having as-received surfaces, since no machining was done in the plane of the sheet. Some of the as-received specimens were annealed to remove surface twins (designated "as received and annealed") and some of these, in turn, were etched in 10% H_2SO_4 to remove cracks and thus provide surfaces entirely free of damage (designated "as received, annealed and etched").

The specimens required for testing in each of the above conditions were removed from the total group of specimens. The remaining specimens, which were to be prepared with ground surfaces, were treated to make certain they were as free of damage as possible prior to grinding. This involved annealing at a time and temperature sufficient to remove twins (as described later) and etching to remove cracks. The samples were then surface-ground to remove 2, 5 or 10 mils in one pass (designated "ground"). All surface grinding was done with a Radiac Par-Os-Way 60 grit wheel, 7 in. diameter x 1-1/4 in. width, at 2,810 rpm. After grinding, some of the specimens were annealed (designated "ground and annealed"), and some of these, in turn, were etched (designated "ground, annealed and etched").

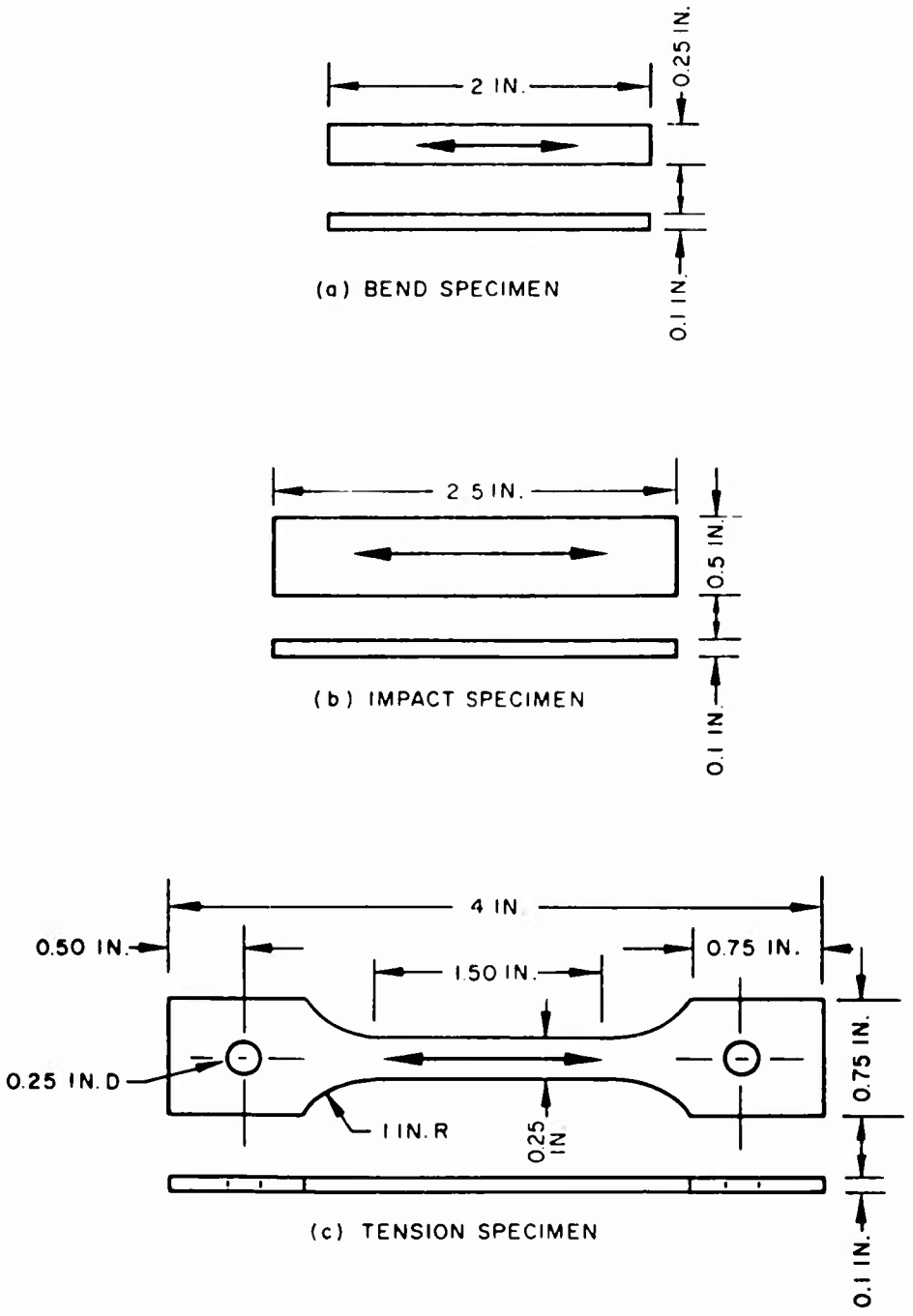

Figure 60 Dimensions of test specimens.

6-2.3 Detection of Surface Damage. Metallographic and electron diffraction techniques were used in this investigation for detecting surface damage. Microradiography with an aluminum tube and a special vacuum camera has been used successfully in detecting defects in beryllium (2, p. 515). For the present study, an aluminum tube was not available, and attempts to use Cr, Fe, and Cu radiation at low voltages were unsuccessful. Further attempts to use microradiography were abandoned, since metallographic techniques proved quite capable of revealing cracks.

(1) Metallographic Techniques. Metallographic examinations were made of specimen surfaces in the as-received and ground conditions, as well as of polished cross sections cut perpendicular to the plane of the sheet (Figure 61).

Normal metallographic techniques for beryllium that employ an electropolishing step were originally used. However, this proved to be unsatisfactory since the edges of the samples became rounded during electropolishing. This rounding off made it very difficult to observe surface damage, which often was confined to a surface layer only one or two grains thick.

After considerable experimentation, the following successful techniques were developed:

(1) Mount in Lucite and grind wet or dry through 3/0 paper.

(2) Swab for 1 minute with solution of 140 cc H_3PO , 200 g CrO_3, 10 cc H_2SO_4 and 1,000 cc H_2O (this removes the damage caused by the previous step).

(3) Polish on Duracloth or Metcloth with a slurry of C-RO polishing abrasive and distilled water until the desired surface is obtained.

The final polishing operation, which required several hours, was conducted on the automatic polishing apparatus shown in Figure 62. Beryllium samples prepared in this manner were free of scratches, pitting or excessive relief, and impurity particles were retained.

(2) Electron Diffraction Techniques. An XRD-5 General Electric X-ray diffractometer was first used in an attempt to observe differences in integrated intensities of the (0002), (10$\bar{1}$0) and (10$\bar{1}$2) peaks in samples with different surface conditions. However, it soon became obvious that the low X-ray absorption coefficient of beryllium makes this technique unsuitable for the detection of differences involving only surface layers.

An electron beam, on the other hand, only penetrates to a depth of the order of 10 Å, and thus diffracts from atomic layers at the surface only. A General Electric electron diffraction unit, operated at 40 kv and 10 ma, was therefore used to obtain the diffraction patterns. The reflection technique was used, with the beam grazing the specimen surface at an angle of less than 1°, as shown in Figure 63. In all cases, the electron beam was perpendicular to the longitudinal axis of the specimen. Since even fingerprints will leave a film that obscures the underlying structure, samples were carefully degreased in toluene or ether, rinsed in ethyl alcohol, and dried. Tweezers were used for all handling.

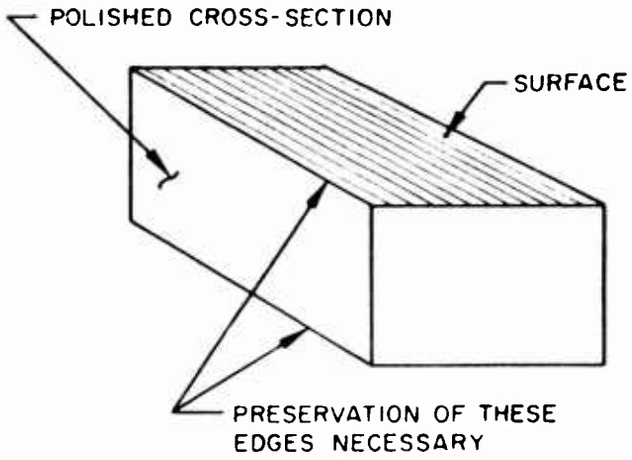

Figure 61 - Schematic diagram of metallographic sample showing relation between sheet surface and polished section.

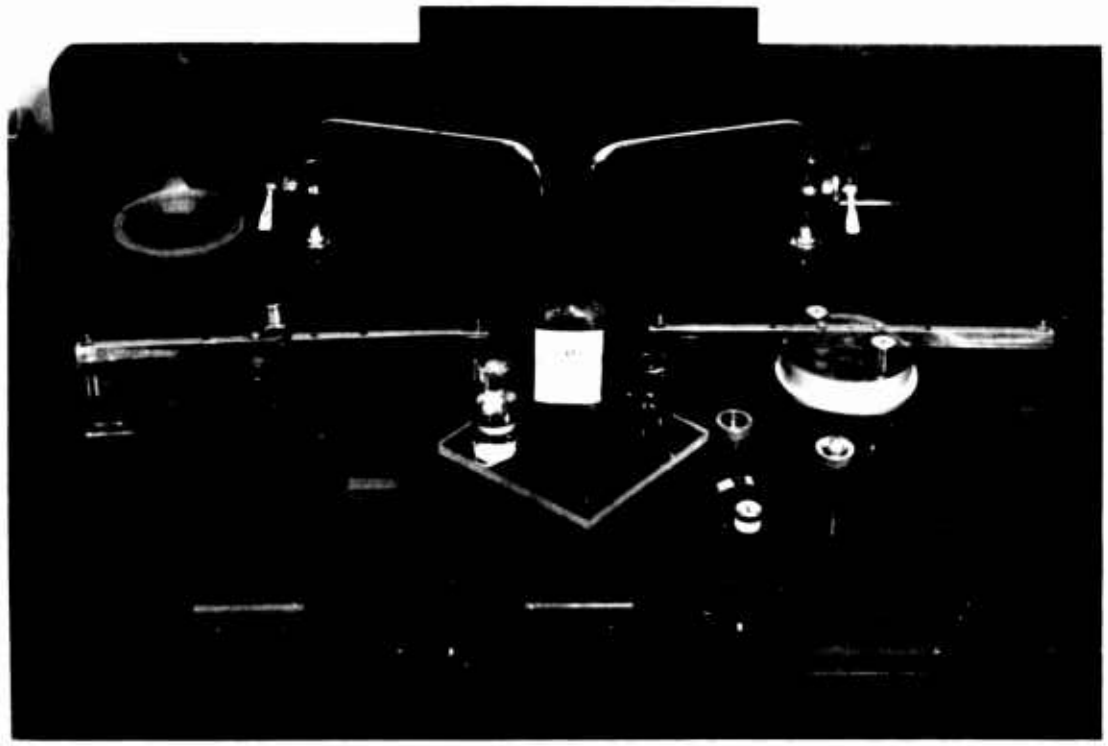

Figure 62 Automatic polishing apparatus used for metallographic preparation of beryllium samples.

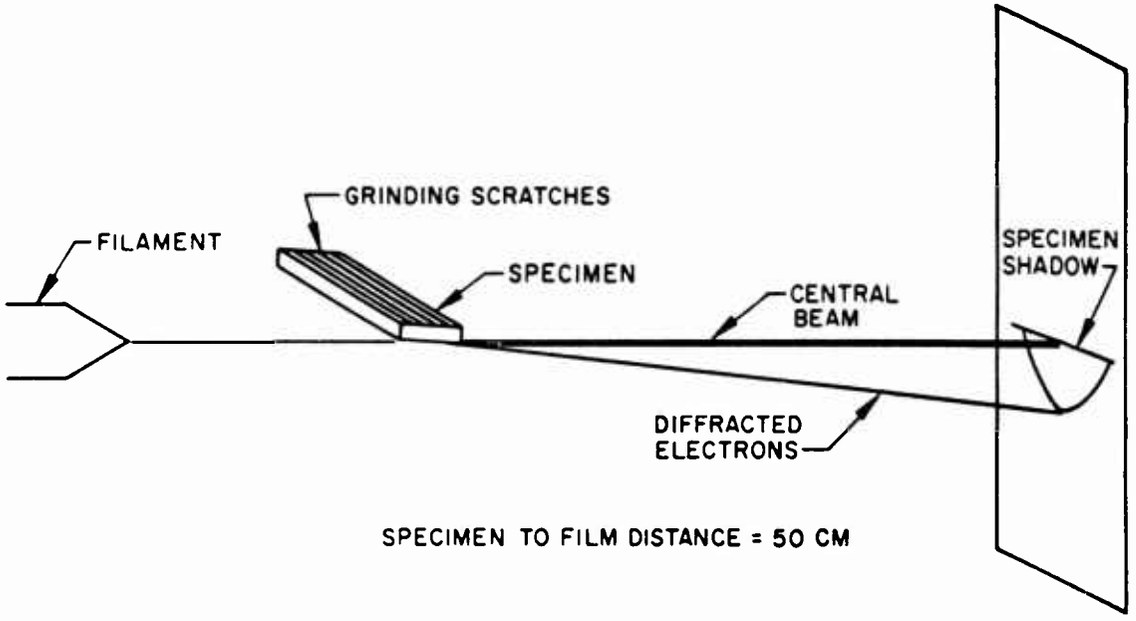

Figure 63 - Electron diffraction technique.

6-2.4 Mechanical Testing Procedures.

(1) Tensile Tests. All tensile tests were performed at room temperature with an Instron tensile machine, using a 10,000 lb load cell. Crosshead speed was 0.01 in./min, which resulted in a strain rate of approximately 0.005 in./in./min.* Ultimate strengths and 0.2% offset yield strengths were computed from the original cross-sectional areas. For a few samples, particularly hot-pressed samples with as-received surfaces, elongation was determined from the load deflection charts by observing the total elongation (assumed to be confined to the 1.5 in. long reduced section of the sample) and then subtracting the elongation due to elastic stresses, slack in the linkage, etc. The resulting net elongation was divided by 1.5 and reported as percent elongation in 1 in. This method was improved when accurate measurements of low elongations were required. All subsequent measurements of elongation were made with microformer extensometers (1 in. gage length) attached to the samples. The extensometers remained attached until fracture of the sample occurred.

(2) Bend Tests. Bend test specimens were deformed as simple beams (3 point loading), using the apparatus shown in Figure 64. The specimen (D) is deflected by a drive screw (G). A synchronous motor (M) drives the screw through changeable gears to apply the bending stress with a 3/32 in. rod at the central point of the beam. The applied load is continuously measured by recording the strain in a calibrated force beam (E) with SR-4 strain gages. Deflection at the center of the bend specimen is measured with a linear variable differential transformer. The strain and applied load are simultaneously recorded on a Honeywell X-Y recorder. The rate of deflection at the center of the sample is approximately 7 mils/min. The supported length is 1.5 in.

Stresses in the outer fibers of the bend specimens were calculated according to the equation:

$$\sigma_{max} = \frac{3}{2} \frac{P\ell}{bh^2}$$

where

σ_{max} = maximum elastic stress

P = applied load

ℓ = supported length = 1.5 in.

b = specimen width

h = specimen thickness

This equation is valid only in the elastic region and, therefore, does not take into account the changes in specimen dimensions. However, as dimensional

- - - - - - - - - - - - - -

* The value of 0.007 in./in./min previously reported in the letter report for March 15 - April 15 was incorrect.

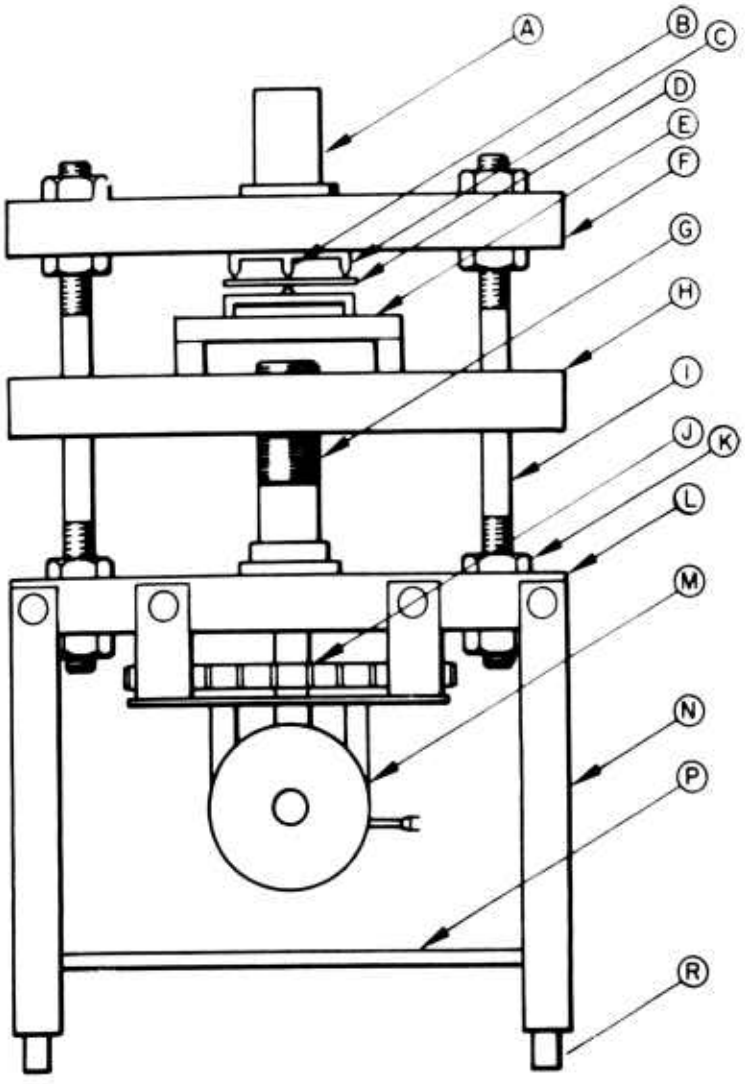

A - Linear Variable Differential Transformer
B - LVDT Core Extension
C - Specimen Support
D - Specimen
E - Calibrated Aluminum I-Beam for Force Measurement using SR-4 Strain Gages
F - Upper Cross Piece
G - Screw Drive
H - Movable Cross Piece
I - Support Rod
J - Drive Gear
K - Retaining Nut
L - Lower Cross Piece
M - Electric Motor
N - Leg
P - Leg Support
R - Leveling Foot

Figure 64 – Bend test apparatus.

changes were for the most part small, it was felt that reporting values of σ_{max} would be more satisfactory than if values of P alone were presented.

(3) Impact Tests. Unnotched Charpy impact tests were made with a Tinius-Olsen Plastic Change-O-Matic impact machine with a capacity of 200 in.-lb. Tests were conducted in a temperature range of -196°C to 600°C. Specimens were heated or cooled by use of the following:

-196°C	liquid nitrogen
0°C	ice-water
100°C	boiling water
100-300°C	silicone oil
>300°C	electric furnace

Each specimen, whether cooled or heated, was held for 15 min. at the selected temperature to ensure equilibrium. Since less than 5 sec elapsed from the time that the specimen was removed from the medium to the time that it was fractured, the drop or rise in temperature was considered negligible. Data are therefore plotted as impact energy vs. temperature, where the temperature is that of the heating or cooling medium.

6-2.5 Microscopic Observation of Deformation and Fracture During Bending. During the course of the investigation, it was found desirable to relate surface damage and fracture mode by observing the process of deformation and fracture on a polished surface. Accordingly, metallographic preparation was carried out on the sides (i.e., the 2 in. by 0.1 in. face shown in Figure 60(a) of several bend specimens. The polishing techniques described in Section 6-2.3 were used. After a satisfactory surface was obtained on the automatic polisher, the specimens were cut from the plastic mount and placed in the modified Flinn Strain Viewer* shown in Figure 65. This is simply a device for bending a specimen in three-point loading. The bending load is applied by a hand-operated screw.

In operation, the Flinn Viewer was placed on a microscope stage, and the specimen was bent until the first crack appeared on the polished section of the sample. This was photographed, and deformation continued until the sample fractured. Several photographs were taken at various stages of deformation to trace the progress of the initial crack.

6-3 RESULTS OF SURFACE DAMAGE STUDIES

6-3.1 Metallographic Studies. The surfaces of as-received and ground sheets are shown in Figures 66, 67, and 68. As-received hot-pressed sheet, Figure 66(a) exhibited a machined surface with numerous particles pulled out of the surface. As-received hot-rolled and hot-upset sheet, Figures 67(a) and 68(a), respectively, had an etched appearance. Except for scratches, which became more severe as depth

- - - - - - - - - - - - -

* Manufactured by Harrow W. Dietert Co., Detroit, Mich. Described in American Foundryman, Sept. 1955.

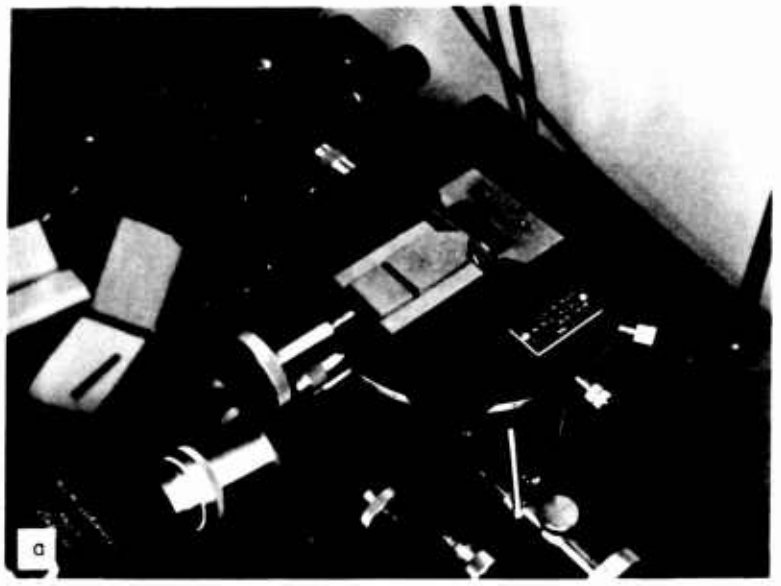

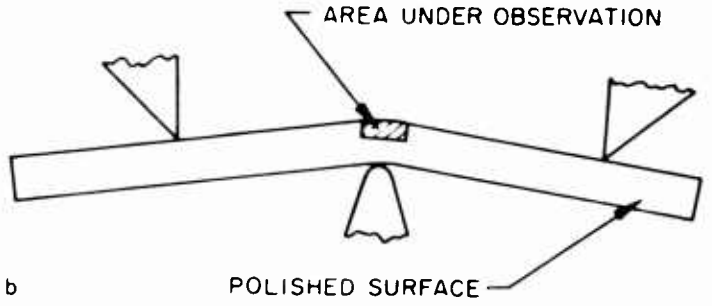

Figure 65 - Setup for bending samples on a microscope stage: (a) Flinn Strain Viewer on stage with specimen in place; (b) area of specimen observed and photographed.

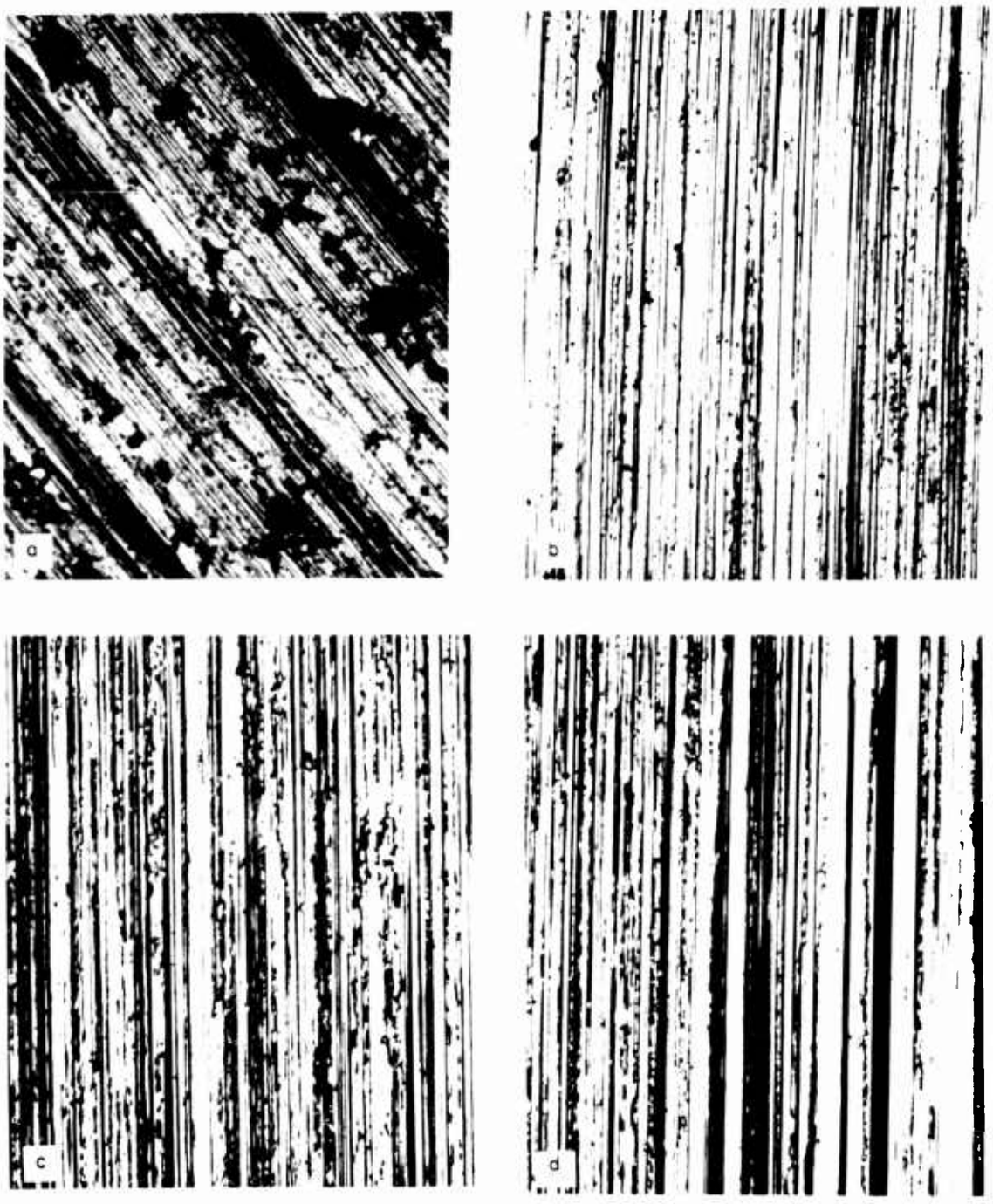

Figure 66 - Surfaces of hot-pressed sheet: (a) as-received; (b) ground 2 mils; (c) ground 5 mils; (d) ground 10 mils. (All photos 250X)

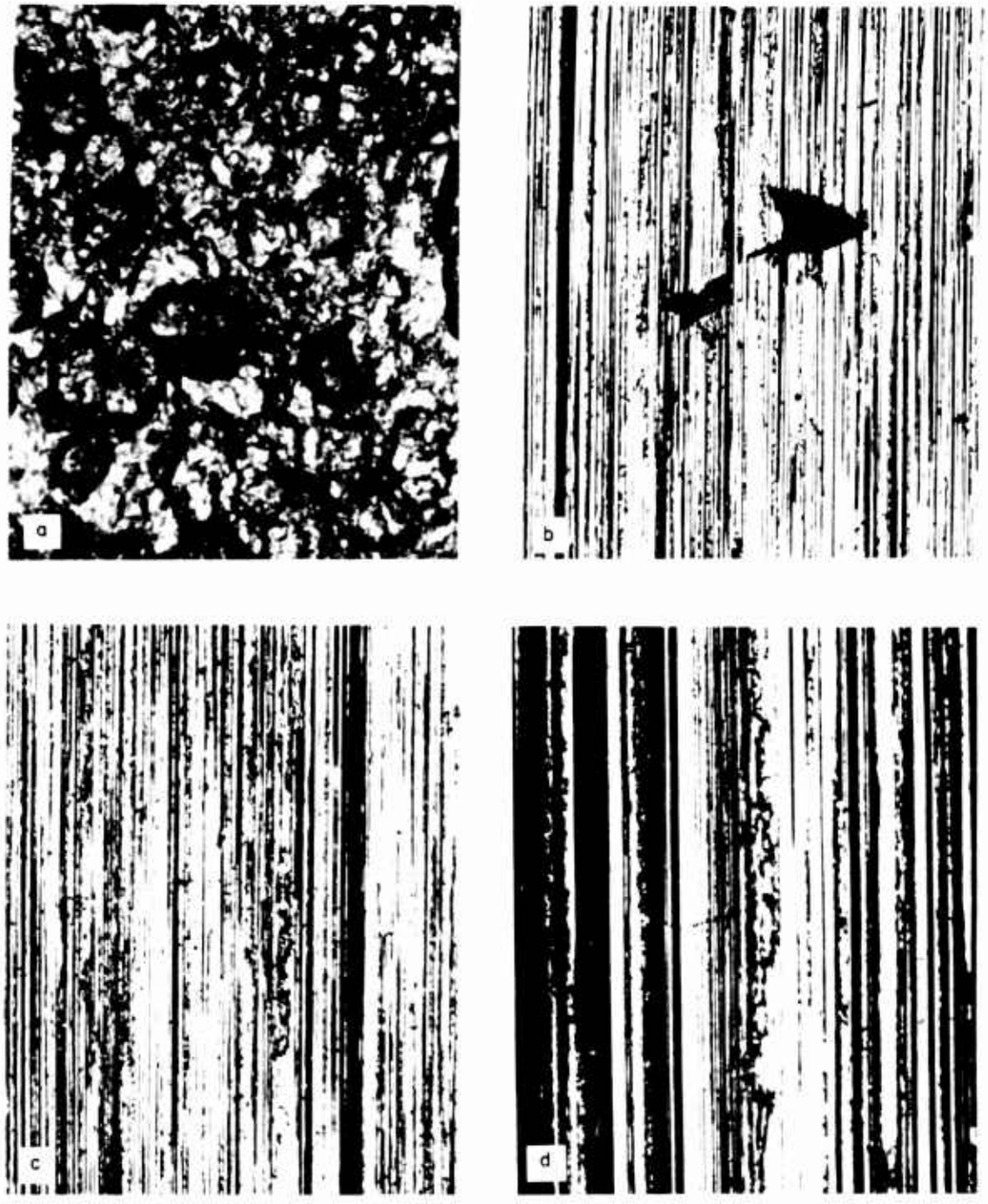

Figure 67 - Surfaces of hot-rolled sheet: (a) as-received; (b) ground 2 mils; (c) ground 5 mils; (d) ground 10 mils. Note grains pulled out in (b) and crack in (d). (All photos 250X)

Figure 68 - Surfaces of hot-upset sheet: (a) as-received; (b) ground 2 mils; (c) ground 5 mils. (All photos 250X)

of grinding increased, the ground specimens exhibited little evidence of damage on the surfaces themselves. Black areas were occasionally visible, where, presumably, material was pulled out of the surface, as in Figure 67(b). A few scattered cracks were also visible, but only where 10 mils were removed, as in Figure 67(d).

Polished cross sections showing damage near the surfaces of hot-pressed, hot-rolled, and hot-upset sheet after various treatments are shown in Figures 69, 70, and 71. Figures 69(a), 70(a), and 71(a) show examples of the damage present in the as-received material. It should be emphasized that the as-received sheet, particularly the hot-pressed and the hot-rolled was rather nonuniform in regard to degree of surface damage. Figures 69(a) and 70(a) are not meant to imply that the extent of twinning and cracking shown are characteristic of the entire sheets. Although many areas did show equivalent damage, there were some portions that showed considerably less or even no damage.

It was believed necessary to remove all evidence of damage in the as-received material prior to inducing controlled degrees of damage by surface grinding. For this purpose, the following treatments were found to be the most satisfactory:

Material	Annealing Treatment	Post-Anneal Etching, Total Thickness Removed
Hot-pressed	2 hr, 800°C	10 mils
Hot-rolled	4 hr, 850°C	10 mils
Hot-upset	4 hr, 900°C	5 mils

Annealing was conducted in vacuum (10^{-4} microns) and the samples allowed to cool to room temperature in a cold portion of the furnace. The above annealing schedules were those found to remove the surface twins in each type of material without providing excessive grain growth. The grain size of hot-pressed and hot-upset sheet did not increase as a result of the annealing treatments, but did increase for hot-rolled sheet. Figures 69(b) and 70(b) show the effects of annealing as-received hot-pressed and hot-rolled sheet respectively. Although the majority of the twins were removed by annealing, a few remained in scattered grains, as the figures show. Similar results were obtained by annealing hot-upset sheet, although no photograph is shown.

Annealing was followed by etching in 10% H_2SO_4 to remove cracks. Although no cracks were observed in the hot-upset sheet, it was nevertheless etched to provide a surface similar to that of the other materials.

Hot-rolled sheet exhibited an apparent increase in the amount of twins at the surface under certain conditions of annealing time and temperature. This matter is discussed in detail in Appendix 6B.

Surface grinding of the annealed and etched materials induced the degrees of damage shown in Figures 69(c, e, f), 70(c, d, e, f), and 71(b,c). As could be expected, the damage became progressively greater as the severity of grinding increased. Damage in the ground samples was more uniform than in the as-received

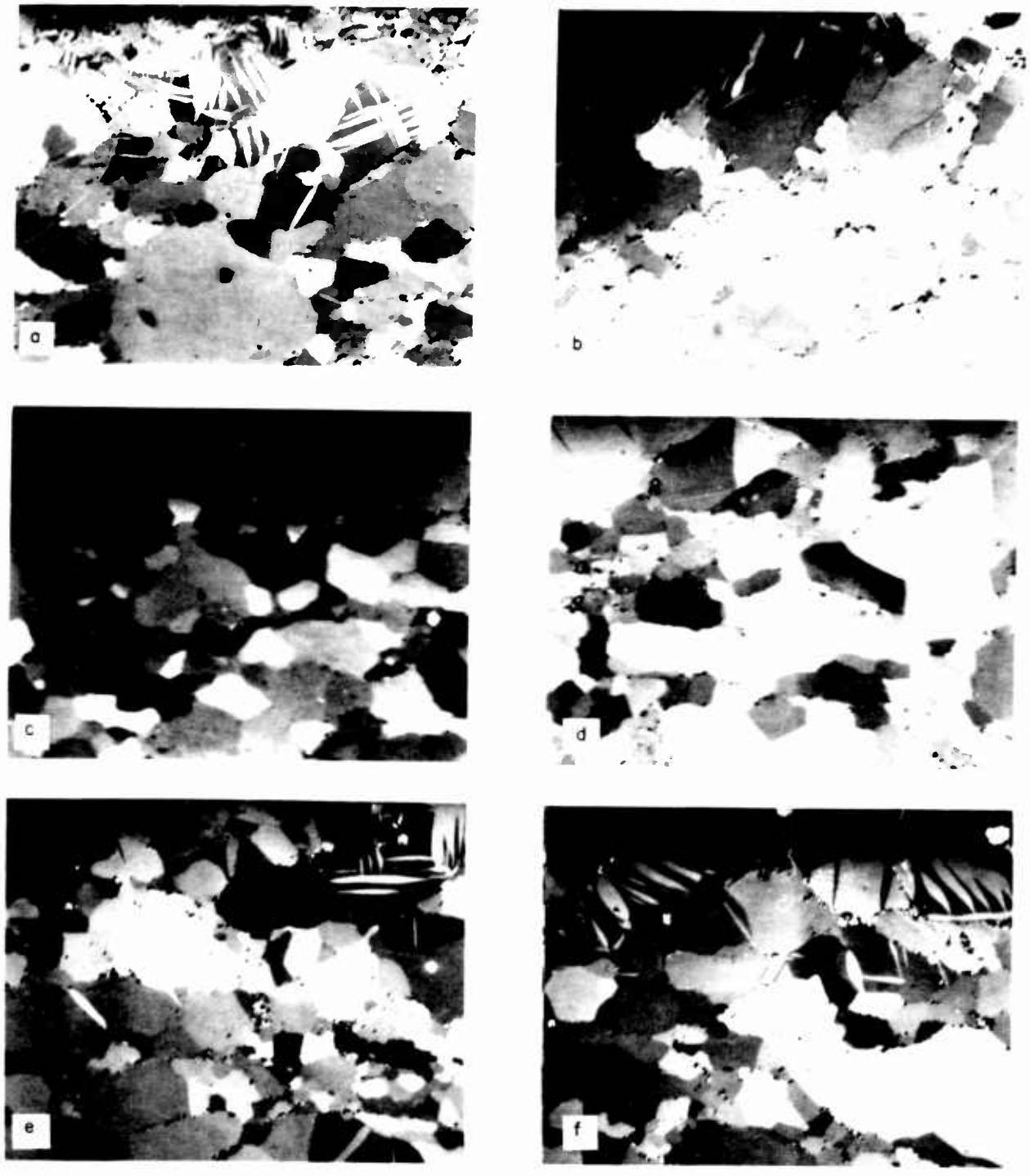

Figure 69 - Cross sections showing damage near surface of hot-pressed sheet: (a) as-received; (b) annealed; (c) ground 2 mils; (d) ground 2 mils and annealed; (e) ground 5 mils; (f) ground 10 mils. (All photos 500X; polarized light)

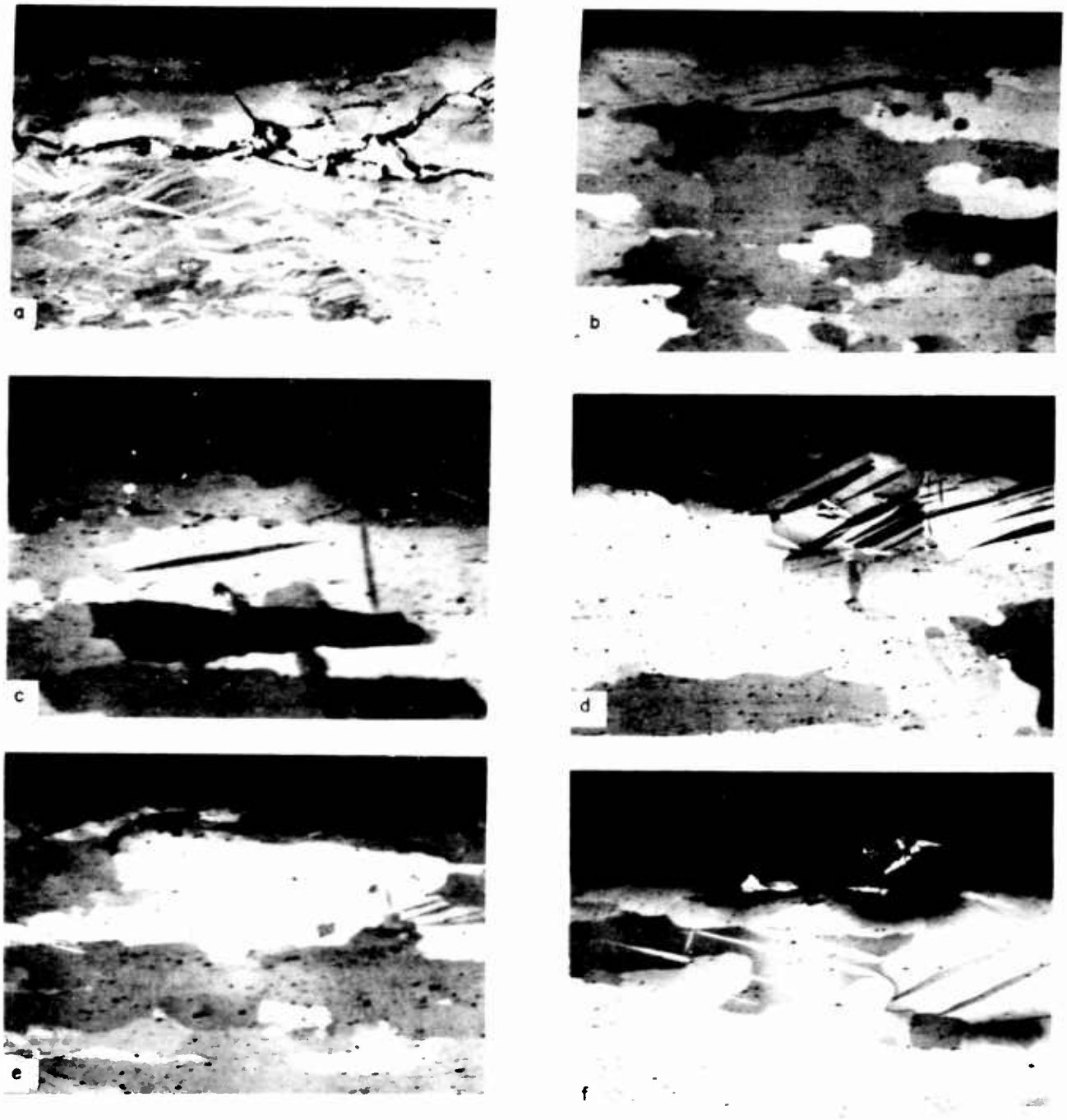

Figure 70 - Longitudinal sections showing damage near surface of hot-rolled sheet: (a) as-received; (b) annealed; (c) ground 2 mils; (d) ground 5 mils; (e) same as (d); (f) ground 10 mils. (All photos 250X; polarized light)

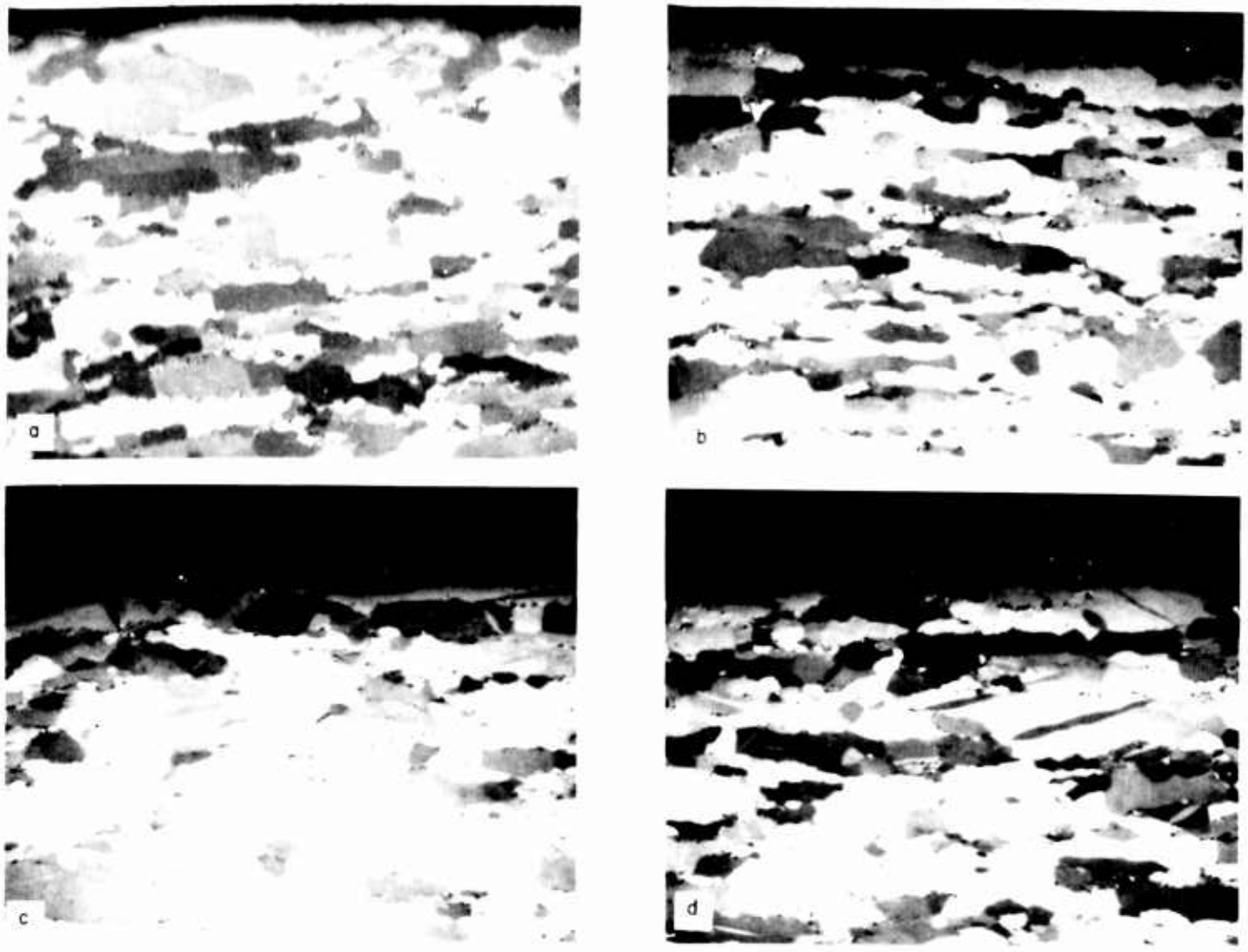

Figure 71 - Cross sections showing damage near surface of hot-upset sheet: (a) as-received; (b) ground 2 mils; (c) ground 5 mils; (d) ground 5 mils and annealed. (All photos 500X; polarized light)

samples. However, some areas sustained more damage than others, as can be seen from Figures 70(d) and (e), both of which are photographs of rolled sheet with 5 mils ground off.

Those samples to be mechanically tested in the ground and annealed condition, and in the ground, annealed, and etched condition, were subjected to the same heat treatments after grinding as before grinding. Again, annealing was very effective in removing the great majority of the twins, but a few did remain as shown in Figures 69(d) and 71(d). It should be mentioned that the areas shown in those photographs are only to indicate that some twins remained. About 90% of the surface grains showed no twins at all. Similar results were obtained for hot-rolled sheet.

No cross sections of samples with as-etched surfaces are shown, simply because the surface grains appear the same as the interior grains, with no surface damage visible.

From an examination of the photomicrographs shown and from more extensive examinations of the samples, it was found that hot-upset sheet was more resistant to induced damage than the other materials.

6-3.2 Electron Diffraction Studies. Electron diffraction patterns were obtained for a number of samples in several different conditions. However, there is little point in presenting all of the patterns here, since the results were basically the same for each type of sheet.

Figure 72 presents a series of patterns from hot-pressed sheet that has been ground 5 mils and then etched in 10% H_2SO_4 for various times up to 60 sec. The as-ground pattern, Figure 72(a) shows a single semicircle with an intense spot at the center. Careful inspection also shows high intensity arcs at each extremity of a semicircle slightly displaced from the one having the central intense spot. The intense central spot is the result of a high concentration of basal planes parallel to the surface of the sheet, a direct result of the plastic flow that occurs in grinding. The arcs occur on the (10$\bar{1}$1) diffraction ring and indicate the tendency for a [10$\bar{1}$0] direction to become aligned parallel to the grinding direction. This pattern, which is typical of all ground samples, is rather diffuse because of the highly worked condition of the metal at the surface.

The pattern in Figure 72(b) is the result of etching the sample for 5 sec in 10% H_2SO_4 which, according to Scott and Wilman[3], removes about 500A from the surface. Line sharpness is seen to have improved considerably over the as-ground sample, and the (0002) and (10$\bar{1}$1) reflections are now resolved. The (0002) spot has spread into an arc that extends to the right of the spot, indicating a less preferred orientation of the basal planes. Other beryllium lines have become visible and are identified in the photograph. Also, note the weak and diffuse BeO rings present between the (10$\bar{1}$2) and (10$\bar{1}$3) rings.

In Figure 72(c), representing an etching time of 10 sec, the (0002) and [10$\bar{1}$0] orientations appear to be growing weaker. BeO lines have become visible below the (0002) line; also, the BeO lines referred to in Figure 72(b) have increased in sharpness and intensity. As etching proceeds, the beryllium is etched away, and the BeO particles stand in relief. Since the grazing angle of

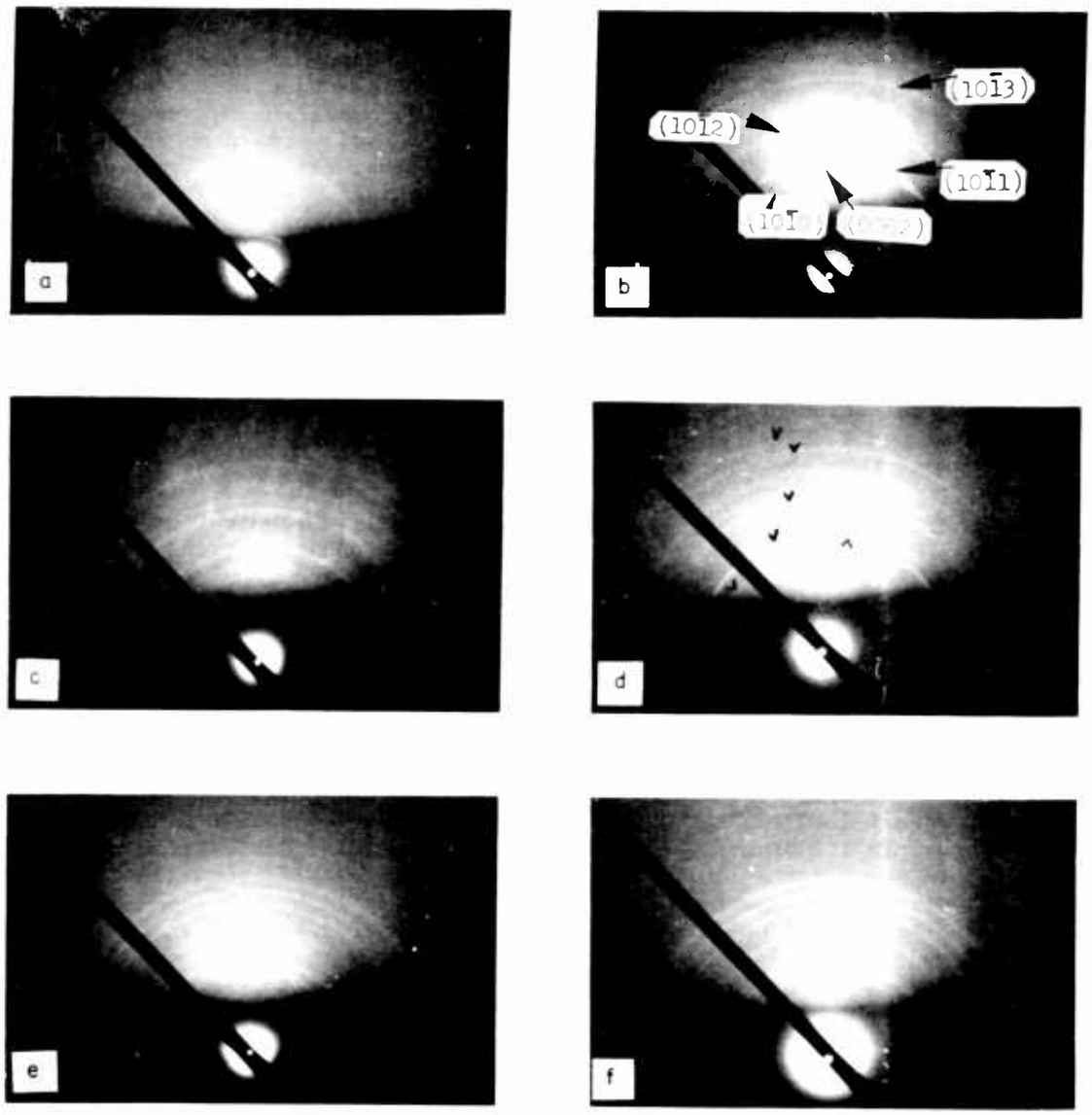

Figure 72 - Electron diffraction photographs of hot-pressed sheet ground 5 mils: (a) as-ground; (b) etched 5 sec, with prominent Be lines identified; (c) etched 10 sec; (d) etched 20 sec; (e) etched 40 sec; (f) etched 60 sec. In (d), marks indicate beryllium lines; all other lines are due to BeO.

the beam is less than 1^{o}, the beam will tend to diffract preferentially from the BeO particles protruding from the surface. As etching time increases to 60 sec, the BeO pattern increases in intensity, until in Figure 72(f) the only lines visible result from diffraction by the BeO. The extent to which the BeO pattern was present was not realized earlier and led to the erroneous statement (in the April 15 - May 15 Letter Report) that at 60 sec the beryllium rings had become continuous.

In Figure 72(c), it may also be noted that the (0002) arc extends to the left of the spot. Because no particular attention was paid to the direction in which the sample was placed in the camera, the displacement of the (0002) arc is understandable; in Figure 72(c) the sample has merely been rotated 180^{o} in its own plane, as compared to Figure 72(b).

Figure 73 shows a similar series of photographs for hot-upset sheet ground 5 mils. Again, the as-ground sample, Figure 73(a) shows only the (0002) spot and the (10$\bar{1}$1) ring, with slightly better resolution than in Figure 72(a). As etching time increases, the (10$\bar{1}$0), (10$\bar{1}$2), and (10$\bar{1}$3) beryllium lines appear. The BeO lines increase in intensity with increased etching time.

A single crystal of beryllium was obtained, and 2 mils were ground from a surface corresponding approximately to the (10$\bar{1}$8) plane. The electron diffraction pattern of the as-ground surface, Figure 74(a) is very faint, but the concentration of basal planes parallel to the surface as a result of grinding is evident. In Figure 74(b) the ground sample has been etched for 10 sec to remove approximately 1000 Å from the surface. The pattern reveals the polycrystalline nature of the surface, with the same beryllium rings observed as in Figures 72(b) and 73(b). After etching to remove 1/2 mil (1.4×10^{5} Å), the polycrystalline rings disappeared and were replaced by single crystal spots, Figure 74(c). Fortunately, the BeO content was low, and only a faint BeO ring appeared near the central spot.

6-4 EFFECTS OF SURFACE CONDITION ON MECHANICAL PROPERTIES

6-4.1 Tensile Properties. The effects of surface condition on the tensile properties of hot-pressed, hot-rolled (tested in the longitudinal and transverse directions), and hot-upset sheet are shown as bar graphs in Figures 75, 76, 77, and 78 respectively. Complete data for each specimen are presented in Appendix 6C, Tables 17, 18, and 19. The averages in these tables were used to plot the bar graphs.

For the hot-pressed material, considering specimens of each basic surface condition as a group (i.e., as-received, ground 2 mils, ground 5 mils), it may be seen (Figure 75) that the lowest values of ultimate tensile strength and elongation within each group were recorded for samples with no annealing or etching treatments; namely, the as-received material and the as-ground samples. When the samples were annealed, or annealed and etched, ultimate tensile strength increased slightly, and elongation increased from around 1% to 2 - 3%. No significant change in yield strength was found in the hot-pressed samples.

Similar remarks apply to the hot-rolled material (Figures 76 and 77. Note, however, that the yield strength of the as-received material drops considerably on annealing for 4 hours at 850^{o}C, reflecting a slight grain growth.

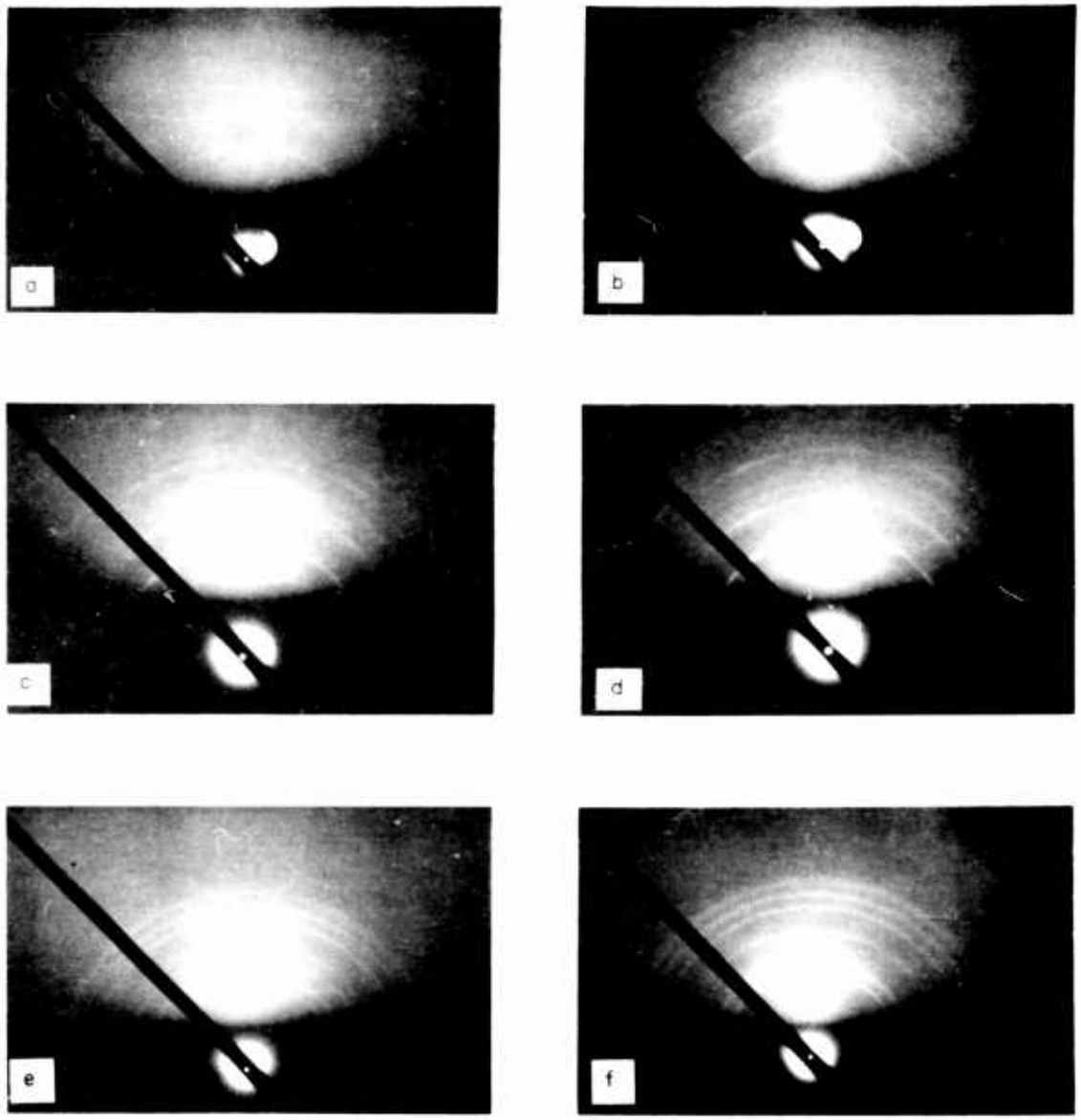

Figure 73 - Electron diffraction photographs of hot-upset sheet ground 5 mils: (a) as-ground; (b) etched 5 sec; (c) etched 10 sec; (d) etched 20 sec; (e) etched 40 sec; (f) etched 60 sec.

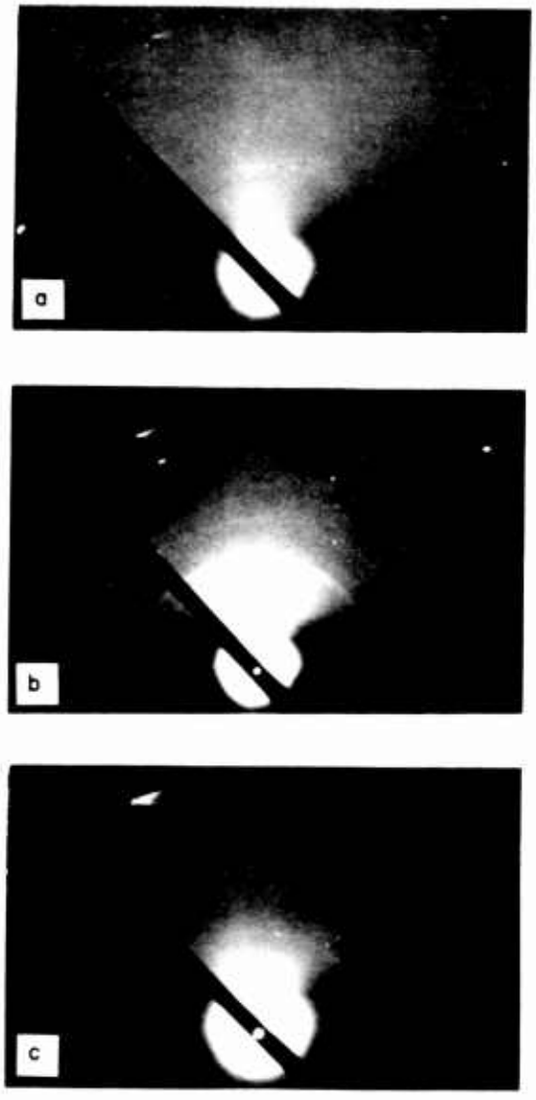

Figure 74 - Electron diffraction photographs of single crystal ground on a $(10\bar{1}8)$ face to remove 2 mils: (a) as-ground; (b) etched 10 sec; (c) etched to remove 1/2 mil. White spot in upper left of each picture is a spurious reflection.

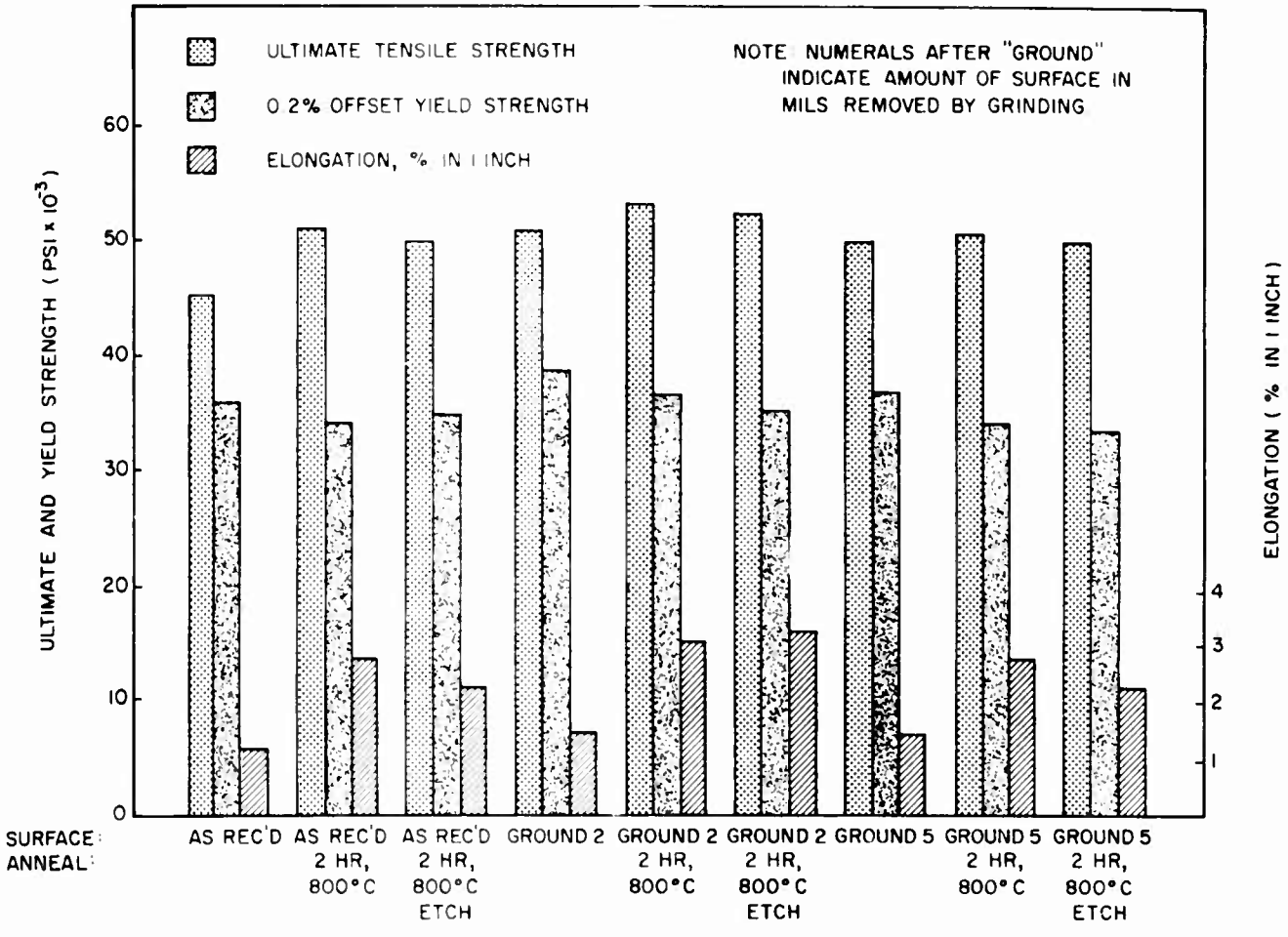

Figure 75 - Tensile properties of hot-pressed beryllium sheet.

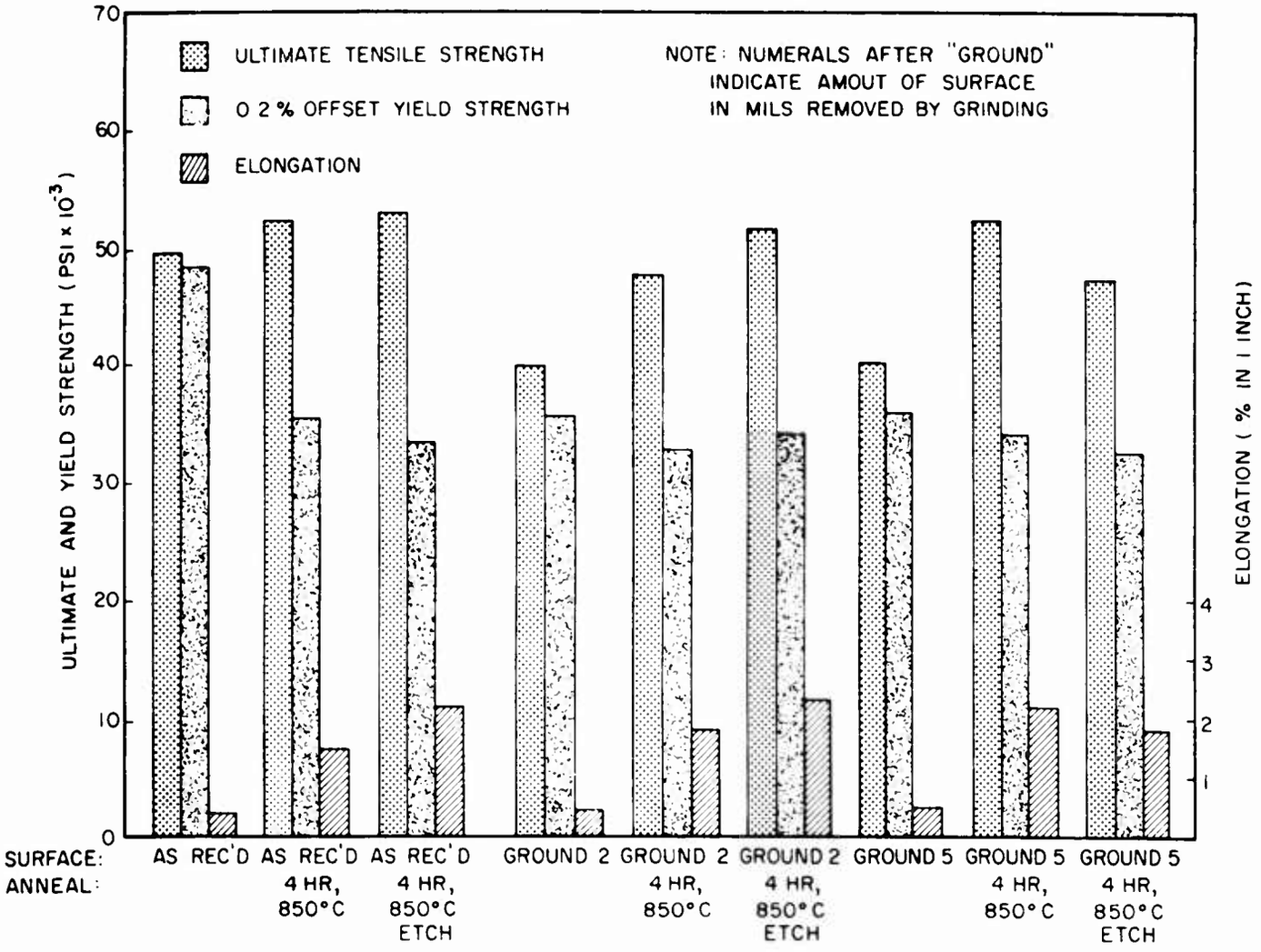

Figure 76 - Tensile properties of hot-rolled beryllium sheet (tested in the longitudinal direction).

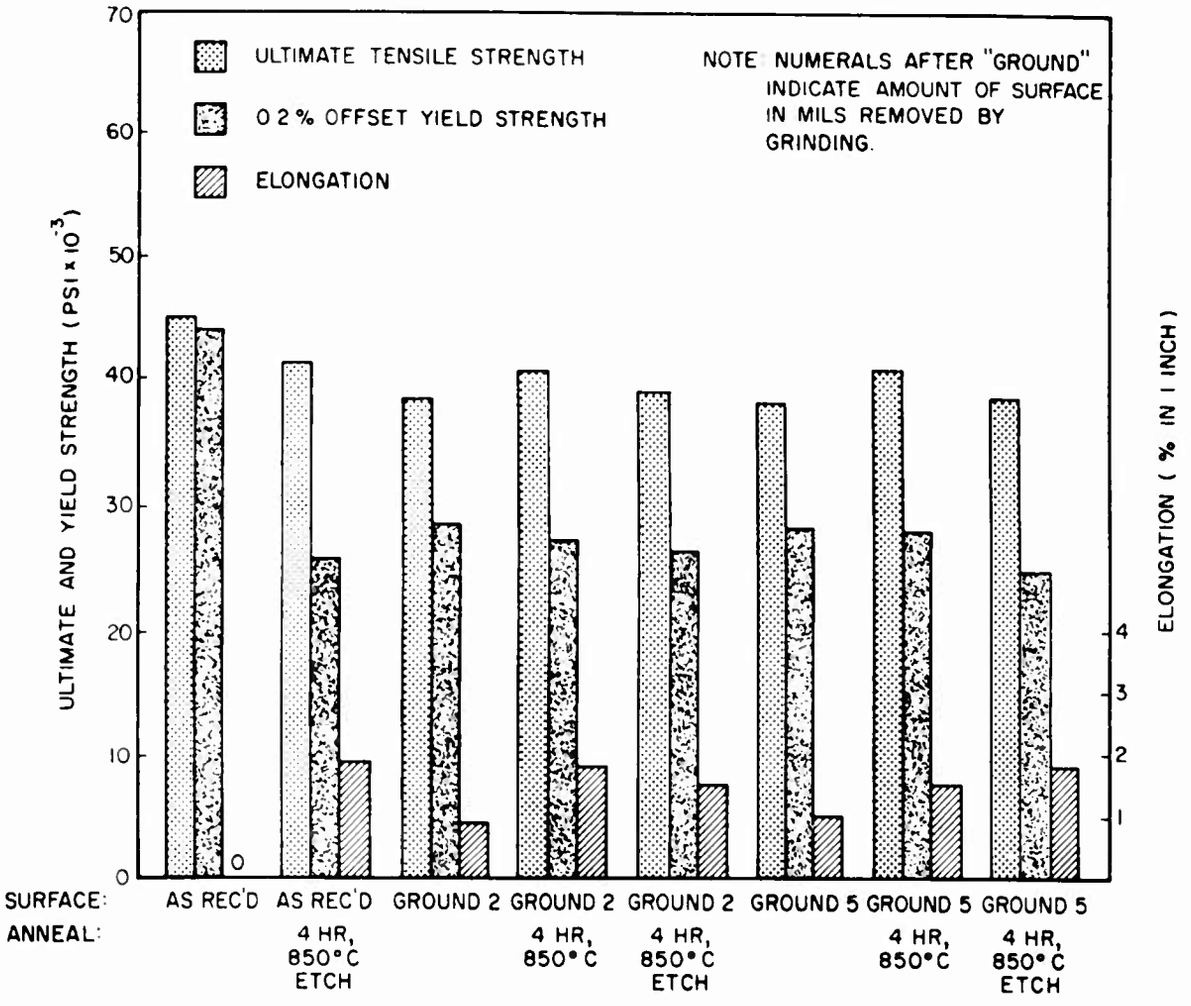

Figure 77 - Tensile properties of hot-rolled beryllium sheet (tested in the transverse direction).

Only 12 tensile samples could be machined from the available hot-upset material. However, relatively high values of ultimate strength and elongation were recorded in the four conditions tested (Figure 78). The elongation of samples ground 5 mils, annealed, and etched was 18.2%, as compared with 8.6% for as-ground samples.

6-4.2 Bend Properties. Bend data are shown in Figures 79, 80, 81, and 82 and in Tables 20, 21, 22, and 23.

Since the maximum tensile stress in bending occurs in the outer fibers of the sample, where surface damage is present, bend tests should distinguish more closely the effects of different surface treatments than tensile tests. This was found to be the case, and some rather striking improvements were noted as the result of annealing treatments.

For hot-pressed material (Figure 79), annealing roughly doubled the values of deflection and permanent bend angle recorded for the as-received or as-ground samples. Etching of the annealed samples produced further slight increases in properties in some cases, and slight decreases in others. Hot-rolled material (Figures 80 and 81) also showed significant improvements on annealing and etching, although the greatest effect again seemed to be due to annealing.

The poor nature of the surface of as-received hot-pressed sheet was shown by the fact that the as-ground samples had better properties. However, strength and ductility decreased as severity of grinding increased. For rolled material, samples ground 2, 5, and 10 mils all had similar properties in the as-ground condition.

Hot-upset sheet (Figure 82) showed some rather interesting results. Strength and ductility of as-received material was sharply increased on annealing for 4 hours at 900°C. The reason for this is not immediately apparent, since damage in the as-received samples was negligible. It is probably not related to the surface at all since the as-ground samples which showed greater surface damage (Figure 71(c)) had much better properties than the as-received material. Annealing improved the properties of the ground samples, and etching improved them still further. The effect of etching appeared to be more pronounced than for the hot-pressed or hot-rolled material.

Figures 83, 84, 85, and 86 show typical samples after bending.

A small investigation was carried out to determine the effects of etching alone on the properties of ground samples. A few untested bend samples were available to make these studies. These were as follows:

(1) Hot-rolled; transverse samples, ground 2 and 5 mils

(2) Hot-pressed; ground 2, 5 and 10 mils

(3) Hot-upset; ground 2 and 5 mils

Only one each of the above was available. A total of 10 mils was removed from the thickness of each sample by etching in 10% H_2SO_4. The results were not plotted, since the figures for this report had already been prepared, but the data are presented in Tables 21, 22, and 23. Although only one sample was tested in each

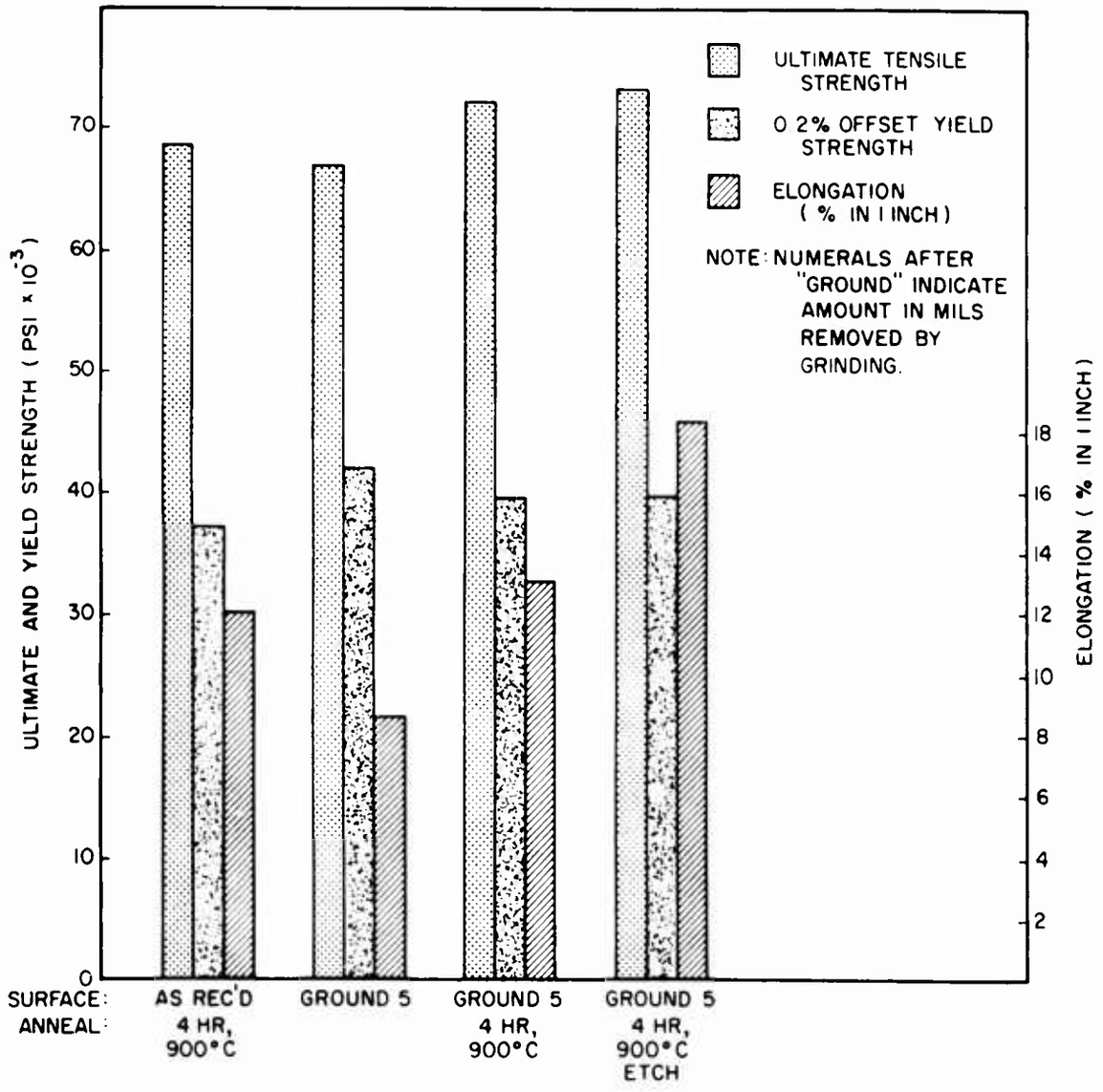

Figure 78 - Tensile properties of hot-upset beryllium sheet.

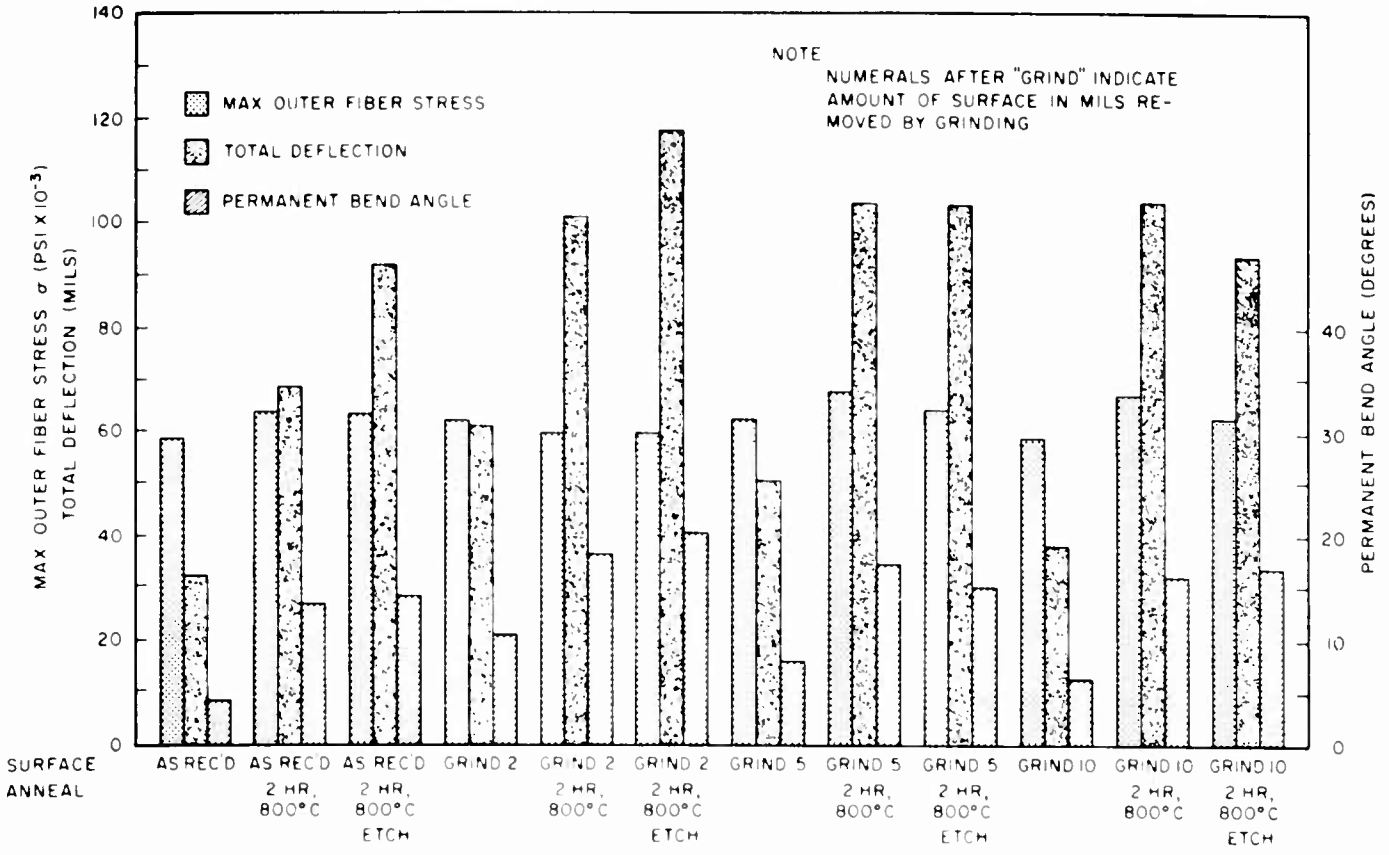

Figure 79 - Bend properties of hot-pressed beryllium sheet.

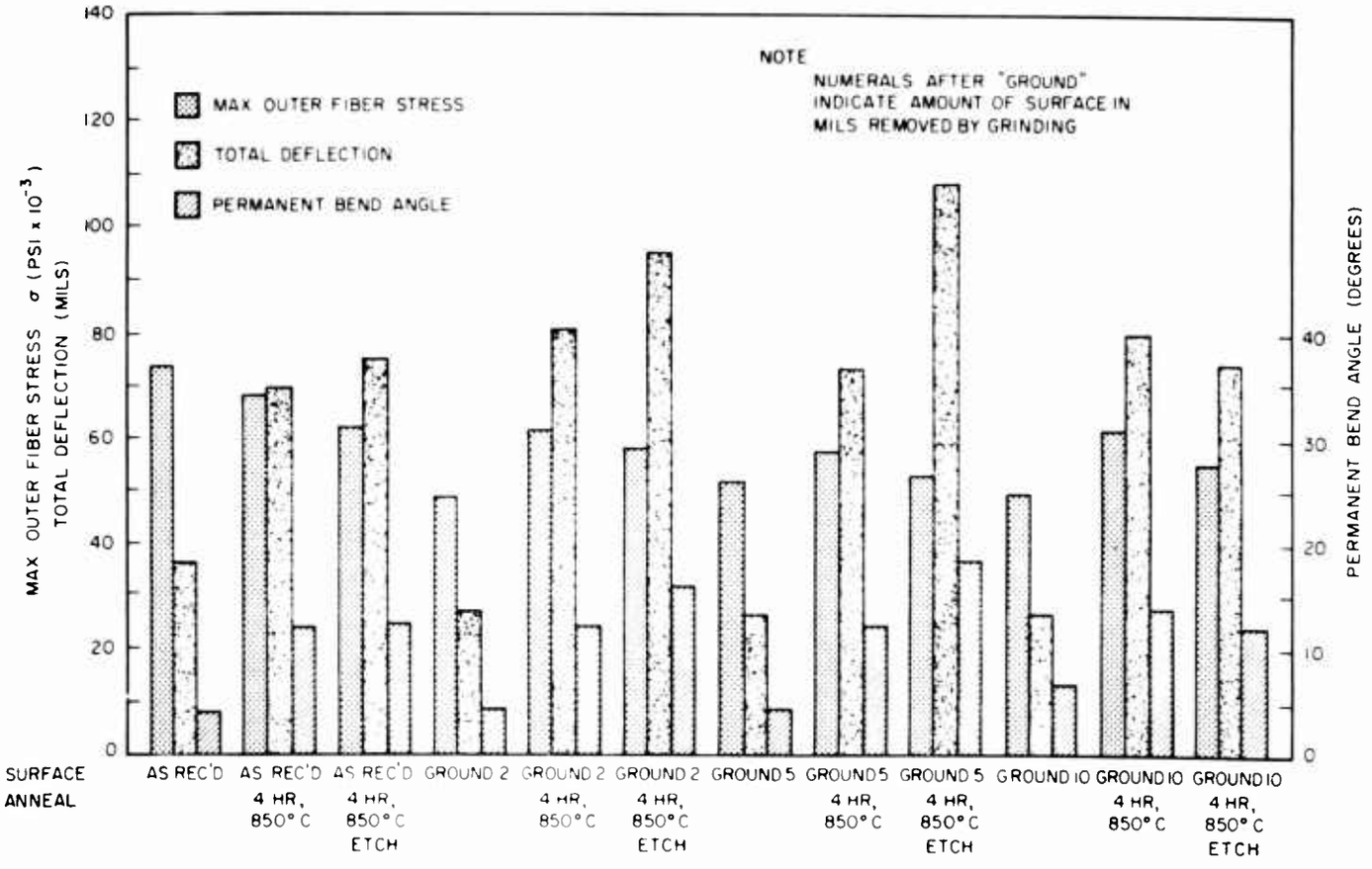

Figure 80 - Bend properties of hot-rolled beryllium sheet (longitudinal specimens).

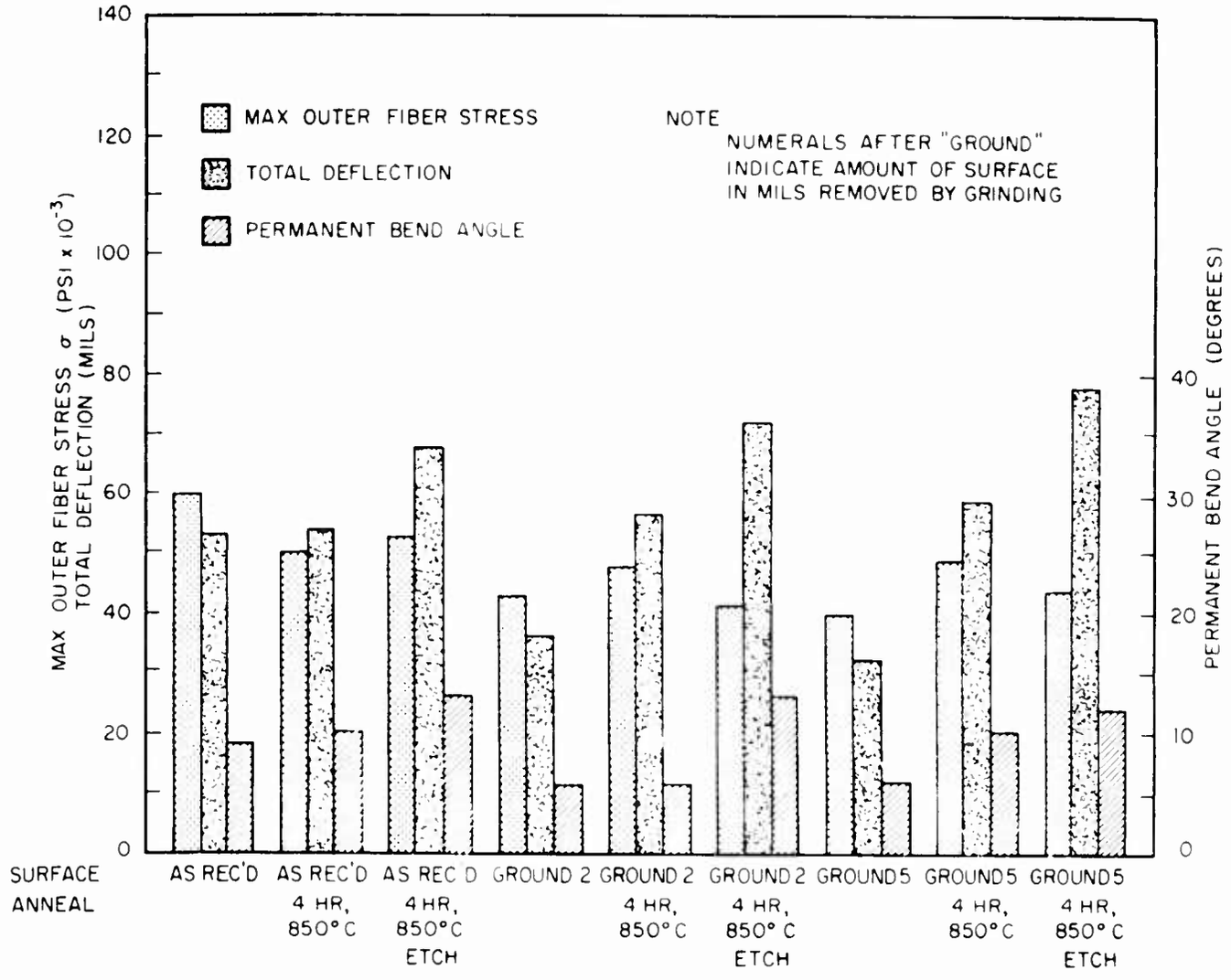

Figure 81 - Bend properties of hot-rolled beryllium sheet (transverse specimens).

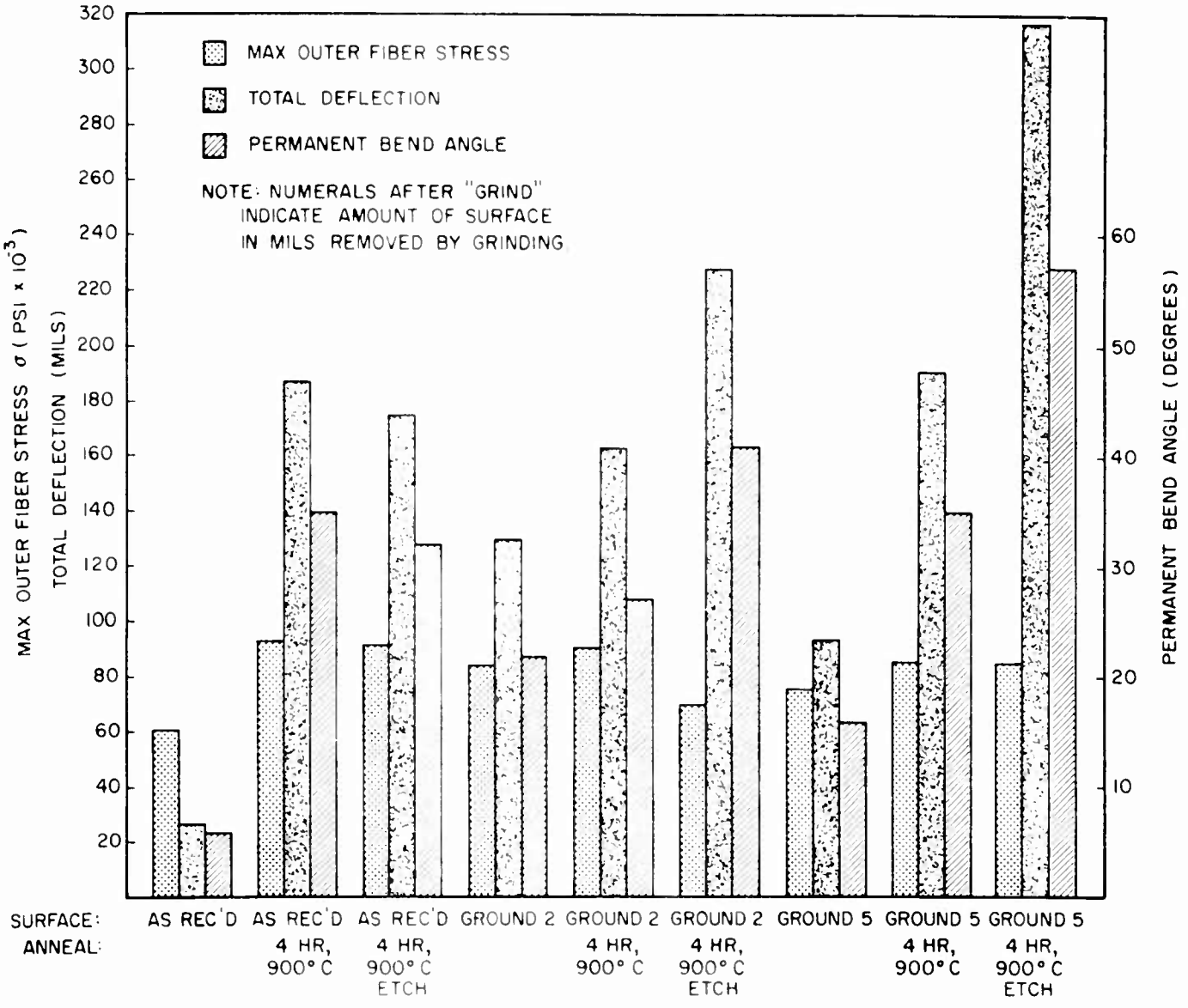

Figure 82 - Bend properties of hot-upset beryllium sheet.

Figure 83 - Bend specimens from hot-pressed sheet.

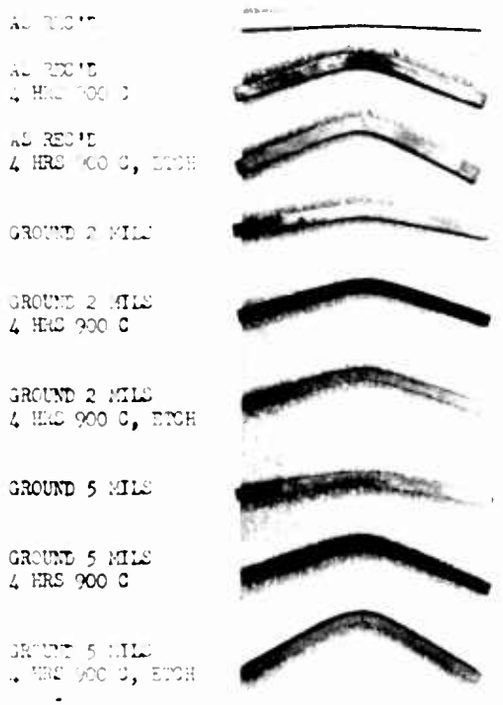

Figure 84 - Bend specimens from hot-upset sheet.

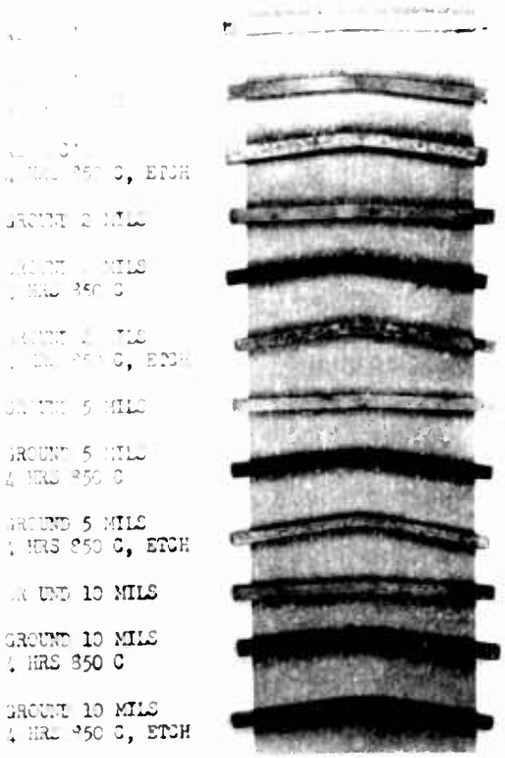

Figure 85 - Longitudinal bend specimens from hot-rolled sheet.

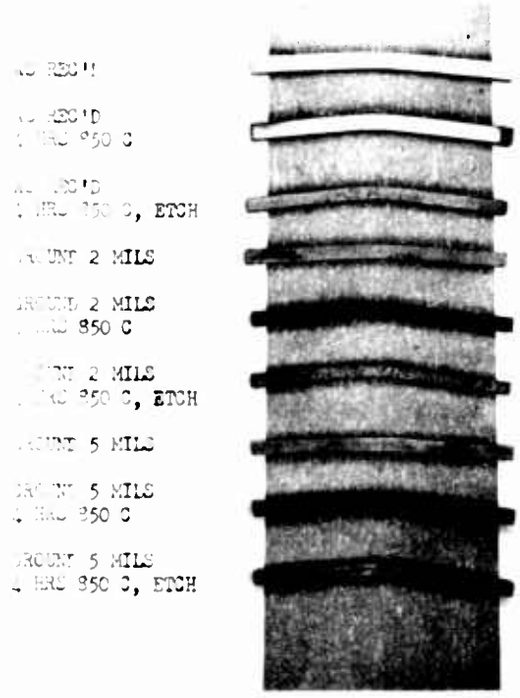

Figure 86 - Transverse bend specimens from hot-rolled sheet.

condition, it is obvious that the properties compare favorably with those obtained for annealed or annealed and etched samples.

6-4.3 Impact Properties. Impact properties are plotted on a semi-logarithmic scale in Figures 87, 88, 89, and 90 with each point representing one specimen only. The curves generally confirm the results obtained in bend tests. It may be noted that the impact curves tend to merge in the vicinity of 500°C, indicating that surface effects are not important at this temperature.

Some samples, particularly in hot-pressed sheet, exhibited a maximum in ductility at 500°C. This is similar to the usually observed tensile behavior, although no evidence of intergranular failure could be seen in the samples tested at 600°C. Tensile failure is usually completely intergranular at 600°C. The high strain rate associated with impact testing has probably moved the transgranular→intergranular fracture transition to a temperature above 600°C.

6-5 RESULTS OF DEFORMATION STUDIES

In this section, four series of photomicrographs are presented to show some of the results obtained when the polished samples described in Section 6-2.5 were bent in the Flinn Strain Viewer. In all of the photographs shown, the tension side of the sample is at the top of the figure. Because of the length of time required to obtain satisfactorily polished surfaces, only a few samples were actually prepared, and these were all from hot-pressed sheet.

Figure 91 shows a sequence of photographs resulting from the bending of as-received sheet. The original structure is shown in Figure 91(a), while 91(b) shows the locations of the first cracks observed. Note both the cleavage cracks forming in twinned regions of the surface grains and the intergranular crack below the surface. This and many subsequent photographs show cleavage cracks as white lines, which might be mistaken for twins. However, this is typical of polarized light pictures, and examination in bright field confirmed the fact that the white areas were cracks and not twins. Additional cleavage cracks have formed in Figure 91(c) and Figures 91(d), (e), and (f) show the spread of these cracks. The large crack at the left is seen to have progressed by a combination of inter- and intracrystalline failure.

Hot-pressed sheet that was annealed and etched to remove surface damage is shown in Figure 92(a) In Figure 92(b), a cleavage crack has been initiated at an impurity particle in a grain boundary. Figure 92(c) shows the progression of this crack and the initiation also at a grain boundary but not at any visible impurity particle, of a new cleavage crack. However, there is a possibility that this crack did originate at an impurity particle slightly below the plane of the photograph. Figure 92(d) shows the further spread of the existing cracks, again by inter- and intracrystalline means. Figure 92(e) shows the nucleation of a cleavage crack in another area, while an intergranular crack is shown in Figure 92 (b) The latter two photomicrographs and the one in 92(b) were all taken at the same applied stress.

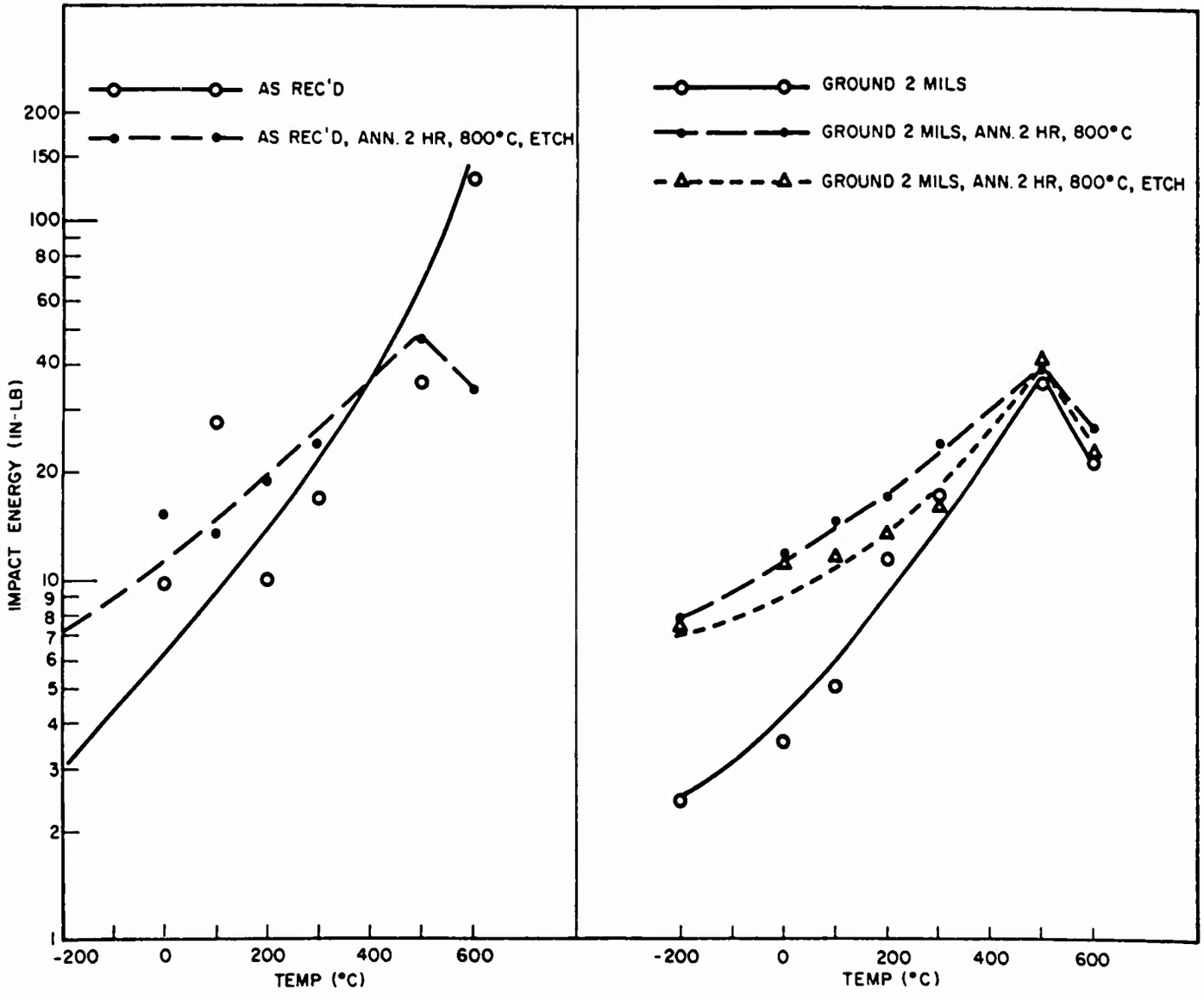

Figure 87 - Impact properties of hot-pressed beryllium sheet.

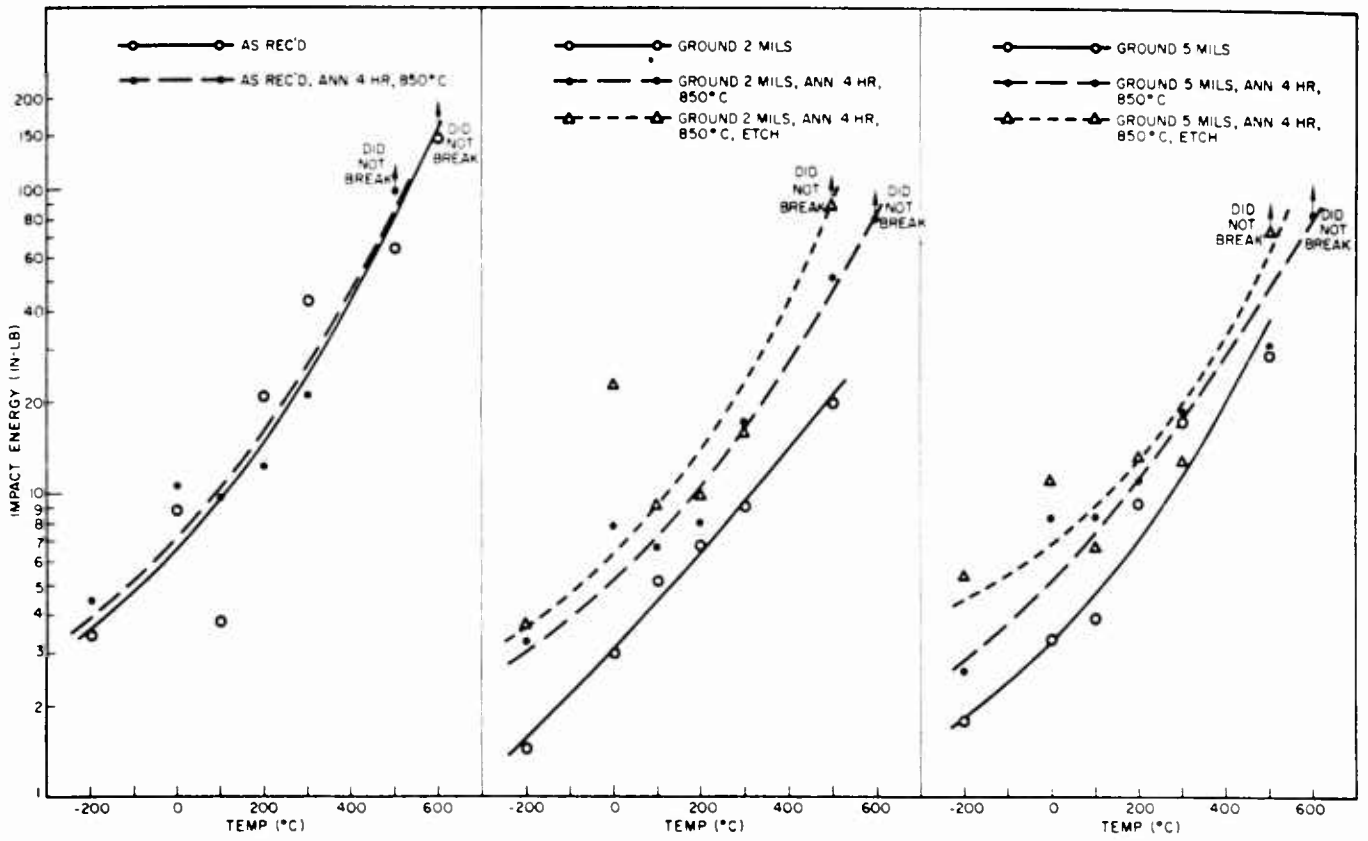

Figure 88 - Impact properties of hot-rolled beryllium sheet (longitudinal specimens).

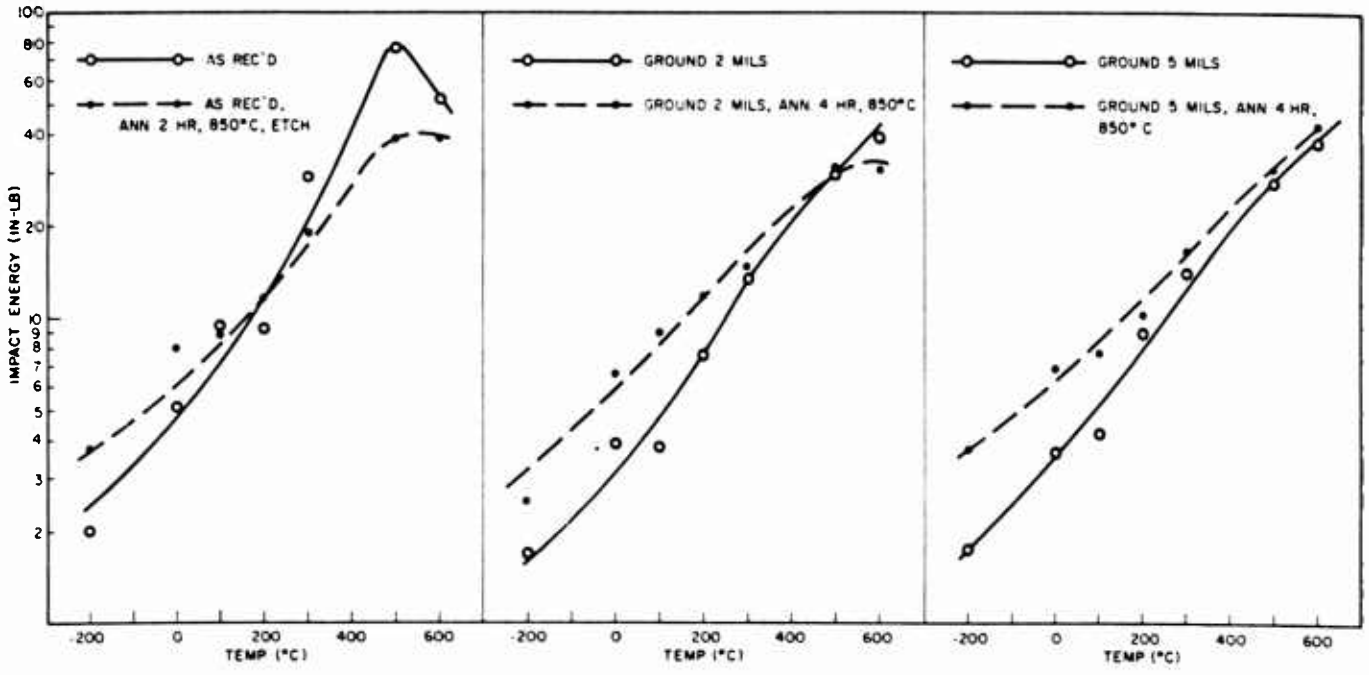

Figure 89 - Impact properties of hot-rolled beryllium sheet (transverse specimens).

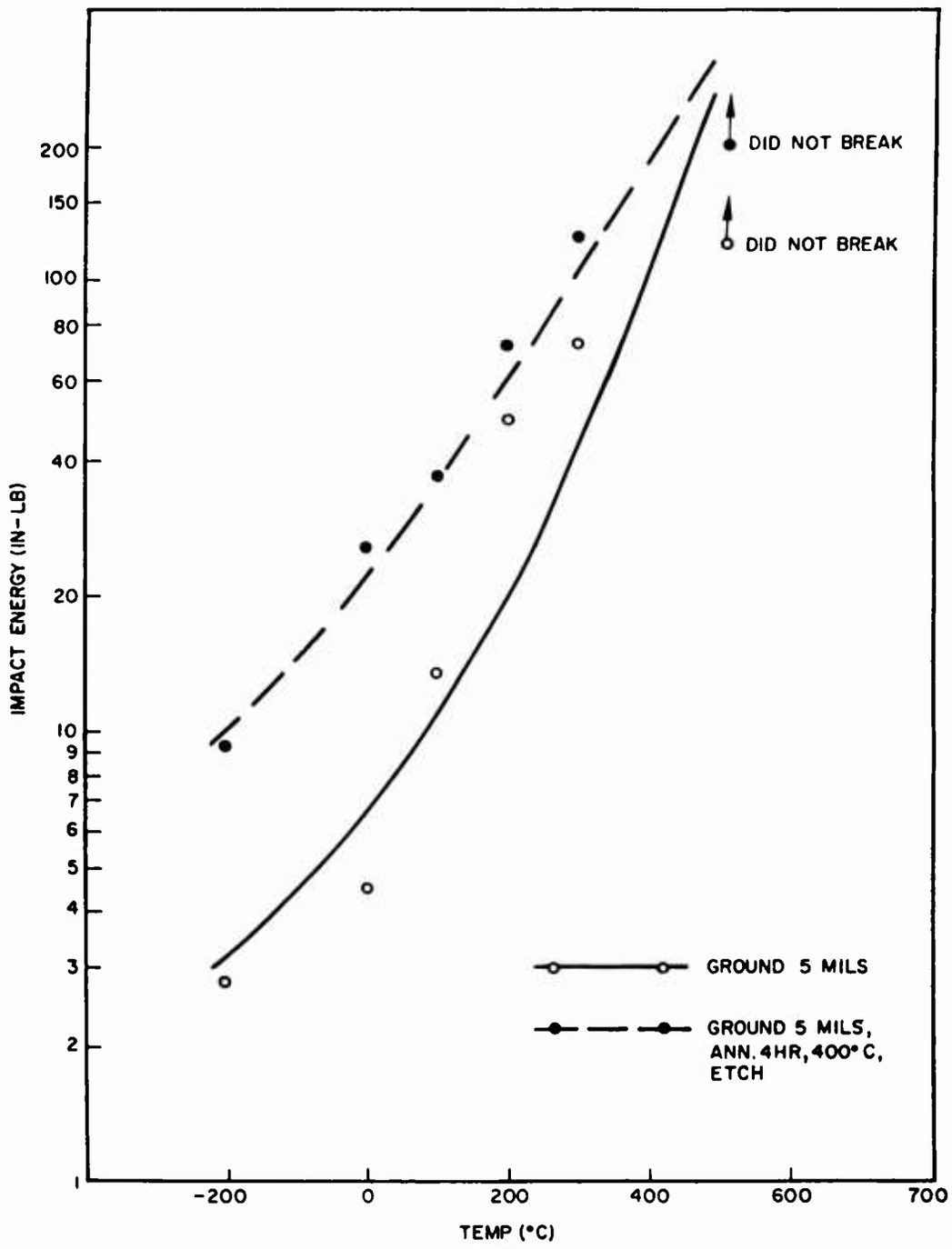

Figure 90 - Impact properties of hot-upset beryllium sheet.

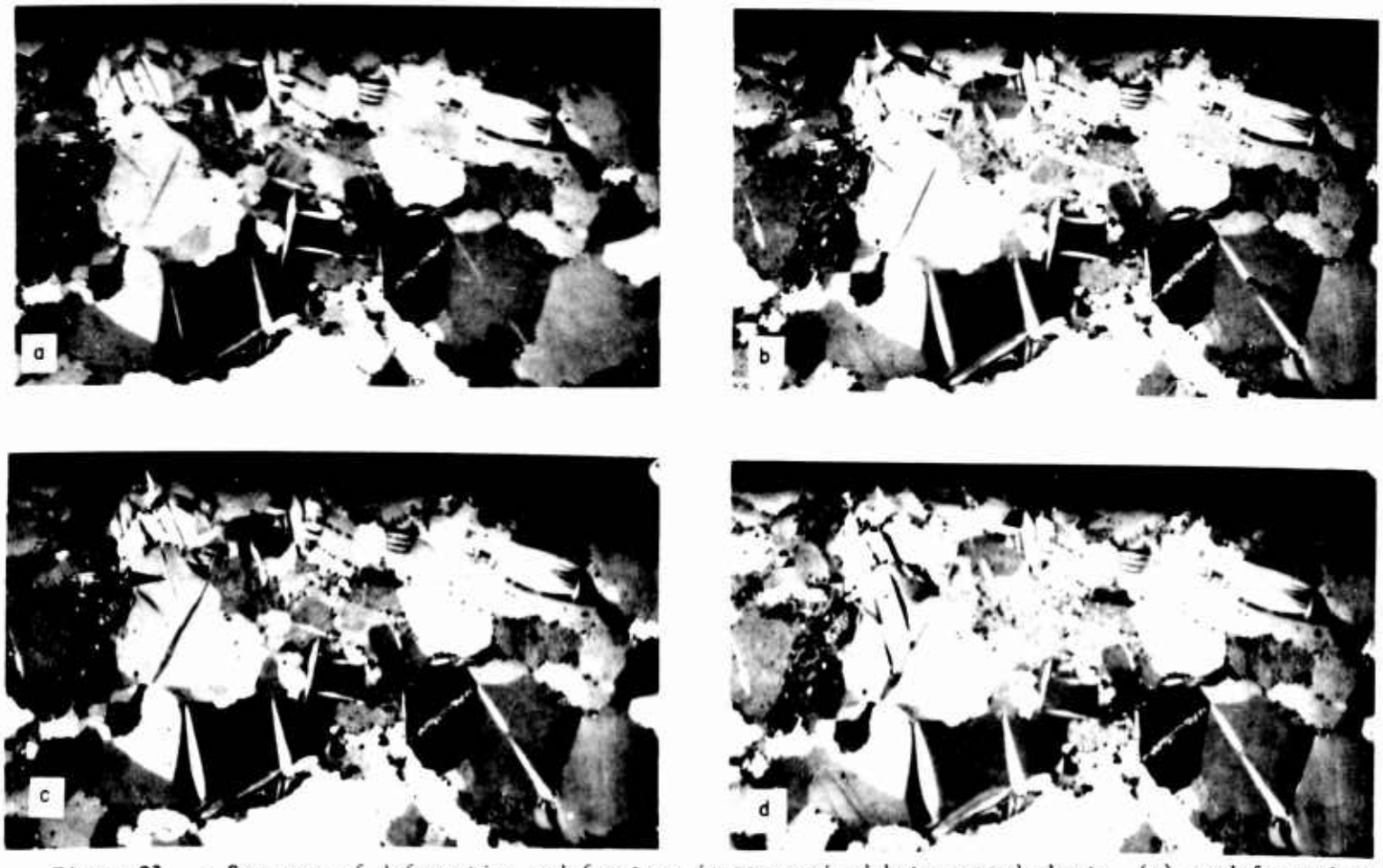

Figure 91 - Sequence of deformation and fracture in as-received hot-pressed sheet: (a) no deformation; (b) cleavage and intergranular cracks (at arrows, upper left and lower right respectively) formed after deformation has begun; (c) additional cleavage cracks (arrow); (d) progression of cleavage cracks. (Sequence continued on following page.)

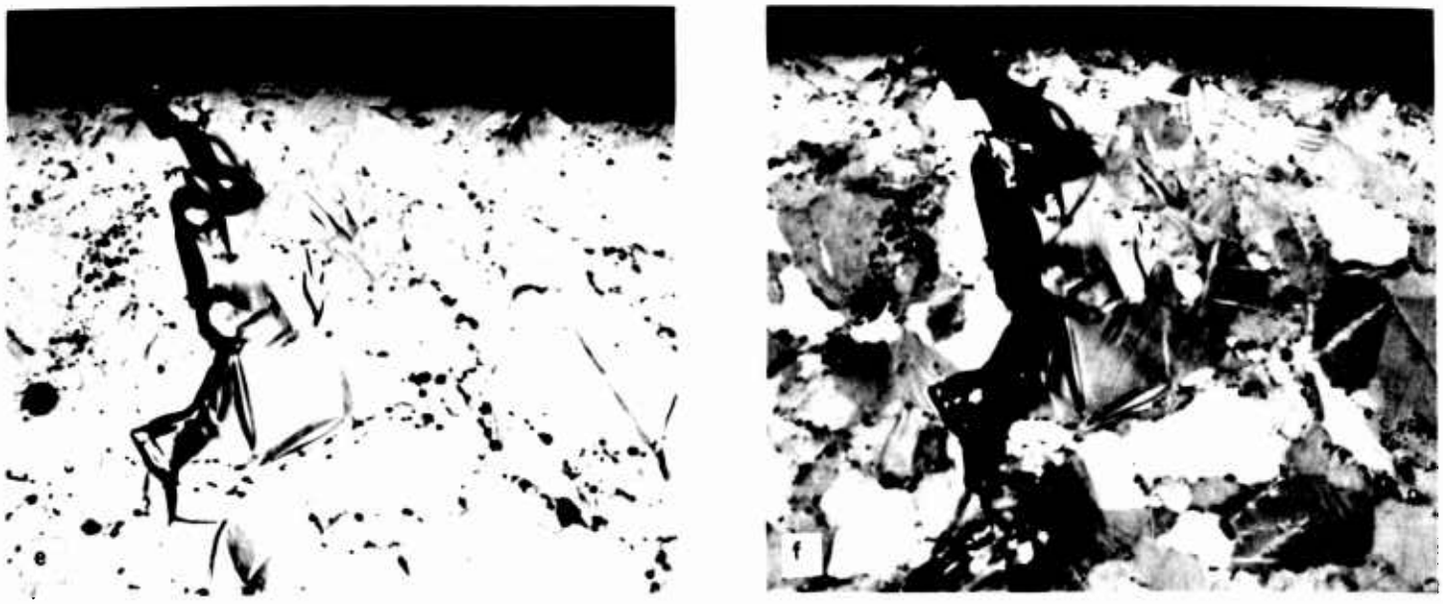

Figure 91 (Cont.) Sequence of deformation and fracture in as-received hot-pressed sheet: (e) advanced stage of fracture (bright light); (f) final fracture. (All photos 500X; polarized light, except (e))

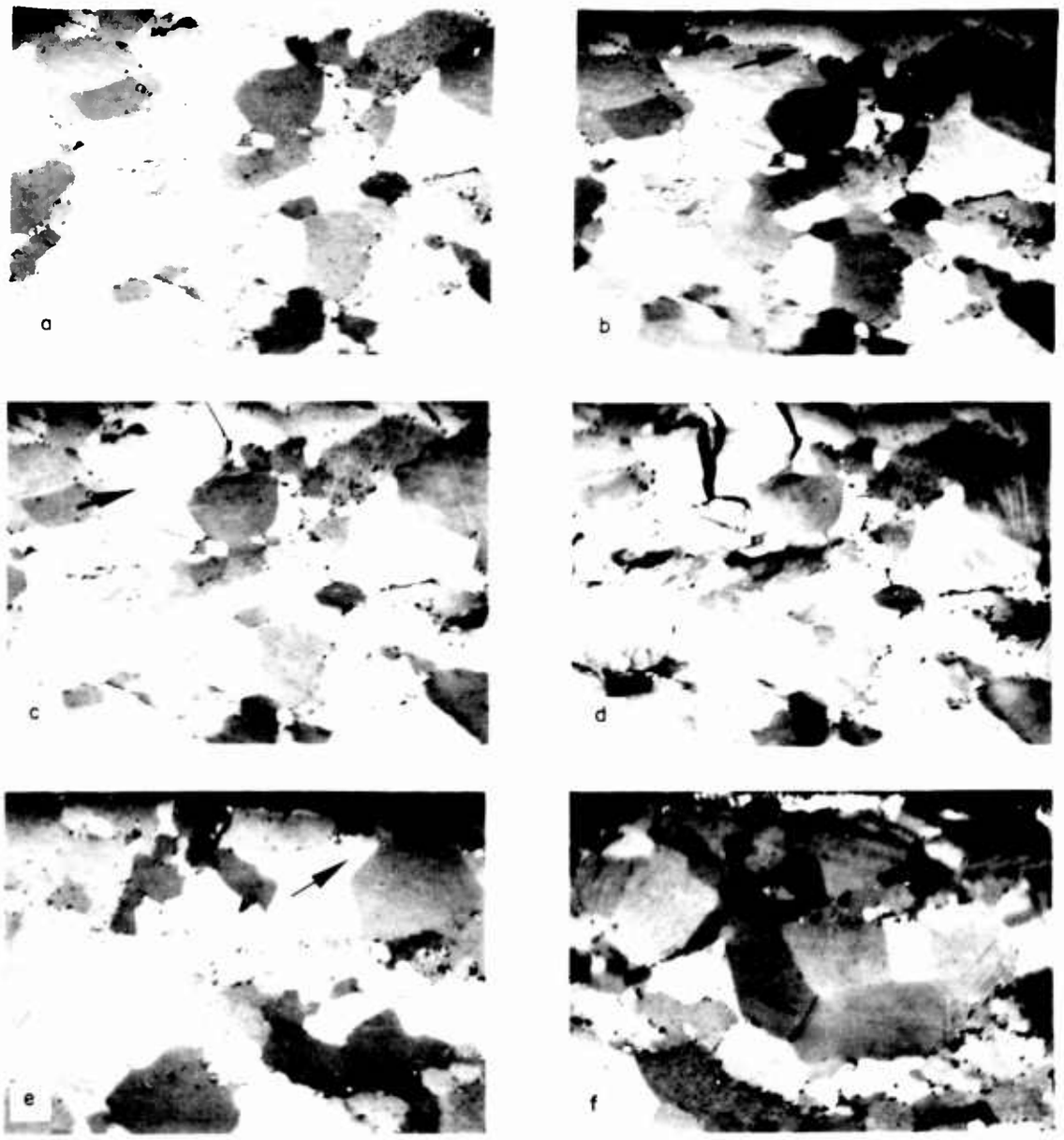

Figure 92 - Sequence of deformation and fracture in hot-pressed sheet after as-received surface was modified by annealing 2 hr at 800°C and etching: (a) no deformation; (b) cleavage crack (arrow) starting at impurity particle in grain boundary; (c) progression of crack in (b) and nucleation of new crack (arrow); (d) crack nucleated in (c) has proceeded both transgranularly and intergranularly; (e) and (f) transgranular and intergranular cracks nucleated at the same time as in (b). (All photos 500X; polarized light)

Hot-pressed sheet with 2 mils ground from the surface is shown in Figure 93(a). In Figure 93(b), cracks have formed at the intersection of a twin and a grain boundary, and at impurity particles in grain boundaries. Figures 93(c), (d), (e), and (f) trace the progress of these and other cracks. The black wavy lines originally seen in Figure 93(b) are slip lines and are not be be confused with cracks.

The sequence of photographs in Figure 94 shows the nucleation of a crack in a heavily twinned grain of a sample that was ground 5 mils. This crack progressed across the twinned region and also along a twin-matrix interface until the grain boundary was reached. In Figure 94(e), the crack is seen to spread along the grain boundary, prior to transmittal to other grains.

6-6 DISCUSSION

The preceding experiments have clearly shown that a relationship exists between surface microstructure and mechanical properties. It has been known for some time that properties of machined samples could be improved by annealing and/or etching treatments[4]. However, the mechanism whereby the properties were improved has not been completely understood.

The metallographic studies in this investigation have demonstrated that surface damage consists of twins and cracks, which increase in extent as severity of machining increases.

The presence of these defects limits the ductility of ground samples or of as-received material. Annealing at a suitable time and temperature removes the great majority of the twins and thereby effects considerable improvements in mechanical properties. Annealing also serves to eliminate the residual stresses that result from machining. The detrimental effect of twins was revealed in the deformation studies of polished surfaces. Cracks can initiate in twinned regions and at the intersections of twins and grain boundaries and can propagate along twin-matrix interfaces.

Etching after annealing removes the machining cracks present, as well as any twins that were not removed in the annealing operation. In the case of hot-pressed and hot-rolled material, etching after annealing sometimes improved properties and at other times effected little or no improvement. For hot-upset sheet, etching clearly improved the tensile and bend properties of ground and annealed samples.

It is not necessary to anneal in order to remove surface damage. Bend tests of ground samples that were only etched clearly demonstrated that etching alone resulted in improvements similar to those obtained for annealed or annealed and etched samples.

The studies in which the deformation and fracture of polished sections were observed revealed some interesting features. For one, impurities were seen to play an important role in room-temperature fracture, as many cleavage fractures were observed to start at impurity particles in grain boundaries. Although many cases were observed in which $(11\bar{2}0)$ bend planes or kink-band boundary planes had clearly formed in a particular grain, no fractures were ever seen associated with them, in contrast to the results obtained by Tuer and Kaufmann for single crystals[5]. It

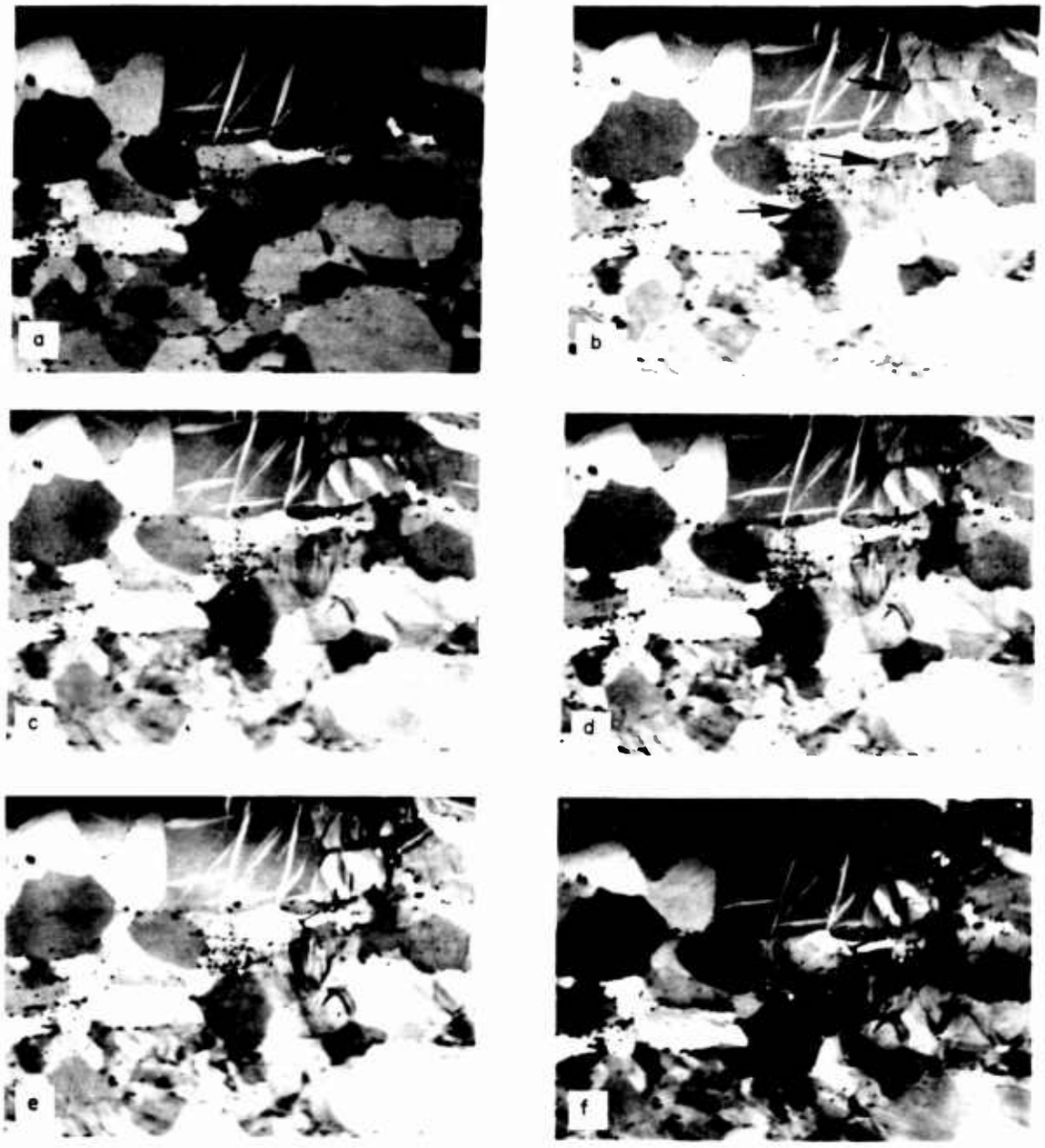

Figure 93 - Sequence of deformation and fracture in hot-pressed sheet ground 2 mils: (a) area prior to deformation -- note small twins (arrow); (b) twins have widened and intergranular crack formed -- transgranular cracks have also started (arrows); (c) black wavy lines (arrow) are slip lines; (d), (e) and (f) progression of deformation features. (All photos 500X; polarized light).

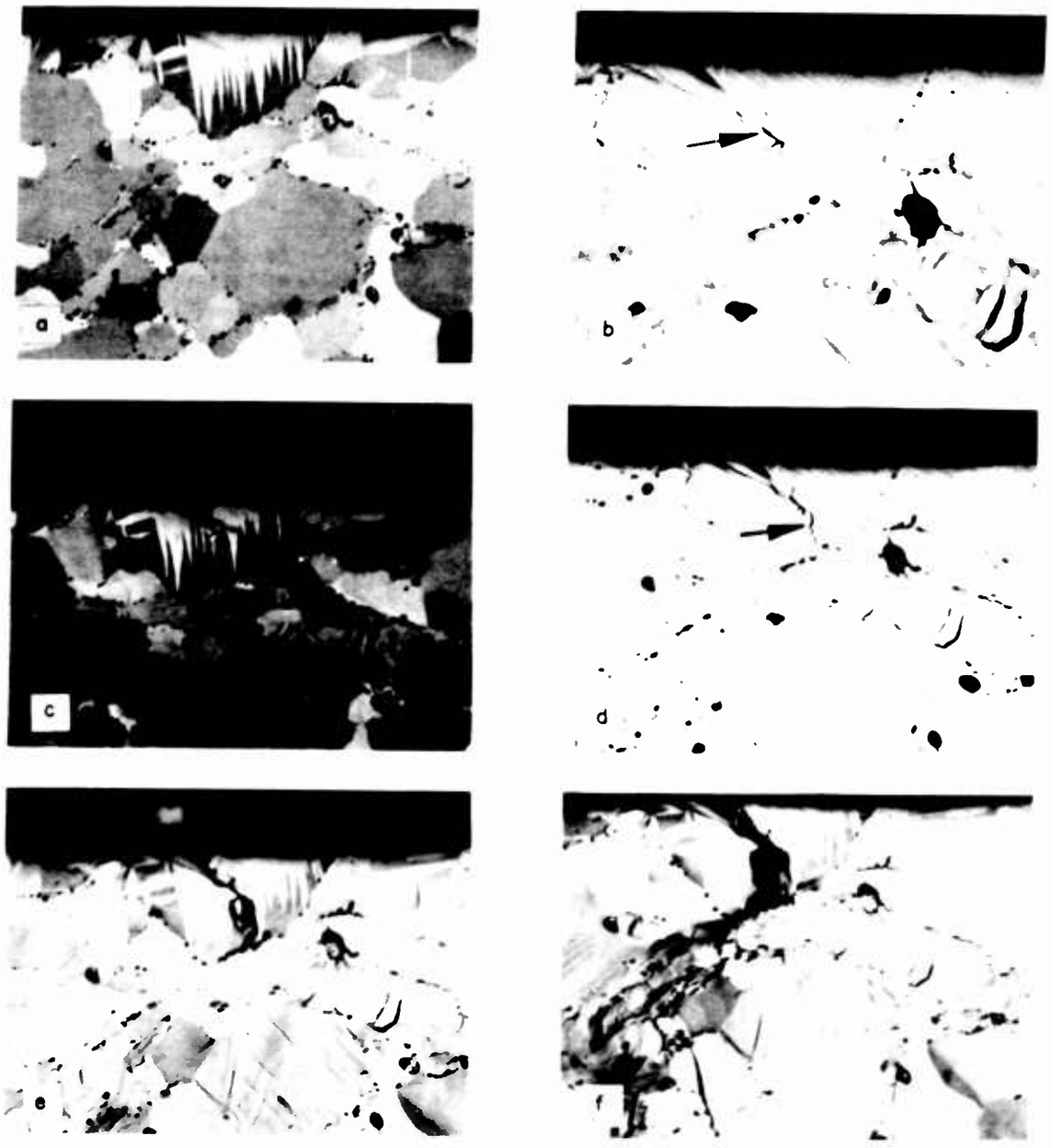

Figure 94 - Sequence of deformation and fracture in hot-pressed sheet ground 5 mils: (a) no deformation (polarized light, 500X); (b) crack (arrow) nucleated after deformation in heavily twinned region (bright light, 750X); (c) crack progressing along twin-matrix interface (polarized light, 500X); (d) same as (c) bright light, 500X); (e) and (f) crack at subsequent stages of deformation (polarized light, 500X).

is possible that the small grain size of the hot-pressed sheet made it difficult to observe the formation of such defects. In those cases where bend planes or kink-band boundaries were observed, fracture had already begun at several other locations. This might have relieved stresses sufficiently to prevent formation of kink-cleavage plane defects. Stroh[6] suggests that grain boundary constraints might prevent the bend-plane fracture mechanisms observed in single crystals from operating in polycrystals.

It was also found that intergranular cracks could form at room temperature, and that cracks could propagate along grain boundaries, at least during the initial stages of crack propagation. The fracture of beryllium at room temperature is usually reported to be transgranular. It is believed that the initial, slowly formed cracks can be either intergranular or transgranular, but once a critical stress level is reached in a local area, crack velocities are so rapid that only cleavage failure occurs. The proportion of cleavage fracture to intergranular fracture is so high that the observed fractured surfaces appear to have failed by transgranular fracture alone.

It might be mentioned here that as-received sheet showed the presence of both intergranular and transgranular cracks. A particularly good example of this is shown in Figure 95, which is a sample of as-received hot-pressed sheet that has been annealed to remove twins.

The fine grain size of hot-upset sheet is no doubt a factor contributing to the lesser amounts of surface damage observed in ground samples of this material. It is difficult to transmit twinning and cracking stresses from grain to grain for any great depth.

The electron diffraction studies showed that grinding produced a thin layer of basal-plane layered material at the surface of the sheet. It was not possible to determine the depth to which this layer extended in polycrystals because of interference from BeO. However, the single crystal study showed that this layer was at least no greater than 1/2 mil (5×10^{-4} in.) deep. Scott and Wilman[3] found that in polycrystalline samples the effects of abrasion persisted to a depth of 1×10^{-4} in., and in single crystals, to a depth of 2×10^{-4} in.

It was concluded that grinding produces a fragmentation of the surface grains to a depth of 500 Å since the single crystal sample showed polycrystalline rings at that depth.

The effect of the highly oriented surface layer on mechanical properties is not clear. However, it would be expected that if the surface consists primarily of basal planes, then $(11\bar{2}0)$ cracks can form either by bending of the basal planes or by tension perpendicular to prior-formed $(11\bar{2}0)$ bend planes (5, p. 403). Removal of this layer would then be expected to result in improvement of properties.

Figure 95 - Intercrystalline crack which begins at surface of hot-pressed sheet, propagates to a depth of approximately 0.002 in., and then proceeds as a transcrystalline crack. (Sheet annealed 2 hr at 800°C. Photo at 1000X; polarized light).

REFERENCES

1. C. O. Matthews, M. I. Jacobson and W. E. Johsman, Beryllium Crack Propagation and Effects of Surface Conditions, WADD Technical Report 60-116, Lockheed Missiles and Space Company, Jan. 1960.

2. M. Udy, Metallography, in The Metal Beryllium, p. 505, Amer. Soc. Metals, Cleveland, Ohio, 1955.

3. V. D. Scott and H. Wilman, Surface Reorientation Caused on Metals by Abrasion, Proc. Roy. Soc. (London), 247:353 (1958).

4. A. R. Kaufmann, P. Gordon, and D. W. Lillie, The Metallurgy of Beryllium, Trans. Amer. Soc. Metals, 42:785 (1950).

5. G. L. Tuer and A. R. Kaufmann, Ductility of Beryllium as Related to Single Crystal Deformation and Fracture, in The Metal Beryllium, p. 372, Amer. Soc. Metals, Cleveland, Ohio, 1955.

6. A. N. Stroh, The Cleavage of Metal Single Crystals, Phil. Mag., 3:597 (1958).

Appendix 6A

DETERMINATION OF PREFERRED ORIENTATION

By R. Bragg, C. Packer, and J. Ho

6A-1 GENERAL

Basal pole figures of the as-received hot-pressed, hot-rolled, and hot-upset beryllium sheets were obtained (Figures **96, 97,** and **98** from nominal 1-inch squares about 0.3 cm thick. The specimens were mounted in a General Electric automatic pole figure goniometer used in conjunction with a GE XRD-5 diffraction unit. Good general discussions of the techniques are available[1,2,3], but certain unusual problems encountered in studying beryllium metal require further discussion. These problems arise because of the deep penetration of the X-ray beam and the near superposition of the (0002) and (1011) reflections. A further difficulty, common to all pole figure determinations, is found in expressing the results relative to random orientation.

The problem of closely juxtaposed lines is most readily solved by resorting to narrow slits and using peak rather than integrated intensities. Because of the low absorption coefficient, the angle 2θ at which a (0002) maximum occurs is a function of α, the angle between the (0002) planes and the specimen surface[4]. It is therefore necessary to determine the correct goniometer setting for each value of α.

6A-2 GEOMETRICAL CORRECTIONS

The finite thickness of the specimen holder of the pole figure goniometer results in an annulus region in which the diffracted beam is blocked by the holder. Therefore, it is not physically possible to obtain the entire pole figure with one radiation at a particular Bragg angle. In and near this "blind" region, the absorption correction is very uncertain because of the long paths followed by the X-ray beam and the large errors in intensity measurements which can be caused by slight deviations from the correct settings. To correct this condition, two radiations were used to overlap the "blind" region. For the (0002) pole figure, measurements were made with molybdenum K_α radiation in transmission (α_T = 0 to 65 degrees) and in reflection (α_R = 80 to 90 degrees), and chromium K_α was also used for reflection measurements (α_R = 60 to 90 degrees).

The diffracted intensities were corrected for absorption by means of the following equations.

Transmission:

$$I_{corr.} = I_{obs}\left[\frac{I\ (\alpha = o)}{I\ (\alpha = \alpha)}\right] = I_{obs}\left[\frac{\left\{\frac{\cos\ (\theta - \alpha)}{\cos\ (\theta + \alpha)} - 1\right\} \mu t \exp\ (-\mu t/\cos\ \theta)}{\cos\ \theta\ \{\exp\ (-\mu t/\cos\ [\theta - \alpha]) - \exp\ (-\mu t/\cos\ [\theta + \alpha])\}}\right]$$

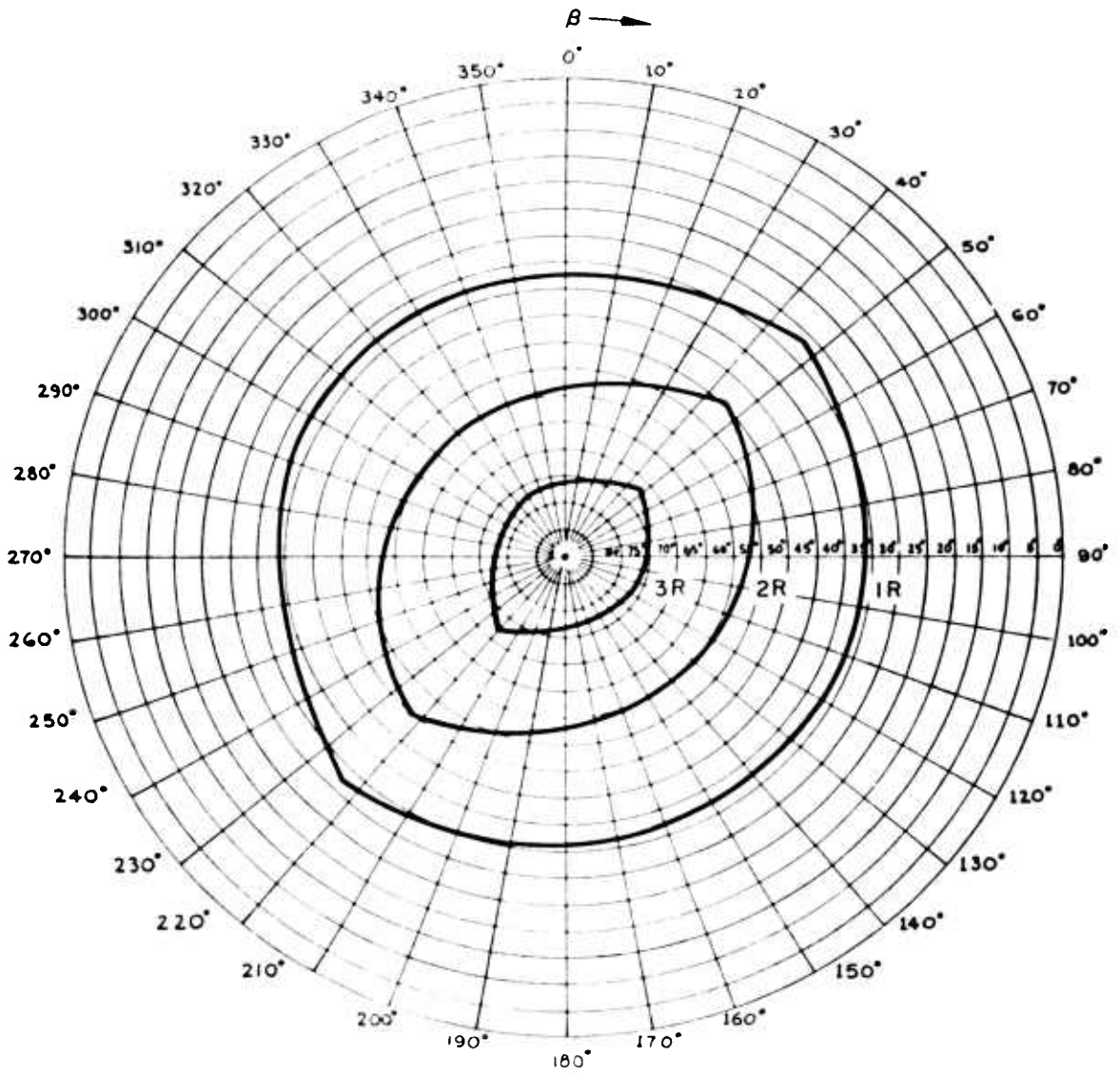

Figure 96 - (0002) pole figure for hot-pressed sheet; pressing direction unknown.

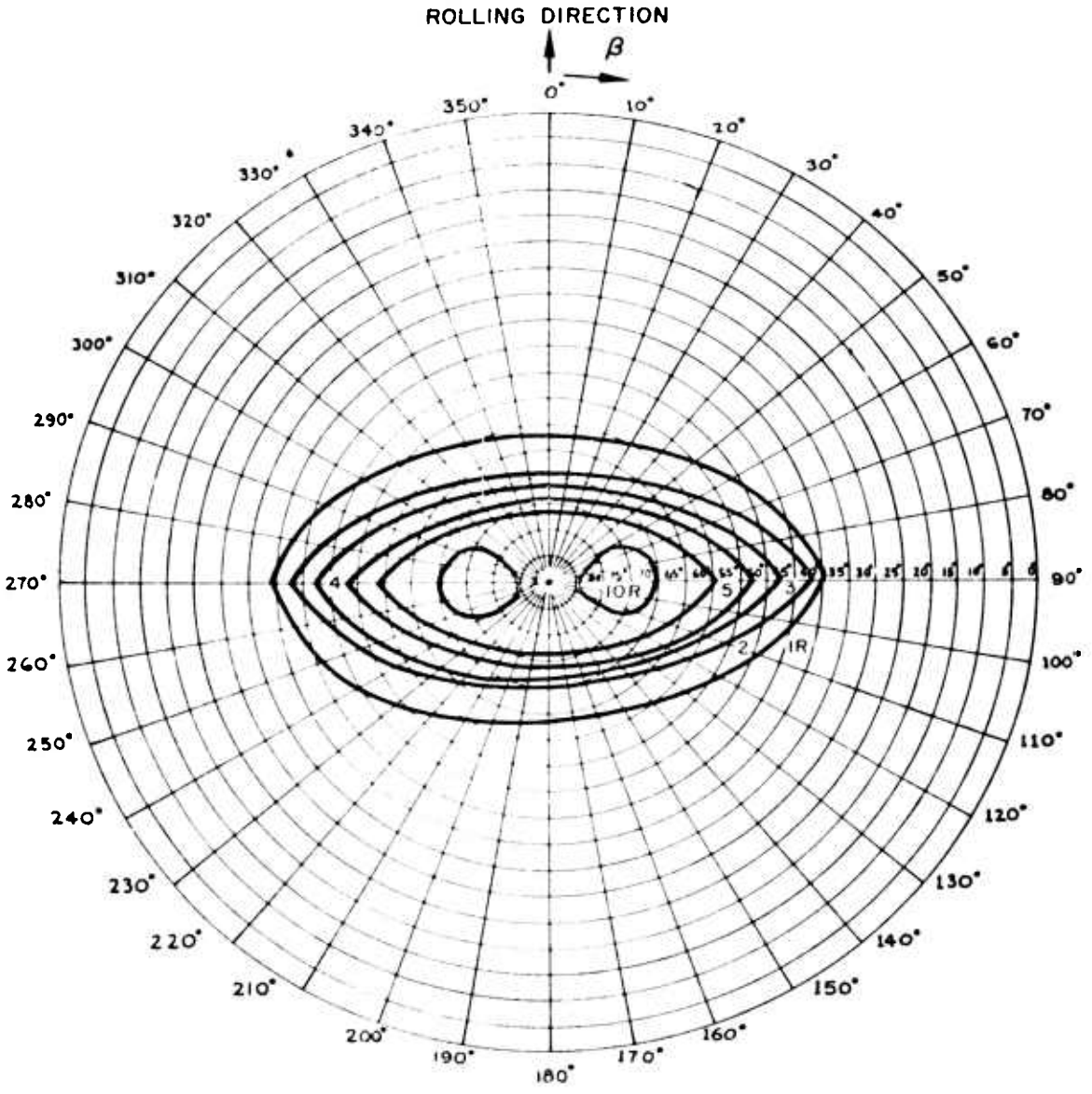

Figure 97 - (0002) pole figure for hot-rolled sheet.

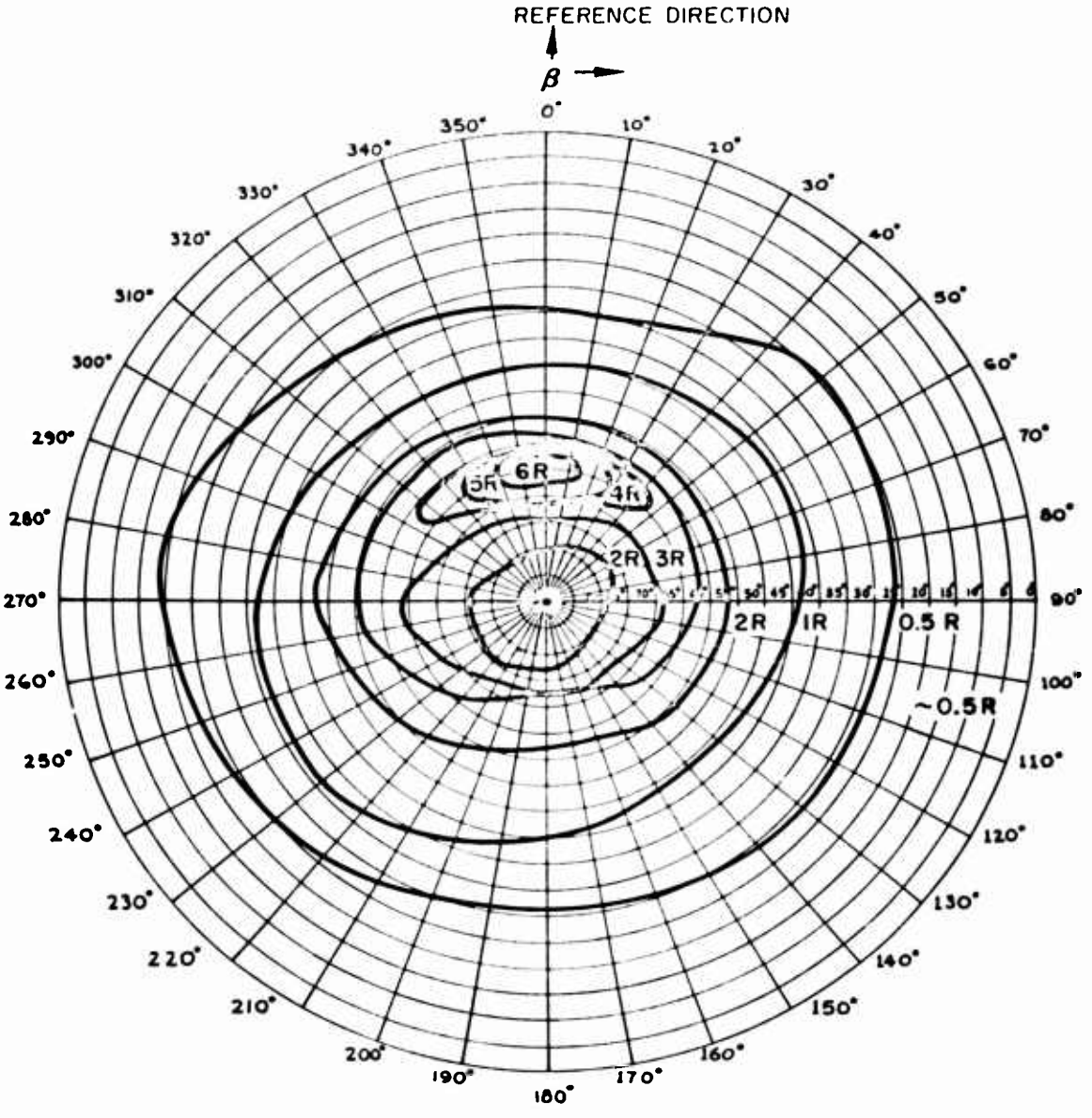

Figure 98 - (0002) pole figure for hot-upset sheet.

Reflection:

$$I_{corr.} = I_{obs}\left[\frac{I\ (\alpha = 0)}{I\ (\alpha = \alpha)}\right] = I_{obs}\left[\frac{1 + \frac{\sin\ (\theta + \alpha)}{\sin\ (\theta - \alpha)}\ \left\{1 - \exp\ (-2\mu t/\sin\ \theta)\right\}}{1 - \exp\left[-\mu t\left[\frac{1}{\sin\ (\theta + \alpha)} + \frac{1}{\sin\ (\theta - \alpha)}\right]\right]}\right]$$

The linear absorption coefficients (μt) of the specimens for the two radiations were measured by counting the (0002) reflection of graphite with and without the specimen in front of the detector slit, and calculating the results according to

$$\ell n \left(\frac{I_0}{I}\right) = \mu t$$

The entire pole figure was first expressed in terms of molybdenum radiation by multiplying the corrected results obtained using chromium radiation by the average ratio of corrected intensities (Mo/Cr) in the range α_R = 80 to 90 degrees. These data were then normalized relative to a randomly oriented specimen using the method described below.

6A-3 NORMALIZATION OF POLE FIGURE

The data as obtained above are proportional to n (α, β), the volume of diffracting material oriented to have the (0002) normal pointing in the solid angle $d\omega$ at α, β. Here β is the angle of rotation in the specimen plane relative to the reference direction. Evidently

$$\iint n\ (\alpha, \beta)\ d\omega = V$$

where V is the total volume of material irradiated by the X-ray beam. Referring α and β to the usual polar coordinates (r, θ, φ), we have the correspondence

$$r \longleftrightarrow r$$
$$\theta \longleftrightarrow 95 \text{ degrees} - \alpha$$
$$\varphi \longleftrightarrow \beta$$

Since $d\omega = \cos \alpha d\alpha d\beta$, then, for the positive half plane (irradiated side of specimen), the relation

$$\int_0^{2\pi} \int_{\pi/2}^{0} n\ (\alpha, \beta) \cos \alpha d\alpha d\beta = V$$

exists.

For the case of a randomly oriented specimen, a similar expression applies except that n (α, β) is independent of α and β. Hence

$$\int_0^{2\pi}\int_{\pi/2}^{0} n\ (\text{random})\ \cos\alpha\, d\alpha\, d\beta = n\ (\text{random}) \int_0^{2\pi}\int_{\pi/2}^{0} \cos\alpha\, d\alpha\, d\beta = V$$

Equating these expressions,

$$n\ (\text{random}) = \frac{\int_0^{2\pi}\int_{\pi/2}^{0} n\ (\alpha, \beta)\ \cos\alpha\, d\alpha\, d\beta}{\int_0^{2\pi}\int_{\pi/2}^{0} \cos\alpha\, d\alpha\, d\beta}$$

Having obtained n (random) by substituting the observed values of n(α, β) in this expression, the data are then normalized by dividing by n (random). Actually n (α, β) is not available as a continuous function, but for discrete values α_i, β_j only. Thus in practice the computation is really reduced by using the approximate formula

$$n\ (\text{random}) \cong \frac{\sum_i \sum_j n\ (\alpha_i, \beta_j)\ \cos\alpha_i\ \Delta\alpha_i\ \Delta\beta_j}{\sum_i \sum_j \cos\alpha_i\ \Delta\alpha_i\ \Delta\beta_j}$$

Finally, taking all increments $\Delta\alpha_i$ and $\Delta\beta_j$ at equal intervals, these can be cancelled out leaving

$$n\ (\text{random}) \cong \frac{\sum_i \sum_j n\ (\alpha_i, \beta_j)\ \cos\alpha_i}{\sum_i \sum_j \cos\alpha_i}$$

REFERENCES FOR APPENDIX 6A

1. B. D. Cullity, Elements of X-Ray Diffraction, pp. 285-295, Addison-Wesley Pub. Co., Inc., Reading, Mass., 1955.

2. G. F. Decker, E. T. Asp, and D. Harker, J. Appl. Phys., 19:382 (1948).

3. M. Field and M. E. Merchant, J. Appl. Phys., 20:741 (1949).

4. D. T. Keating and B. E. Warren, Rev. Sci. Instr., 23:519 (1952).

Appendix 6B

REMOVAL OF TWINS IN THE SURFACE GRAINS OF BERYLLIUM SHEET

The as-received beryllium sheet for this study contained numerous surface (and interior) twins which had to be removed before the effects of deliberately induced surface damage could be evaluated. Twins can be removed by annealing at some temperature near the recrystallization temperature. For the present study, it was desirable to keep the annealing time short enough to prevent excessive grain growth.

Recrystallization has been observed to take place in the range 750 - 900°C, depending on fabrication history. Therefore, samples of as-received sheet were annealed at 750°C (1382°F), 800°C (1472°F), 850°C (1562°F) and 900°C (1652°F) for 1/4, 1/2, 1, 2, 4, 8, 16, 32, and 64 hours. These treatments were performed as described in the sections on experimental procedure.

Metallographic examination showed that annealing of hot-pressed sheet for 2 hours at 800°C removed the majority of twins with no observable grain growth. A suitable treatment for hot-upset sheet was found to be four hours at 900°C.

Annealing of hot-rolled sheet did not produce the same effect as for hot-pressed and hot-upset material. Instead of removing the twins in the surface grains, annealing in the temperature range of 750 - 900°C caused an increase in quantity and depth of twins. At a particular temperature, twinning increased to a maximum with time (Figures 99 and 100). After 2 hours at 850°C, a maximum number of surface twins were produced. Eight hours at 850°C removed the heavy twinning but produced excessive grain growth. As a compromise, it was decided to anneal the hot-rolled sheet for 4 hours at 850°C. This treatment removed the majority of the mechanical twins without producing excessive grain growth.

The above observations in as-received hot-rolled sheet were made on samples taken from the edge of the sheet. However, the microstructure of the sheet was not uniform, and the extent of twinning was greater near the central portion of the sheet (compare Figures 100 and 70(a)). This may have been the result of nonuniform deformation, since it was observed that the outer edges of the sheet were several thousandths of an inch thinner than the central portions.

That the twins in the surface grains were not introduced by metallographic polishing was confirmed by the following experiment. A sample of as-received hot-rolled sheet was metallographically polished so that the plane of polish was perpendicular to the sheet surface. Then a Vickers micro-hardness indention (100 g load) was made on the polished surface. No twins could be seen around the hardness indentation. The specimen was repolished along with five annealed samples on the automatic polisher, until the hardness indentation was removed. Metallographic examination showed that no twins were introduced by the polishing method. Also, the structure of the annealed samples remained the same; i.e., the twins in the surface grains could not be removed by polishing.

Since the observed increases in the amount of twinning when hot-rolled sheet was annealed were contrary to the results expected, an explanation for this behavior was sought.

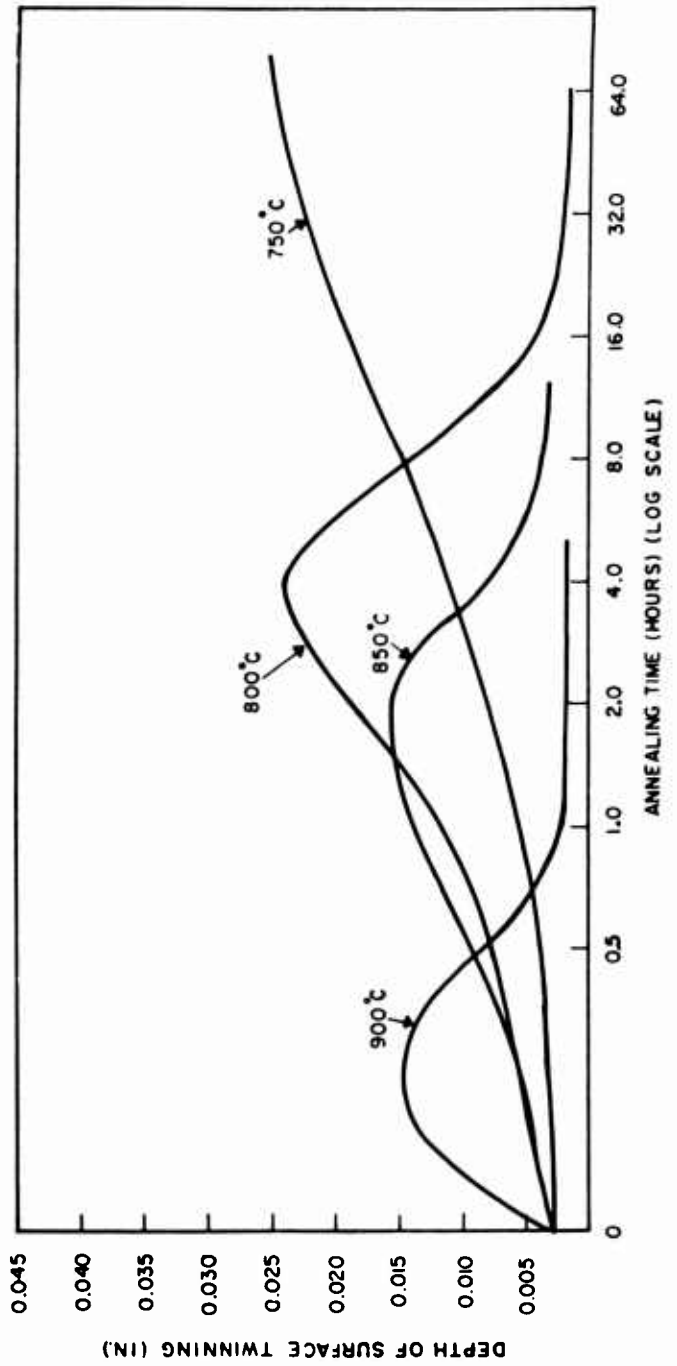

Figure 99 - Effect of annealing time on depth of twinning.

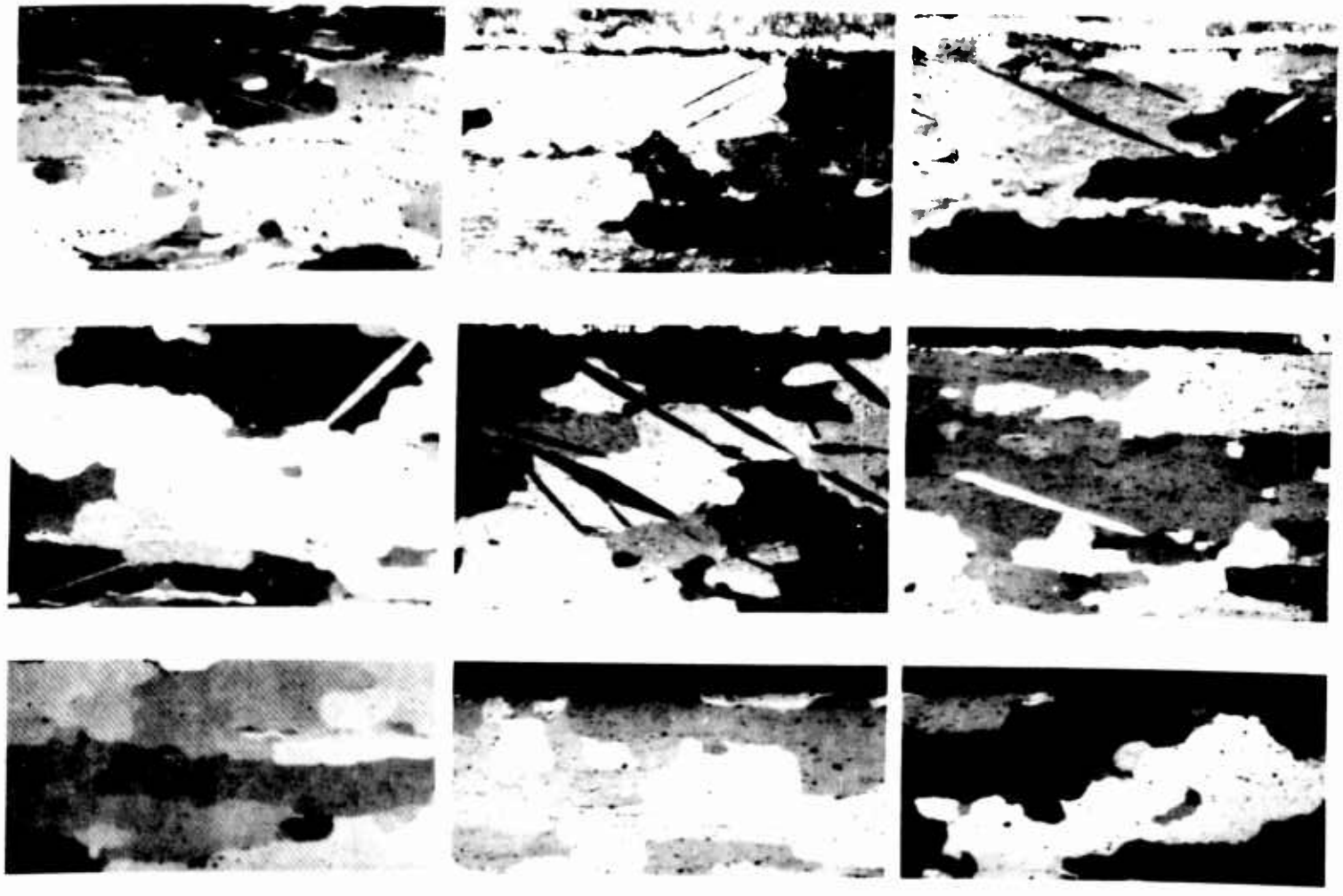

Figure 100 - Effect of annealing time on formation of surface twins in hot-rolled sheet annealed at 800°C. Annealing times: top row, left to right -- 0, 1/2 hr, 1 hr; center row -- 2 hr, 4 hr, 8 hr; bottom row -- 16 hr, 32 hr, 48 hr. (Polarized light; 200X)

One possibility is that the increase was due to the formation of annealing twins. Annealing twins occur frequently in fcc metals and are believed to initiate from stacking faults[1,2]. If the (111) plane of an fcc lattice is called the A plane, then the fcc lattice is built up by stacking additional planes of atoms in the B and C positions, as shown in Figure

The stacking order can be written

ABCABCABC

Without destroying the close packing, breaks may occur in the stacking order, as indicated by the arrow below:

ABCABCBACBACBA
↑

The planes to the right of the arrow are arranged as a mirror image of the planes to the left of the arrow; i.e., the arrow indicates a stacking fault which corresponds to a twin boundary. These stacking faults are of low energy and are relatively easy to produce during annealing in an fcc metal.

In hcp metals, the arrangement of the atoms in the basal planes is the same as in the (111) planes of fcc metals, i.e., the A Arrangement. The next layer of atoms is in the B positions, but the third layer is directly over the first, so that the stacking may be written as

ABABABAB

A break in the correct stacking order would result in the following sequence

ABAB ↑ CBCBCB

However, the arrangement ABAB is crystallographically indistinguishable from CBCB, so that the stacking fault does not correspond to a twin boundary.

In the preceding discussion, it is recognized that the basal plane in beryllium is not a coherent twin boundary, since twinning occurs on $\{10\bar{1}2\}$ and possibly other pyramidal planes. In order to form stacking faults on pyramidal planes in beryllium or other hcp metals extremely high energies would be required. The reason for this is that there is virtually no stacking of atoms above or below the $(10\bar{1}2)$ planes, the most common twinning plane for beryllium and other hexagonal metals. This is easily seen by a line perpendicular to the $(10\bar{1}2)$ plane through any atom in the plane. The line will not intersect any other atom in the lattice. Lee and Brick[3] conclude that $(10\bar{1}2)$ twins have to be over 100 atom layers thick in order to be stable. The probability of forming such twins by formation and growth of stacking faults during annealing is indeed small.

No cases have been found in the literature in which annealing twins form in hcp metals. It might be added further that all the twins observed in the annealed sample, if they had resulted from annealing, would be expected to show blunt ends.

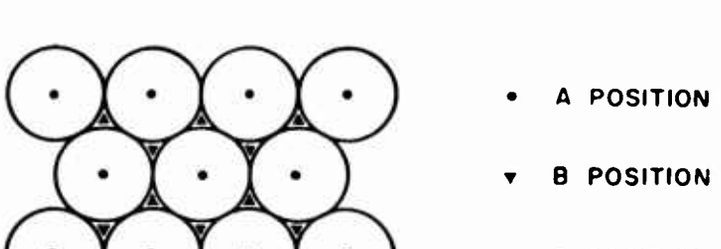

Figure 101 - Stacking in an fcc lattice.

However, the great majority showed sharp ends, indicating they were formed by shear. Where twins with blunt ends were observed, it is believed that they were in the process of being consumed by the lattice.

A second possibility is that the formation of twins is the result of "thermal-ratcheting". In the thermal treatment of uranium, zinc, and other noncubic metals, it has been reported that deformation occurs by slip, twinning, localized distortions at grain boundaries, and grain boundary migrations[4-7]. Other investigators have reported dimensional changes as a result of thermal treatments[6-10]. These deformations and dimensional changes are produced by thermal cycling, which consists of successively heating and cooling a specimen a number of times within a certain temperature range.

Boas and Honeycombe[4] attributed slip and twinning observed in thermally cycled Zn, Cd, and Sn to stresses arising from the anisotropy of thermal expansion in the crystals. They also found that long cycles produced greater amounts of deformation than short cycles.

Burke and Turkalo[11] studied the deformation of zinc bicrystals as the result of thermal cycling and proposed the "thermal ratchet" mechanism to explain the irreversible distortion that occurred between the two grains of the bicrystal. The two grains are shown schematically in Figure **102** with α_1 and α_2 as the coefficients of expansion in the directions indicated ($\alpha_1 > \alpha_2$). On heating, grain 1 attempts to become longer than grain 2, but is constrained by grain 2. Thus, grain 1 is loaded in compression and grain 2 in tension, and a shearing stress is developed across the boundary. As temperature increases, stresses build up and grain 1 (with its slip planes at 45° to the grain boundary) will be plastically deformed by slip, since the greater stress is resolved on its slip planes. Eventually, partly as a result of grain boundary flow, grain 1 grows longer than grain 2. It is interesting that twinning was observed near the grain boundary in zinc bicrystals.

The above argument can be modified to apply to beryllium. Suppose α_1 indicates the coefficient of expansion in the c direction for grain 1, and α_2 indicates the coefficient of expansion in the a direction for grain 2. Assume that the plane in grain 1, which is shown as a slip plane, is now a $(10\bar{1}2)$ plane. If so, the angle marked θ would be 42°. The coefficients of expansion for beryllium at 800°C are 22.0×10^{-6} per $^\circ$C in the a direction, and 18.3×10^{-6} per $^\circ$C in the c direction[12], so that on heating, grain 2 will attempt to expand more than grain 1. Thus, a tensile stress will develop in grain 1. The approximate magnitude of this stress can be calculated by a formula proposed by Boas and Honeycomb[4].

$$\sigma = \left(\alpha_1 - \alpha_2\right) \Delta T \left(\gamma_1^2 - \gamma_2^2\right) \frac{E_1 E_2}{E_1 + E_2}$$

where

α_1 and α_2 = The coefficients of expansion in the a and c direction respectively

ΔT = Temperature rise

γ_1, γ_2 = Cosine of angle between c axis and grain boundary for grain 1 and grain 2 respectively

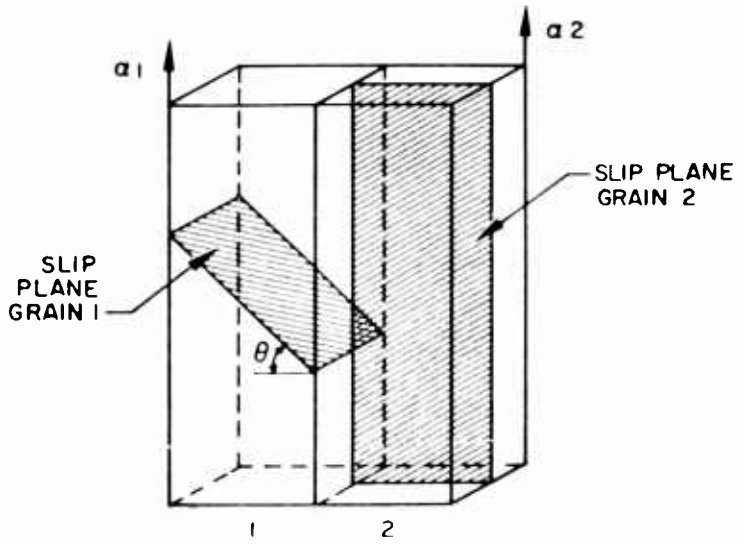

Figure 102 - Bicrystal of an anisotropic metal with slip plane of grain 1 lying 45° to grain boundary and slip plane of grain 2 at 90° to boundary (after Burke and Turkalo[11]).

E_1 and E_2 = Young's modulus for grain 1 and grain 2 respectively

σ = Calculated stress

It may be seen that the maximum stress results when the c axes are at right angles to each other; i.e., when $\left(\gamma_1^2 - \gamma_2^2\right) = 1$.

For beryllium, $(\alpha_1 - \alpha_2)$ is approximately equal to 4×10^{-6} per ^{o}C at all temperatures. At $850^{o}C$, we assume $E_1 = E_2 = 10 \times 10^6$ psi[13]. If the situation is as shown in Figure 6B-4, then the calculated tensile stress on grain 1 is 17,000 psi, which amounts to a resolved shear stress in the twinning plane of about 8500 psi.

For a polycrystalline sample, the constraints of neighboring grains would make it very difficult to perform a calculation of this sort, but let us assume the stresses of this order of magnitude can result. This stress is not sufficient to cause twinning, or else increases in the amount of twinning would have been observed in hot pressed and hot upset sheet annealed at various times and temperatures unless, of course, the effect of the high degree of texture present in the hot rolled sheet is significant. It is felt that the residual compressive stress present in the hot rolled sheet[14] (25,000 psi) may be the underlying difference in the behavior of the three sheets. The relief of these residual stresses and the resulting deformation associated with this relief may be the source of twinning. Yans, Wolff and Kaufmann[15] report that large amounts of $(10\bar{1}2)$ twinning were observed to occur in single crystals deformed by rolling at temperatures as high as $1070^{o}C$.

It is proposed, therefore, that the observed increase in the number of twins in hot-rolled sheet during certain time-temperature treatments occurs by the combined effects of thermal anisotropy and relief of residual stresses. Under suitable conditions of time and temperature, the twins are absorbed by the matrix and disappear. Recall that Boas and Honeycombe[4] found increased amounts of deformation with longer cycling times. This may also apply to beryllium, where increased amounts of twinning are observed with increasing time at a particular temperature. It is recognized that the annealing treatments used in this investigation did not comprise repeated cycles. It is proposed, however, that the observed effects resulted from only one heating cycle.

REFERENCES FOR APPENDIX 6B

1. H. G. Van Bueren, Chps. 13 and 21 in Imperfections in Crystals, Interscience Pub. Co., New York, 1960.

2. A. Seeger, in Dislocations and Mechanical Properties of Crystals (J. Fisher et al, Eds.), p. 243, John Wiley, New York, 1957.

3. H. T. Lee and R. M. Brick, Trans. Am. Soc. Met., 48:1003 (1956).

4. W. Boas and R. W. K. Honeycombe, Proc. Roy. Soc. (London), Series A, 186:57 (1946).

5. F. G. Foot, Nuclear Metallurgy Symposium A.I.M.E., Oct. 1955.

6. H. H. Chiswick, Trans. Am. Soc. Met., 49:622 (1957).

7. S. T. Zegler et al, Trans. Am. Soc. Met., 50:905 (1958).

8. R. M. Mayfield, Trans. Am. Soc. Met., 50:926 (1958).

9. J. E. Burke and A. M. Turkalo, Trans. Am. Soc. Met., 50:943 (1958).

10. L. T. Lloyd and R. M. Mayfield, Trans. Am. Soc. Met., 50:954 (1958).

11. J. E. Burke and A. M. Turkalo, Trans. A.I.M.E., 194:651 (1952).

12. P. Gordon, J. Appl. Phys., 20:908 (1948).

13. W. J. Salmen, Tensile Properties of Beryllium at Various Temperatures from Room Temperature to 1600°F, LMSC-800446, Lockheed Missiles and Space Company, Sunnyvale, Calif., Jan 1961.

14. C. O. Matthews, M. I. Jacobson, and W. E. Jahsman, Beryllium Crack Propagation and Effects of Surface Condition, WADD Technical Report 60-116, Jan 1960.

15. F. M. Yans, A. K. Wolff, and A. R. Kaufmann, Development of Randomly Ori[illegible] Wrought Beryllium Sheet, WADD Technical Report 60-403, Dec 1960.

Appendix 6C

TABULATION OF MECHANICAL PROPERTIES OF BERYLLIUM SHEET

Tensile and bend properties of the various categories of beryllium sheet - properties which were determined by this study - are detailed in the seven tables which constitute this appendix.

Table 17. TENSILE PROPERTIES OF HOT-ROLLED BERYLLIUM SHEET

Condition	Specimen	Longitudinal Direction			Transverse Direction		
		Ultimate Tensile Strength (psi x 10^{-3})	0.2% Offset Yield Strength (psi x 10^{-3})	Elongation (% in 1 in.)	Ultimate Tensile Strength (psi x 10^{-3})	0.2% Offset Yield Strength (psi x 10^{-3})	Elongation[a] (% in 1 in.)
As-received	A	48.6	48.3	0.2	45.4	45.4	0
	B	48.9	48.3	0.3	-	41.2	(b)
	C	51.6	48.9	0.7	-	46.2	(b)
	Av.	49.7	48.5	0.4	45.4	44.3	0
As-received; 4 hr, 850°C	A	52.9	36.8	1.0			
	B	51.6	34.2	1.2			
	Av.	52.3	35.5	1.1			
As-received; 4 hr, 850°C; etch 5 mils	A	53.3	32.8	2.3	42.4	26.2	1.9
	B	53.2	33.8	2.2	41.5	25.8	2.0
	C	51.4	33.5	2.0	41.1	25.8	1.7
	Av.	52.6	33.4	2.2	41.7	25.9	1.9
Ground 2 mils	A	41.4	35.2	0.6	38.6	30.1	0.8
	B	36.8	35.9	0.2	38.7	26.6	1.0
	C	42.1	36.6	0.5	-	-	-
	Av.	40.1	35.9	0.4	38.7	28.4	0.9
Ground 2 mils; 4 hr, 850°C	A	41.3	29.2	1.7	40.1	25.7	2.0
	B	51.5	34.5	2.0	42.0	28.1	1.8
	C	50.6	34.7	1.7	40.1	27.9	1.6
	Av.	47.8	32.8	1.8	40.7	27.2	1.8
Ground 2 mils; 4 hr, 850°C; etch 5 mils	A	51.5	33.4	2.3	39.4	26.6	1.7
	B	51.1	34.8	2.3	38.9	25.9	1.3
	Av.	51.3	34.1	2.3	39.2	26.3	1.5

Table 17 (Continued)

Condition	Specimen	Longitudinal Direction			Transverse Direction		
		Ultimate Tensile Strength (psi x 10^{-3})	0.2% Offset Yield Strength (psi x 10^{-3})	Elongation (% in 1 in.)	Ultimate Tensile Strength (psi x 10^{-3})	0.2% Offset Yield Strength (psi x 10^{-3})	Elongation[a] (% in 1 in.)
Ground 5 mils	A	38.7	35.7	0.3	38.0	29.1	0.9
	B	42.3	36.2	0.6	38.6	27.4	1.0
	Av.	40.5	36.0	0.5	38.3	28.3	1.0
Ground 5 mils; 4 hr, 850°C	A	52.3	35.2	2.1	41.6	26.9	1.6
	B	53.2	33.2	2.6	39.4	28.4	1.4
	C	50.6	33.9	1.9	-	-	-
	Av.	52.0	34.1	2.2	40.5	27.7	1.5
Ground 5 mils; 4 hr, 850°C; Etch 5 mils	A	50.9	32.7	2.2	38.2	22.6	1.8
	B	40.9	32.2	1.0	39.5	27.1	1.8
	C	50.0	32.5	2.2	-	-	-
	Av.	47.3	32.5	1.8	38.9	24.8	1.8

(a) All values determined with microformer extensometer.
(b) Failed outside gage length.

Table 18. TENSILE PROPERTIES OF HOT-PRESSED BERYLLIUM SHEET

Condition	Specimen	Ultimate Tensile Strength (psi x 10^{-3})	0.2% Offset Yield Strength (psi x 10^{-3})	Elongation (% in 1 in.)
As-received	A	46.3	36.2	1.4*
	B	46.6	35.8	1.1*
	C	42.5	35.5	0.7*
	Av.	45.1	35.8	1.1
As-received; 2 hr, 800°C	A	49.2	35.0	2.0*
	B	51.2	32.6	2.6*
	C	52.1	34.6	3.4*
	Av.	50.8	34.1	2.7
As-received; 2 hr, 800°C; etch 5 mils	A	45.6	34.2	1.6*
	B	49.2	34.5	2.1*
	C	54.0	35.8	3.3*
	Av.	49.6	34.8	2.3
Ground 2 mils	A	50.6	38.5	1.3
	B	51.2	39.3	1.4
	C	50.4	38.7	1.5
	Av.	50.7	38.8	1.4
Ground 2 mils; 2 hr, 800°C	A	54.4	36.1	3.8
	B	51.9	39.2	2.2
	C	52.4	34.6	2.9
	Av.	52.9	36.6	3.0
Ground 2 mils; 2 hr, 800°C; Etch 5 mils	A	51.4	34.6	3.0
	B	52.8	36.0	3.5
	C	52.8	34.9	3.2
	Av.	52.3	35.2	3.2
Ground 5 mils	A	50.5	36.4	1.6
	B	48.2	37.3	1.2
	C	51.4	37.4	1.5
	Av.	50.0	37.0	1.4
Ground 5 mils; 2 hr, 800°C	A	50.7	33.6	2.8
	B	50.0	34.8	2.5
	C	51.8	-	-
	Av.	50.8	34.2	2.7
Ground 5 mils; 2 hr, 800°C; etch 5 mil	A	50.2	33.0	2.5
	B	49.7	33.1	2.0
	C	50.0	34.8	2.1
	Av.	50.0	33.6	2.2

*Elongation determined from crosshead separation. All other values determined with microformer extensometer.

Table 19. TENSILE PROPERTIES OF HOT-UPSET BERYLLIUM SHEET

Condition	Specimen	Ultimate Tensile Strength (psi x 10^{-3})	0.2% Offset Yield Strength (psi x 10^{-3})	Elongation (% in 1 in.)
As-received;	A	-	(a)	(a)
4 hr, 900°C	B	65.1	36.0	8.2(b)
	C	71.4	37.9	16.0(b)
	Av.	68.3	37.0	12.1
Ground 5 mils	A	62.8	44.6	(a)
	B	67.0	41.2	(a)
	C	71.1	40.6	8.6
	Av.	67.0	42.1	8.6
Ground 5 mils;	A	71.5	39.9	13.0
4 hr, 900°C	B	71.2	39.0	11.1
	C	73.0	39.4	14.8
	Av.	71.9	39.4	13.0
Ground 5 mils;	A	72.0	38.5	14.6
4 hr, 900°C;	B	73.4	37.6	19.2
etch 5 mils	C	74.2	42.0	21.0
	Av.	73.2	39.4	18.3

(a) Failed outside gage length.
(b) Elongation determined from crosshead separation. All other values determined with microformer extensometer.

Table 20. BEND PROPERTIES OF HOT-ROLLED BERYLLIUM SHEET IN THE LONGITUDINAL DIRECTION

Condition	Specimen	Max. Outer Fiber Stress (psi x 10^{-3})	Total Deflection (mil)	Permanent Bend Angle (degrees)
As-received	A	84.3	71.1	8
	B	67.6	18.2	2
	C	68.7	18.2	2
	Av.	73.5	35.8	4
As-received; 4 hr, 850°C	A	65.0	58.2	10
	B	73.2	72.8	12
	C	65.6	78.2	13
	Av.	67.9	69.7	12
As-received; 4 hr, 850°C; etch 5 mils	A	60.1	65.5	10
	B	63.0	82.0	12
	C	62.0	76.5	13
	Av.	61.7	74.7	12
Ground 2 mils	A	48.7	26.4	4
Ground 2 mils; 4 hr, 850°C	A	-	-	10
	B	60.4	89.2	16
	C	62.6	72.8	10
	Av.	61.5	81.0	12
Ground 2 mils; 4 hr, 850°C; etch 5 mils	A	59.0	96.5	16
	B	55.5	89.5	17
	C	60.5	98.2	14
	Av.	58.3	94.7	16
Ground 5 mils	A	54.2	31.9	4
	B	48.6	21.8	4
	Av.	51.4	26.9	4
Ground 5 mils; 4 hr, 850°C	A	60.7	82.5	12
	B	54.0	69.2	12
	C	57.0	67.4	12
	Av.	57.2	73.0	12
Ground 5 mils; 4 hr, 850°C; etch 5 mils	A	52.9	109	20
	B	52.0	111	17
	C	53.0	103	16
	Av.	52.6	108	18

Table 20 (Continued)

Condition	Specimen	Max. Outer Fiber Stress (psi x 10^{-3})	Total Deflection (mil)	Permanent Bend Angle (degrees)
Ground 10 mils	A	53.6	31.9	7
	B	44.6	18.2	4
	Av.	49.1	25.1	6
Ground 10 mils; 4 hr, 850°C	A	57.5	64.6	10
	B	60.5	81.0	14
	C	62.3	91.0	15
	Av.	60.1	78.9	13
Ground 10 mils; 4 hr, 850°C; etch 5 mils	A	56.7	94.6	16
	B	48.2	51.0	8
	C	56.5	72.8	13
	Av.	53.8	72.8	12

Figure 21. BEND PROPERTIES OF HOT-ROLLED BERYLLIUM SHEET IN THE TRANSVERSE DIRECTION

Condition	Specimen	Max. Outer Fiber Stress (psi x 10^{-3})	Total Deflection (mil)	Permanent Bend Angle (degrees)
As-received	A	61.1	40.0	7
	B	58.6	60.0	10
	C	61.0	60.0	10
	Av.	60.2	53.3	9
As-received; 4 hr, 850°C	A	54.3	54.6	11
	B	47.2	51.0	10
	C	48.6	54.6	10
	Av.	50.0	53.4	10
As-received; 4 hr, 850°C; etch 5 mils	A	52.2	65.5	12
	B	53.0	69.2	14
	C	52.6	67.4	13
	Av.	52.6	67.4	13
Ground 2 mils	A	43.2	34.6	6
	B	43.4	36.4	6
	C	42.6	38.6	7
	Av.	43.1	36.5	6
Ground 2 mils; 4 hr, 850°C	A	49.2	58.2	12
	B	47.1	55.5	11
	C	48.2	57.2	10
	Av.	48.2	57.0	11
Ground 2 mils; 4 hr, 850°C; etch 5 mils	A	43.4	72.8	12
	B	40.8	78.3	14
	C	40.9	65.5	12
	Av.	41.7	72.2	13
Ground 2 mils; etch 5 mils	A	38.0	78.2	12
Ground 5 mils	A	28.2	40.1	6
	B	30.9	39.8	6
	C	28.8	40.9	6
	Av.	29.3	40.3	6
Ground 5 mils; 4 hr, 850°C	A	49.9	58.4	10
	B	48.9	58.4	10
	C	48.9	58.6	10
	Av.	49.2	58.5	10

Table 21 (Continued)

Condition	Specimen	Max. Outer Fiber Stress (psi x 10^{-3})	Total Deflection (mil)	Permanent Bend Angle (degrees)
Ground 5 mils; 4 hr, 850°C; etch 5 mils	A	42.7	82.0	12
	B	42.0	80.2	12
	C	46.5	73.5	13
	Av.	43.7	78.6	12
Ground 5 mils; etch 5 mils	A	37.0	72.7	14

Table 22. BEND PROPERTIES OF HOT-PRESSED BERYLLIUM SHEET

Condition	Specimen	Max. Outer Fiber Stress (psi x 10^{-3})	Total Deflection (mil)	Permanent Bend Angle (degrees)
As-received	A	62.0	36.4	6
	B	52.7	18.2	4
	C	60.3	40.0	2
	Av.	58.3	31.5	4
As-received; 2 hr, 800°C	A	66.0	72.8	13
	B	65.0	72.8	13
	C	60.1	67.3	12
	Av.	63.7	71.0	13
As-received; 2 hr, 800°C etch 5 mils	A	67.8	87.5	11
	B	64.4	91.1	15
	C	55.5	94.6	16
	Av.	62.6	91.1	14
Ground 2 mils	A	62.6	58.3	10
	B	62.9	60.0	10
	C	60.2	63.8	10
	Av.	61.9	60.7	10
Ground 2 mils; 2 hr, 800°C	A	62.2	94.5	17
	B	64.8	100.0	16
	C	67.0	100.9	20
	Av.	64.7	98.5	18
Ground 2 mils; 2 hr, 800°C; etch 5 mils	A	60.7	107	21
	B	58.2	127	19
	Av.	59.5	117	20
Ground 2 mils; etch 5 mils	A	52.6	116	20
Ground 5 mils	A	66.6	58.2	9
	B	59.4	51.0	8
	C	60.2	41.0	7
	Av.	62.1	50.1	8
Ground 5 mils; 2 hr, 800°C	A	68.7	106	17
	B	68.3	100	17
	C	65.3	102	18
	Av.	67.4	103	17

Table 22 (Continued)

Condition	Specimen	Max. Outer Fiber Stress (psi x 10^{-3})	Total Deflection (mil)	Permanent Bend Angle (degrees)
Ground 5 mils; 2 hr, 800°C; etch 5 mils	A	64.4	106	17
	B	62.5	100	12
	Av.	63.5	103	15
Ground 5 mils; etch 5 mils	A	46.4	84.0	14
Ground 10 mils	A	60.0	36.4	6
	B	61.6	45.5	7
	C	54.5	31.8	5
	Av.	58.7	37.9	6
Ground 10 mils; 2 hr, 800°C	A	65.5	101	15
	B	67.2	107	17
	C	67.8	103	16
	Av.	66.7	104	16
Ground 10 mils; 2 hr, 800°C; etch 5 mils	A	62.3	89.2	16
	B	62.2	97.5	18
	Av.	62.3	93.4	17
Ground 10 mils; etch 5 mils	A	49.4	115	18

Table 23. BEND PROPERTIES OF HOT-UPSET BERYLLIUM SHEET

Condition	Specimen	Max. Outer Fiber Stress (psi x 10^{-3})	Total Deflection (mil)	Permanent Bend Angle (degrees)
As-received	A	67.4	25.5	6
	B	57.1	27.3	6
	C	58.5	29.1	6
	Av.	61.0	27.3	6
As-received; 4 hr, 900°C	A	97.0	231	44
	B	86.0	133	23
	C	100.0	197	37
	Av.	94.3	187	35
As-received; 4 hr, 900°C; etch 2 mils	A	84.6	133	23
	B	96.8	246	46
	C	90.7	146	28
	Av.	90.7	175	32
Ground 2 mils	A	84.6	147	29
	B	83.2	112	14
	Av.	83.9	130	22
Ground 2 mils; 4 hr, 900°C	A	90.7	166	30
	B	90.6	158	23
	Av.	90.7	162	27
Ground 2 mils; 4 hr, 900°C; etch 5 mils	A	87.3	291	49
	B	71.0	164	32
	Av.	79.2	228	41
Ground 2 mils; etch 5 mils	A	67.0	258	44
Ground 5 mils	A	76.8	94.6	16
	B	65.6	56.5	11
	C	82.8	129.0	22
	Av.	75.1	93.4	16
Ground 5 mils; 4 hr, 900°C	A	88.1	172	39
	B	81.9	208	30
	Av.	85.0	190	35
Ground 5 mils; 4 hr, 900°C	A	80.5	324	56
	B	88.6	310	58
	Av.	84.6	317	57
Ground 5 mils; etch 5 mils	A	66.5	292	52

Aeronautical Systems Division, Dir/Materials & Processes, Metals & Ceramics Lab, Wright-Patterson AFB, Ohio.
Rpt Nr ASD-TDR-62-509 Vol I. BERYLLIUM RESEARCH AND DEVELOPMENT PROGRAM. Final report, Oct. 1962, 214 pp. incl illus, tables, & 78 refs.

Unclassified Report

Summary of work conducted for the period April 1, 1960 through September 30, 1961 aimed at making Be more useful as an Air Force structural material. Report describes work in the field of purification, joining and flow and fracture. Volume I describes the preparation of high purity Be by the decomposition of BeI_2, the joining of Be by ultrasonic welding and the resistance spot welding of Be. Also, a study of the distribution of BeO and voids in Be by replication electron microscopy, an investigation of the brittle behavior of Be by transmission electron microscopy, and a study of surface damage in Be are described.

1. Beryllium
2. Metallurgy
3. Welding
4. Surface Properties
I. AFSC Proj 7351-04
II. Contr Nr AF 33(616)-7065
III. Nuclear Metals, Inc. Concord, Mass.
IV. S. H. Gelles, Coordinator
V. Aval fr OTS
VI. In ASTIA collection

Aeronautical Systems Division, Dir/Materials & Processes, Metals & Ceramics Lab, Wright-Patterson AFB, Ohio.
Rpt Nr ASD-TDR-62-509 Vol I. BERYLLIUM RESEARCH AND DEVELOPMENT PROGRAM. Final report, Oct. 1962, 214 pp. incl illus, tables, & 78 refs.

Unclassified Report

Summary of work conducted for the period April 1, 1960 through September 30, 1961 aimed at making Be more useful as an Air Force structural material. Report describes work in the field of purification, joining and flow and fracture. Volume I describes the preparation of high purity Be by the decomposition of BeI_2, the joining of Be by ultrasonic welding and the resistance spot welding of Be. Also, a study of the distribution of BeO and voids in Be by replication electron microscopy, an investigation of the brittle behavior of Be by transmission electron microscopy, and a study of surface damage in Be are described.

1. Beryllium
2. Metallurgy
3. Welding
4. Surface Properties
I. AFSC Proj 7351-04
II. Contr Nr AF 33(616)-7065
III. Nuclear Metals, Inc. Concord, Mass.
IV. S. H. Gelles, Coordinator
V. Aval fr OTS
VI. In ASTIA collection

Aeronautical Systems Division, Dir/Materials & Processes, Metals & Ceramics Lab, Wright-Patterson AFB, Ohio.
Rpt Nr ASD-TDR-62-509 Vol I. BERYLLIUM RESEARCH AND DEVELOPMENT PROGRAM. Final report, Oct. 1962, 214 pp. incl illus, tables, & 78 refs.

Unclassified Report

Summary of work conducted for the period April 1, 1960 through September 30, 1961 aimed at making Be more useful as an Air Force structural material. Report describes work in the field of purification, joining and flow and fracture. Volume I describes the preparation of high purity Be by the

(over)

decomposition of BeI_2, the joining of Be by ultrasonic welding and the resistance spot welding of Be. Also, a study of the distribution of BeO and voids in Be by replication electron microscopy, an investigation of the brittle behavior of Be by transmission electron microscopy, and a study of surface damage in Be are described.

1. Beryllium
2. Metallurgy
3. Welding
4. Surface Properties
I. AFSC Proj 7351-04
II. Contr Nr AF 33(616)-7065
III. Nuclear Metals, Inc. Concord, Mass.
IV. S. H. Gelles, Coordinator
V. Aval fr OTS
VI. In ASTIA collection

Aeronautical Systems Division, Dir/Materials & Processes, Metals & Ceramics Lab, Wright-Patterson AFB, Ohio.
Rpt Nr ASD-TDR-62-509 Vol I. BERYLLIUM RESEARCH AND DEVELOPMENT PROGRAM. Final report, Oct. 1962, 214 pp. incl illus, tables, & 78 refs.

Unclassified Report

Summary of work conducted for the period April 1, 1960 through September 30, 1961 aimed at making Be more useful as an Air Force structural material. Report describes work in the field of purification, joining and flow and fracture. Volume I describes the preparation of high purity Be by the

(over)

decomposition of BeI_2, the joining of Be by ultrasonic welding and the resistance spot welding of Be. Also, a study of the distribution of BeO and voids in Be by replication electron microscopy, an investigation of the brittle behavior of Be by transmission electron microscopy, and a study of surface damage in Be are described.

1. Beryllium
2. Metallurgy
3. Welding
4. Surface Properties
I. AFSC Proj 7351-04
II. Contr Nr AF 33(616)-7065
III. Nuclear Metals, Inc. Concord, Mass.
IV. S. H. Gelles, Coordinator
V. Aval fr OTS
VI. In ASTIA collection